U.S. Department
of Transportation

Federal Highway
Administration

Load Transfer for Drilled Shafts in Intermediate Geomaterials

FOREWORD
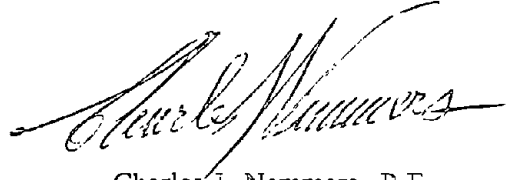
This report summarizes investigations on the resistance of load-settlement behavior of axially loaded drilled shafts in geomaterials at the boundary between soil and rock, termed "intermediate geomaterials." Two predictive models were developed, namely, a finite element model based on drilled shafts with smooth and rough interfaces in cohesive geomaterials, and a model based on an approximate elasticity solution and correlations of geomaterial properties with standard penetration test results in cohesionless geomaterials. The models are recommended for use pending local calibration.

Charles J. Nemmers, P.E.
Director, Office of Engineering
Research and Development

NOTICE

1. Report No. FHWA-RD-95-172	2. Government Accession No. PB97-117477	3. Recipient's Catalog No.
4. Title and Subtitle LOAD TRANSFER FOR DRILLED SHAFTS IN INTERMEDIATE GEOMATERIALS		5. Report Date November 1996
		6. Performing Organization Code
7. Author(s) M.W. O'Neill, F.C. Townsend, K.M. Hassan, A. Buller, P.S. Chan		8. Performing Organization Report No. 91143.10
9. Performing Organization Name and Address PSC Associates, Inc. 1185 Terra Bella Mountain View, CA 94043		10. Work Unit No. (TRAIS) 3E3a
		11. Contract or Grant No. DTFH61-91-Z-00041
12. Sponsoring Agency Name and Address Office of Engineering and Highway Operations R&D Federal Highway Administration 6300 Georgetown Pike McLean, VA 22101-2296		13. Type of Report and Period Covered Final Report 1991-1995
		14. Sponsoring Agency Code

15. Supplementary Notes

Contracting Officer's Technical Representative (COTR):
Carl Ealy, HNR-10

16. Abstract

This study investigated the resistance and load-settlement behavior of axially loaded drilled shafts in geomaterials at the boundary between soil and rock, termed "intermediate geomaterials." The primary objective of the study was to develop or adapt simple design-level models to predict resistance and load-settlement behavior. Two models are proposed. The first is based on finite element modeling of drilled shafts with smooth and rough interfaces in cohesive geomaterials, while the second is based on approximate elasticity solution and correlations of geomaterial properties with standard penetration test results in cohesionless geomaterials. Loading tests on seven full-scale drilled shafts were considered as a means to verify the accuracy of the design models and to develop recommendations concerning the inputs to the models. The models are recommended for use pending local calibration.

17. Key Words Drilled Shafts, Design Soft Rock, Hard Clay, Residual Soil, Glacial Till, Load Testing, Load Transfer	18. Distribution Statement No restrictions. This document is available to the public through the National Technical Information Service, Springfield, Virginia 22161.	
19. Security Classif. (of this report) Unclassified	20. Security Classif. (of this page) Unclassified	21. No. of Pages 194	22. Price

Form DOT F 1700.7 (8-72)   Reproduction of completed page authorized

Preface

In order to complete the research study presented in this report, the authors were assisted by numerous generous individuals and organizations who received the authors for personal visits, reviewed materials, permitted access to data bases, and made test sites available and accessible. These individuals and organizations are listed below.

Clyde Baker, Jr.
Jean-Louis Briaud
John Carter
Ian Johnston
Chris Haberfield
Robert Horvath
Fred Kulhawy
James Long
Reniere Majano
Paul Mayne
Michael McVay
Priscilla Nelson
P. J. N. Pells
Harry Poulos
Lymon Reese
Kerry Rowe
Julian Seidel
Keith Tucker
Willem Van Impe
Adrian Williams

ADSC: The International Association of Foundation Drilling
Georgia Department of Transportation
Haley and Aldrich, Inc.
Kentucky Transportation Cabinet
Southwestern Laboratories, Inc.
Trow, Inc.

SI* (MODERN METRIC) CONVERSION FACTORS

APPROXIMATE CONVERSIONS TO SI UNITS

Symbol	When You Know	Multiply By	To Find	Symbol
LENGTH				
in	inches	25.4	millimeters	mm
ft	feet	0.305	meters	m
yd	yards	0.914	meters	m
mi	miles	1.61	kilometers	km
AREA				
in²	square inches	645.2	square millimeters	mm²
ft²	square feet	0.093	square meters	m²
yd²	square yards	0.836	square meters	m²
ac	acres	0.405	hectares	ha
mi²	square miles	2.59	square kilometers	km²
VOLUME				
fl oz	fluid ounces	29.57	milliliters	mL
gal	gallons	3.785	liters	L
ft³	cubic feet	0.028	cubic meters	m³
yd³	cubic yards	0.765	cubic meters	m³

NOTE: Volumes greater than 1000 l shall be shown in m³.

Symbol	When You Know	Multiply By	To Find	Symbol
MASS				
oz	ounces	28.35	grams	g
lb	pounds	0.454	kilograms	kg
T	short tons (2000 lb)	0.907	megagrams (or "metric ton")	Mg (or "t")
TEMPERATURE (exact)				
°F	Fahrenheit temperature	5(F-32)/9 or (F-32)/1.8	Celcius temperature	°C
ILLUMINATION				
fc	foot-candles	10.76	lux	lx
fl	foot-Lamberts	3.426	candela/m²	cd/m²
FORCE and PRESSURE or STRESS				
lbf	poundforce	4.45	newtons	N
lbf/in²	poundforce per square inch	6.89	kilopascals	kPa

APPROXIMATE CONVERSIONS FROM SI UNITS

Symbol	When You Know	Multiply By	To Find	Symbol
LENGTH				
mm	millimeters	0.039	inches	in
m	meters	3.28	feet	ft
m	meters	1.09	yards	yd
km	kilometers	0.621	miles	mi
AREA				
mm²	square millimeters	0.0016	square inches	in²
m²	square meters	10.764	square feet	ft²
m²	square meters	1.195	square yards	yd²
ha	hectares	2.47	acres	ac
km²	square kilometers	0.386	square miles	mi²
VOLUME				
mL	milliliters	0.034	fluid ounces	fl oz
L	liters	0.264	gallons	gal
m³	cubic meters	35.71	cubic feet	ft³
m³	cubic meters	1.307	cubic yards	yd³
MASS				
g	grams	0.035	ounces	oz
kg	kilograms	2.202	pounds	lb
Mg (or "t")	megagrams (or "metric ton")	1.103	short tons (2000 lb)	T
TEMPERATURE (exact)				
°C	Celcius temperature	1.8C + 32	Fahrenheit temperature	°F
ILLUMINATION				
lx	lux	0.0929	foot-candles	fc
cd/m²	candela/m²	0.2919	foot-Lamberts	fl
FORCE and PRESSURE or STRESS				
N	newtons	0.225	poundforce	lbf
kPa	kilopascals	0.145	poundforce per square inch	lbf/in²

* SI is the symbol for the International System of Units. Appropriate rounding should be made to comply with Section 4 of ASTM E380.

(Revised September 1993)

iii

Table of Contents

Table of Contents
(continued)

Table of Contents
(continued)

List of Figures

List of Figures
(continued)

List of Tables

CHAPTER 1: INTRODUCTION

BACKGROUND

Drilled shafts are foundation elements for bridges and other transportation structures that are often cost-effective alternatives to driven piles or spread footings. They are commonly constructed by excavating a circular borehole into a geomaterial (soil or rock), setting a reinforcing cage, and then placing concrete; and they can be designed to carry axial load, lateral load, or a combination of loads. A schematic of a typical drilled shaft foundation is shown in figure 1.
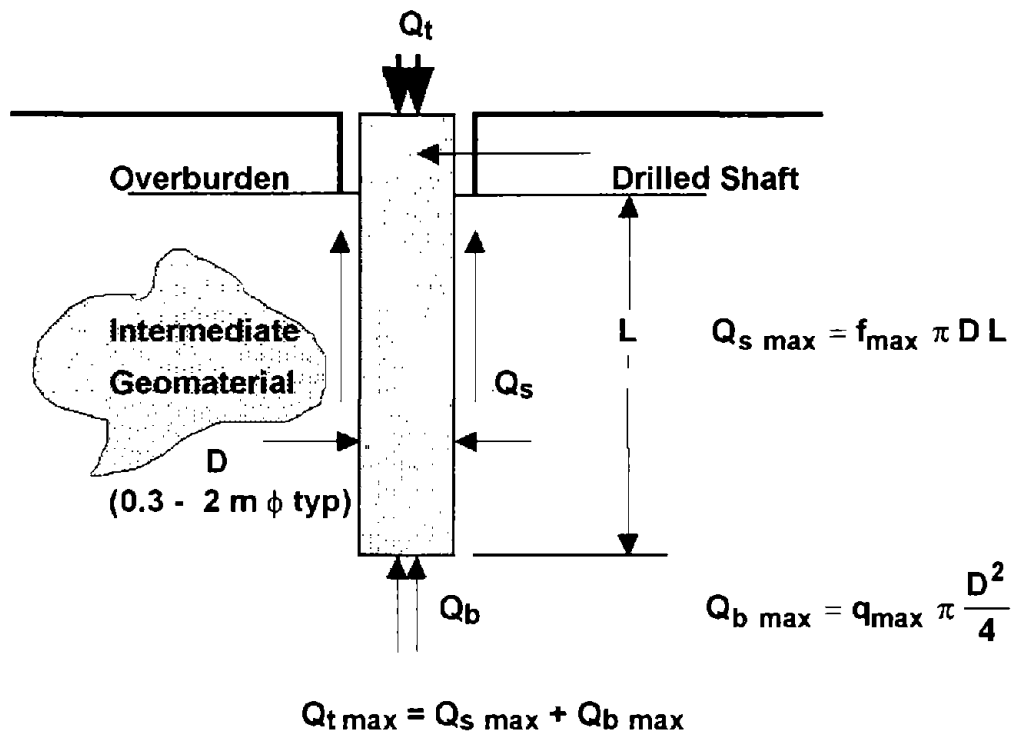
Figure 1. Schematic of a typical drilled shaft foundation.

Drilled shaft foundations are particularly attractive for use in "intermediate geomaterials," or geomaterials at the boundary between soil and rock; since boreholes in such geomaterials are relatively stable, the geomaterials are not usually difficult to excavate, and the geomaterial provides excellent resistance to load. Driven piles, the most common alternative to drilled shafts, are often more difficult to install and are sometimes damaged in intermediate geomaterials. Drilled shafts in intermediate geomaterials are most often constructed so as to provide most of their resistance to working load by means of side resistance, as opposed to base resistance. This report recommends methodologies for estimating axial (side and base) resistance and settlement of drilled shafts under axial loading in these geomaterials. Ordinarily, the unit shaft resistance at failure f_{max} is estimated by an appropriate method, some of which are described later; the unit base resistance at failure q_{max} is estimated by an appropriate method; and the ultimate capacity $Q_{t\,max}$ is computed as indicated in figure 1.

1

Intermediate Geomaterials

For purposes of this report, three categories of intermediate geomaterials (IGM's) will be considered:

1. _Argillaceous geomaterials:_ heavily overconsolidated clays, clay shales, saprolites and mudstones that are prone to smearing when drilled.

2. _Calcareous rocks:_ limestone and limerock and argillaceous geomaterials that are not prone to smearing when drilled.

3. _Very dense granular geomaterials:_ Residual, completely decomposed rock and glacial till with SPT N values between 50 and 100 blows / 0.3 m.

Geomaterials in Categories 1 and 2, above, are cohesive. For purposes of definition, the compressive strength range q_u of such geomaterials will be taken to be 0.5 to 5.0 MPa. Geomaterials in Category 3 are primarily cohesionless and will be considered to possess a standard penetration test (SPT) blow count of 50 - 100 blows / 0.3 m. Since soils and soft rocks in these three categories behave differently, separate design procedures are recommended for each category.

Study Objective

Design of drilled shafts in IGM's is currently problematical. For example, figure 2 shows the variation of the proportionality factor (α) between the shear strength s_u (normalized by atmospheric pressure p_a), or one-half of the compressive strength q_u (normalized by atmospheric pressure p_a), of cohesive geomaterials and the maximum unit side shearing resistance in drilled shafts ($f_{max} = Q_s / \pi DL$, figure 1), obtained experimentally from loading tests. It is clear that correlation to geomaterial strength alone, which is currently common practice, will force designers to employ very conservative methods for estimating side resistance. It is obvious, therefore, that design methods should be identified that relate more closely to the controlling parameters in the shaft/geomaterial system and yet be simple enough to apply in practice. For example, Kulhawy and Phoon recommend that $\overline{\alpha}$ be taken near the upper bound of data in figure 2 for rough boreholes and near the lower bound for smooth boreholes.[2] They also point out that it is critical to use recommended values of $\overline{\alpha}$ together with appropriate laboratory tests for defining s_u or q_u. The isotropically consolidated, undrained compression (CIUC) triaxial test is probably the most appropriate test for such correlation; however, only unconsolidated, undrained (UU) data are commonly available in most site investigations, and such data can be used conservatively. The objective of this study and the primary focus of this report was to identify the controlling parameters and to describe methods for the design of drilled shafts loaded in compression that are appropriate for IGM's. Designs for dynamic loading, loading due to downdrag or swelling soils, and uplift loading are not considered explicitly.

Study Methodology

This report is a succinct description of the design methods recommended for transportation structure foundations developed using the following methodology.

1. The technical literature on the subject was reviewed, and personal visits were made to researchers and practitioners in the United States (University of Illinois; Lymon C. Reese and Associates; Keith Tucker, Consulting Engineer; University of Texas at Austin; STS Consultants, Ltd.), Canada (Trow, Inc.; University of Western Ontario; McMaster University;University of Toronto), Australia (VicRoads - the road authority of the State of Victoria; New South Wales Road and Traffic Authority; Coffey Partners, Ltd.; University of Sydney; and Monash University), and Belgium (University of Ghent) to discuss their perspectives on design and to obtain loading test data. Informal discussions were also held with representatives of the Federal Highway Administration, ADSC (The International Association of Foundation Drilling), and several state departments of transportation in the United States.
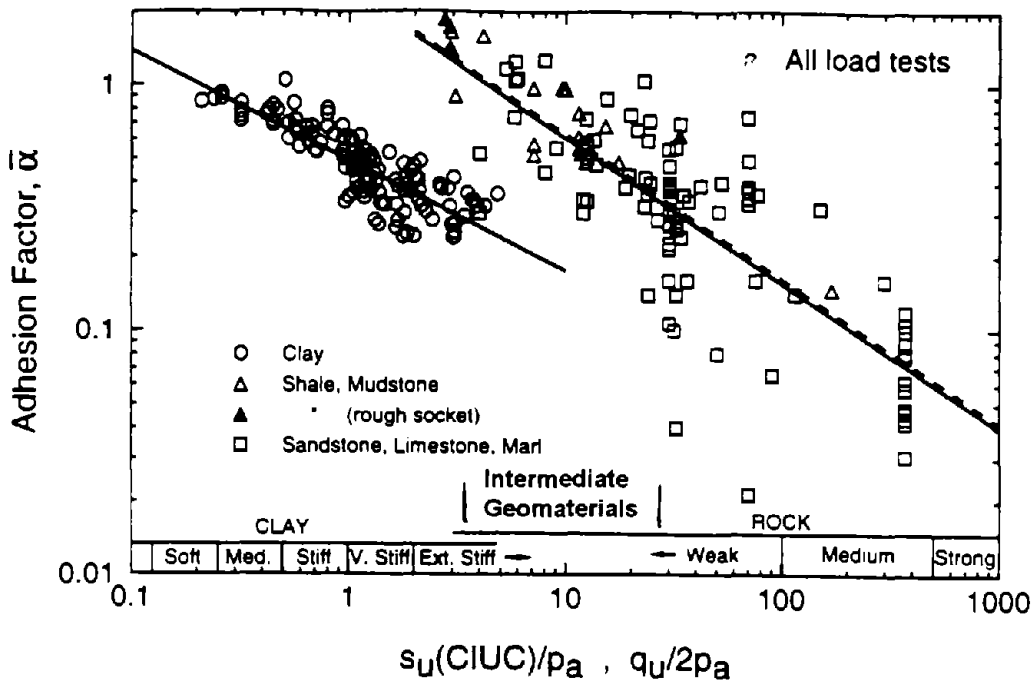
Figure 2. Variation in factor $\overline{\alpha}$ based only on geomaterial strength.[1] (Reproduced by permission of ASCE, New York)

3

2. Trial design methods were selected from among those identified in Step 1.

3. Geomaterial characterization and loading test data were extracted from numerous papers and reports that were found in the literature search and provided by human contacts These site-specific loading test data were input into a data base. Results of 139 load tests were used in further steps.

4. Predictions of side resistance at failure (Q_{smax}) were made for the tests in the data base using nine commonly used design methods identified in the literature search that prescribe side resistance based on geomaterial strength, and values of Q_{smax} that were computed were compared to the measured side resistances. In the loading tests in the data base (Step 3) there was a low degree of correlation between predictions and measurements for all nine methods, not surprisingly in view of the information presented in figure 2. Although this substudy included only side resistance, the general conclusions (lack of correlation to geomaterial strength) can be assumed to apply to total resistance (sides plus base).

5. In order to provide a basis for developing an improved design model, the effects of such variables as shaft/geomaterial interface roughness, geomaterial smear, depth and geomaterial stiffness on load transfer, and load-settlement response were quantified through a systematic study of drilled shafts in cohesive geomaterials that was conducted using the finite element method. Based on this analysis, new predictive procedures were developed for estimating both resistance and load-settlement behavior of drilled shafts in cohesive (Category 1 and 2) geomaterials. Parameters were verified, and in some cases optimized, by comparing results of the finite element analyses directly with selected load test data from the data base for argillaceous geomaterials. The results of this step apply to Category 1 and 2 geomaterials.

6. A method for estimating the resistance and load-settlement behavior of drilled shafts in Category 3 intermediate geomaterials was adapted from a method developed by others, partially from field data gathered for this study (Step 7, below).

7. Full-scale loading tests on instrumented drilled shafts were conducted or observed in Category 1 and 3 geomaterials. These tests included a shallow drilled shaft in clay-shale (Dallas, Texas); a deep drilled shaft in clay-shale (College Station, Texas); a deep drilled shaft in sandy shale (Owensboro, Kentucky); a deep drilled shaft in completely decomposed rock (Coweta County, Georgia); and a deep drilled shaft in glacial till (Boston, Massachusetts). Two other tests conducted by others outside of the scope of this research were also documented in detail.

8. The design procedures were tested against the loading tests referenced in Step 7 and were modified slightly where necessary to provide better predictions.

9. A design procedure for ultimate side resistance based on the analogy between a small-diameter plug and a drilled shaft was also investigated. Grout plugs were installed at each of the test sites referenced above, except for the site in Boston, and at other sites at which drilled shaft loading tests had been conducted. The results of these tests were compared with measured unit side resistances in order to evaluate the accuracy of this direct method of estimating unit load transfer.

10. Final conclusions were drawn, considering the results of Steps 1 through 9, and recommendations are provided in this report.

DOCUMENTATION OF DETAILS

Details of the literature search, data base study, finite element analyses, and field loading tests are not provided in the main text of this report. They can be found in Appendices A through D, which are bound separately, referenced as follows:

- Appendix A. *Load Transfer Between Drilled Shafts and Intermediate Geomaterials: A Literature Review.*

- Appendix B. *Evaluation of Skin Friction Design Methods for Drilled Shafts Socketed into Intermediate Geomaterials.*

- Appendix C. *Finite Element Analyses and Field Tests for Drilled Shafts in Soft, Argillaceous Rock.*

- Appendix D. *Results of Deep Loading Test in Glacial Till - Boston Central Artery Project.*

Separate reports describe the field plug tests. These reports, summarized briefly in chapter 7 of the present report, are as follows:

- C. Dunkelberger, F. C. Townsend, D. Bloomquist, and B. Johnsen, "Pullout Tests on Drilled Shafts, Dallas Site," *FHWA Contract DTFH61-92-01211*, Federal Highway Administration, Turner-Fairbank Highway Research Center, McLean, VA, June, 1992.

- B. Johnsen, F. C. Townsend, D. Bloomquist, and C. Dunkelberger, "Pullout Tests on Drilled Shafts, Coweta County, Georgia Site," *FHWA Contract DTFH61-92-01211*, Federal Highway Administration, Turner-Fairbank Highway Research Center, McLean, VA, October, 1992.

- F. C. Townsend, P. Hirshman-Cox, D. K. Crapps, and J. W. Goodwin, "Pullout and Osterberg Load Cell Tests on Drilled Shafts - Owensboro Bridge," *FHWA Contract DTFH61-92-01211*, Federal Highway Administration, Turner-Fairbank Highway Research Center, McLean, VA, May, 1993.

- F. C Townsend and M. W. O'Neill, "Pullout and Load Tests on a Drilled Shaft - National Geotechnical Site - Texas A and M," *Progress Report, FHWA Contract DTFH61-91-Z-00041*, Federal Highway Administration, Turner-Fairbank Highway Research Center, McLean, VA, June, 1994.

ORGANIZATION OF REPORT

The main body of this report is organized in the following way:

- Chapter 2, which follows this introduction, reviews significant phenomena that impact design identified from the literature review and summarizes existing methods for analysis and design

- Chapter 3 describes the data base and reviews the data base study.

- Chapter 4 describes the proposed new design models.

- Chapter 5 describes the geomaterial and borehole conditions for the field tests.

- Chapter 6 describes the field loading tests and compares predicted and measured performance in IGM's.

- Chapter 7 addresses small-scale plug tests as methods for site investigations.

- Chapter 8 provides conclusions and recommendations.

References are provided following chapter 8.

Chapters 2 and 3 provide details of phenomena that have been found in earlier studies by others to have effects on drilled shaft performance in hard soils, soft rocks, and very dense granular soils. These studies comprise the general background for the new design methods that are proposed in chapter 4. It is recommended that these chapters be thoroughly reviewed. However, the reader who wishes to proceed directly to the description of the proposed new design methods may turn to chapter 4.

CHAPTER 2: LITERATURE SURVEY AND VISITS

GENERAL

Rational design methods for drilled shafts in intermediate geomaterials (IGM's) require determination of both their ultimate resistances and expected settlements. A number of current design methods were identified in this study, in most of which the maximum unit side shear resistance (f_{max}) and the maximum unit base resistance (q_{max}) are predicted using empirical correlations between the results of field loading tests in the geographical area of the agency's or individual consultant's practice and:

- s_u (undrained shear strength) or q_u (unconfined compression strength) from rock cores (Category 1 and 2 IGM's).
- Rock Quality Designation (RQD) (Category 1 and 2 IGM's).
- Standard Penetration Tests (SPT) (Category 3 IGM's).

RQD is defined in equation 1:

$$\mathbf{RQD} = \frac{\sum \textbf{lengths of core fragments of IGM} \geq \textbf{100 mm long}}{\textbf{total length cored}} \tag{1}$$

Although the settlement of foundations in IGM's can be significant, settlement is often ignored in design calculations. When settlement calculations are judged to be necessary, load-settlement response in the range of working load is determined from rules developed from parametric finite element solutions or analytical solutions, many of which, in turn, employ empirical correlations with simple geomaterial indexes (such as q_u and RQD) to assess the elasticity characteristics of the rock and ultimate side and base resistances.

More advanced design methods, applied in public transportation and private practice in Canada and Australia, include additional parameters, such as:

- Interface roughness and dilatancy characteristics.
- Cohesion and internal friction characteristics of the geomaterial mass and the interface.
- Mass elastic moduli of the geomaterial.
- Size and frequency of discontinuities and soil seams, if any, in the geomaterial.
- Young's modulus of the drilled shaft concrete.
- Shaft geometry.
- Initial hydrostatic concrete pressure.

"Mass" properties of geomaterials are properties for the geomaterial mass as a whole, including effects of seams and discontinuities. Mass properties are not equivalent to properties measured by tests on intact geomaterial cores, which yield the properties of the geomaterial between the seams and discontinuities. Intact core samples are normally

much stronger and stiffer than the geomaterial mass, making it necessary to modify the values obtained in core tests to apply to the geomaterial mass.

EXAMPLES OF DESIGN METHODS FOR IGM'S

Several selected design methods are described. These methods, which were all developed from the perspective that the geomaterial is a soft rock or dense, residual granular material, form the conceptual foundation for the new design model that is recommended for Category 1 and 2 IGM's in chapter 4. In the case of Category 3 IGM's, an existing method reviewed in this chapter is recommended directly for design use in transportation structures, with some adaptation based on the research reported here. Existing methods require the evaluation of critical geomaterial parameters, often different ones in each method, and the summary descriptions of the various methods in this chapter will serve to indicate to the reader which geomaterial parameters require evaluation in the subsurface exploration and testing program.

Some of the methods involve both the computation of capacity, or resistance, and of settlement. The methods have some similarities and some differences, and some are even contradictory. The reader is urged to consult the original publication referenced in this report before applying any method in a design context in order to obtain the full benefit of the commentary and interpretations by the developers of the method.

Drilled shafts are often installed through soil, or overburden material, into IGM's, as illustrated in figure 1. The design methods considered in this report do not address the side resistance developed in the overburden materials or the effect thereof upon settlement. Appropriate approximations of the response of the overburden soils to load can be obtained by consulting chapter 11 of reference 2. Side shear reactions in the soil overburden generally reduce the amount of load applied to the head of the shaft that reaches the elevation of the top of the IGM. The load on the shaft considered here is the load that is present at the elevation of the top of the IGM. It is usually conservative to ignore the effects of the overburden soils, as is suggested in figure 1, and to assume that the load applied to the shaft is equivalent to the load present at the top of the IGM.

Design Method of Williams *et al.*

Williams *et al.* developed a design method based on observations of axial loading tests of drilled shafts and shaft segments in Melbourne mudstone in Victoria, Australia, and upon elastic pile-soil interaction analyses.[3] The method is applied through the concept of normalized elastic and inelastic side shear and base resistances to predict the load-settlement response of soft rock sockets. This method, which allows for the computation of both settlement and resistance, is most appropriate for Category 2 IGM's and is described here to provide an example of an advanced semi-empirical method that is used in routine practice in Australia, both in Victoria and New South Wales. The writers[1]

---

[1] The term "writers" is used in this report to signify the authors of the report or paper being described. The term "authors" is used to indicate the authors of this report.

employed the elastic solution of a pile in a semi-infinite half space to predict the total elastic load, Q_e, at a given target settlement, as:

$$Q_e = \frac{w_t E_m D}{I},$$ (2)

in which w_t = target settlement of the shaft head, E_m = average mass modulus of elasticity of the IGM along the drilled shaft , D = shaft diameter, and I = an elastic influence factor, based on the geometry of the shaft, determined from analytical procedures for elastic behavior and shown in figure 3. In figure 3, E_c is the composite Young's modulus of elasticity of the drilled shaft concrete and reinforcing steel.

The percentage of Q_e that is transferred to the base, defined as Q_{be}, is then determined by reference to figure 4, also based on analytical procedures for elastic behavior. The portion of Q_e carried in side shear, Q_{se}, is then equal to Q_e - Q_{be}. The "elastic" unit side shear, f_e, and the "elastic" end bearing, q_e, are then determined as:

$$f_e = \frac{Q_{se}}{\pi L D}, \text{ and}$$ (3)

$$q_e = \frac{4 Q_{be}}{\pi D^2}.$$ (4)

The value of f_{max} (f at failure) is then determined, for example, using the relation suggested by the writers in figure 5 for soft rock without open discontinuities or borehole wall disturbance, in which.

$$f_{max} = \alpha \, q_u,$$ (5)

where q_u is the unconfined compression strength of representative, intact IGM cores. Note that $\alpha \neq \bar{\alpha}$ in figure 2. If the IGM has soft soil seams within the matrix of the harder material constituting the cores, f_{max} is determined from figures 5 and 6 using:

$$f_{max} = \alpha \, \beta \, q_u,$$ (6)

in which E_m = Young's modulus of elasticity of the rock mass, including the effects of seams, and E_i = Young's modulus of elasticity measured from the intact rock cores. E_m/E_i in figure 6 can be estimated from observation of high-quality IGM cores by using:
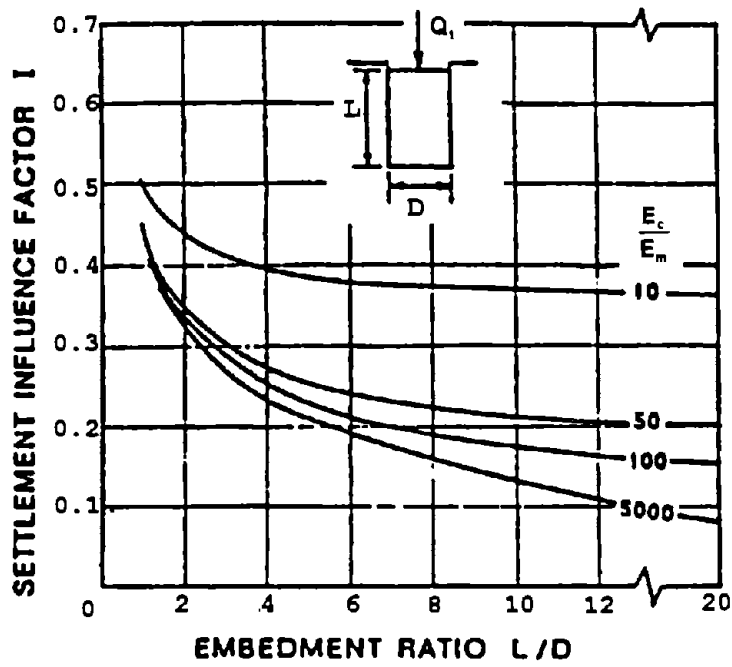
Figure 3. Influence Factor I.[3]
(Reproduced by permission of A. A. Balkema, Rotterdam, Netherlands)
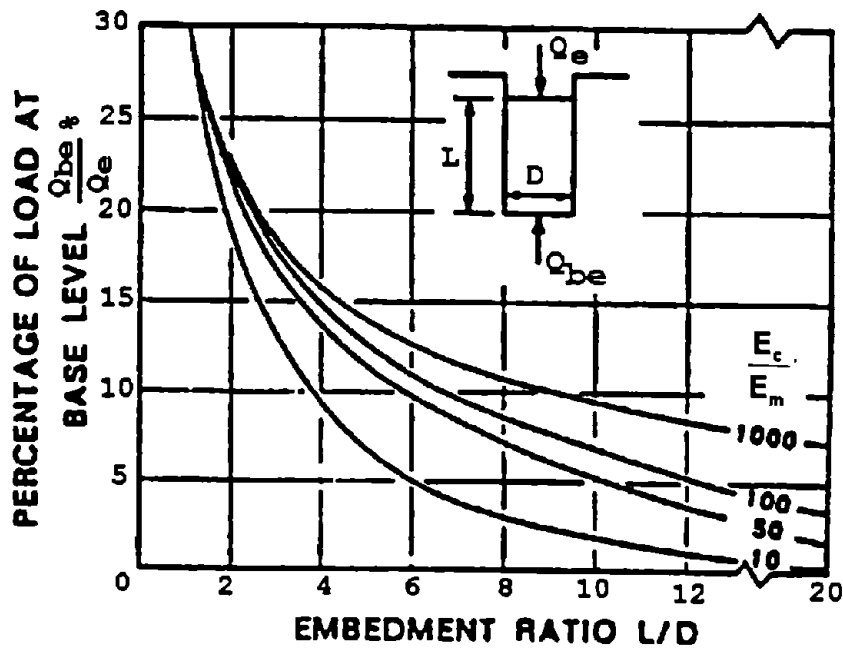
Figure 4. Q_{be} / Q_e [3]
(Reproduced by permission of A. A. Balkema, Rotterdam, Netherlands)
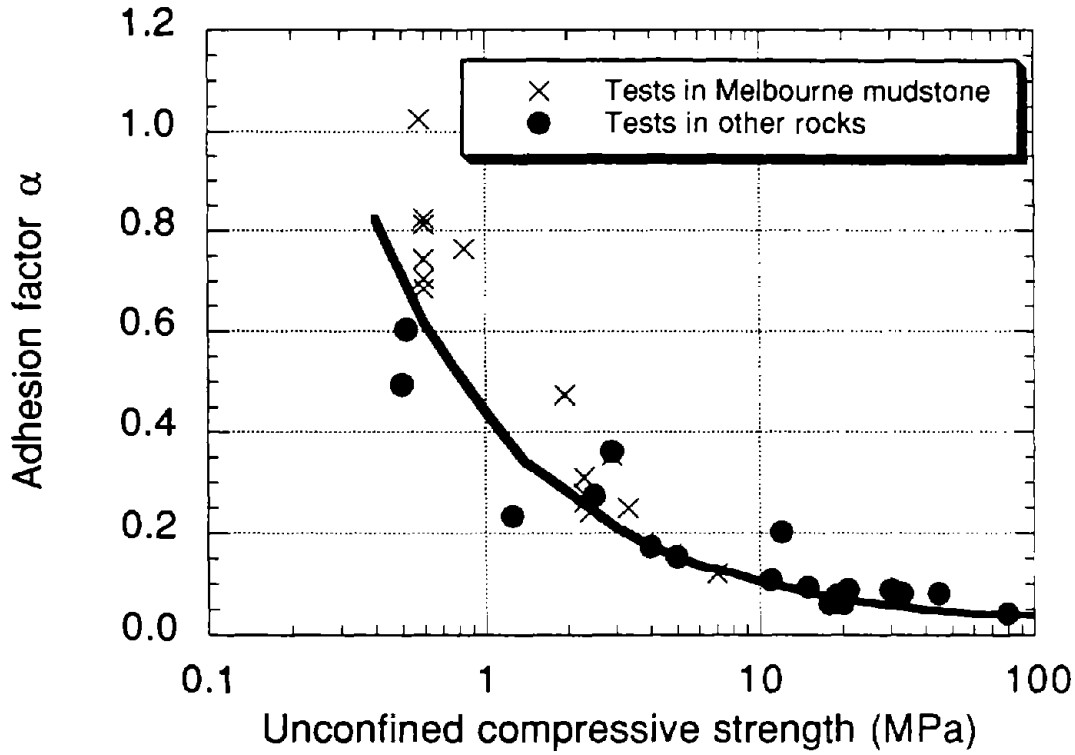
Figure 5. α vs. q_u.[3]
(Reproduced by permission of A. A. Balkema, Rotterdam, Netherlands)
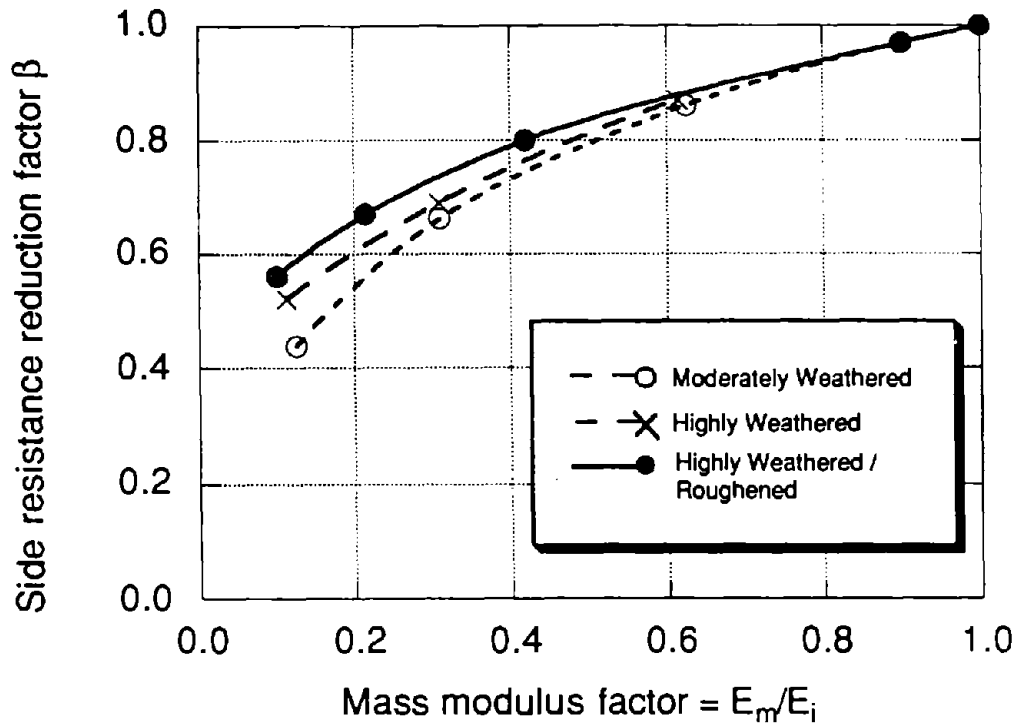
Figure 6. β vs. mass factor.[3]
(Reproduced by permission of A. A. Balkema, Rotterdam, Netherlands)

$$\frac{E_m}{E_i} = \frac{L_c}{\left[\frac{E_i}{E_s}\right]\sum t_s + \sum t_i} \quad , \tag{7}$$

where L_c is the length of geomaterial cored, E_s = estimated Young's modulus of elasticity of the material in the seams, t_s = thickness of each seam, and t_i = thickness of each segment of intact IGM. If the IGM is strongly layered (as distinguished from possessing thin seams), f_{max} for each ith layer, denoted f_{maxi}, is computed from equation 5 or 6, as appropriate, using properties for layer i, with thickness L_i, and a weighted average is computed as:

$$f_{max} = \frac{\sum f_{maxi} L_i}{L} \tag{8}$$

The elastic side shear ratio, f_e/f_{max}, is then calculated.

Actual load-settlement behavior will not be elastic. The deviation from elastic behavior is quantified by using the normalized graph shown in figure 7, which was derived with empirical evidence from full-scale loading tests on rough-walled sockets in Melbourne mudstone. Factors termed f_e and f_p are shown in that figure. Factor f_p is the loss of unit shaft resistance that occurs due to plastic yielding for the value of settlement, w_t, selected for equation 2. Therefore, the shaft resistance Q_s corresponding to the target settlement w_t is given by:

$$Q_s = (f_e - f_p)\, \pi\, L\, D \quad . \tag{9}$$

The ultimate unit base resistance, q_1, is defined as the net bearing stress corresponding to a settlement of 0.01 D. For cohesive IGM free of discontinuities and seams:

$$q_1 = N_s\, q_u \quad , \tag{10}$$

in which N_s is given as a function of L/D in figure 8.

Base resistance is also decreased through plastic losses, so q_e must be reduced by an amount q_p according to figure 9. Finally, the base resistance for the selected value of w_t is:

$$Q_b = (q_e - q_p)\, \frac{\pi\, D^2}{4} \quad , \text{ and} \tag{11}$$

$$Q_t = Q_s \text{ (equation 9)} + Q_b \quad . \tag{12}$$
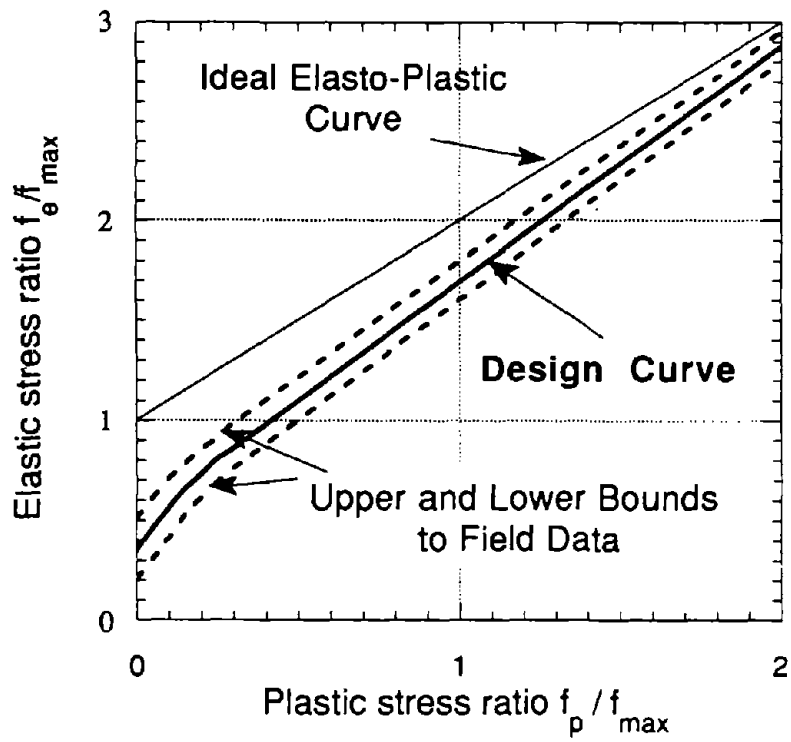
Figure 7. Design curve for side resistance. [3]
(Reproduced by permission of A. A. Balkema, Rotterdam, Netherlands)
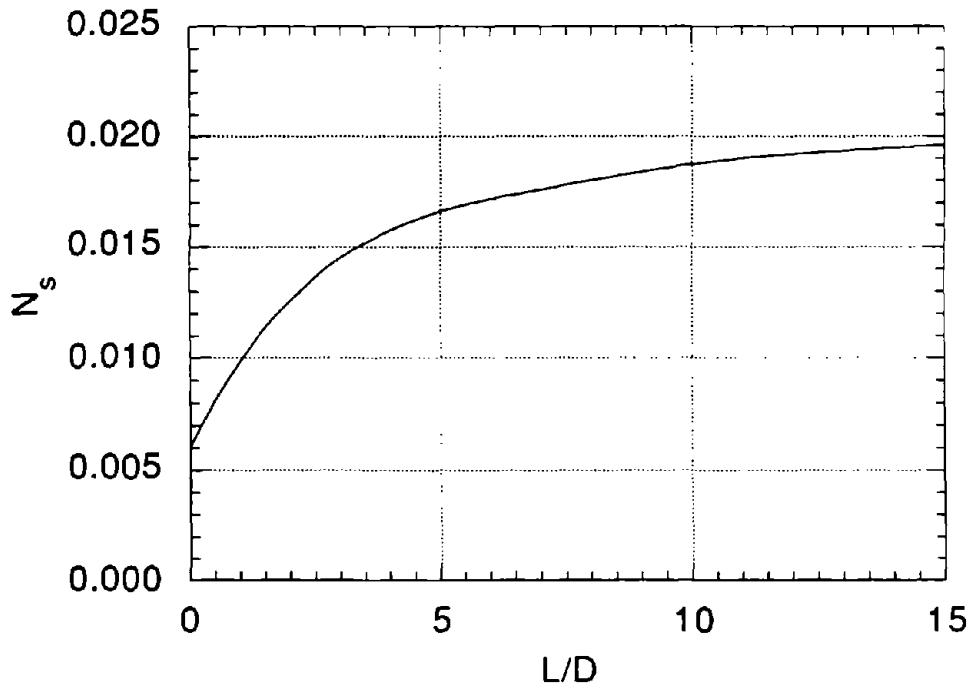
Figure 8. Base bearing capacity factor N_s. [3]
(Reproduced by permission of A. A. Balkema, Rotterdam, Netherlands)
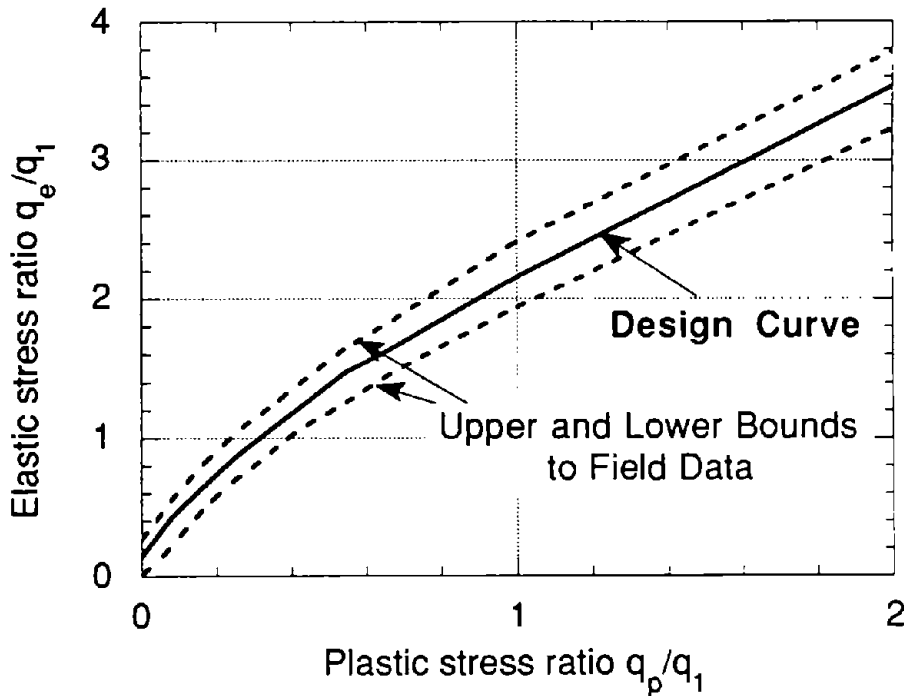
Figure 9. Design curve for base resistance. [3]
(Reproduced by permission of A. A. Balkema, Rotterdam, Netherlands)

In equation 11, Q_t is the relaxed (actual) load at the top of the shaft corresponding to the target settlement w_t. Other values of w_t may be chosen and the procedure repeated to synthesize a load-settlement curve

At this point, $Q_s/\pi DL$ and $4Q_b/\pi D^2$ should be compared to f_{max} and $q_{max} = q_1$ to ensure that adequate factors of safety exist in each component of resistance. The authors suggest that if the applied load Q_t is a factored load, partial factors of safety of about 1.4 and 2.0 are appropriate for side and base resistance when the geomaterial properties are well defined, unless the shaft supports only side resistance, in which case the partial factor of safety for side resistance should be at least 2.0.

Design Method of Kodikara et al.

Kodikara et al. extended the method of Williams et al. by deriving α factors for Category 2 IGM's and stronger soft rock that incorporate explicitly, through a rational mathematical model, the effect of roughness at the shaft-IGM interface, in addition to the strength of the IGM.[4] The method takes account of dilatancy at the interface, assuming that dilatancy occurs at constant radial stiffness. The phenomenon of dilatancy is discussed in more detail in the description of the method of Carter and Kulhawy later in

14

this chapter. Results from mathematical model calculations were confirmed by large-scale direct shear tests conducted on concrete-soft rock interfaces with varying degrees of controlled roughness under drained, constant normal stiffness conditions. Since the method assumes constant normal interface stiffness, due to the elastic restraint of the soft rock adjacent to the dilating rough interface, it is necessary to characterize such stiffness by estimating the Young's modulus of the rock mass (E_m). The magnitude of radial strain, and therefore radial stiffness, produced by a dilating interface is a function of shaft diameter for any given roughness pattern, so that a shaft diameter is implicit in the results. That diameter can be taken to be 0.5 m (1.6 ft) through 2.0 m (6.6 ft) for the values of α given here. In theory, the results will be conservative for smaller diameters and unconservative for larger diameters.

With this method, the roughness pattern of the excavated interface must be estimated and characterized as "smooth," "medium," or "rough" according to the roughness characteristics in table 1. The roughness patterns described in table 1 apply to boreholes that are roughened naturally by the routine drilling process, not to boreholes in which grooves or shear keys are cut by a contractor to enhance side resistance. Roughness is modeled assuming that asperity patterns in the sides of the borehole are not regular, or harmonic, which is typical of the natural roughness of drilled shafts in the Melbourne mudstone.

Table 1 Characterization of borehole roughness.[4]

Parameter	Range of Values for Sockets in Melbourne Mudstone		
	Smooth	Medium	Rough
i_m (°)	10 - 12	12 - 17	17 - 30
i_{sd} (°)	2 - 4	4 - 6	6 - 8
h_m (mm)	1 - 4	4 - 20	20 - 80
$\dfrac{h_{sd}}{h_m}$	0.35		
D (mm)	500 - 2000		
q_u (bars)	5 - 100		
	(s_u = 2.5 - 50 bars)		
E_{mass} (MPa)	50 - 3000		

The factor i_m in table 1 is the mean value of the angle between the face of the asperity and the vertical. i_{sd} is the standard deviation of i_m, h_m is the mean double-amplitude height of the asperities, and h_{sd} is the standard deviation of h_m. Statistical distributions of the asperity angles and heights are considered Gaussian in this method.

15

The factor α is then estimated from graphs such as those given in figure 10, using the estimated IGM modulus, E; the unconfined compression strength of the IGM, q_u; and the roughness classification and the initial radial pressure on the interface, σ_{no}, which, according to the writers, can be taken as the estimated fluid pressure produced by the concrete. E/q_u is properly the ratio of the respective values for the IGM mass; however, the experience of the authors and the developers of other design methods suggests that mass values for both E and q_u are reduced from their intact values by about the same amount if seams and discontinuities exist in the geomaterial, so that for design purposes, these can be taken as the values obtained from intact cores.

Figure 10 was developed for $E/q_u = 300$, which is appropriate for many IGM's; however, figures for other values of E/q_u are given by the writers in reference 4. As an approximation, the values for α are reduced to approximately 0.7 times the values shown in figure 10 when E/q_u is reduced to 100. If soil seams are inferred to be present from the sample cores, equations 6 and 7 and figure 6 should be employed in evaluating f_{max}. Otherwise, equation 5 is used.
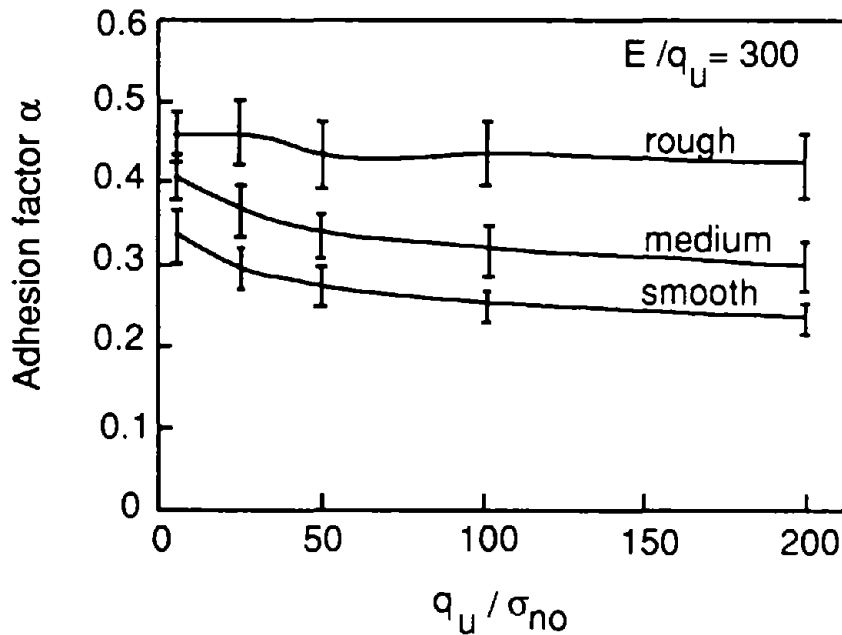
Figure 10. α vs. borehole roughness.[4]

This method does not address either settlement or base resistance, so that other methods need to be used if these parameters are to be evaluated by the designer.

16

Design Method of Horvath *et al.*

Horvath *et al.* proposed a method for evaluating α that is applicable for artificially roughened borehole walls, based on the analysis of loading tests in cohesive IGM's and harder rock in southern Ontario.[5] In this method:

$$\alpha = 0.8RF^{0.45} = 0.8\left[\frac{\Delta r}{r}\left(\frac{L_t}{L_s}\right)\right]^{0.45} \tag{13}$$

The terms in equation 13 are defined in figure 11.
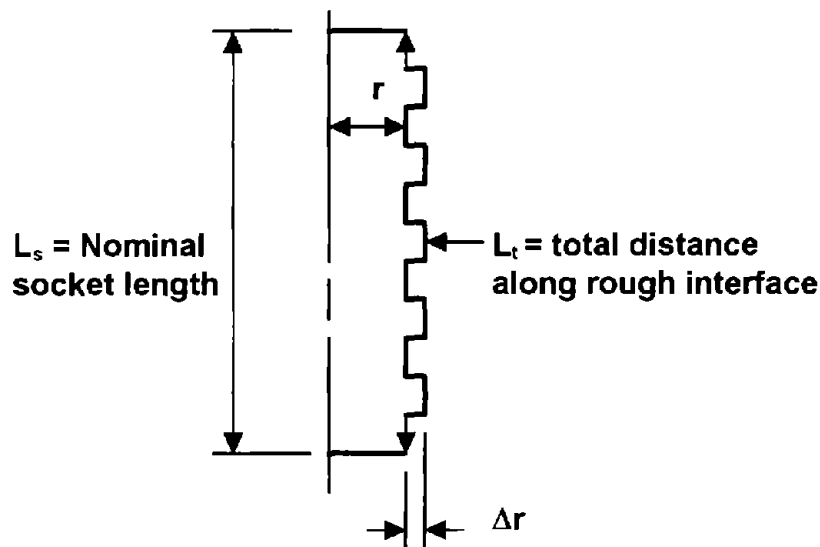
Figure 11. Definition of terms in equation 13.

As with the method of Kodikara *et al.*, this method is not intended to address settlement or base resistance.

Design Method of Rowe and Armitage

Rowe and Armitage developed a comprehensive design method that can be used in cohesive IGM's for evaluating both side and base resistance and for conducting detailed settlement analyses.[6] The method for computing settlement allows for the implicit consideration of both dilation at the concrete-IGM interface and progressive slip along the interface, so that the method can simulate nonlinear behavior. Maximum unit side and

17

base resistances are evaluated empirically, however. The specific resistance computation for f_{max} is:

$$f_{max}(MPa) = \left[1 - S + S\left(\frac{f_s(MPa)}{\lambda\sqrt{q_u(MPa)}}\right)\right]\lambda\sqrt{q_u(MPa)} \; , \tag{14}$$

where $S = (\Sigma\text{ seam thicknesses})/L_s$, f_s = maximum unit side resistance in the seam material (which is equal to 0.5 s_u or 0.25 q_u of the seam material), $\lambda = 0.60$ for clean boreholes with roughness characterized by grooves or undulations greater than 10 mm deep, greater than 10 mm wide, and spaced 50 to 200 mm on centers, or 0.45 for other roughness conditions.

Because of the variability of IGM properties around a particular site, Rowe and Armitage recommend that f_{max} be reduced to f_{maxd}, where

$$f_{maxd} = 0.5 \text{ to } 0.7\ f_{max} \tag{15}$$

The maximum base resistance is computed from:

$$q_{max} = 2.5\ q_u \; ; \tag{16}$$

however, the maximum (working) design value for base resistance q_{maxd} is given by:

$$q_{maxd} = q_u \tag{17}$$

Equations 16 and 17 apply only to soft rock that is free of seams and voids beneath the base of the shaft. If horizontal seams or voids exist beneath the base, a more appropriate means of computing q_{max} is the base resistance equation from the *Canadian Foundation Manual* (given subsequently).

It remains to determine the distribution of shaft and base resistance to ensure that neither the design values nor the maximum values of unit base resistance (equations 17 and 16, respectively) are exceeded. This is accomplished as follows. Reference is made to figure 1 and figure 12.

- Estimate a relative shaft penetration, $(L/D)_{max}$, into the intermediate geomaterial assuming that all of the applied design load Q_t is carried in side resistance. That is, let

$$\left[\frac{L}{D}\right]_{max} = \frac{Q_t}{\pi D^2 f_{maxd}} \tag{18}$$

- Estimate the average mass Young's modulus E_m of the IGM over distance L, using equation 7 if soft soil seams are encountered within the IGM. Estimate also the

18

composite Young's modulus of the drilled shaft, E_c. Finally, determine whether the mass Young's modulus of the IGM immediately beneath the base, E_b, is significantly higher or lower than that along the sides. If so, the designer should refer to the original paper of Rowe and Armitage for guidance. If E_m/E_b can be assumed for design purposes to be 1, continue.

- Referring to figure 12, construct a straight line between $Q_b/Q_t = 0$ percent and the selected value of $(L/D)_{max}$ and $Q_b/Q_t = 100$ percent and $L/D = 0$.

- Select a target settlement value for the top of the "socket" in the IGM, w_t, and then compute a settlement influence factor I

$$ I = \frac{w_t E_m D}{Q_t} $$

(19)
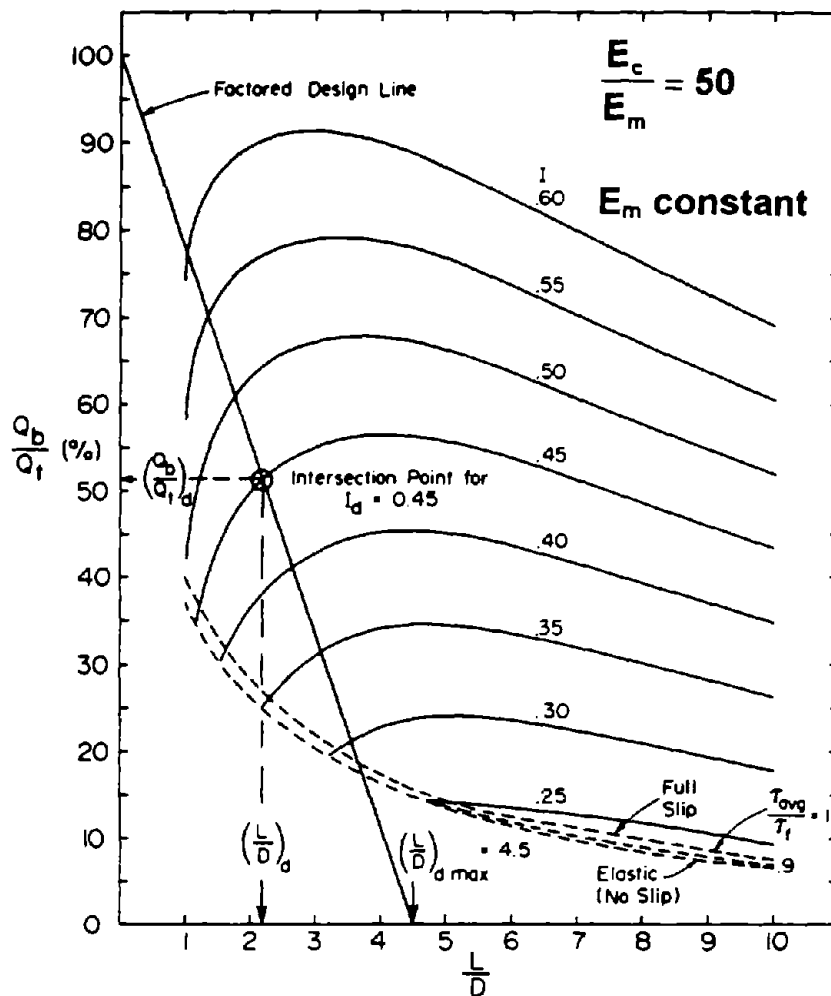
Figure 12. Design chart for Rowe and Armitage's method.[6]
(Reproduced by permission of Canadian National Research Council, Ottawa)

19

- Where the line constructed in the preceding step crosses the curve with the value of I computed in equation 19, read horizontally across to find the ratio Q_b/Q_t, and read down to find the minimum value of L/D that is required to produce this ratio of Q_b/Q_t. If an intersection is found, it is the design value for L/D for the socket.

- If no intersection is found, it may not be possible to design the drilled shaft for the given conditions, or the behavior may be entirely elastic. To determine whether the behavior is elastic, consult figure 3. Draw a horizontal line from the computed value of I for the curve representing the value of E_c/E_m for the shaft under consideration.

- If there is an intersection in this figure, draw a line vertically downward and read the required value of L/D. This will then be the necessary value for design. Then, consult figure 4 to determine the ratio Q_b/Q_t. If no intersection can be found in figure 3, the shaft cannot be designed for the given conditions, so a new (larger) diameter D should be selected and the process repeated.

- Ensure that the base resistance, both under load Q_t using both the nominal value for shaft resistance inferred from the solution and at the shaft resistance corresponding to side shear failure, does not cause excessive base settlement. This is done by satisfying both equations 20 and 21.

$$q_b = 4 \frac{Q_b}{\pi D^2} \le q_u \quad . \tag{20}$$

$$Q_t - 0.43 f_{max\,d}\, \pi\, D\, L \le q_{max}\, A_b \quad , \tag{21}$$

where A_b = cross-sectional area of the cylindrical shaft. Equation 21 operates with a partial factor of safety of approximately 3.33 on the nominal computed value for f_{max} $(0.43 \times 0.7)^{-1}$.

It is clear that the above calculations not only ensure safety against excessive settlement but also provide an estimate of settlement, w_t.

Canadian Foundation Manual Method

The *Canadian Foundation Manual* method, as used here, concerns only the estimation of base resistance.[7] Maximum unit base resistance q_{max} is expressed for rock formations that are primarily stratified horizontally. The design equation is also assumed to apply to IGM's and is given by:

$$q_{max} = 3 \Delta K_{sp}\, [q_u(\text{beneath base})] \quad , \tag{22}$$

where:

$$\Delta = \text{depth factor} = 1 + 0.4\,\frac{L}{D} \le 3.4 \ , \quad \text{and} \tag{23}$$

$$K_{sp} = \frac{3 + \dfrac{s_d}{D}}{10\left(1 + 300\,\dfrac{t_d}{s_d}\right)^{0.5}} \ , \tag{24}$$

in which:

s_d = the vertical spacing of horizontal or near-horizontal discontinuities beneath the base, t_d = thickness of the discontinuities, and the application of equation 24 is limited to $0.05 < s_d/D < 2$, $t_d/D < 0.02$, and $D > 0.3$ m.

Method of Carter and Kulhawy

Carter and Kulhawy provide closed-form solutions for drilled shafts socketed into rock that can presumably be used to predict the load versus settlement for Category 1 or 2 IGM's at the high end of the compressive strength range for IGM's.[8] Separate solutions are given for response in the elastic range (prior to slip or initial shear failure at the concrete-rock interface) and in the range beyond the elastic range. Separate solutions are also given for various loading conditions, including compression loading of a full socket (i.e., a socket that develops both side and base resistance).

This method also cites procedures for computing q_{max} in jointed rock, developed earlier by the junior writer, in which the joints are vertical. If the rock has relatively uniform mass strength below the base (e.g., there are no soil or softer rock layers below the base), three failure conditions are envisioned:

- Vertical joints are open and spaced horizontally at a distance less than shaft diameter, D. Here:

$$q_{max} = q_u \ (\textbf{rock mass}) \tag{25}$$

- Vertical joints are closed and spaced horizontally at a distance less than the shaft diameter, D. Here, Bell's bearing capacity theory for shear wedge failure is used, which assumes that no friction is developed along the joints. For practical approximations, the gross bearing capacity can be computed as:

$$q_{max}(\text{gross}) = (1 + N_q/N_c)\,c\,N_c + 0.3\,D\,\gamma\,N_\gamma + (1 + \tan\phi)\,\gamma\,L\,N_q \ , \tag{26}$$

in which N_c, N_γ, and N_q are Bell's bearing capacity factors, c and ϕ are the cohesion and angle of internal friction of the rock mass, and γ is the unit weight of the rock mass (buoyant if the rock is beneath the phreatic surface). It is noted that the effect of

21

confinement at the base of the shaft provided by overburden material is not included in
equation 26 by the authors. The bearing capacity factors are evaluated in figure 13.
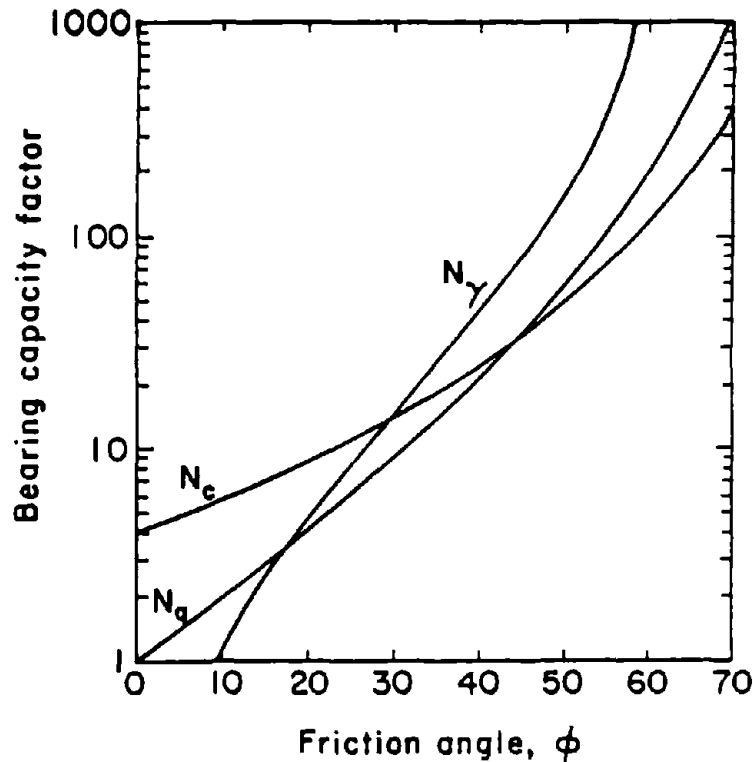
Figure 13. Bearing capacity factors for Bell's theory.[8]
(Copyright © 1988. Reproduced by permission of Electric Power Research Institute
[EPRI], Palo Alto, CA)

- Vertical joints are open or closed and spaced horizontally at a distance greater than the
  shaft diameter, D. In this case, vertical splitting of the rock beneath the base of the
  shaft will occur, and failure will be governed by that condition. The appropriate
  equation is:

$$q_{max} = J \, c \, N_{cr} \qquad (27)$$

N_{cr} is a bearing capacity factor that is based on the horizontal spacing of the rock joints
S relative to the base diameter D and the angle of internal friction of the rock mass,
given in figure 14. J is a correction factor for spacing of horizontal joints, if they exist,
with a vertical spacing of H, given in figure 15. Finally, c is the cohesion of the rock
mass.

Carter and Kulhawy also give solutions for q_{max} in sloping jointed rock in reference 8.
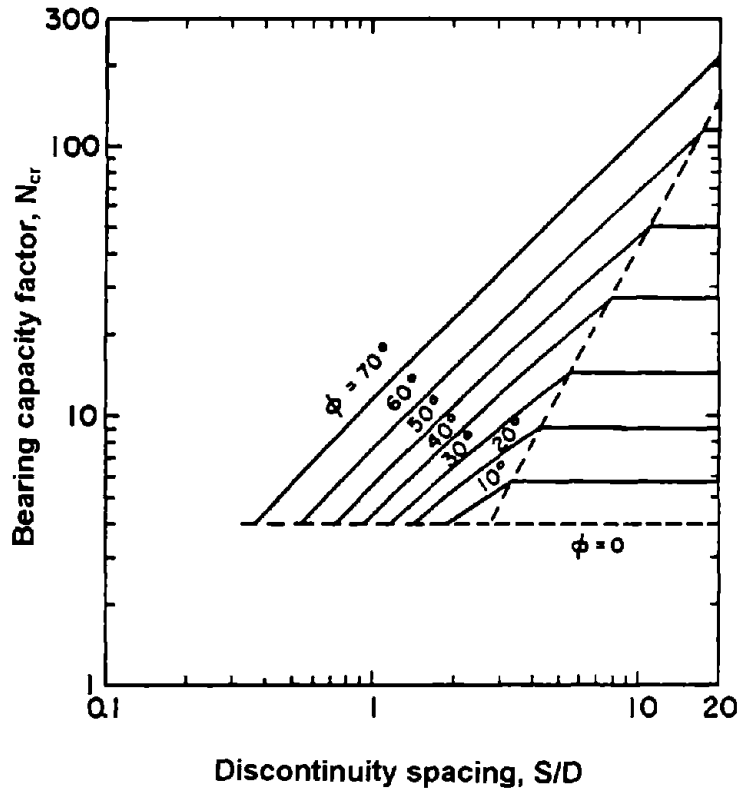
Figure 14. N_{cr} vs. S/D.[8]
(Copyright © 1988. Reproduced by permission of EPRI, Palo Alto, CA)
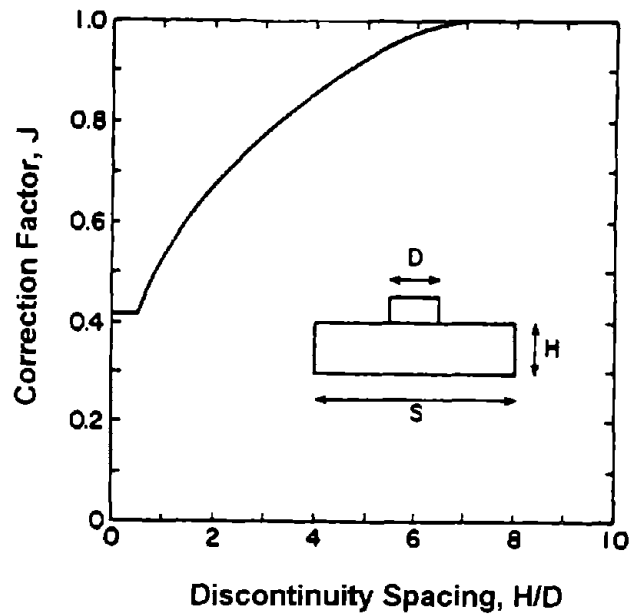
Figure 15. J vs. rock discontinuity spacing.[8]
(Copyright © 1988. Reproduced by permission of EPRI, Palo Alto, CA)

Note is made that q_{max} as used here is a gross bearing capacity for which the weight of the shaft must be considered part of the load. If q_{max} is to represent the net bearing capacity, for which the weight of the shaft is not added to the load, N_q from figure 13 must be reduced by subtracting 1 from the value read from the figure. In all of the equations in this method, c and ϕ are rock mass properties, not properties measured from tests on rock cores (intact rock). Carter and Kulhawy suggest that the value of ϕ for the rock mass be taken to be about one-half of the value measured from the intact rock, if ϕ for the intact rock is measured through direct shear or triaxial shear testing on rock cores in the laboratory. Values for ϕ for intact rock are dependent on the crystalline structure of the rock, microdiscontinuities, and other factors, and are therefore difficult to generalize. Conservatively, ϕ for the rock mass can be taken as zero in the calculation of base resistance. Equation 28 is used to estimate the equivalent q_u of the rock mass.

$$q_u(mass) = \alpha_E \, q_u(intact) \qquad (28)$$

Factor α_E can be obtained accurately if the RQD, percent core loss, Young's modulus of the intact rock, and normal stiffness of the material in the joints are known. Appropriate graphs are given by Carter and Kulhawy to evaluate α_E for the case when such detailed information is available for the rock. However, a simple approximation for most rock is to take $\alpha_E = 0.1$ for RQD equal to or less than 70 percent, $\alpha_E = 0.6$ for RQD = 100 percent, and to assume a linear variation of α_E between RQD of 70 and 100 percent.

Once $\phi(mass)$ and $q_u(mass)$ are evaluated, $c(mass)$ can then be computed from:

$$c(mass) = \frac{q_u(mass)}{2 \tan \left[45° + \phi(mass)/2 \right]} \qquad (29)$$

Carter and Kulhawy also give closed-form solutions for load-movement relationships for five cases of rock-socketed drilled shafts:

- Complete socket (combined base and side resistance) loaded in compression.
- Socket with side resistance only (implying a void beneath the base) loaded in compression.
- Socket with side resistance only loaded in uplift at the head of the socket.
- Socket with side resistance only loaded in uplift at the base of the socket.
- Socket with side resistance only loaded in uplift at the base of the socket by jacking upward on the base with a compression reaction against the rock at the bottom of the void.

Commentary is provided here only on the first condition, which is the condition that most often concerns transportation geotechnical engineers. However, Carter and Kulhawy note through mathematical modeling that each of the different loading conditions can produce different resistances and load-settlement characteristics. The implication of this statement

is primarily that of caution in applying the results of one loading condition in a loading test to that of another condition for design.

The load-settlement curve at the head of the socket is presumed to have the shape shown in figure 16. In the initial part of the curve, both side interface and base response is linear, and there has been no debonding of the concrete in the shaft from the rock walls. At point A, slip begins to occur between the concrete and the rock at the sides of the socket at some point along the shaft, and slip then progresses along the shaft until point B is reached. In this sense, slip can be viewed as debonding of the shaft concrete from the rock. Beyond point B, base response remains elastic, while side shear response is frictional-dilative, rather than cohesive, as is the case for the elastic region of loading. At some point beyond point B, collapse (fracturing) of the rock at the base can occur (i.e., q_{max} can be developed) and/or displacement-softening behavior will occur at the concrete-rock interface as the asperities along the interface (described subsequently) are sheared, which will cause the curve to flatten or the resistance to decrease with increasing settlement. This ultimate failure condition is not considered in this method.
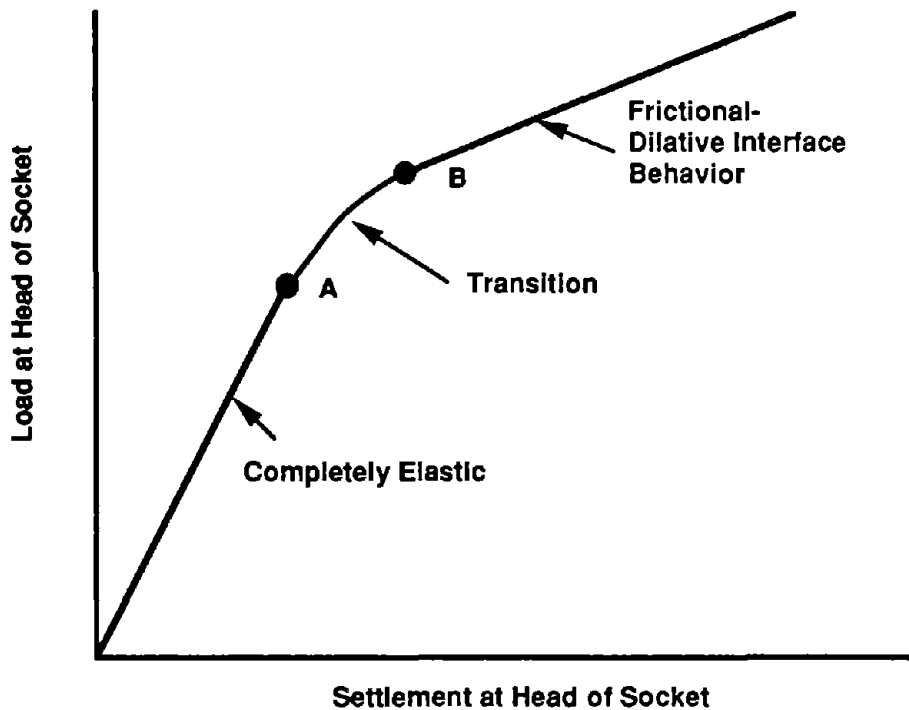
Figure 16. Conceptual load-settlement curve for rock socket.

25

Within the elastic range, the settlement at the top of the socket w_t can be related to the load at the top of the socket Q_t by using equation 30, which is shown here for the case where the elastic stiffness of the rock mass below the base is equal to the elastic stiffness along the sides of the shaft. Other, more general, conditions are described in reference 8.

$$w_t = \left[\frac{2Q_t}{DG_m}\right] \frac{1 + \left(\frac{4}{1-v}\right)\frac{1}{\pi\lambda}\left(\frac{2L}{D}\right)\left(\frac{\tanh(\mu L)}{\mu L}\right)}{\left(\frac{4}{1-v}\right) + \left(\frac{2\pi}{\zeta}\right)\left(\frac{2L}{D}\right)\left(\frac{\tanh(\mu L)}{\mu L}\right)} \tag{30}$$

The value of the load carried by the base under elastic conditions is:

$$Q_b = \frac{Q_t\left(\frac{4}{1-v}\right)\left(\frac{1}{\cosh\mu L}\right)}{\left(\frac{4}{1-v}\right) + \left(\frac{2\pi}{\zeta}\right)\left(\frac{2L}{D}\right)\left(\frac{\tanh(\pi L)}{\pi L}\right)} \tag{31}$$

Several variables need to be defined for equations 30 and 31:

G_m = shear modulus of the rock mass = $E_m/2(1 + v)$.
v = Poisson's ratio of the rock mass.
$\lambda = E_c / G_m$, where E_c is the composite Young's modulus of the shaft material.

μ and ζ are defined by equations 32 and 33, respectively.

$$\mu = \frac{2}{D}\sqrt{\frac{2}{\lambda\zeta}} \tag{32}$$

$$\zeta = \ln\left[5(1-v)\frac{L}{D}\right] \tag{33}$$

The settlement of the base w_b can then be computed approximately from:

$$w_b = \frac{Q_b}{A_b}\frac{\pi}{2}\left(\frac{1-v^2}{E_m}\right)\frac{D}{2} \tag{34}$$

in which A_b is the bearing area of the base. Generally v is not measured. For most problems, its value can be safely taken in the range of 0.25 to 0.30 for soft rock. E_m can be evaluated according to equation 7 or by:

$$E_m = \alpha_E E(\text{intact}) \tag{35}$$

26

Note that equations 30 and 31 are essentially the equivalents of equations 2 and 4 in the method of Williams *et al.*, although the analytical methods from which the relationships of Williams *et al.* were derived were different from those used by Carter and Kulhawy, so that the two methods do not give identical solutions for elastic load vs. settlement. Q_t in equations 30 and 31 is equivalent to Q_e in equation 2, and Q_b in equation 31 is equivalent to Q_{be} in equation 4, which is evaluated from figure 4. The method of Williams *et al.* also differs from this method in that it presumes a small deviation from elastic conditions prior to point A in figure 16, whereas Carter and Kulhawy presume linearity to that point. It is the authors' opinion that point A can be assumed for design purposes to occur whenever w_t equals or exceeds 7.0 mm or w_b equals or exceeds 3.5 mm, whichever occurs first. Point B corresponds approximately to complete debonding of the concrete from the rock, which occurs at:

$$Q_s = Q_t - Q_b = c \text{ (interface) } \pi \, D \, L \quad . \tag{36}$$

Note that c(interface), the adhesive bond strength between the concrete and rock, can be as high as the value of c(mass) (equation 29) if the interface is free of any remolded rock or "smear." It should be made clear, however, that the value of c for the rock is usually less than $q_u(\text{mass})/2$, because the rock will ordinarily drain during loading and behave as a frictional material. It is reasonable that equation 29 be employed using an estimate of ϕ for the interface, rather than $\phi(\text{mass})$ to evaluate c. Measurements of $\phi(\text{interface})$ for a clay shale were part of the original research reported herein and are described in chapter 5. A possible alternate means for assessing c for intact rock is given in the method of McVay *et al.*, considered subsequently. Carter and Kulhawy include a method for estimating c(interface) from field loading tests on sockets without base resistance.

In order to predict the load-settlement relationship beyond point B, an analytical solution that involves frictional resistance at the concrete-rock interface is employed. It is also assumed that dilation occurs at the interface, as is also assumed in the methods of Rowe and Armitage, and Kodikara *et al.* The dilatancy phenomenon is illustrated conceptually in figure 17, which shows the concrete and rock in the vicinity of the interface. Asperities, or peaks and valleys in the rock and concrete surface caused naturally by drilling or intentionally with a grooving tool, control the behavior of the interface. A regular interface pattern with an asperity angle ψ is shown in figure 17. Angle ψ is also known as the "angle of interface dilation." This angle is equivalent to angle i_m in the method of Kodikara *et al.* (table 1); however, in figure 17, $i_{sd} = 0$, since the interface is harmonic. If the concrete is considered to be much stronger and much less deformable than the rock, which is an appropriate assumption for IGM's, as the concrete shaft is thrust downward (settles) a distance w in response to application of an axial load, the rock moves downward by an amount Δw, due to the development of shearing strains in vertical planes in the rock mass. Δw is less than w because of slippage at the interface following debonding. The rock is forced kinematically to move radially outward by an amount $\Delta v = \Delta w \tan \psi$. The rock surrounding the interface can be considered elastic, so the outward movement, Δv, produced in response to the settlement of the shaft, w, creates an increased normal force on the interface, as symbolized by the springs. Since the interface

is frictional, the shearing resistance on the interface increases as w increases, which explains the positive slope of the load-settlement curve beyond point B in figure 16. As the slip mechanism develops, it is assumed that c (interface) drops to zero. The interface asperities in the rock and in the concrete are both assumed to be nondeformable. The behavior of the rock in the field beyond the interface is entirely elastic.
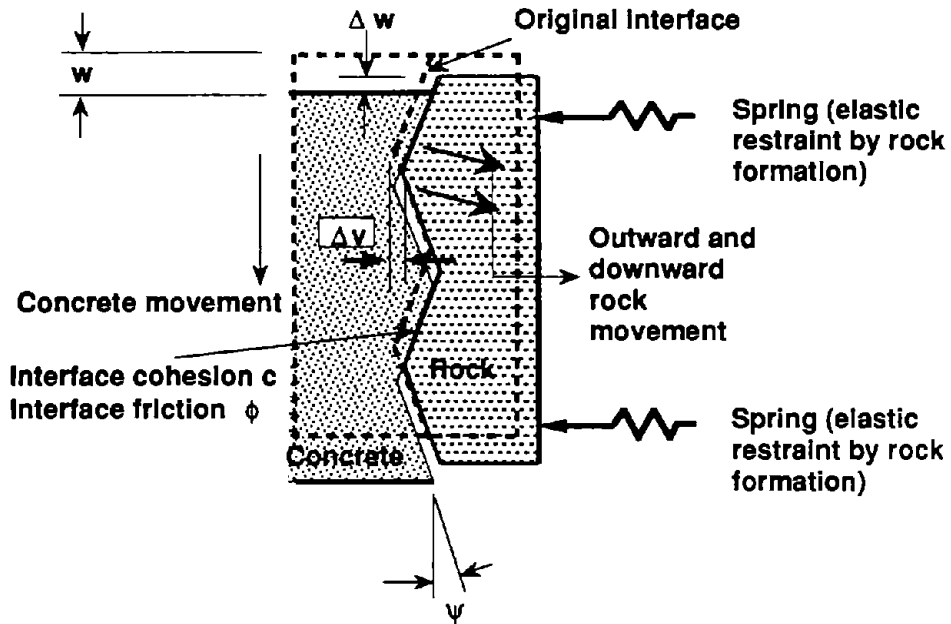
Figure 17. Schematic of the interface dilatancy phenomenon.

In order to make the calculations for load vs. settlement and the distribution of base and side resistances in the range beyond point B, which are straightforward but lengthy, the following material and geometric properties must be estimated:

- E_m (along sides of socket); E_m (beneath base).
- v (along sides of socket); v (beneath base).
- D.
- L.
- E_c (mean value for composite concrete/steel cross-section).
- c, ϕ (interface).
- ψ.

The reader is referred to the original reference for the equations to be used in making these calculations

The heights of the asperities are not used in the solution of Carter and Kulhawy. Values for the heights of the asperities (e.g., h_m in table 1) are needed in any model that predicts the complete shearing failure stress f_{max} at the interface, since the ultimate shearing resistance of the rock asperities must be calculated in such a model. This is done in the

28

Kodikara *et al.* model, but not in the model of Carter and Kulhawy. In the model of Rowe and Armitage, side shear failure is assumed to occur when the shearing resistance calculated to occur during dilative shear reaches the empirical value of f_{max}, defined in the section describing that model. The maximum settlement beyond point B to which the curve in figure 16 might be assumed to be valid could be determined for design purposes for IGM's by computing the unit base resistance q and unit side resistance f corresponding to trial values of settlement using the equations of Carter and Kulhawy for post-slip conditions and ensuring that the conditions established by Rowe and Armitage in equations 20 and 21 are met. The maximum value of such settlement would represent the limit of the validity of the solution.

Method of McVay *et al.*

McVay *et al.* proposed a design method for side-resistance-only drilled shaft sockets that applies to Category 2 IGM's and harder rock, specifically Florida limestone.[9] This method addresses only side resistance, and it does not include an estimation of settlement or base resistance. Base resistance is often omitted in limestone and limerock because random occurrences of solution cavities and slots make the use of base resistance problematical without extensive and costly probing beneath the bases of the drilled shafts. The writers' position is that settlement is not a major design concern in these geomaterials. If settlement and/or base resistance calculations are required, this method can presumably be augmented with other methods developed primarily for Category 1 and 2 IGM's, described previously in this chapter, or by the new design model addressed in chapter 4.

Through a detailed finite element analysis of drilled shaft sockets in a geomaterial that possesses both cohesion and internal friction (i.e., a "c-ϕ," or Mohr-Coulomb, material), which is characteristic of limestone, it was discovered that the ultimate shearing resistance at the interface was approximately equal to the value of cohesion (c) of the limestone. Because experience with small-scale physical tests had revealed that the shear failure surface at the IGM-concrete interface occurred in the IGM, and not precisely at the interface, no specific interface model was used, and interface dilation was not prescribed. Principal variables in the finite element study were c (0.5 to 1.4 MPa), ϕ (30 to 50 degrees), E_m (0 14 to 1.4 GPa), and E_c (27.6 GPa). The coefficient of earth pressure at rest (K_o) prior to simulated compression loading of the socket was 0.5. The IGM was modeled as a bilinear elasto-plastic material.

Since for design purposes $f_{max} = c$, some simple method is needed to evaluate c in a c-ϕ material. Note that c is not equal to $q_u/2$ in such a case. If cores of the geomaterial can be recovered, and if unconfined compression and split tensile tests can be performed on those cores, then f_{max} (which is equal to c) can be evaluated from:

$$f_{max} = 0.5 \sqrt{q_u} \sqrt{q_t} \quad , \tag{37}$$

where q_t is the split tensile strength of the geomaterial. Equation 37 is derived from a consideration of the Mohr's circles at failure for unconfined compression and split tensile

tests. Alternatively, if ϕ is known or can be estimated, f_{max} can be determined only from q_u, as follows:

$$f_{max} = q_u \frac{1 - \sin\phi}{2\cos\phi} \qquad (38)$$

The writers applied equation 37 to the estimation of the average value of f_{max} in seven loading tests at sites in limestone throughout Florida. Values of q_u varied from approximately 1.2 to 10 MPa, and q_t varied in the approximate range of 0.6 to 1.2 MPa. Six of the tests were pullout tests on short segments 0.15 m in diameter by about 1 m long, while one was a compression test on a 0.76-m-diameter socket 2.4 m long, whose base was 10.7 m below the surface. Base resistance was minimized in the latter shaft by casting the shaft on a Styrofoam pad. The magnitude of f_{max} observed in the various loading tests varied from approximately 0.5 to 1.7 MPa, and these values were predicted with equation 37 with a standard error of estimate of about 0.53 kPa. The largest error was less than 10 percent. It is noted that the standard error of the estimate is defined as $[\Sigma(\text{measured values} - \text{estimated values})^2 / n]^{0.5}$, where n is the number of observations (in this case, seven).

The writers caution that the variability in strength of limestones in Florida is significant and that such variability should be taken into account when arriving at values of f_{max}. It is suggested that the variability in a given property, such as q_u or q_t, be expressed by picking a value for design as the mean value m from among n tests minus the standard error of the mean, σ_m, not to be confused with the standard deviation of the individual test results. Therefore, for q_u:

$$q_u \text{ (design)} = m_{q_u} - \sigma_{mq_u} , \qquad (39)$$

where:

$$\sigma_{mq_u} = \frac{t\,\sigma_{q_u}}{\sqrt{n}} , \qquad (40)$$

in which t is the confidence level from a student t distribution (which is equal to 2.58 for a 99-percent confidence level) and σ_{q_u} is the standard deviation of the individual unconfined compression strengths. A similar procedure could be applied to obtain q_t (design). It is obvious that the value of σ_m decreases, and the value of f_{max}(design) increases, as the number of strength tests that are performed increases. The designer must weigh the cost of obtaining large numbers of core samples versus the cost of conducting one or more full-scale loading tests, versus designing with very conservative values of f_{max}.

30

Method of Mayne and Harris

In completely decomposed, residual granular rock in which undisturbed samples cannot be recovered, a relatively straightforward method for computing f_{max} and q_{max} based on the standard penetration test (SPT) has been described by Mayne and Harris.[10] This method, therefore, potentially applies to Category 3 IGM's. It has been used by Mayne to predict the behavior of drilled shafts in Piedmont residuum in the Eastern United States.

At a given depth, perhaps the mid-depth of the socket, the vertical effective stress (total soil pressure on a horizontal plane minus the water pressure in the pores) in the ground, σ'_{vo}, is estimated. From the blow count N_{60}, in B/0.3 m, from an SPT log in which the energy transferred to the top of the drive string is 60 percent of the drop energy of the SPT hammer (or 285 N-m per blow), or the blow count N has been corrected to N_{60}, the preconsolidation pressure of the geomaterial σ_p' can be estimated from:

$$\sigma_p' = 0.2 \, N_{60} \, \sigma_P \quad , \tag{41}$$

where $\sigma_P = 1$ atmosphere (e.g., 101 kPa if σ'_p is in kPa and N_{60} is in B/0.3 m), and the overconsolidation ratio (ratio of maximum past vertical effective stress to present vertical effective stress), OCR, is given by:

$$OCR = \frac{\sigma_p'}{\sigma_{vo}'} \tag{42}$$

The effective angle of internal friction of the geomaterial, ϕ', can be estimated from:

$$\phi' = \arctan\left\{ \left[\frac{N_{60}}{12.2 + 20.3\left(\dfrac{\sigma_{vo}'}{\sigma_p}\right)} \right]^{0.34} \right\} \tag{43}$$

The shaft-geomaterial interface is considered rough but nondilatant unless heavy mudcake buildup has been allowed during drilling. It is assumed that if concrete is placed rapidly after excavation, the *in situ* ground stresses can be assumed to be maintained; f_{max} is given by the simple friction equation:

$$f_{max} = K_o \tan \phi' \, \sigma_{vo}' \quad , \tag{44}$$

in which the coefficient of horizontal earth pressure remains equal to K_o prior to excavation, which is given by the correlative expression:

$$K_o = (1 - \sin \phi')OCR^{\sin\phi'} \qquad (45)$$

The use of equations 41 through 45 assumes that side shear failure occurs under drained conditions. Below the base, undrained failure can be assumed conservatively. It is assumed that undrained failure will occur in a full-scale loading test and that it is consistent with present practice to design with values appropriate for loading tests. In this case:

$$s_u = 0.23 \, \sigma_{vo}' \, OCR^{0.8} \qquad , \qquad (46)$$

where s_u is the operational undrained shearing strength of the geomaterial beneath the base and σ_{vo}' is the value of vertical effective stress at the elevation of the base. Finally, q_{max} is given by:

$$q_{max} = 9.33 \, s_u \qquad (47)$$

The above method is appropriate for N_{60} values in the range of 100 B/0.3 m or less. The method should be applied with caution for higher values of N_{60}.

Load-deformation behavior of drilled shaft sockets in this type of IGM can be computed using methods similar to those described for drilled shafts in cohesive IGM's. A total load-settlement method, as originally developed by Randolph and Wroth, is recommended.[11] This method also forms the basis for computing settlement in the method of Carter and Kulhawy.

In the following, only the load-settlement behavior of the socket is described. Elastic shortening in the overburden (generally 0.25 to 2.0 mm, depending on load and socket depth) will need to be added to the computed settlement to obtain the settlement at the shaft head.

As shown in figure 18, the socket load-settlement relation is a three-branched curve. For a given load Q_t at the top of the socket, the corresponding elastic settlement along segment 1, w_t, is computed from equation 48, which is equivalent to equation 2, except for a slight change in notation:

$$w_t = \frac{Q_t I}{E_{sL} D} \qquad (48)$$

Here, E_{sL} is taken to be the Young's modulus of the granular geomaterial along the sides of the socket at the base level (as distinguished from the geomaterial below the base.)

Based on correlations between energy-corrected SPT tests and Young's moduli determined from dilatometer testing in Piedmont residuum, Mayne and Harris suggest:
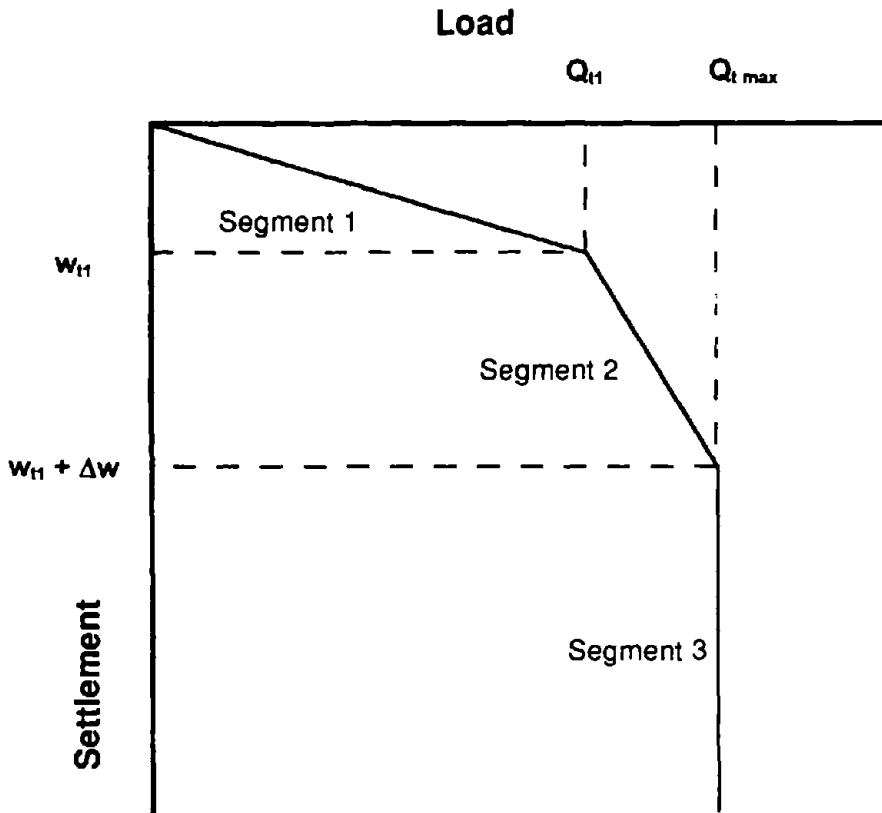
Load

Figure 18. Hypothetical load-settlement relationship for method of Mayne and Harris.

$$E_s = 22 \, \sigma_p \, N_{60}^{0.82} \quad , \tag{49}$$

in which N_{60} is again in B/0.3 m. If pressuremeter, dilatometer, or seismic data are available at the site, more accurate estimates of E_s (and K_o) might be possible.

Mayne and Harris provided a closed-form solution for I for straight-sided shafts from the original solution of Randolph and Wroth, given in equation 50:

$$I = 4(1+v) \; \frac{1 + \dfrac{8 \tanh(\mu L)L}{\pi \lambda (1-v) \xi (\mu L) D}}{\dfrac{4}{(1-v)\xi} + \dfrac{4\pi \dfrac{E_{sm}}{E_{sL}} \tanh(\mu L)L}{\varsigma (\mu L) D}} \; . \tag{50}$$

Several parameters appearing in equation 50 require definition and interpretation:

- $v =$ Poisson's ratio of the geomaterial, which can be taken as approximately 0.3 for intermediate geomaterials unless evidence indicates otherwise.
- $L =$ socket length.
- $\mu L =$ a lateral extent influence factor for elastic settlement, which can be taken to be $2\,(2\,/\,\zeta\lambda)^{0.5}$ (L/D), in which
- $\zeta =$ $\ln\{[0.25 + (2.5\,(E_{sm}/E_{sL})\,(1 - v) - 0.25)\xi]\,(2L/D)\}$.
- $\lambda =$ $2\,(1 + v)\,E_c/E_{sL}$.
- $E_c =$ Young's modulus of the composite (steel and concrete) cross section of the drilled shaft.
- $E_{sm} =$ Young's modulus of soil at the mid-depth of the socket. [Where the decomposed rock becomes stronger with depth (N increases with depth along the socket), E_{sm}/E_{sL} can ordinarily be taken to be 0.5.]
- $\xi = \dfrac{E_{sL}}{E_b}$, in which
- $E_b =$ Young's modulus of the geomaterial beneath the base of the drilled shaft, which can be different from E_{sL}. In modeling drilled shaft load tests in Piedmont residuum in the Atlanta, Georgia, area, E_b must be taken to be about 0.4 E_{sL} to obtain an optimum match with the measured load-settlement relations. That is, $\xi = 2.5$.

A schematic of the variation of soil moduli for this method is shown in figure 19.

Equation 48 is used to model load vs. settlement only until the maximum side resistance, $Q_{s\ max}$, has been reached (segment 1, figure 18).

$$Q_{s\ max} = f_{max}\,(\pi\ D\ L)\ ,\tag{51}$$

and

$$Q_t\ (\text{end of segment 1}) = Q_{t1} = \frac{Q_{s\,max}}{1 - \left\{\dfrac{1}{[\xi\cosh(\mu L)]\,[(1- v)(1+ v)]}\right\}}\tag{52}$$

Equation 52 is valid approximately for $\xi < 20$. w_{t1}, the settlement at the top of the socket at the end of segment 1, can be determined by letting $Q_t = Q_{t1}$ in equation 48.

Equations 48 and 52 define the end of linear segment 1 and the beginning of linear segment 2. At this point, Q_{b1} (load on the base at the end of segment 1) = $Q_{t1} - Q_{s\ max}$.

34
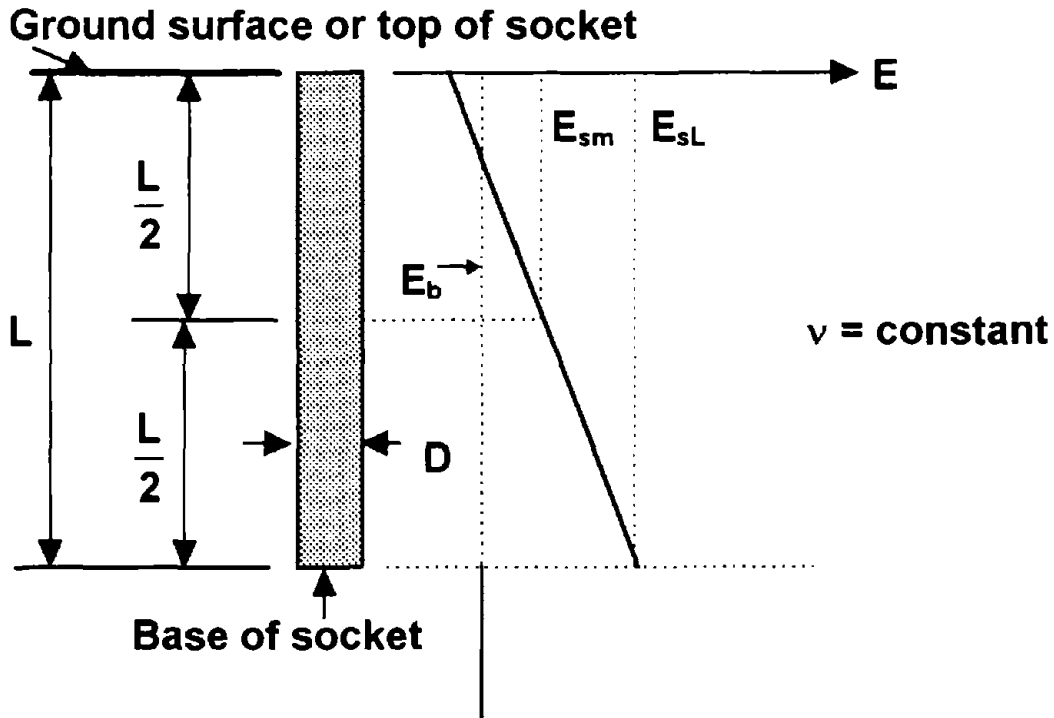
Figure 19. Potential soil modulus variation for computing settlement in granular, decomposed rock (Category 3 IGM).

The load at the end of segment 2 is the maximum total resistance of the shaft in the given geomaterial, $Q_{t\,max} = Q_{s\,max} + Q_{b\,max}$. If the side resistance is perfectly plastic (no load-softening or hardening after a movement of w_{t1}), then:

$$Q_{tmax} = f_{max} (\pi D L) + q_{max} \left[\frac{\pi D^2}{4} \right]$$ (53)

The corresponding settlement at the end of segment 2 is approximately w_{t1} plus the base settlement, Δw_b, due to the increment of base load $Q_{t\,max} - Q_{t1}$, which is given by:

$$\Delta w_b = (Q_{t\,max} - Q_{t1}) \frac{(1-v)(1+v)}{E_b D}$$ (54)

Finally, the end of segment 2 is defined by $Q_{t\,max}$ and $(w_{t1} + \Delta w_b)$. Segment 3 is a line defining continued settlement at no increase in load, which is probably conservative for most decomposed rock.

Long-Term Settlement of Drilled Shafts in Intermediate Geomaterials

The preceding methods address resistance and short-term settlement. Long-term settlement is also possible in some IGM's. Such settlement is produced by consolidation and by creep. The former can be estimated by standard methods found in textbooks. There is relatively little information on the latter effect; however, Horvath and Chae provide some guidance on creep settlement of predominantly side-resistance drilled shafts in soft, natural shale.[18] They define normalized settlement S_N by:

$$S_N = \frac{E_m D}{2 Q_{socket}} w_{socket} \quad , \tag{55}$$

where E_m is the secant mass modulus at one-half of the compressive strength of the soft rock, and the subscript "socket" refers to load (Q) or deflection (w) at the top of a rock socket with diameter D. If creep settlement is defined as the settlement occurring in the period after 1 day of sustained load, ΔS_N can be expressed as:

$$\Delta S_N = c_{nrp} \log_{10} [t_p\,(days)] + c_{nrs} \log_{10} [t(days) - t_p(days)] \quad . \tag{56}$$

In the above expression, c_{nrp} is a normalized primary creep coefficient in mm/log cycle of time in days, c_{nrs} is a secondary creep coefficient in the same units, t_p is the time required to achieve primary creep (approximately 100 days for the tests reported), and t is the time after application of the sustained load for which ΔS_N is desired. If $t < t_p$, only the first term is applied.

Test results indicated that both creep coefficients are dependent on the roughness of the borehole wall. For smooth interfaces [RF(equation 13) = 0.025], c_{nrp} is approximately 0.1, and c_{nrs} is approximately 0.03. For rough interfaces (RF > 0.08), c_{nrp} is approximately 0.06, and c_{nrs} is approximately 0.01, which indicates that rough interfaces are less prone to creep. Further research is necessary to establish the validity of these expressions for a wider range of IGM's and for situations in which substantial load is carried by the base.

Comparison of Methods

Eight published methods for the estimation of the performance of drilled shafts in intermediate geomaterials have been reviewed. These methods are different in their approach to the problem, although some have common attributes. Table 2 provides a concise summary of the attributes of the methods that have been reviewed.

Numerous other methods can be found in the literature for estimating f_{max} in rock sockets, which can be assumed tentatively to apply to IGM's. Virtually all of these methods apply

36

to Category 1 and Category 2 IGM's and involve correlations of measured shaft resistance to q_u of rock cores or to SPT N values. Expressions for estimating f_{max} from these additional methods are summarized in table 3.

Table 2. Summary of methods reviewed

Method \ Attribute	Williams	Kodikara	Horvath	Rowe	CFM	Carter	McVay	Mayne
IGM category	2	2	2	1,2	1,2	1,2	2	3
Primary method of sampling IGM:								
Cores	X	X	X	X	X	X	X	
SPT								X
Method for assessing f_{max}:								
Empirical	X		X	X				
Analytical		X				X	X	X
None					X			
Method for assessing q_{max}:								
Empirical	X			X	X			
Analytical						X		X
None		X	X				X	
Explicit interface dilation and friction?	N	Y	N	Y	-	Y	N	N
Interface degradation?	N	N	N	Y	N	N	N	N
Settlement calculations:								
Empirical	X							
Elasticity/FEM	X			X		X		X
None		X^2	X		X		X	
Load versus settlement to failure?	Y	N	N	N	Y	Y	N	Y

---

[2] Kodikara developed a method for estimating deformation that is not covered in the referenced paper and is not considered in this report.

Table 3. Estimation of f_{max} from additional references.

Reference	Expression for f_{max} in tons per square foot[3]
Horvath and Kenney[12]	$0.67 \, q_u^{0.5}$
Carter and Kulhawy[8]	$1.42 \, q_u^{0.5}$
Rosenberg and Journeaux[13]	$1.11 \, q_u^{0.51}$
Reynolds and Kaderabek[14]	$0.3 \, q_u$
Gupton and Logan[15]	$0.2 \, q_u$
Reese and O'Neill[2]	$0.15 \, q_u$
Toh[16]	$0.25 q_u$ or $10 \, N \, (B \, / \, 0.3m)^4$
Crapps[17]	$0.01 \, N \, (B \, / \, 0.3 \, m)$ or $-5.54 + 0.41 \, N \, (B \, / \, 0.3 \, m)$

In the first three entries in table 3, and in the methods of Williams et al., Horvath, and Rowe and Armitage described in more detail earlier in this chapter, the relationship between f_{max} and q_u is a power function of q_u, while in the next four entries, a linear relation exists. All of these expressions were developed from back-analysis of loading tests at locations in which at least some cores were recovered and tested in unconfined compression. Whether an expression is a power function or is linear depends mainly on the range in q_u represented in the data base that was used by the writer to develop the expression. For example, the linear expression of Reese and O'Neill is specified to apply only to a range of q_u of approximately 1.7 to 2.0 MPa (18 to 21 tons per square foot), predicated on load tests in three midwest clay-shale formations. Power function expressions such as that of Horvath and Kenney apply to a wide range of q_u. In the power function relations, $\alpha = f_{max}/q_u$ reduces with increasing values of q_u. Properties of the IGM, such as the angle of internal friction, the angle of interface dilation, the formation stiffness, and the initial coefficient of lateral earth pressure; factors related to construction, such as interface roughness, the cleanliness of the interface, the initial lateral concrete pressures, and the length of time that the borehole remains open prior to concreting; and factors

---

[3] Units are given as presented in the references. Values for q_u are also in tons per square foot. 1 ton per square foot = 95.8 kPa.

[4] Units in Toh's method are kPa for both q_u and f_{max}.

related to the way in which the loading test was conducted, such as socket details (length, diameter, destroyed or intact base resistance), method of loading (uplift, compression, jacking upward from the base) can affect the expression. Because these factors are not considered in simple correlations with q_u, it is not surprising that the various methods give widely different expressions. Under these circumstances, load testing of representative drilled shafts remains an essential element of design. Further details of construction effects are given in reference 19.

There is clearly a need for improved methods for computing both resistance and settlement in axially loaded drilled shafts in all IGM categories. It is also clear that any such method, to be successful, must include as a minimum some quantification of borehole roughness, geomaterial degradability, and strength and stiffness of the geomaterial.

CHAPTER 3: DATA BASE

GENERAL INFORMATION

A data base was developed by reviewing the literature and reports of loading tests that were obtained by the research team. The purpose of this data base was to provide measurements against which the various methods documented in chapter 2 could be investigated. The particular data base that was chosen for use was originally developed at the University of Florida for drilled shaft tests in Florida soils and limestone. It was modified at the University of Houston by appending additional data fields appropriate for other types of IGM's, including clay-shales, mudstones, and residual soils. The complete data base is available on microfloppy disks from either the University of Florida, Department of Civil Engineering, or the University of Houston, Department of Civil and Environmental Engineering. It can be accessed using a DOS-based microcomputer through either *Lotus 123*® (Lotus Development Corporation) or *Excel*® (Microsoft, Inc.).

CONTENTS OF DATA BASE

A total of 139 loading tests were documented in the data base for this study. An additional 106 cases for soil and limestone, developed previously by the University of Florida, are also contained in the data base. A listing of the loading tests included in the data base that were used in this study is provided in table 4, which also gives pertinent information about the test, including data base file number, test location, type of intermediate geomaterial, date of test, shaft geometry, IGM strength as represented by the mean unconfined compression strength (q_u), and rudimentary failure load and settlement information.

According to Reese and O'Neill, a settlement of 5 percent of the shaft diameter is required to produce failure in a drilled shaft in which bearing develops at the base.[2] In most of the tests reviewed, the maximum settlement was less than 5 percent of the shaft diameter, so that a less favorable definition of failure had to be adopted. The criterion of Davission, commonly used in interpreting conservatively the failure load for pile foundations, was therefore used.[20]

In many of the tests in the data base, only side resistance was tested. A side resistance test is often accomplished by casting the test shaft with a void beneath the base, for example, by placing a weak, crushable pad on the bearing material before placing concrete. Table 4 indicates those tests in which voids were included. For such tests, the Davisson criterion is a satisfactory predictor of side resistance.

It is noted that testing a drilled shaft in compression with a void beneath its base will, in theory, yield a value of ultimate side resistance that is different from that which would have been achieved had base resistance been developed because of: (1) the increased lateral strain, and therefore the increased normal stress at the interface, produced in the shaft concrete in response to increased axial load resulting from the base resistance in a

Table 4. Summary of the data base load tests.

File No.	Location	IGM type	Date	Diam. (mm)	Length (m)	Over-burden thickness (m)	Socket † length (m)	q_u (MPa)	Voided-Base ?	Failure Load Q_{max} (MN)	Settlement at 50 % of Q_{max} (mm)	Rank
1001	SOUTH AFRICA	WEA. DIABASE	1976	610	12.2	2.1	10.1	0.77-1.03	NO	3.47	3.05	B
1002	SOUTH AFRICA	WEA. DIABASE	1976	610	12.2	2.1	10.1	0.77-1.03	NO	2.67	2.54	B
1003	SOUTH AFRICA	WEA. DIABASE	1976	610	12.2	2.1	10.1	0.77-1.03	YES	2.22	2.03	A
1004 ‡	DALLAS, TEXAS	SHALE	1991	610	9.1	3.0	6.1	0.83	YES	1.65	1.24	A
1005	OKLAHOMA	SHALE	1976	762	8.8	2.7	6.2	0.39-0.84	NO	4.45	2.79	C
1006	OKLAHOMA	SHALE	1976	762	11.1	2.7	8.5	1.45	NO	6.94	3.56	C
1007	PENNSYLVANIA	SHALE	1978	610	5.2	5.2	0.0	1.45	NO	1.42	2.79	B
1008	PENNSYLVANIA	SHALE	1978	762	6.7	5.2	1.5	1.45	YES	2.22	4.06	A
1009	PENNSYLVANIA	SHALE	1978	762	6.1	5.2	0.9	1.45	YES	2.22	3.30	A
1010	PENNSYLVANIA	SHALE	1978	610	6.1	5.2	0.9	1.45	YES	1.07	2.29	A
1011	PENNSYLVANIA	SHALE	1978	457	6.1	5.2	0.9	1.45	YES	0.89	2.03	A
1012	PENNSYLVANIA	SHALE	1978	457	6.1	5.2	0.9	1.45	YES	0.89	1.78	A

42

Table 4. Summary of the data base load tests (cont'd).

File No.	Location	IGM type	Date	Diam. (mm)	Length (m)	Over-burden thickness (m)	Socket length (m)	q_u (MPa)	Voided-Base ?	Failure Load Q_{max} (MN)	Settlement at 50 % of Q_{max} (mm)	Rank
1013	PENNSYLVANIA	SHALE	1978	457	5.2	2.7	2.5	1.45	NO	0.89	1.78	B
1014	PENNSYLVANIA	SHALE	1978	610	6.1	5.2	0.9	1.45	YES	1.25	2.03	A
1015	PENNSYLVANIA	SHALE	1978	762	5.2	5.2	0.0	1.45	NO	1.25	3.30	B
1016	PENNSYLVANIA	SHALE	1978	457	7.2	5.2	2.0	1.45	NO	1.78	4.32	C
1017	COLORADO	CLAY-STONE	1970	305	3.5	0.6	2.9	1.08	YES	0.27	2.54	C
1018	COLORADO	CLAY-STONE	1970	305	3.5	0.6	2.9	1.08	YES	0.31	1.27	C
1019	SINGAPORE	DEC. ROCK	1988	610	6.0	0.8	5.2	NA	NO	1.25	0.76	A
1020	SINGAPORE	DEC. ROCK	1988	610	6.0	2.3	3.7	NA	NO	0.95*	0.76	A
1021	SINGAPORE	DEC. ROCK	1988	610	7.0	3.0	4.0	NA	YES	1.07	1.02	A
1022	SINGAPORE	DEC. ROCK	1988	610	7.0	5.0	2.0	NA	NO	0.62	1.02	A
1023	NORTHERN IRELAND	MARL	1976	762	13.3	5.0	8.3	0.61-0.74	YES	3.11*	10.16	B
1024	NORTHERN IRELAND	MARL	1976	762	16.0	5.0	10.0	0.41-0.81	NO	5.12*	1.27	B
1025	TORONTO, CANADA	GLACIAL TILL	1989	762	**	1.8	**	0.48	NO	-	NA	B

Table 4. Summary of the data base load tests (cont'd).

File No.	Location	IGM type	Date	Diam. (mm)	Length (m)	Over-burden thickness (m)	Socket length (m)	q_u (MPa)	Voided-Base ?	Failure Load Q_{max} (MN)	Settlement at 50 % of Q_{max} (mm)	Rank
1026	TORONTO, CANADA	TILL	1989	762	**	3.4	**	0.28-1.0	NO	-	NA	B
1027	TORONTO, CANADA	TILL	1989	762	**	0.0	**	0.28-1.0	NO	-	NA	B
1028	BRAZIL	HARD CLAY	1989	1951	12.2	1.5	10.7	0.14-0.33	NO	2.10	1.78	B
1029	ROANOKE, TEXAS	SHALE	1988	914	3.0	1.2	1.9	0.33	NO	1.60	0.63	C
1030	ROANOKE, TEXAS	SHALE	1988	914	3.0	1.2	1.9	0.41-1.63	NO	8.90	2.16	C
1031	NOVA SCOTIA, CANADA	TILL & SHALE	1967	813	9.1	0.0	9.1	0.23	NO	1.11	5.08	B
1032	NOVA SCOTIA, CANADA	TILL & SHALE	1967	610	6.1	0.0	6.1	0.23	NO	1.42	2.54	B
1033	NOVA SCOTIA, CANADA	TILL & SHALE	1967	610	13.7	0.0	13.7	0.23	NO	3.11	3.81	B
1034	CLEVELAND, OHIO	TILL & SHALE	1983	762	64.5	0.0	64.5	37.23	NO	11.12	7.87	C
1035	ONTARIO, CANADA	SHALE	1983	711	2.4	0.0	2.4	5.39	YES	3.56	2.79	A
1036	ONTARIO, CANADA	SHALE	1983	711	2.4	0.0	2.4	11.10	NO	4.45	4.57	A
1037	ONTARIO, CANADA	SHALE	1983	711	2.4	0.0	2.4	5.60	YES	4.45	5.08	A
1038	ONTARIO, CANADA	SHALE	1983	711	2.4	0.0	2.4	5.50	NO	6.49	4.83	A

44

Table 4. Summary of the data base load tests (cont'd).

File No.	Location	IGM type	Date	Diam. (mm)	Length (m)	Over-burden thickness (m)	Socket length (m)	q_u (MPa)	Voided-Base ?	Failure Load Q_{max} (MN)	Settlement at 50 % of Q_{max} (mm)	Rank
1039	ONTARIO, CANADA	SHALE	1983	711	2.4	0.0	2.4	5.39	YES	6.41	4.32	A
1040	IRVING, TEXAS	SHALE	1989	762	14.1	0.0	14.1	2.41-3.45	YES	3.11	1.27	A
1041	IRVING, TEXAS	SHALE	1989	762	14.1	0.0	14.1	2.41-0.345	YES	4.80	2.79	A
1042	CHICAGO, ILLINOIS	HARD CLAY	1972	762	9.4	4.9	4.6	0.57-1.14	NO	1.16	2.54	B
1043	CHICAGO, ILLINOIS	HARD CLAY	1972	762	9.4	4.9	4.6	0.57-1.14	YES	1.87	3.30	B
1044	CHICAGO, ILLINOIS	HARD CLAY	1972	762	9.4	4.9	4.6	0.57-1.14	NO	1.87	3.05	C
1045	NEW MEXICO	SHALE	1981	610	15.8	0.0	15.8	4.18-4.78	NO	8.90*	6.35	B
1046	NEW MEXICO	SHALE	1981	610	16.9	0.0	16.9	4.18-4.78	NO	8.90*	6.35	B
1047	ALAMO, NEVADA	HARD CLAY	1982	648	4.3	0.0	4.3	NA	NO	0.89*	0.76	B
1048	ALAMO, NEVADA	HARD CLAY	1982	648	2.7	0.0	2.7	NA	NO	0.85*	2.29	B
1049	CHICAGO, ILLINOIS	HARD-PAN	1921	2499	18.3	15.2	3.0	0.43-0.77	NO	8.63*	7.62	C
1050	CHICAGO, ILLINOIS	HARD-PAN	1921	1285	18.3	15.2	3.0	0.43-0.77	NO	2.67	7.62	C
1051	CHICAGO, ILLINOIS	TILL	1972	1930	20.7	14.3	6.4	0.43-0.72	NO	6.05	8.64	C

Table 4. Summary of the data base load tests (cont'd).

File No.	Location	IGM type	Date	Diam. (mm)	Length (m)	Over-burden thickness (m)	Socket length (m)	q_u (MPa)	Voided-Base ?	Failure Load Q_{max} (MN)	Settlement at 50 % of Q_{max} (mm)	Rank
1052	MONTOPOLIS, TEXAS	SHALE	1975	737	7.3	5.8	1.5	1.42	NO	4.71	2.54	B
1053	MONTOPOLIS, TEXAS	SHALE	1975	787	7.3	5.8	1.5	1.42	NO	3.38	2.54	B
1054	MONTOPOLIS, TEXAS	SHALE	1975	737	7.3	5.8	1.5	1.42	NO	3.74	2.54	B
1055	DALLAS, TEXAS	SHALE	1975	889	7.6	5.8	1.8	0.62	NO	3.11	3.05	B
1056	MELBOURNE, AUSTRALIA	WEA. BASALT	1984	1524	1.9	0.0	1.9	2.80	NO	9.79	3.05	B
1057	MELBOURNE, AUSTRALIA	WEA. BASALT	1984	1600	2.1	0.0	2.1	2.80	NO	13.34	1.78	B
1058	MELBOURNE, AUSTRALIA	WEA. BASALT	1984	1600	15.8	0.0	15.8	3.60	NO	13.79	3.81	B
1059	MELBOURNE, AUSTRALIA	WEA. BASALT	1984	1524	11.0	0.0	11.0	2.80	NO	6.67	2.29	B
1060	MELBOURNE, AUSTRALIA	WEA. BASALT	1984	1499	18.0	0.0	18.0	3.60	NO	11.96*	1.02	B
1061	COVENTRY, ENGLAND	SILT-STONE	1975	1067	8.5	4.9	3.7	1.20-4	NO	4.45	6.60	B
1062	SOUTH AFRICA	MUD-STONE	1976	660	6.1	3.0	3.0	1.10	NO	1.16	3.30	B
1063	SOUTH AFRICA	MUD-STONE	1976	889	6.1	3.0	3.0	1.10	NO	0.36	1.52	B
1064	SOUTH AFRICA	MUD-STONE	1976	889	6.1	3.0	3.0	1.10	NO	0.52	2.29	B

Table 4. Summary of the data base load tests (cont'd)

File No.	Location	IGM type	Date	Diam. (mm)	Length (m)	Over-burden thickness (m)	Socket length (m)	q_u (MPa)	Voided-Base ?	Failure Load Q_{max} (MN)	Settlement at 50 % of Q_{max} (mm)	Rank
1065	SAN ANTONIO, TEXAS	SHALE	1982	457	10.5	4.1	6.4	0.23-0.69	NO	1.16	3.56	B
1066	SAN ANTONIO, TEXAS	SHALE	1982	762	11.0	4.1	6.9	0.23-0.69	NO	1.78	2.29	B
1067	SAN ANTONIO, TEXAS	SHALE	1968	457	10.4	4.1	6.2	0.23-0.69	NO	0.71	1.27	C
1068	SAN ANTONIO, TEXAS	SHALE	1968	762	8.2	5.5	2.7	0.57-0.63	NO	6.23	3.56	C
1069	LITTLEBROOK, ENGLAND	CHALK	1975	1049	26.8	18.3	8.5	1.03	NO	6.23	6.35	B
1070	CHICAGO, ILLINOIS	TILL	1987	762	15.2	14.0	1.2	0.37-1.13	NO	2.49	2.54	B
1071	OAHU, HAWAII	WEA. BASALT	1991	813	16.8	0.0	16.8	0.97-1.13	NO	11.79*	7.87	B
1072	OAHU, HAWAII	WEA. BASALT	1991	838	12.0	0.0	12.0	0.97-1.13	NO	7.12	6.60	B
1073	OAHU, HAWAII	WEA. BASALT	1991	813	17.1	0.0	17.1	0.97-1.13	NO	10.85*	4.57	B
1074	SOUTH CAROLINA	MARL	1990	610	45.7	30.8	14.9	NA	NO	2.94	3.56	B
1075	SOUTH CAROLINA	MARL	1990	610	41.8	30.8	11.0	NA	NO	3.56*	4.06	B
1076	SOUTH CAROLINA	MARL	1991	610	25.8	10.2	15.5	NA	NO	2.85	2.79	C
1077	SASKATCH-EWAN, CANADA	TILL	1967	610	8.2	5.5	2.7	NA	YES	0.76	1.27	C

47

Table 4. Summary of the data base load tests (cont'd).

File No.	Location	IGM type	Date	Diam. (mm)	Length (m)	Over-burden thickness (m)	Socket length (m)	q_u (MPa)	Voided-Base ?	Failure Load Q_{max} (MN)	Settlement at 50 % of Q_{max} (mm)	Rank
1078	DALLAS, TEXAS	SHALE	1960	457	14.2	8.1	6.1	1.57-1.79	NO	2.94	4.57	C
1079	DENVER, COLORADO	DENVER BLUE	1990	457	15.7	2.4	13.2	1.54	NO	1.42	3.05	B
1080	DENVER, COLORADO	DENVER BLUE	1990	457	10.6	2.4	8.2	1.63	NO	2.22	5.84	B
1081	DENVER, COLORADO	DENVER BLUE	1990	457	6.2	2.4	3.7	0.52	NO	0.20	1.78	B
1082	DENVER, COLORADO	DENVER BLUE	1990	762	16.3	2.4	13.9	1.54	YES	0.76	2.29	B
1083	DENVER, COLORADO	DENVER BLUE	1990	762	11.4	2.4	9.0	1.63	YES	3.25*	3.30	B
1084	DENVER, COLORADO	DENVER BLUE	1990	762	6.9	2.4	4.5	0.52	YES	0.40	2.03	B
1085	DENVER, COLORADO	DENVER BLUE	1990	762	7.9	2.4	5.5	0.52	YES	0.67	1.78	B
1086	DENVER, COLORADO	DENVER BLUE	1990	610	3.0	0.0	3.0	0.95	NO	2.85	4.83	B
1087	PHOENIX, ARIZONA	CEMENT-COLLUV	1971	737	5.4	2.1	3.3	NA	NO	4.18	4.06	B
1088	PHOENIX, ARIZONA	CEMENT-COLLUV	1971	762	4.7	2.1	2.6	NA	NO	4.00	3.81	B
1089	PHOENIX, ARIZONA	CEMENT-COLLUV	1971	762	4.9	2.1	2.8	NA	NO	4.45	3.56	B
1090	PHOENIX, ARIZONA	CEMENT-COLLUV	1971	762	5.2	2.1	3.1	NA	NO	4.00	3.81	B

Table 4. Summary of the data base load tests (cont'd)

File No.	Location	IGM type	Date	Diam. (mm)	Length (m)	Over- burden thickness (m)	Socket length (m)	q_u (MPa)	Voided- Base ?	Failure Load Q_{max} (MN)	Settlement at 50 % of Q_{max} (mm)	Rank
1091	PHOENIX, ARIZONA	CEMENT- COLLUV.	1971	762	5.5	2.1	3.4	NA	NO	5.34	3.81	B
1092	PHOENIX, ARIZONA	CEMENT- COLLUV.	1971	762	5.6	2.1	3.4	NA	NO	8.01	3.81	B
1093	PHOENIX, ARIZONA	CEMENT- COLLUV.	1971	914	5.7	2.1	3.6	NA	NO	6.23	3.56	B
1094	PHOENIX, ARIZONA	CEMENT- ALLUV.	1971	813	6.5	2.1	4.4	0.28	NO	1.96	2.54	B
1095	PHOENIX, ARIZONA	CEMENT- ALLUV.	1971	762	5.0	2.1	2.8	0.28	NO	1.78	2.54	B
1096	PHOENIX, ARIZONA	CEMENT- ALLUV.	1971	742	10.9	2.1	8.8	0.28	NO	4.00	4.32	B
1097	PHOENIX, ARIZONA	CEMENT- ALLUV.	1971	610	9.5	2.1	7.4	0.28	NO	4.63	2.54	B
1098	PHOENIX, ARIZONA	CEMENT- ALLUV.	1971	762	9.7	2.1	7.6	0.28	NO	3.91	4.32	B
1099	PHOENIX, ARIZONA	CEMENT- ALLUV.	1971	919	4.9	2.1	2.8	0.28	NO	1.51	2.03	B
1100	PHOENIX, ARIZONA	CEMENT- ALLUV.	1971	762	4.9	2.1	2.7	0.28	NO	1.60	2.29	B
1101	PHOENIX, ARIZONA	CEMENT- ALLUV.	1971	914	4.9	2.1	2.7	0.28	NO	1.11	3.05	B
1102	PHOENIX, ARIZONA	CEMENT- ALLUV.	1971	762	6.2	2.1	4.1	NA	NO	6.67	3.05	B
1103	PHOENIX, ARIZONA	CEMENT- ALLUV.	1971	914	4.8	2.1	2.6	NA	NO	3.38	3.56	B

Table 4. Summary of the data base load tests (cont'd).

File No.	Location	IGM type	Date	Diam. (mm)	Length (m)	Over- burden thickness (m)	Socket length (m)	q_u (MPa)	Voided- Base ?	Failure Load Q_{max} (MN)	Settlement at 50 % of Q_{max} (mm)	Rank
1104	PHOENIX, ARIZONA	CEMENT- ALLUV.	1971	914	4.9	2.1	2.7	NA	NO	4.00	4.06	B
1105	PHOENIX, ARIZONA	CEMENT- ALLUV.	1971	762	4.9	2.1	2.8	NA	NO	1.60	2.54	B
1106	PHOENIX, ARIZONA	CEMENT- ALLUV.	1971	762	6.4	2.1	4.3	NA	NO	2.85	2.03	B
1107	PHOENIX, ARIZONA	CEMENT- ALLUV.	1971	762	5.2	2.1	3.0	NA	NO	1.78	5.08	B
1108	PHOENIX, ARIZONA	CEMENT- ALLUV.	1971	762	6.9	2.1	4.7	NA	YES	5.07	2.29	C
1109	PHOENIX, ARIZONA	CEMENT- ALLUV.	1971	762	5.1	2.1	3.0	NA	YES	2.67	3.81	B
1110	PHOENIX, ARIZONA	CEMENT- ALLUV.	1971	914	5.1	2.1	3.0	NA	YES	3.56	3.56	B
1111	PHOENIX, ARIZONA	CEMENT- ALLUV.	1971	610	6.7	2.1	4.6	NA	YES	3.29	1.27	C
1112	VIENNA, VIRGINIA	DEC. ROCK	1989	914	10.2	6.1	4.1	NA	YES	4.98	4.83	B
1113	FORT COLLINS, COLORADO	SHALE	1983	457	13.7	10.7	3.0	3.75	NO	1.78	2.29	B
1114	HONG KONG	DEC. ROCK	1982	1295	7.4	0.0	7.4	NA	YES	5.78	5.33	C
1115	HONG KONG	DEC. ROCK	1980	1499	30.5	12.8	17.7	NA	NO	8.90	6.35	B
1116	HONG KONG	DEC. ROCK	1980	1499	22.6	12.2	10.4	NA	NO	4.89	4.32	B

Table 4. Summary of the data base load tests (cont'd).

File No.	Location	IGM type	Date	Diam. (mm)	Length (m)	Over-burden thickness (m)	Socket length (m)	q_u (MPa)	Voided-Base ?	Failure Load Q_{max} (MN)	Settlement at 50 % of Q_{max} (mm)	Rank
1117	HONG KONG	DEC. ROCK	1980	1499	21.9	9.8	12.2	NA	NO	2.22	4.83	C
1118	HONG KONG	DEC. ROCK	1980	1333	48.2	23.2	25.0	NA	NO	6.94	6.60	B
1119	HONG KONG	DEC. ROCK	1980	1499	51.8	29.0	22.9	NA	NO	10.96*	5.84	B
1120	MELBOURNE, AUSTRALIA	MUD-STONE	1977	660	2.5	0.0	2.5	0.83	YES	1.78*	2.03	A
1121	MELBOURNE, AUSTRALIA	MUD-STONE	1977	1118	3.6	0.0	3.6	0.55	YES	4.45	1.78	A
1122	MELBOURNE, AUSTRALIA	MUD-STONE	1977	1168	3.5	0.0	3.5	0.61	YES	4.45	1.27	A
1123	MELBOURNE, AUSTRALIA	MUD-STONE	1978	1219	13.5	0.0	13.5	2.50	YES	4.27	1.78	A
1124	TORONTO, CANADA	SHALE	1968	635	6.8	5.5	1.3	14.74	NO	4.45	4.80	C
1125	ST. P'BURG, FLORIDA	LIME-STONE	Un-dated	711	27.7	17.1	10.7	0.34-0.62	NO	8.90*	5.33	C
1126	SAN DIEGO, CALIFORNIA	HARD CLAY	Un-dated	483	6.3	0.0	6.3	NA	YES	1.33*	1.02	B
1127	JACKSONVILLE, FLORIDA	LIME-STONE	Un-dated	914	17.4	8.2	9.1	3.28-7.2	NO	4.00	2.29	C
1128	DADE COUNTY, FLORIDA	LIME-STONE	1986	1067	7.7	2.4	5.3	1.93-5.12	NO	8.90*	14.48	C
1129	TEMPE, ARIZONA	HARD CLAY	1990	914	36.6	33.5	3.0	0.97	NO	12.45*	3.81	A

51

Table 4. Summary of the data base load tests (cont'd).

File No.	Location	IGM type	Date	Diam. (mm)	Length (m)	Over-burden thickness (m)	Socket length (m)	q_u (MPa)	Voided-Base ?	Failure Load Q_{max} (MN)	Settlement at 50 % of Q_{max} (mm)	Rank
1130	TEMPE, ARIZONA	HARD CLAY	1990	914	36.6	34.4	2.1	0.48-0.83	NO	8.90*	2.54	A
1131	SAN ANTONIO, TEXAS	SHALE	1989	610	15.2	7.6	7.7	0.77-1.35	NO	0.36	2.29	B
1132	SAN ANTONIO, TEXAS	SHALE	1989	610	15.2	7.6	7.7	0.77-1.35	NO	2.67	0.76	B
1133	SHREVEPORT, LOUISIANA	HARD CLAY	1978	711	24.0	12.2	11.8	0.77	YES	8.01*	5.08	B
1134	SOUTH CAROLINA	LIME-STONE	1988	610	13.7	9.9	3.8	13.51	NO	3.56*	2.03	C
1135	SOUTH CAROLINA	LIME-STONE	1988	610	12.4	10.1	2.3	10.23	NO	1.07	1.27	C
1136	REGINA, SASK., CANADA	TILL	1980	610	15.2	12.0	3.2	0.34	YES	1.07	1.27	B
1137	FOREST GLEN, MARYLAND	DEC. ROCK	1991	914	10.5	4.7	5.8	NA	NO	5.43	2.54	B
1138	FOREST GLEN, MARYLAND	DEC. ROCK	1991	914	15.2	3.2	12.0	NA	NO	3.56	2.79	B
1139 ‡	COWETA CO., GEORGIA	DEC. ROCK	1992	914	19.2	14.6	4.6	NA	NO	5.34	4.57	A

* Failure not achieved according to the Davisson failure criterion. Resistances were calculated on the basis of the maximum applied loads.

** End bearing test with shaft length not reported.

† Penetration length in the IGM.   ‡ Test performed specifically for this project.

NA: Neither unconfined compressive strength nor UU triaxial compression results available (either SPT or other strength tests were used).

52

"complete" shaft (the so-called "Poisson's effect") and (2) the decreased confining stresses near the base of a complete shaft that lead to decreased IGM strength along the shaft near the base. It is assumed here that the two effects approximately cancel each other and that the results of voided-base tests are relevant for evaluating methods for predicting shaft resistance.

The final entry in table 4 is a test rank. The rank value, A, B, or C, indicates the perceived reliability of the test. A Rank A test is one in which the installation details are documented, in which considerable IGM strength information is available, and in which testing details are well-documented. In some cases, tests in which the authors took part were placed in Rank A because of the authors' familiarity with site conditions, construction details, and testing procedures. A Rank B test is generally identical to a Rank A test except that only sparse data were reported on the IGM tested. A Rank C test was usually judged to be deficient in geotechnical information. Only Rank A and B tests were used in the analyses that follow.

FILE FORMAT

An example file from the data base is presented in table 5. Note that the original format created previously by the University of Florida ends with the double line on the third page of the file. Below that double line is a set of data created specifically for this project at the University of Houston. Also note that some blank fields in the data base file have been eliminated for printing and that in some cases, the file numbers in table 4 do not correspond with the final file numbers in the data base. In such cases, the desired file is easily found by location and IGM type.

CORRELATIONS DEVELOPED USING DATA BASE

The most appropriate screening test for the various design methods is the comparison of the predicted and measured side resistances. Such comparisons were made using the only measure of geomaterial and interface strength that was available in a significant number of loading tests in the data base: the unconfined compression strength, q_u. Comparisons were made using the methods of Williams, Rowe, Horvath, Carter, Reynolds, Gupton, Reese, Toh, and Rosenberg in Category 1 and 2 IGM's, which utilize only the unconfined compressive strength (q_u). (Some of the methods have additional corrections for soft seams and other factors, but since such data were not generally reported in the literature or loading test reports, those features of the methods were not included.) Category 3 IGM's were not studied in this phase of the research because too few tests existed in the data base.

Correlations between predicted and measured side resistance at failure among the nine methods studied are shown separately for mudstone, clay-shale, and limestone in figures 20, 21, and 22, respectively. Details of these correlations can be found in Appendix B.

53

Table 5. Example data base file.

```
DATA BASE FILE NUMBER:              1014
LOCATION:                          ALLEGHENY COUNTY, PENNSYLVANIA, USA, SHAFT 7
DATE OF LOAD TEST:                 1978
GEOLOGIC FORMATION:                CLAY SHALE OF CONEMAUGH FORMATION
```

```
              ENGINEER REFERENCE :           SPANOVICH & GRAVIN
SHAFT DATA
_____ .

SHAFT DIAM (IN):                    24
TOTAL SHAFT LENGTH (FT)             20
SHAFT LENGTH EMBEDED IN SOIL (FT):  20
TYPE OF HOLE RESTRAINT:             1          1 = DRY   2 = SLURRY
CASING :           0 FEET   ( 0 " DIAMETER)              3 = CASING

TYPE OF SHAFT BASE:                 1          1 = STRAIGHT
              DIAMETER BELL :       0          2 = BELL
              LENGTH BELL  :        0
```

```
SHAFT CONCRETE DATA
_____  _____ .

SLUMP OF CONCRETE, AVG (IN) =        NR

REINFORCED CONCRETE =                2          (1 = YES, 2 = NO)

CONCRETE STRENGTH
AT TIME OF TESTING (PSI) =          3120.00

YOUNG'S MODULUS OF CONCRETE =       3183.8     KSI
```

```
ANY OTHER CONCRETE INFORMATION

W/C :
AIR CONTENT
```

```
LOAD-SE  ERR MSG
_____ _____ _
```

* LOAD-SETTLEMENT AT THE TOP OF THE PILE *

LOAD (TONS)	SETTLEMENT (IN)	
0.00	0.00	
50.00	0.03	
75.00	0.08	
100.00	0.16	
125.00	0.30	
150.00	0.47	
175.00	0.71	
200.00	1.20	
225.00	1.82	
230.00	2.27	
220.00	2.30	
100.00	2.27	
0.00	2.15	
	0.00 (ONLY FOR DAVISSON CRITERIA)	0
	0.35	0

Table 5. Example data base file (cont'd).

0.43   230.00

IN-SITU TEST RESULTS
─────────────────── ─

SPT :
CPT :   N A
GROUNDWATER DEPTH :   999 FEET

DEPTH (FT)	SPT (BLOWS)	SOIL
2.00	7	MED TO STIFF CLAY SILT
4.00	6	
7.00	8	
10.00	7	
12.00	9	
14.00	5	
16.00	5	

INPUT DATA FOR SHAFTUF PROGRAM
─────────────────────

SOIL LAYERS :   3

LAYER 1		125	UNIT WEIGHT
	CLAY	17	LAYER THICKNESS
		0	SOIL TYPE
LAYER 2		150	UNIT WEIGHT
	IGM	10	LAYER THICKNESS
		2	SOIL TYPE
LAYER 3		130	UNIT WEIGHT
	IGM	3	LAYER THICKNESS
		2	SOIL TYPE
LAYER 4			UNIT WEIGHT
			LAYER THICKNESS
			SOIL TYPE
LAYER 5			UNIT WEIGHT
			LAYER THICKNESS
			SOIL TYPE

0   DIRECT (0)
           CPT (1)

POINTS IN CLAY   NUMBER OF Cu PTS
LAYERS   (MIN 2 PTS.)

IF THE CLAY	2	DEPTH	1
LAYER IS AT THE	0.35	Cu (TSF)	
SURFACE PUT FIRST	6	DEPTH	2
POINT AT 5 FEET	0.6	Cu (TSF)	
	12	DEPTH	3
DEPTH SHOULD BE	1	Cu (TSF)	
AT THE BOUNDARIES		DEPTH	4
		Cu (TSF)	
IF THE CLAY		DEPTH	5
LAYER IS AT THE		Cu (TSF)	

Table 5 Example data base file (cont'd).

```
BOTTOM PUT MIN.              DEPTH              6
 POINTS ( ONE PT.           Cu (TSF)
  LLOW  THE SHAFT )          DEPTH              7
                            Cu (TSF)


                            Cu (TSF)
                            DEPTH              9
                            Cu (TSF)
```

ROCK LAYERS

```
                    0        UF METHOD          0
                             WILLIAMS           1
                             OWN VALUES         2
```

```
    qu =              TSF
    ql =              TSF     ( ONLY FOR UF METHOD )
    qb =     =VALUE:  TSF
```

OTHER UH DATA

SHAFT DESIGN

TYPE OF LOAD TEST:	2	(1 = SIDE SHEAR DESTROYED.
		2 = END BEARING DESTROYED,
		3 = COMPLETE SHAFT INSTRUMENTED)
TYPE OF LOADING :	1	(1 = COMPRESSION. 2 = UPLIFT)
TIME TO FAILURE :	2	(1 = QUICK TEST,
		2 = MAINTAINED LOAD OR OTHER TESTS)
DEPTH OF TOP OF SHAFT :	0	FT
DEPTH OF NO FRICTION :	0	FT

OTHER GEOMATERIAL DATA

LAYER # 1

DEPTH TO TOP =	0	FT
DEPTH TO BOTTOM =	17	FT
GEOMATERIAL TYPE:	0	MED. TO STIFF CLAY SILT

SHEAR STRENGTH

UNCONFINED =	7.1	PSI
UU TRIAXIAL =		PSI
CD TRIAXIAL =		PSI & DEGREES
DIRECT SHEAR =		PSI & DEGREES

PMT DATA

PL* =		PSI
PMT MODULUS =		PSI

SPT DATA

Table 5. Example data base file (cont'd).

AVG COUNT =	8	BLOWS.FT
DIRECT INTERFACE =		PSI & DEGREES
YOUNG'S MODULUS =		PSI
OCR =		
Ko =		
TESILE STRENGTH =		PSI
RQD =		
% RECOVERY =		
WATER CONTENT =	20	%

LAYER # 2

DEPTH TO TOP =	17	FT
DEPTH TO BOTTOM =	27	FT
GEOMATERIAL TYPE:	2	BROWN CLAY SHALE
		SOFT TO MED. HARD

SHEAR STRENGTH

UNCONFINED =	105	PSI
CU TRIAXIAL =		PSI
CD TRIAXIAL =		PSI & DEGREES
DIRECT SHEAR =		PSI & DEGREES

PMT DATA

PL* =		PSI
PMT MODULUS =		PSI

SPT DATA

AVG COUNT =		BLOWS/FT

DIRECT INTERFACE =		PSI & DEGREES
YOUNG'S MODULUS =	1000000	PSI
OCR =		
Ko =		
TESILE STRENGTH =		PSI
RQD =		
% RECOVERY =		
WATER CONTENT =	9.1	%

LAYER = 3

DEPTH TO TOP =	27	FT
DEPTH TO BOTTOM =	30	FT
GEOMATERIAL TYPE:	2	GRAY SHALE

Table 5. Example data base file (cont'd).

SHEAR STRENGTH

UNCONFINED =	105	PSI	
UU TRIAXIAL =		PSI	
CD TRIAXIAL =		PSI & DEGREES	
DIRECT SHEAR =		PSI & DEGREES	

PMT DATA

PL* =	PSI	
PMT MODULUS =	PSI	

SPT DATA

AVG COUNT =	BLOWS/FT	

DIRECT INTERFACE =   PSI & DEGREES

YOUNG'S MODULUS   =   1000000   PSI

OCR   =

Ko   =

TESILE STRENGTH   =   PSI

RQD   =

% RECOVERY   =

WATER CONTENT   =   9.1   %

LAYER # 4

DEPTH TO TOP =   FT
DEPTH TO BOTTOM =   FT

GEOMATERIAL TYPE:

SHEAR STRENGTH

UNCONFINED =	PSI	
UU TRIAXIAL =	PSI	
CD TRIAXIAL =	PSI & DEGREES	
DIRECT SHEAR =	PSI & DEGREES	

PMT DATA

PL* =	PSI	
PMT MODULUS =	PSI	

SPT DATA

AVG COUNT =	BLOWS FT	

DIRECT INTERFACE   =   PSI & DEGREES

YOUNG'S MODULUS   =   PSI

OCR   =

Ko   =

TESILE STRENGTH   =   PSI

Table 5. Example data base file (cont'd).

RQD   =

% RECOVERY   =

WATER CONTENT   =   %

SIDE SHEAR & END BEARING VALUES
————————————————

Qs LAYER = 1	=	0.72	KSF
Qs LAYER = 2	=	7.344	KSF
Qs LAYER = 3	=	7.344	KSF

Qb   =   KSF

JUDGED RELIABILITY OF DATA   :   7

OTHER COMMENTS:

FAILURE LOAD IS ASSUMED TO BE 150 TONS
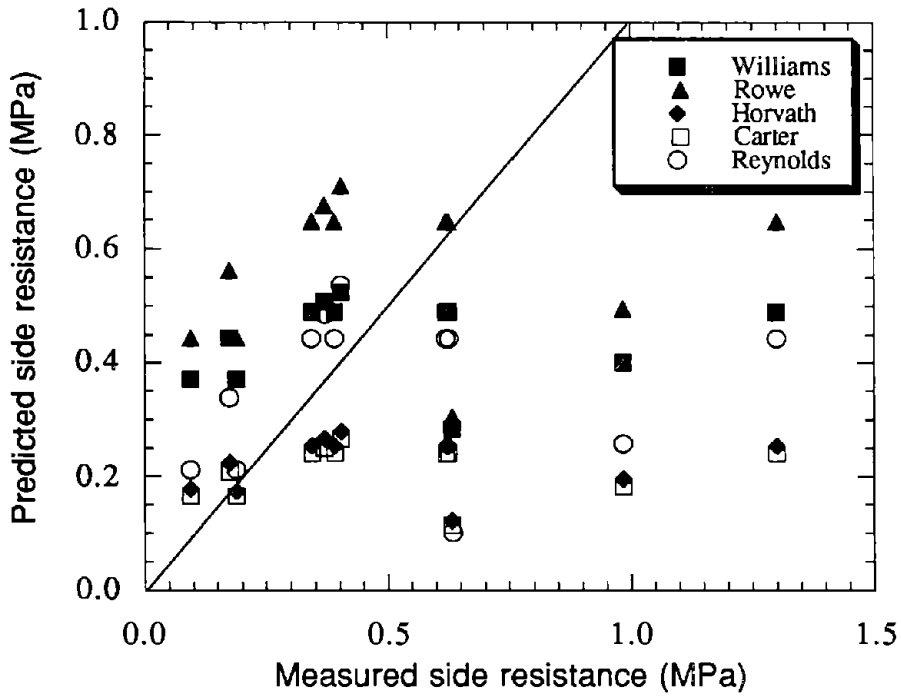
a. Williams, Rowe, Horvath, Carter, and Reynolds' methods.

b. Gupton, Reese, Toh, and Rosenberg's methods.

Figure 20. Predicted vs. measured side resistance in mudstone.

60

a. Williams, Rowe, Horvath, Carter, and Reynolds' methods.
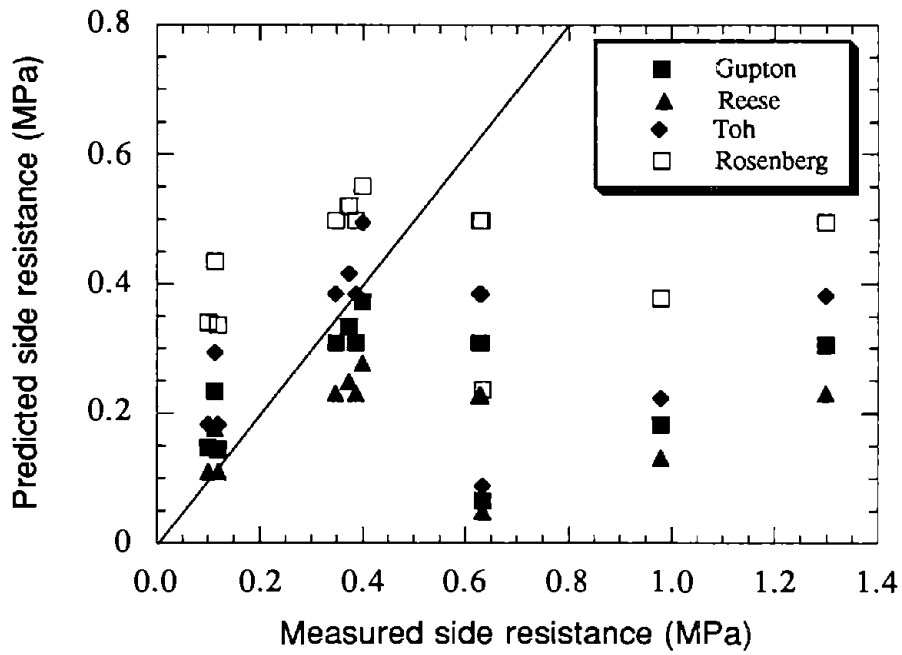
b. Gupton, Reese, Toh, and Rosenberg's methods.

Figure 21. Predicted vs. measured side resistance in clay-shale
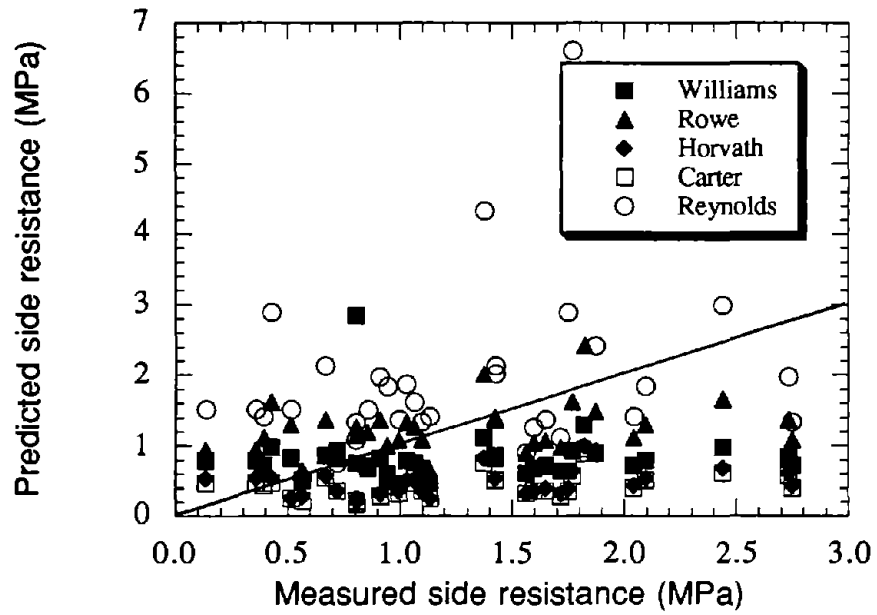
a. Williams, Rowe, Horvath, Carter, and Reynolds' methods.
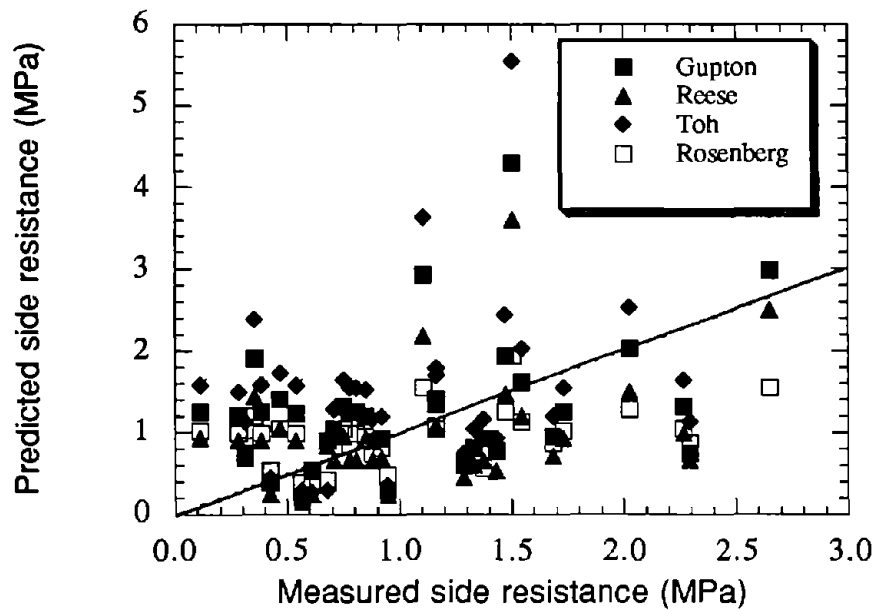
b. Gupton, Reese, Toh, and Rosenberg's methods.

Figure 22. Predicted vs. measured side resistance in limestone.

None of the methods gave consistently accurate solutions over a wide variety of test sites for any of the three classes of Category 1 and 2 IGM's considered. It is concluded in Appendix B that:

- **Unique α values do not exist, implying that more parameters than just q_u are required to make accurate predictions of f_{max}.**

- **Nonlinear correlations of α with q_u are more accurate than linear correlations.**

- **The design correlations of Williams, Rowe, and Rosenberg provide the best estimation of unit side resistance in Category 1 and 2 IGM's.**

- **Reese's method gives the best predictions among the linear α correlations; however, it is very conservative on the average.**

- **Both linear and nonlinear correlative methods tend to overestimate f_{max} (i.e., are unconservative) for relatively small values of q_u, and tend to underestimate f_{max} for higher values of q_u.**

Appendix B also develops a preliminary conclusion that McVay's two-parameter correlation appears to provide an improvement over the methods tested against the data base, but that further research is needed over a substantial number of cases before that statement can be confirmed.

Further correlations, such as for base resistance and settlement, were not performed because of relatively sparse stress-strain data for the IGM's tested and because of the poor performance of the design methods in computing side resistance.

NEW DESIGN METHODS

The data base study reviewed briefly here clearly points out the need for a new design method for Category 1 and 2 IGM's. McVay's method should be an improvement because it uses two parameters to compute f_{max} to be equivalent to interface cohesion, which is different from (lower than) $q_u/2$ in frictional geomaterials. Furthermore, the technique proposed by McVay leads to a unique value of f_{max} that is not totally dependent on q_u for the formation being tested. McVay's method also requires the assumption that interface dilation does not occur, which can serve to elevate f_{max} to a value higher than the interface cohesion. Further improvement in McVay's method can be made if construction effects such as interface roughness and smear (IGM degradation due to drilling) are included.

Observation of the load-settlement relations in the data base suggests that settlement can be as important a design consideration as resistance, particularly when base resistance is present. It is therefore important to include a simple procedure for computing settlement from readily obtainable geotechnical data. Chapter 4 reviews such an improved method

63

developed in this study from finite element parametric studies and tested against new full-scale loading tests in Category 1 IGM's and an existing loading test in Category 2 IGM's.

Less guidance is available for development of an appropriate design model for Category 3 IGM's. An existing method (Mayne and Harris), which computes both resistance and settlement, is adopted and tested later against load tests in a residual granular IGM and a dense, granular glacial till performed as a part of this study.

CHAPTER 4: DESIGN MODELS FOR AXIALLY LOADED DRILLED SHAFTS IN INTERMEDIATE GEOMATERIALS

BACKGROUND

Numerous methods were outlined in chapter 2 to compute resistances (and in some cases settlements) of drilled shafts in hard soils and soft rocks. In chapter 3, it was shown that the most basic of the computations—determination of average maximum unit side resistance, f_{max}— was not predicted well by any of the methods. Part of this deficiency may be due to differences in characterizing the properties of the soil or rock among test sites, but part may have been due to characteristics of the design models, namely relating f_{max} only to the compressive strength of the IGM.

Two design models, denoted Model 1 and Model 2, are proposed in this chapter for axially loaded drilled shafts in IGM's. The proposed models build on the concepts outlined in chapter 2. Model 1 is intended for cohesive IGM's (Category 1 and Category 2), and Model 2 is intended for cohesionless IGM's (Category 3). Specific definitions of the three categories of IGM's are given below:

- Model 1 is used with Category 1 IGM's, which are cohesive, argillaceous (clay-based) geomaterials with q_c between 0.5 and 5 MPa that exhibit the characteristic of excessive strength loss upon exposure to water (defined subsequently). Examples are hard clays (heavily overconsolidated sedimentary or residual soils) and mudstones (claystones, siltstones, or clay-shales), as ordinarily classified by geologists. An important characteristic of these geomaterials is their propensity to slake or soften when exposed to water or remolded during drilling. Morganstern and Eigenbrod identify water-sensitive argillaceous geomaterials as: (a) having q_c at natural moisture content of less than 3.5 MPa, (b) experiencing a loss of undrained compressive strength of 60 percent or more of the original compressive strength when exposed to water, and (c) simultaneously experiencing an increase in natural water content exceeding 1 percent.[21] The appropriate identification tests are conducted upon cylindrical laboratory samples of IGM's having a diameter of no more than 50 mm, that are allowed to imbibe distilled water freely for 3 days in a triaxial cell when confined at approximately 350 kPa pressure, and that are then tested to failure in undrained compression perpendicular to the bedding planes.

If any one of these properties exists, the IGM may tend to remold and soften at the concrete-IGM interface during shaft construction, and the design should proceed assuming that the borehole is "smooth" unless artificial grooves at least 25 mm deep are cut into the sides of the boreholes to act as shear keys on a vertical spacing of no more than 0.3 m, in which case the borehole may be considered to be "rough." The design can also proceed assuming that the borehole is rough in these geomaterials if: (a) "rough" conditions according to the definition in table 1 can be verified for representative drilled shafts and the estimated thickness of softened IGM ("smear") remaining on the borehole wall at the time of concreting does not exceed 2.5 mm at

any place on the wall, (b) RF (defined in equation 13) can be verified to exceed 0.10 and smear does not exceed 2.5 mm in thickness, or (c) rough conditions can be verified through load testing of representative drilled shafts, as indicated by values of load transfer that correspond to calculated values obtained by using Model 1 with rough interface classification. Measurements necessary to establish roughness and smear conditions are discussed under the section entitled "Calculations for Design Model." If rough, non-smeared conditions cannot be verified, the shaft should always be designed as if it were smooth.

- Model 1 is also used with cohesive, argillaceous geomaterials that have a natural q_c exceeding 3.5 MPa; experience an undrained strength loss of less than 40 percent of the original q_c after being exposed to water for 3 days at 350 kPa confining pressure; and whose water content increases less than 1 percent while imbibing water. These IGM's are generally insensitive to exposure to water. These IGM's and cohesive, carbonaceous/siliceous-cemented geomaterials such as limestones, limerock, and sandstones having q_c of 0.5 to 5 MPa, which normally exhibit the same response to exposure to water as insensitive argillaceous IGM's, are considered Category 2 IGM's. Category 2 IGM's are distinguished from Category 1 IGM's by the potential strength loss at the face of the borehole due to drilling, especially where any free water may be present in the formation or where water is used to assist in the drilling process. It is not considered necessary to verify the existence of non-smeared zones on the face of the borehole because these materials are insensitive to exposure to water; thus, it is only necessary to estimate whether the borehole is smooth or rough, using the methodology described above for Category 1 IGM's.

  The commentary provided here on the smear potential of IGM's should be considered preliminary until further research on smear potential can be conducted, as other factors, such as excessive exposure to the atmosphere, drilling slurries, and similar effects, may contribute to borehole smear.

- Model 2 is used with all cohesionless IGM's, such as granular tills, granular weathered rock, and similar granular geomaterials having an SPT blow count exceeding 50 blows per 0.3 m, which are defined as Category 3 IGM's. (IGM's with cobbles and boulders are excluded from this definition, as cobbles and boulders can affect N considerably.) These IGM's are distinguished from ordinary sands, which exhibit SPT blow counts of 50 or less and for which adequate design methods already exist (e.g., reference 2). Design of drilled shafts in Category 3 IGM's using Model 2 requires only SPT N values, water table (piezometric) position, and unit weight of the soil. In chapter 6, it will be demonstrated that design predictions can be made reasonably accurately using this model as long as N is restricted to no more than 100 blows per 0.3 m.

- The present FHWA design manual for drilled shafts under axial loading, issued in 1988, defines intermediate geomaterials as transitional cohesive materials having q_u between about 0.4 MPa (4 tsf) and 1.7 MPa (18 tsf) [2] Weaker cohesive materials are

treated as clay, and stronger cohesive materials are treated as rock for design purposes. Computation of unit shaft and base resistances for such geomaterials is performed by linear interpolation between the maximum unit side or base resistance value for "clay" (q_u = 0.4 MPa) and the minimum value for "rock" (q_u = 1.7 MPa), using q_u as the interpolation variable. The present FHWA method does not recognize the difference between moisture-susceptible and non-moisture susceptible cohesive IGM's, nor does it address cohesionless IGM's (Category 3). The present research includes these important characteristics and extends the range of strengths for cohesive IGM's on the high end to 5.0 MPa because such materials are classified as very soft rocks, which, up to q_u = 3.5 MPa, can be prone to softening to a soil-like consistency during drilling. The further extension to 5 MPa is somewhat arbitrary, but it is intended to cover cohesive geomaterials whose strength extends to about one-fifth that of normal drilled shaft concrete (f'_c = 24 to 28 MPa), beyond which most cohesive geomaterials would truly behave as a rock, that is, would not degrade to soil-like material during drilling. The lower bound of 0.5 MPa was based on the generally lowest average values of q_u available for full-scale test sites in this research (0.4 to 0.5 MPa). It is reasonable, however, to extend the method down to q_u = 0.4 MPa, the upper limit for "clays" in reference 2.

Both models predict load-settlement behavior and not resistance directly. It is expected that the user of these models would define resistance at failure according to an acceptable settlement criterion for the problem at hand.

Factors that are considered, either explicitly or implicitly, in Model 1 are:

- Undrained compression strength of the IGM.
- Angles of internal friction and dilation of the IGM.
- Characterization of roughness of interface between IGM and drilled shaft concrete.
- Angle of interface friction (angle of interface dilation is considered explicitly by the roughness characterization, which allows for the deformation and compression of IGM asperities).
- Smearing characteristics of the interface (presence of remolded geomaterial between the concrete and undisturbed IGM).
- Young's modulus of the IGM and of the concrete.
- Thickness and moduli of soft seams within the IGM.
- Initial interface pressure between the concrete in the shaft and the IGM.
- Depth and diameter of the socket.

The basic method is the result of a parametric finite element study, described in this chapter, that was validated by comparison with field loading tests on full-scale test shafts that were an integral part of this research project and by selected, well-documented tests in the literature, discussed in chapter 6. The method is therefore comprehensive. Numerical characterization of all of the parameters listed above is difficult in practice. Model 1 is therefore presented in simplified form that requires estimation of:

- Young's moduli of the IGM and concrete.
- Unconfined compressive strength of the IGM.
- General interface roughness pattern ("smooth" or "rough").
- Vertical effective stress at the top of the socket.
- Fluid pressure of the concrete at the mid-depth of the socket (function of specified slump and rate of placement of the concrete).
- Socket geometry.

Model 1 makes use of typical values for IGM's and correlations between parameters to include the effects of parameters not normally measured. Conservative estimates can be made of any or all of the parameters listed above for design purposes. However, the accuracy of the prediction of load-settlement behavior depends on the accuracy of parameter evaluation, which depends, in turn, on the quality of sampling and laboratory or in situ testing.

Model 1 can be applied directly or by using the method to produce unit load transfer functions that can be used in available software to synthesize load-settlement behavior.

Factors that are included in Model 2 are:

- Young's moduli of the IGM and concrete.
- Drained angle of internal friction of the IGM.
- Coefficient of earth pressure at rest in the IGM.
- Vertical effective stresses in the IGM.
- Socket geometry.

Recognizing that measurements of the first four properties are not normally made directly, the correlative procedure of Mayne and Harris described in chapter 2 is proposed to allow the use of standard penetration test results to compute the load-settlement relation.[10] In this case, a method for computing unit load transfer functions is not available.

MODEL 1 (Category 1 and 2 IGM's)

Finite Element Analysis

Model 1 was derived through intensive, parametric finite element modeling. Details are presented in Appendix C, but a summary is given here. Figure 23 describes the geometric conditions modeled and the boundary conditions used. The geometry of the IGM socket was not varied in the finite element analysis except to validate solutions for selected values of L (and therefore L/D) different from that used in the parametric study. The absolute value of the shaft diameter was not varied in the finite element study. Expanding cavity theory, which can be used crudely to compute radial stresses caused by dilation of the socket during axial loading, suggests that there is an effect of diameter on load transfer. This effect is to reduce side shearing resistance with increasing D, regardless of L. Experimental evidence, including that presented in chapter 6, suggests that the effect is

generally small for D greater than about 0.61 m; however, caution should be used in applying the method to shafts of very large diameters (greater than 1.53 m). The surcharge load shown in figure 23 was varied to facilitate modeling the effect of the depth of the socket. D was set equal to 0.61 m, and L was set equal to 6.1 m for the parametric analyses. Axisymmetric meshes were established to model both rough and smooth interfaces, as shown in figures 24 and 25.

Rough interfaces were modeled by a sinusoidal pattern shown in figure 26. This shape is typical of shapes observed in sockets drilled with augers in soft clay-shale formations by the authors. A frictional/noncohesive surface was used to represent argillaceous geomaterials at the interface at which slide elements were used to allow relative shearing movements and separation of IGM from concrete as interface slippage occurred. In the rough interface, the asperities in both the rock and concrete were modeled by deformable elements described using the parameters for the undisturbed IGM or by parameters that represented some degree of softening (smear) at the interface due to drilling. These points are illustrated by a typical deformed mesh in the vicinity of a rough interface in figure 27.
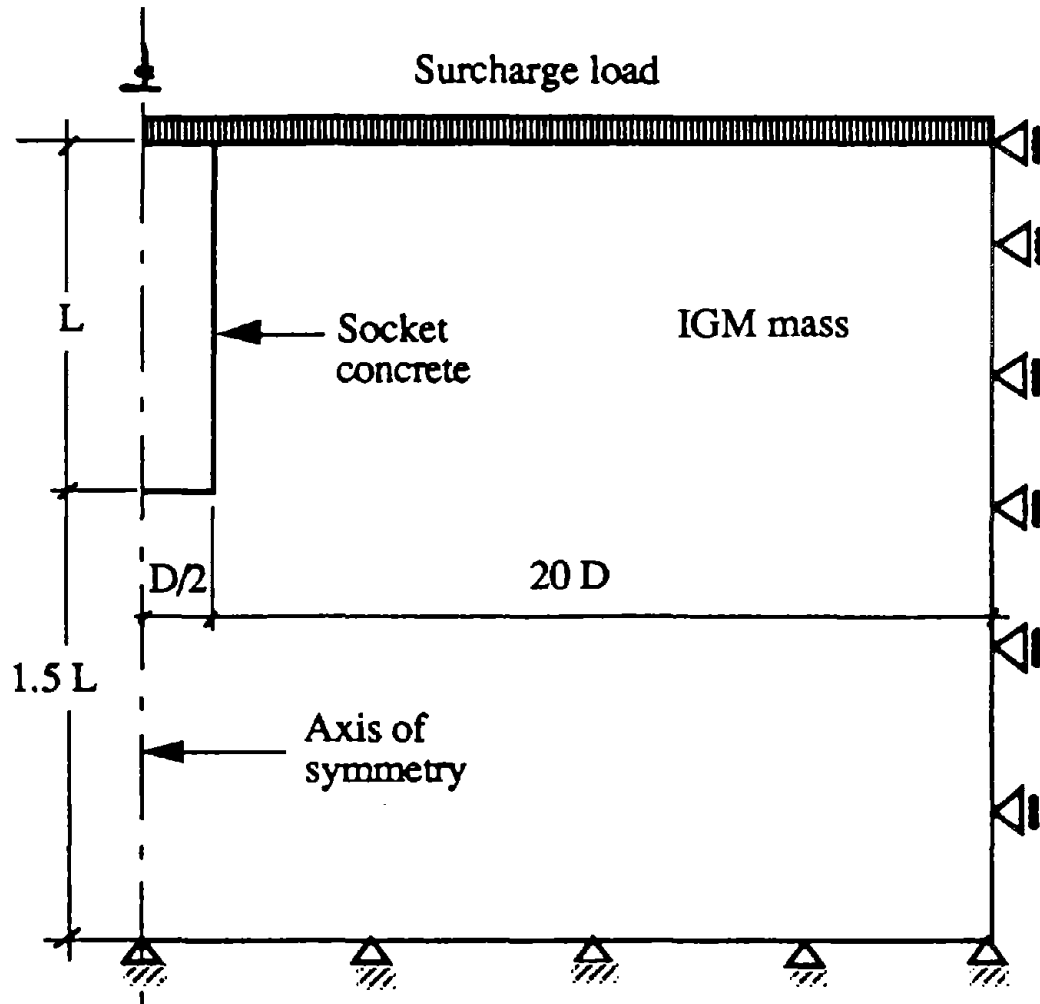
Figure 23. Loading and boundary conditions for finite element analyses.

Socket Detail
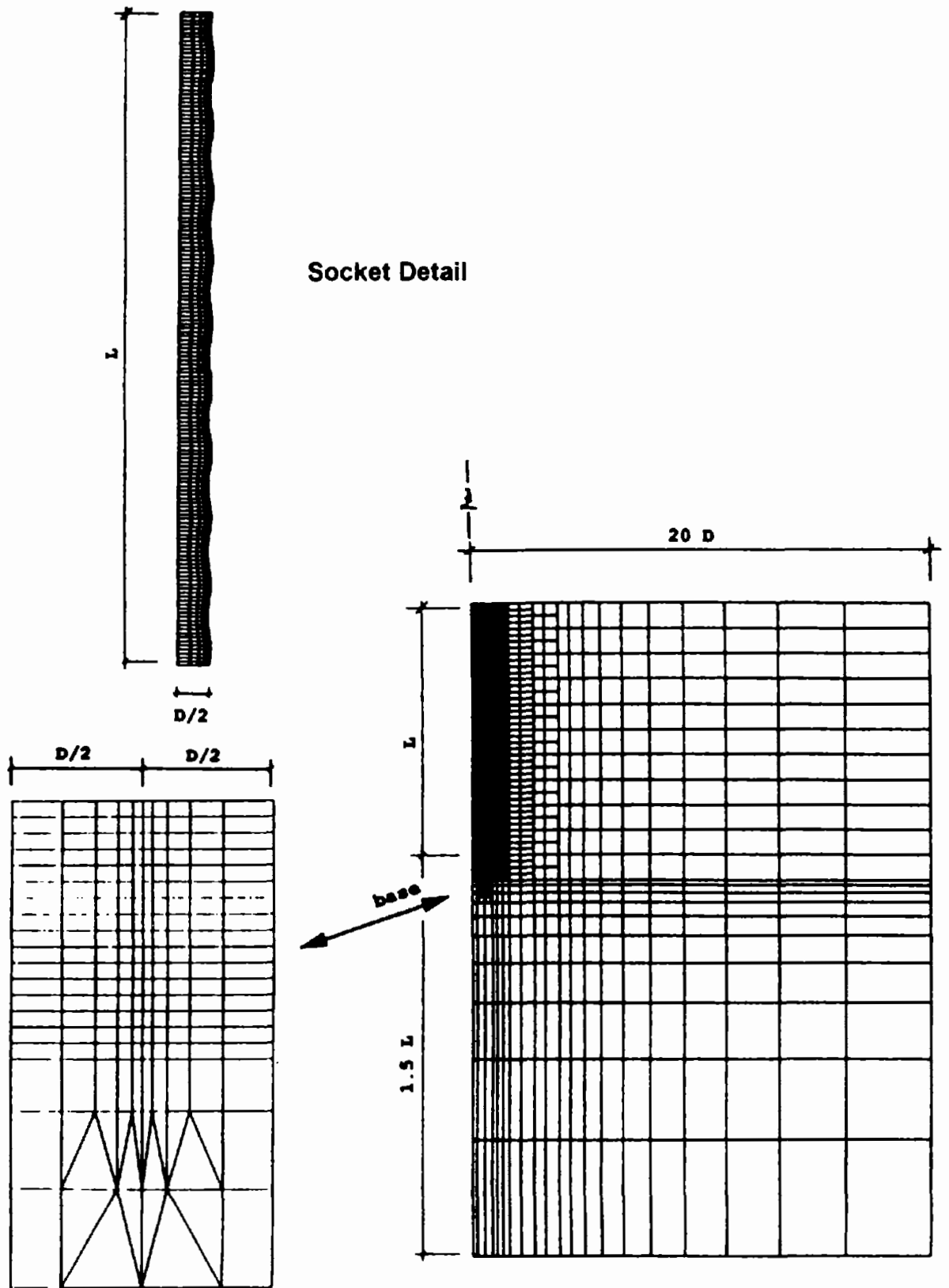
Figure 24. Finite element mesh for rough socket analysis.
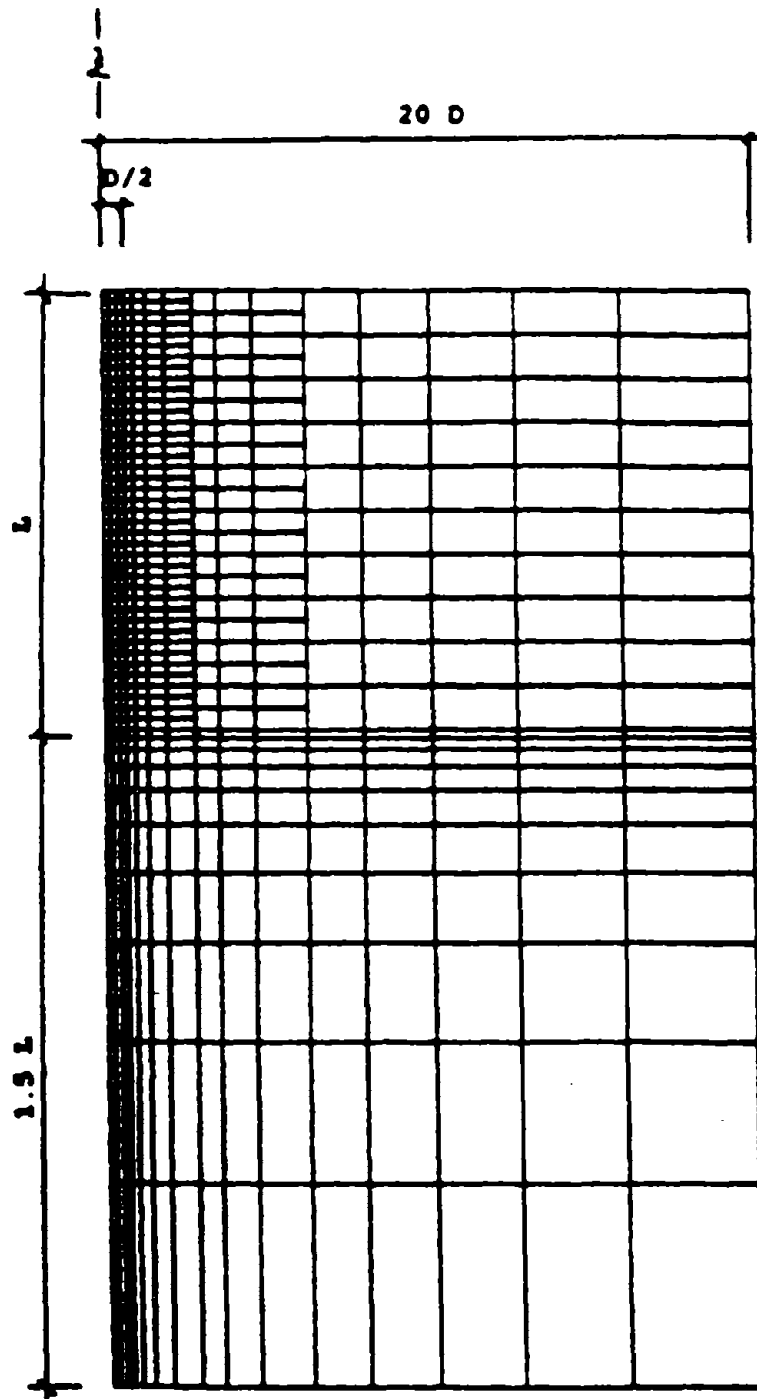
Figure 25. Finite element mesh for smooth socket analysis.

71
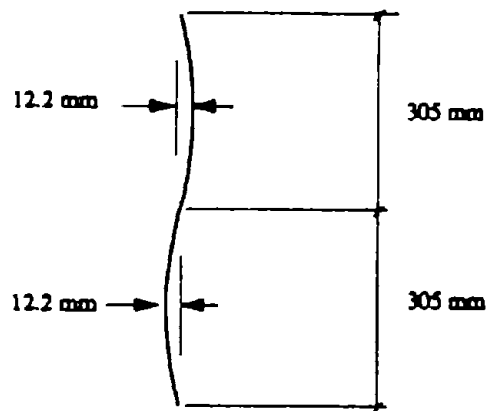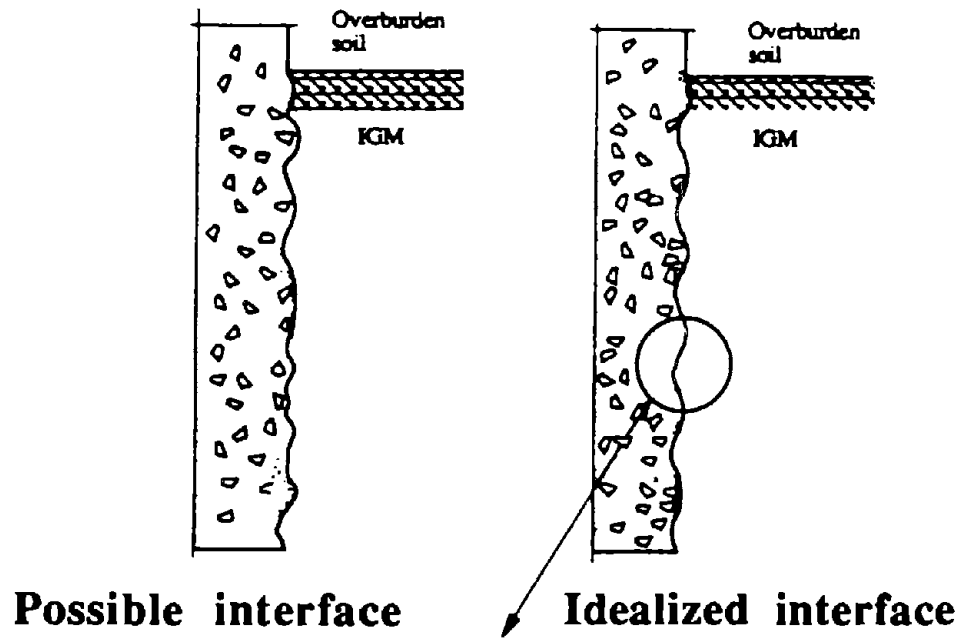
Figure 26. Idealization of rough concrete-IGM interface.
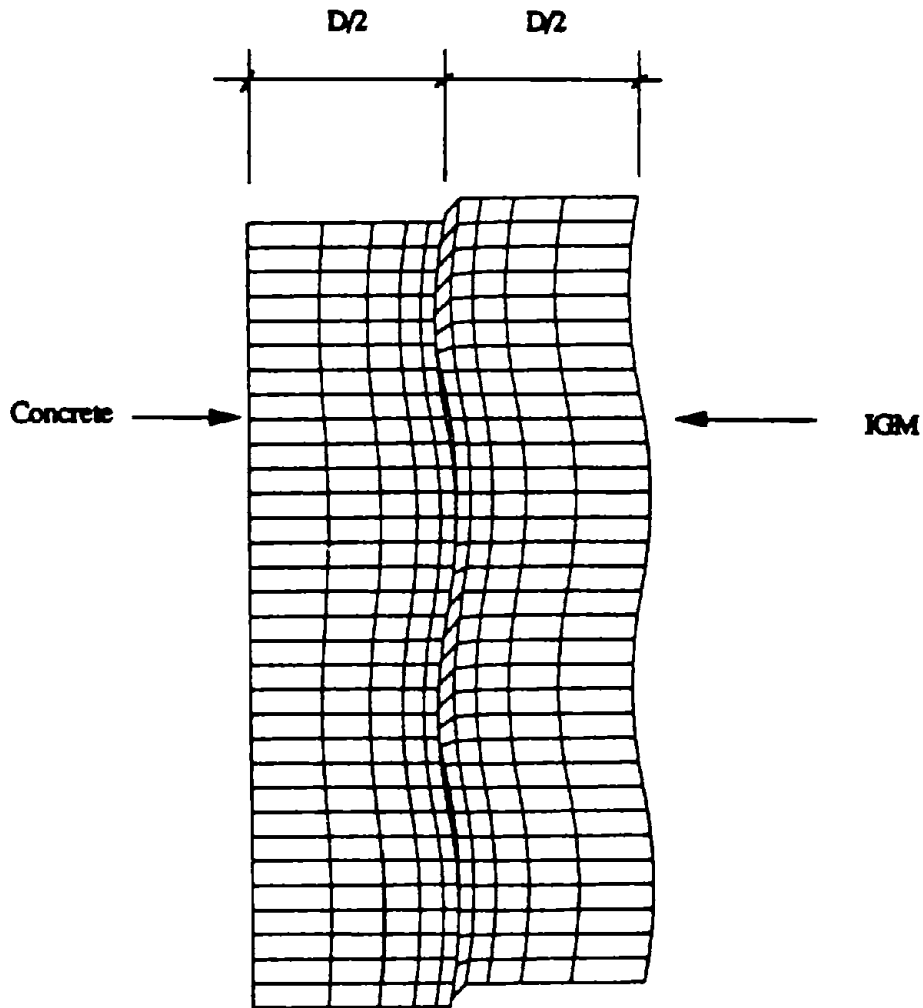
Figure 27. Displaced mesh in the vicinity of concrete-IGM interface at 25-mm settlement at top of socket.

The IGM was simulated with a Drucker-Prager nonassociated flow model using eight-noded isoparametric elements. The concrete was assumed to be elastic. Computations were performed with the ABAQUS code.[22] Ranges of values of the significant parameters used in the finite element analyses are described in table 6. In the computations used to develop the design equations, the interface was frictional ($\phi = \phi_{rc}$), but the mass geomaterial was homogeneous, undrained, and nonfrictional ($\phi = 0$). The consequences of this assumption are relatively minor and are discussed in Appendix C. Where the interface is cohesive (e.g., sockets in which cement paste penetrates the matrix of Category 2 IGM's and slip does not occur), McVay's method (chapter 2) may be more appropriate for assessing f_{max} than the method given here, which assumes no interface cohesion. If f_{max} from McVay's method is used to evaluate side resistance, however, the method presented in this chapter for estimation of settlement will usually overpredict settlement significantly.

73

Table 6. Range of values for parameters for finite element analysis.

Description of parameter	Units	Symbol	Value
Socket diameter	m	D	0.61
Socket length	m	L	6.1
Unit weights of overburden, IGM, and concrete	kN/m^3	γ	20.4
Vertical effective stress at top of socket (represents depths of 3.05 m and 15.24 m if overburden is not submerged)	kPa	σ'_{vt}	62, 311
Compressive strength of the IGM	MPa	q_u	0.48-4.8
Mass Young's modulus of the IGM	-	E_m	$(58\text{-}576)q_u$
Poisson's ratio of IGM	-	ν_r	0.30
Angle of internal friction of the IGM	deg.	ϕ_r	0, 37
Angle of internal dilation of the IGM	deg.	ψ_r	0, 18.5
Angle of interface friction	deg.	ϕ_{rc}	30
Initial normal (horizontal) stress at concrete-IGM interface	atm.	σ_n	1.25, 3.75
Coefficient of earth pressure at rest in IGM	-	K_o	1
Young's modulus of concrete shaft	GPa	E_c	27.6
Poisson's ratio of concrete shaft	-	ν_c	0.15
Interface asperity height	mm	h_a	0, 25.4
Interface asperity wave length	mm	l_a	305

The design model described in this chapter was developed by fitting the side load-settlement relations produced by multi-load finite element solutions with a simple function. Base resistance-settlement behavior was also obtained from the finite element analyses, as the shafts whose behavior was synthesized were all complete shafts. It was found that side shearing resistance-settlement behavior can be decoupled from base resistance in uniform geomaterials, although the ratio of base resistance to side resistance affects the mean lateral strains in the concrete along the socket, the resulting lateral stresses produced at the interface by the Poisson's effect in the concrete, and the side load-settlement behavior. This behavior is captured in the design model for sockets with L = 6.1 m. The design model is slightly conservative for shorter sockets, where the ratio of base resistance to side resistance is relatively high. For longer sockets, the proportion of applied load reaching the base for any given set of conditions is smaller than for shorter sockets, which results in a smaller Poisson's effect near the base of the socket and somewhat lower side load transfer than is predicted by the design model. It is intended that Model 1 be applied only to sockets within the range 2 ≤ L/D ≤ 20.

Cylindrical geometry was used to represent the shaft in both the overburden and IGM socket. No step change in diameter was assumed to occur at the top of the IGM. However, if casing is used to drill through the overburden, the diameter of the shaft in the overburden will be greater than the diameter in the socket, and a shoulder will be formed

at the top of the socket (bottom of the casing). The effect of such a step change in diameter was not addressed in this study.

K_o was taken to be 1.0, which is consistent with data obtained from Menard-type pressuremeter tests in clay-shale at the Dallas test site described in chapter 5 and with suggestions by geological engineers that K_o approaches 1.0 in all rock as time increases without bound. K_o had little effect on the behavior of the shaft in the finite element model, since the condition modeled for development of the design method was undrained IGM mass behavior and drained interface behavior. Justification for these drainage conditions is given in Appendix C. At the interface, the normal effective stress is influenced most strongly by the pressure applied by the concrete (assumed to be equal to the fluid pressure in the concrete at the time of casting).

Base resistance is not large compared to side resistance at settlements at the top of the socket of less than 25 mm for $L = 6.1$ m. It may be sufficient for design purposes to consider only the side resistance component when computing load-settlement behavior up to a settlement of 25 mm and independently adding the end bearing resistance proposed in equation 10 to the side shear developed at a settlement of 25 mm to obtain the limiting resistance of the socket. Base resistance may be excluded entirely in karst terrane or in formations in which the IGM strength is extremely variable.

Before proceeding to the design model, several characteristics of the finite element solutions are discussed. These discussions, which are illustrated by solutions for specific sets of conditions, are meant only to describe general phenomena and should not be generalized to all cases.

Stress distribution around interface and defined value of f_{max}

The distribution of stress at the interface is quite complex. Contours of mean normal stresses (σ_m) are shown in figure 28 for a shaft with $\sigma_n = 3.75\ \sigma_p$, where σ_p = atmospheric pressure, $q_u = 1.2$ MPa, $\phi_r = 0$, $\phi_{rc} = 30$ deg., $h_a = 24$ mm, and $l_a = 305$ mm ("rough" interface), at a settlement of 25.4 mm. The mean normal stresses are lowest near the roots of the IGM asperities and highest on the top faces of the peaks of the IGM asperities. All stresses remain compressive at this point (as indicated by the + sign). Figure 29 contains contours of shearing stresses on vertical surfaces in the vertical direction (τ_{rz}). The contour marked "8" represents the shear strength of the IGM, which is $q_u/2$ in this "reference" problem. The zone around the peak of the asperity and penetrating down obliquely into the IGM is in a plastic condition. However, the IGM near the root of the asperity has low shearing stresses at this point. Further yielding in the asperity, which will occur with further settlement, will eventually produce yielding at the root of the asperity. At this point, the mean unit side shear along the socket will either be equal to the shear strength of the IGM at the interface if the IGM is ductile and does not strain soften, or less than the shear strength at the interface if the IGM is brittle and undergoes strain softening (which was not modeled here).

75

Since the maximum average unit side shearing resistance occurs in rough-interface shafts at settlements exceeding 25 mm, it is suggested, for design purposes, that f_{max} be taken as the mean shearing stress along the interface at a settlement of 25 mm. Investigation of figure 29 indicates that f_{max} according to this definition will be less than $q_u/2$. The proposed design model will allow this value to be evaluated. If settlement criteria for the structure require settlements of less than 25 mm at the ultimate limit state, the load-settlement characteristics of the proposed design model can be employed to estimate f_{max} for that settlement criterion. The method should not be used, however, for estimating f_{max} for settlements greater than 25 mm.

The small mean normal stresses at the roots of the asperities in figure 28 are partially the result of the development of tensile stresses in the vertical direction, which will produce horizontal fractures in the IGM, as indicated in figure 30. This effect would be expected to be especially severe in horizontally laminated IGM's, such as some clay-shales. Although no fracture mechanics studies were conducted of this phenomenon, the tension fractures appear to be stable (will not propagate further until more load is added to the socket) based on more detailed finite element analyses reported in Appendix C, and they do not have an appreciable effect on short-term load-settlement behavior up to settlements

$\sigma_m \quad (kPa)$

1	+4
2	+257
3	+508
4	+761
5	+1015
6	+1269
7	+1523
8	+1776

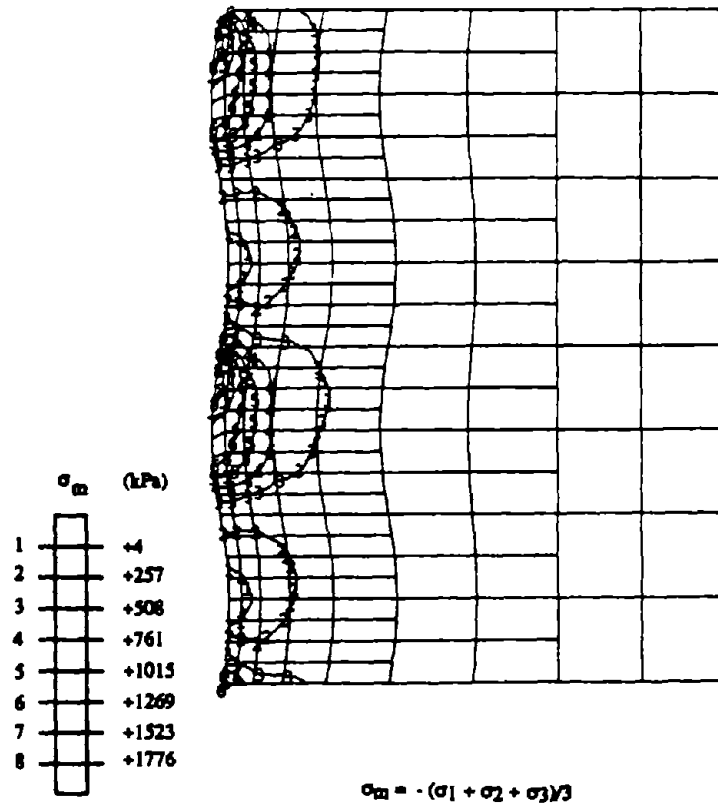$\sigma_m = -(\sigma_1 + \sigma_2 + \sigma_3)/3$

Figure 28. Contours of mean normal stresses, σ_m, at settlement of 25 mm.
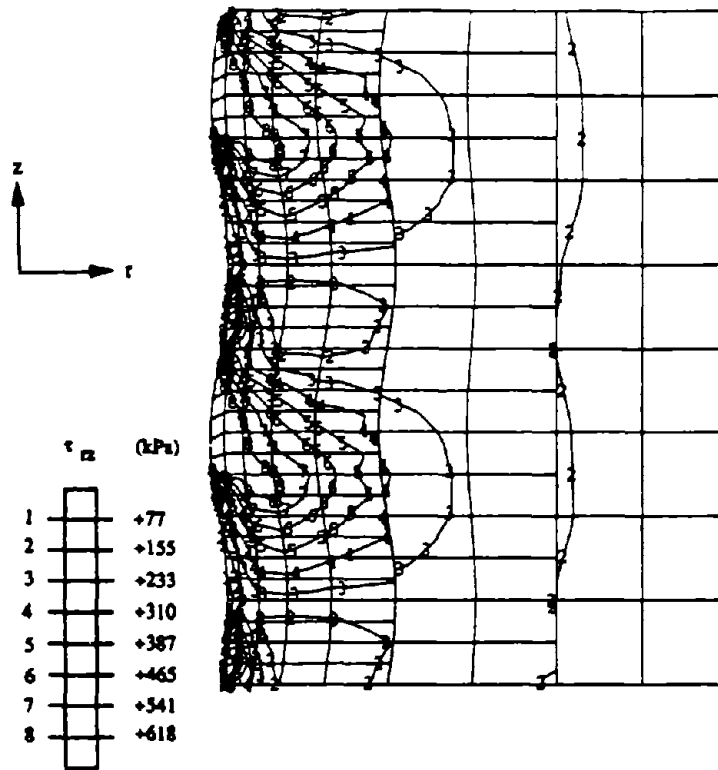
76

Figure 29. Contours of shear stresses, τ_{rz}, at settlement of 25 mm.
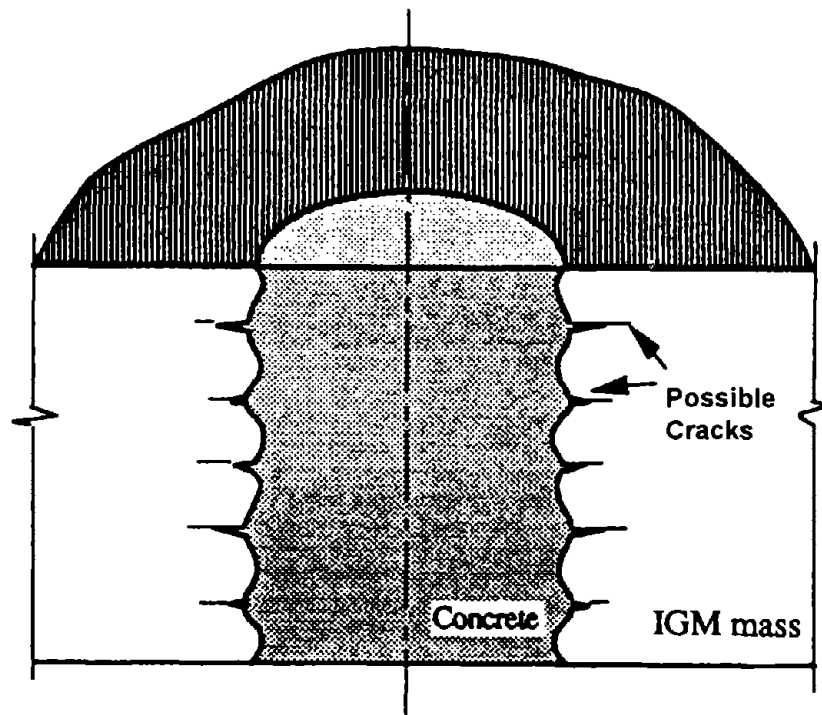
Figure 30. Fracture pattern in IGM indicated by finite element analyses.

of up to 25 mm. This phenomenon suggests that long-term creep may occur in side resistance, however. The design method presented here does not address creep. However, guidance on simple estimation of settlement of drilled shafts in shale due to creep is given by Horvath and Chae and summarized by O'Neill and Hassan.[18, 19]

Effect of borehole roughness

The average value of f (side shear resistance) is plotted against the settlement of the top of the socket in figure 31 for the conditions shown on the figure, for σ_n/σ_p = 1.25 (shallow socket). It is observed that the average value of f at a settlement of 25 mm ("f_{max}") is approximately three times as large in the rough socket (h_a = 24 mm, l_a = 305 mm) as in the smooth socket, and the corresponding values of α (equation 5) are 0.09 and 0.28. Borehole roughness is therefore a critical condition to be evaluated by the designer.

Effect of disturbed geomaterial ("smear") on the face of the borehole

Limited finite element analyses were conducted for the condition depicted in figure 32, in which a 15-mm-thick zone of degraded IGM, or "smear," was present between the undisturbed IGM and the concrete shaft in an otherwise rough interface (h_a = 24 mm and l_a = 305 mm). Results of analyses for a shallow socket (σ_n/σ_p = 1.25) with q_u = 2.4 MPa are given in figure 33 for the other conditions shown. The two load-settlement relations represent a smooth-faced socket and a rough socket in the same material, but with a smear zone in which q_u = 0.20 q_u in the undisturbed IGM and E_m = 0.25 E_m in the undisturbed IGM. The two sockets have very nearly the same behavior, even though the thickness of the smear zone is smaller than the asperity height. This observation suggests that if there

Figure 31. Example of effect of interface roughness on load-settlement behavior in finite element analyses.

Figure 32. Schematic of smeared interface in finite element analyses.

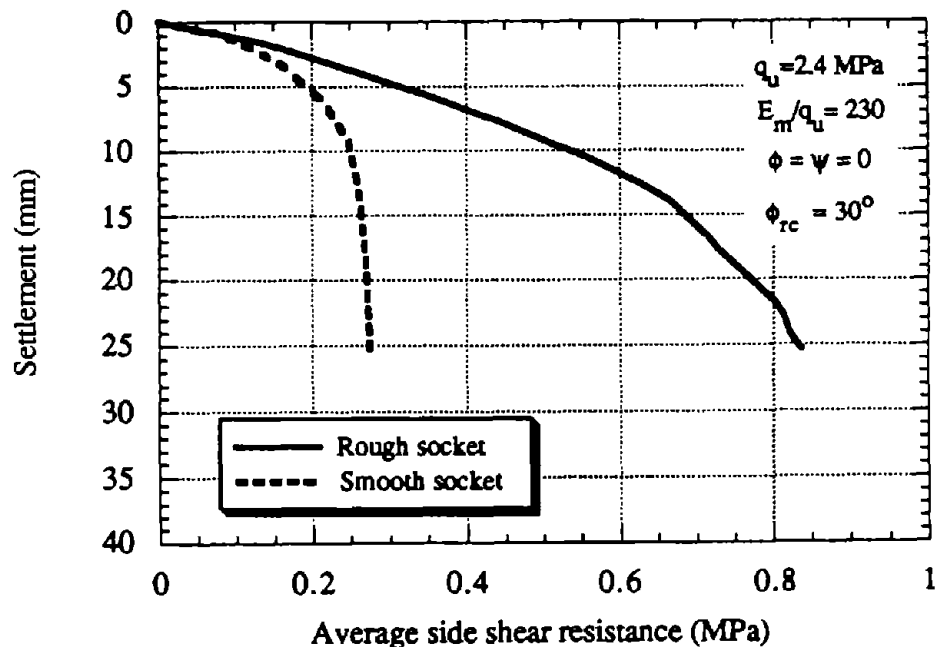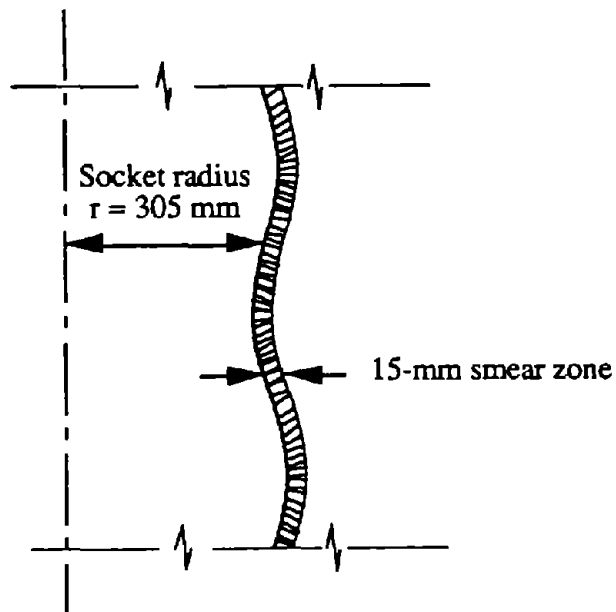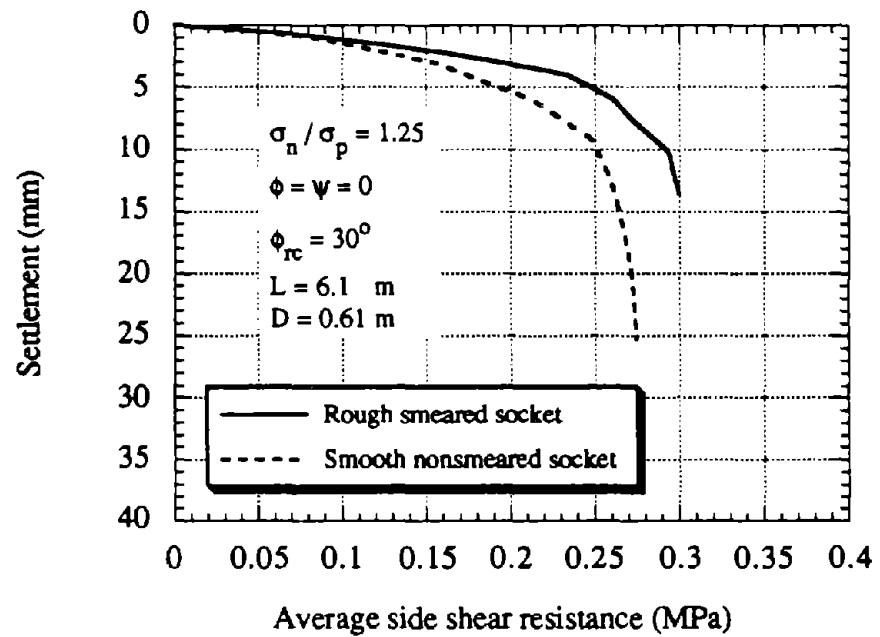Figure 33. Relative behavior of rough smeared socket and smooth socket.

is any doubt that a degraded interface will exist after drilling, the shaft should be designed as a smooth shaft, even if it is expected to be rough after completion of drilling.

Calculations for Design Model

Direct load-settlement simulation

In a design context, while many important parameters were identified during the development of design Model 1, it is not presently normal practice to measure precisely the values of each parameter for every construction site. Only one parameter for Model 1 must be measured (M), while others can be estimated (E), and values can be calculated from simple correlations for others (C). Still others are inherent in Model 1, but standard values have already been included and are not required to be provided by the designer (S). The factors used in Model 1 are:

- q_c or q_u of the IGM .... M
- Young's modulus of the IGM and the concrete................................. C
    [Standard formulas can be used for the concrete if f'_c is known
    E_m (mass Young's modulus of IGM) can be taken as 115 q_u for
    Category 2 IGM's and 250 q_u for Category 1 IGM's for design
    purposes if modulus measurements are not made, provided
    soft seams and open fractures are not present. Other procedures
    are given in the following for the case where the IGM is not massive
    and possesses soft seams or fractures.]
- Initial interface pressure between concrete and IGM........................ C
- Roughness classification of interface ("smooth" or "rough")............ E
- Smear classification of interface ("smeared" or "non-smeared").......... E
- Thickness of and moduli of seam material within the IGM.................. E
    [These factors affect E_m and unit side and base resistances
    in IGM that is not massive and that contains soft seams.
    Their effects can be considered indirectly by using core
    recovery properties of the geomaterial samples, described later.]
- Depth and diameter of the socket .... E
    [Model 1 is intended to apply for 2 < L/D < 20, D < 1.54 m.]
- Angles of internal friction and dilation of the IGM............................ S
- Angle of interface friction... S
    [30 degrees is used as a standard value The unit side shear may be
    be revised by the designer if evidence exists that the value of this
    parameter will be other than 30 degrees. A suggestion for this
    revision is made in chapter 8, based on experimental observations in
    field tests described in chapters 5 and 6.]

The parameter evaluation activity that goes beyond present geotechnical practice in most design agencies is the classification of boreholes as smooth or rough and smeared or non-

smeared. Suggestions for making the classification estimates are given in the ensuing material.

A typical design procedure would be as follows:

- Obtain sufficient samples of the IGM at the construction site to characterize the subsurface geomaterials using the best methods available for sample recovery. Category 1 and 2 IGM's may sometimes be difficult to sample because of heterogeneity (e.g., seams, fractures). Soft IGM's can sometimes be sampled with thin-walled tube samplers, whereas harder IGM's may require core barrels, and extremely heterogeneous IGM's may require Dennison barrels or even drive samplers. The order of preference for sampling tools is given below based on generally decreasing quality of samples:

    - Thin-walled tube samplers (75-mm diameter / 50-mm diameter).[23]
    - Triple-walled core barrel samplers.[24] The detail of the design of the core barrel sampler used in IGM's is critical, since cores are often difficult to recover and remove from the sampler. It is important that the inner barrel has a swivel head connection with the barrel unit and that there exists a non-rotating liner (third tube, split if possible) to preserve the sample.
    - Double-walled core barrel samplers.[25] As with the triple-walled sampler, the inner tube should be non-rotating.
    - Dennison barrel samplers (large-diameter core barrels with thin-walled inner tubes).[24]
    - Ring-lined driven barrel samplers.[26]
    - Split-spoon drive samplers.[27]

It may sometimes be necessary to use a combination of tools at any one site or in any one sample borehole. For example, the IGM is sampled with the triple-walled core barrel, but core recovery suddenly falls below 50 percent. In that event, the more desirable core barrel sampler should be replaced with a Dennison barrel sampler, or even a drive sampler, to recover as much material as possible for evaluation and testing. Laboratory tests, discussed subsequently, that are conducted on drive samples are likely to give very conservative strength results; however, such samples may be the only source of strength data and must be used. In some instances, even drive samples will not be recovered; in which case, SPT blow counts will need to be used to characterize the geomaterial. In such an extreme case, the compressive strength, q_c, of Category 1 and 2 IGM's can be estimated crudely from q_c (kPa) = $N/0.075$, with a recommended upper limit on N of 100. N-correlated strengths of cohesive geomaterials are very unreliable, and the latter method should be used only as a last resort.

Details of operation and usage of geomaterial samplers is beyond the scope of this report. The reader is referred to the appropriate references from the above list for more information.

- Obtain representative values of the compressive strength of the IGM, q_c. The most appropriate standard laboratory test for obtaining q_c is the unconsolidated, undrained triaxial compression test. In this test, the IGM can be considered as rock and tested under ASTM D2664, in which case q_c will be the compressive stress required to produce failure, or more precisely, the total principal stress difference at failure.[28] In the event that triaxial compression tests cannot be performed (for example, due to the lack of appropriate testing equipment), the next most suitable testing method is the unconfined compression test.[29] In this case, the value of q_c should be taken to be equal to q_u, the unconfined compression strength of the IGM core. Other laboratory strength tests may be substituted for the triaxial and unconfined compression tests (e.g., direct shear tests on short cores or triple-ring drive samples); however, it will be incumbent on the engineer to provide an appropriate conversion from the shear strength so obtained to q_c, considering the fundamental differences in the tests, location of bedding planes relative to maximum shear planes, and similar factors.

- The specimens chosen for compression testing should be selected so as to represent an average consistency from among the primary geomaterial in the cores or sample tubes and loaded to failure with the samples oriented vertically. Identification of the primary geomaterial can be accomplished through visual inspection of all of the samples recovered at a particular site. Any soft seams that are included within the matrix of stronger, primary IGM and that are recovered in the sampling process should be tested separately, where possible, by means of direct shear tests, torvane tests, or pocket penetrometer tests to obtain an approximate measure of the shear strength of such included materials. The total thickness of all soft seam materials, Σt_s, in the length of rock drilled, L_c, should also be measured, if possible.

If no direct measurement of seam material strength is possible, it will be conservative to estimate Σt_s to be $(1 - r)L_c$, where r is the recovery ratio, or "percent recovery" expressed as a ratio. In such a case, the thickness of all primary material, Σt_i, can be assumed to be rL_c. This information is to be used in equation 7 to compute the ratio E_m/E_i. E_m/E_i is then used in figure 6 (or in table 8, presented later in this section, which extrapolates figure 6 to lower values of E_m/E_i than are considered in figure 6) to compute the side resistance reduction factor β. β is then used in equation 6 to compute f_{max} for IGM's that are bedded with seams of softer materials

For purposes of computing E_m/E_i, the designer must also estimate E_i/E_s, in which E_i is the Young's modulus of the cores of the primary, intact geomaterial and E_s is the Young's modulus of the seam material, unless E_m is measured directly. E_i can be measured through standard techniques during the performance of the triaxial test as the initial slope of the stress-strain curve. The value obtained will probably be conservative if the sample is relatively undisturbed and possibly highly conservative (too small) if the core sample is disturbed. Although it is not common practice, E_s can possibly also be measured in the laboratory (if the seams are thick) through simple shear tests or other innovative laboratory tests. Often, however, such tests on seam

material will be virtually impossible to conduct and/or may be extraordinarily expensive, so that one of the following approximate approaches must be used.

- By far the most reliable approximate way to determine E_m/E_i is to measure E_i as noted above and then to conduct a loading test on a drilled shaft at the construction site. The test need not be conducted to failure, but enough load should be applied to obtain the initial (elastic) slope of the load-settlement relation. If the IGM profile is relatively uniform with depth, E_m can be related to the ratio of applied load (Q) to settlement (w) as indicated below. For a drilled shaft in a cohesive IGM with L/D = 10, $E_m = (0.13 - 0.33)\dfrac{Q}{wD}$. The smaller coefficient should be used when the q_u of the IGM is near the lower limit of 0.5 MPa, and the larger one used when q_u is near 5 MPa. Values intermediate between 0.13 and 0.33 should be used when IGM strengths are between the upper and lower limits. For other conditions (different L/D values, layered geomaterial), the reader may consult reference 30.

- If loading tests cannot be conducted during the design phase, representative samples of both the primary, intact geomaterial and the softer seam material can be tested for strength in the laboratory. For design purposes, E_i/E_s can be taken to be equal to $\dfrac{q_{ci}}{2s_{us}}$, where q_{ci} is the average compressive strength of the primary, intact geomaterial and s_{us} is the average undrained shear strength of the softer seam material. Use of this information will allow a reformulation of equation 7, as follows:

$$\frac{E_m}{E_i} = \frac{1}{\dfrac{q_{ci}}{2s_{us}}(1-r) + r} \quad , \quad r > 0 \quad . \tag{57}$$

- If loading tests cannot be conducted and if adequate samples of the primary, intact geomaterial are recovered for testing, but the softer seam material is not recovered, or is recovered but cannot be tested, which often occurs with IGM's, E_m/E_i can be estimated conservatively from table 7 based on RQD, the rock quality designation index, defined in equation 1. Table 7 is adapted from references 2 and 8. If the designer is in doubt about the condition of the joints (open or closed), the IGM should be assumed to have open joints. If RQD is less than 20 percent, the correlation with RQD should not be used. This method should be considered much less reliable than the previous method involving loading of drilled shafts and less reliable than the preceding method involving measurement of the shear strength of the soft seam material.

- Where the correlation in table 7 is not recommended (RQD < 20 percent), rational design cannot proceed according to this method. It is suggested that in such cases, more careful attempts should be made to sample the geomaterials to obtain the highest quality samples feasible, for example, with triple-wall core barrel samplers, and the RQD should be redetermined. If such an exercise is not successful, rational design can proceed only by making direct measurements of drilled shaft side and base resistances through full-scale loading tests to failure in order to measure f_{max} and q_{max} directly.[31] Discussion of the details of loading tests is beyond the scope of this report.

Table 7. Estimation of E_m/E_i based on RQD.

RQD (percent)	E_m/E_i	
	(closed joints)	(open joints)
100	1.00	0.60
70	0.70	0.10
50	0.15	0.10
20	0.05	0.05

Note: Values of E_m/E_i for RQD values between those shown can be estimated by linear interpolation on RQD.

It may also be possible to estimate E_m directly from diametrically loaded borehole jacks, self-boring pressuremeter tests (initial loading curves), or from the Menard pressuremeter test (reloading curves). It is expected, however, that moduli from such tests may be different from the operational E_m, since jacks and pressuremeters of standard size (75-mm diameter) do not stress a large enough volume of geomaterial to be truly representative of the mass as appropriate for drilled shaft analysis. Not enough information exists to confirm the validity of this approach, and it is not recommended at present.

Other methods for determining E_m directly that have not been verified in this research are the rigid plate load test method and the flexible plate load test method.[32, 33]

- Decide whether the IGM in which the drilled shaft is to be placed requires subdivision into sublayers for analysis. If the IGM is relatively uniform, the behavior of axially loaded drilled shafts can probably be simulated satisfactorily for design purposes as a uniform geomaterial using the simple direct procedure outlined in the following. If there is significant layering in the IGM in the depth range of the socket, a load transfer function analysis requiring the use of a digital computer model, for example, as described in reference 2, will be required. Development of inputs for such an analysis is detailed later in this chapter. "Significant layering" would exist if the IGM at the base of the socket is considerably stronger and stiffer than that surrounding the sides and/or if large changes in stiffness and strength of the IGM occur along the sides of

the socket. If L/D in the socket is less than 2 or greater than 20, load transfer function analysis should be conducted, as the direct method is not intended to be used outside of that range of L/D.

- Classify the surface of the borehole as "smooth" or "rough." Roughness can be quantified approximately by making electronic or mechanical caliper logs of the borehole and comparing the borehole wall profiles to the patterns expressed in table 1 or to RF, defined in equation 13. If RF exceeds 0.10, the borehole can be considered rough. Electronic borehole calipers are available commercially from many oil field service companies in diameters up to 2 m. Examples of such caliper logs will be shown in chapter 6. Measurements of the thickness of the smear zone can be made by sending personnel downhole inside safety casing after a borehole is completed to probe the side of the borehole at several locations with conical probes or similar devices, or to expose the non-smeared IGM by digging into the wall down to the undisturbed IGM, followed by measurement of the thickness of the smear zone with a scale. Downhole, sidehole mudcake samplers that are used to determine cake thickness in slurried boreholes can also sometimes be used to take sidewall samples in soft IGM's that can be returned to the surface for smear zone thickness measurements. It may be possible to use other downhole tools, such as specially fitted downhole cameras having attached distance probes, to observe both roughness and smear thickness beneath drilling fluids.

A rough borehole condition can be ensured by cutting or rifling a shear key pattern into the side of the borehole. When such procedures are not used, the borehole may or may not be rough. Since roughness and borehole disturbance are affected by the details of the interaction of the specific drilling tool (soil auger, rock-tooth auger, core barrel, etc.) with the IGM and the presence of free water during drilling, laboratory tests cannot be relied upon to provide the necessary information on roughness and smear. For boreholes that are not planned to be artificially roughened, information on the result of using a specific drilling technique on roughness in a particular geologic formation must be collected in one or more full-sized boreholes that are excavated at the construction site during the design phase of the project. Such full-sized excavations are currently recommended for observation of hole stability, water inflow, natural obstructions, and similar factors that might affect construction.[2] In geologic settings familiar to the designer, full-sized excavations for investigating constructability may become unnecessary after experience with sloughing, water inflow, and similar effects has been gained and has been routinely dealt with. Similarly, it is expected that rules can be developed over time from full-scale excavations with local drilling procedures made during the design phase and subsequent pre-construction trial shaft construction that indicate whether such procedures produce rough sockets, smooth sockets, or rough sockets with smear. Then, future designs can then proceed accordingly without full-sized excavations during the design phase for every project. General quantification of the effect of various drilling tools and procedures on borehole roughness in various types of geological formations is a subject for future

85

research. If there is any doubt in the designer's mind that the borehole will be "rough," it should be designed as if it were "smooth."

Calipering of every borehole and performing smear zone thickness measurements are not practical economically under production conditions, except on the largest of projects. However, these measurements may be used to verify the design assumptions on selected, representative shaft excavations or in situations in which geologic conditions or drilling procedures change during the course of a construction project.

- Note that end bearing (q_{max}) calculations require knowledge of the thickness and spacing of discontinuities in the IGM within about 2D beneath the base. If such discontinuities exist, and they are primarily horizontal discontinuities, equations 22 through 24 are appropriate for estimating q_{max}. If they are primarily vertical discontinuities, equations 25 through 27 are appropriate. Otherwise, if discontinuities are minimal or nonexistent (for example, core recovery of 100 percent and RQD > 90 percent), equation 16 can be used. It is usually not appropriate to estimate discontinuity parameters (spacing, thickness, etc.) from small-diameter cores. Instead, nearby cuts should be observed, full-sized excavations should be made with ensuing downhole measurement by personnel, or large-diameter cores (> 0.5 m diameter) should be recovered for measurement. The only alternative is to perform load tests on the IGM at the level of the base of the shaft (e.g., as described in references 32, 33, and 34), perform full-scale load tests on complete shafts, disregard end bearing in the design, or use conservative prescriptive end bearing values for which experience exists in the geological formation at the site.

- Estimate f_a, the apparent maximum average unit side shear at infinite displacement. Note that f_a is not equal to (is less than) f_{max}, which is defined at a deflection prescribed by the user in this method.

<u>Category 1 or 2 IGM, rough borehole</u>: Use:

$$f_a = c_r + \sigma_n \tan \phi_r \quad , \tag{58}$$

where c_r is the drained cohesion of the IGM, σ_n is the normal (horizontal) stress at the borehole wall before loading the shaft, and ϕ_r is the drained angle of internal friction for the IGM. Determination of σ_n is discussed in the following. Parameters c_r and ϕ_r can be evaluated by drained constant normal stress direct shear testing of the geomaterial.

If the IGM interface shear strength parameters are not known, use the following approximation:

$$f_a = \frac{q_u}{2} \quad . \tag{59}$$

Category 1 or 2 IGM, smooth borehole: Use

$$f_a = \alpha \, q_u \quad , \tag{60}$$

where α is a constant of proportionality that is determined from figure 34, based on the finite element simulations using the parameters outlined in table 6. The factor σ_p in figure 34 is the value of atmospheric pressure in the units employed by the designer. The maximum value of α that is permitted is 0.5. Figure 34 is based on the use of $\phi_{rc} = 30$ degrees, which is a value that was measured at a test site in clay-shale (chapter 5) that is believed to be typical of clay-shales and mudstones in the United States. If evidence indicates that ϕ_{rc} is not equal to 30 degrees, then α should be adjusted to:

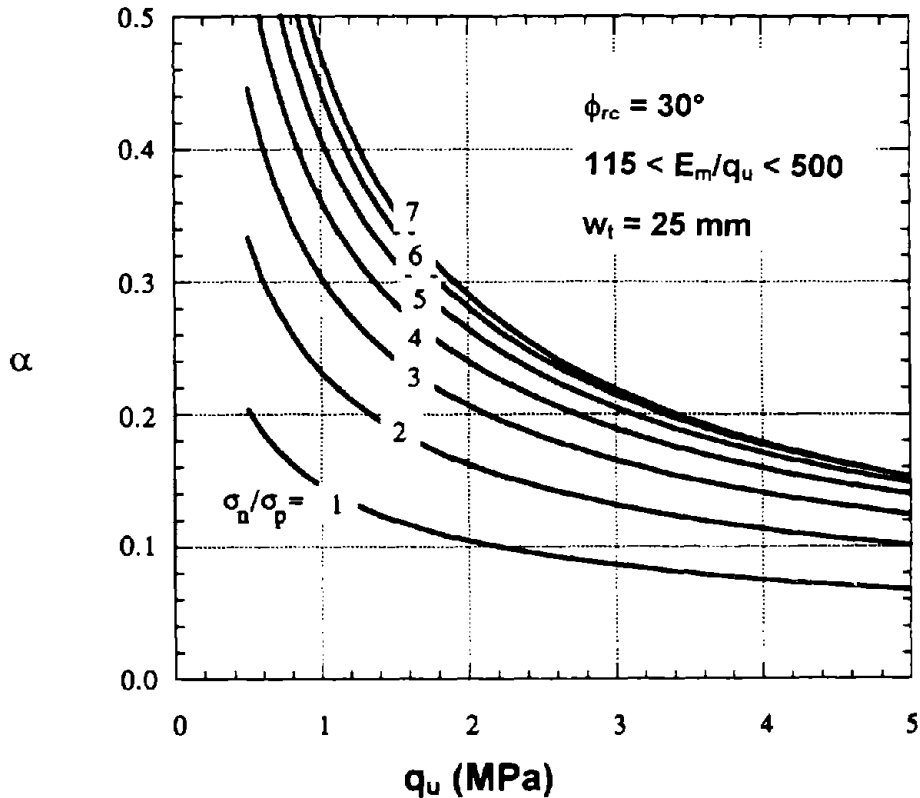$$\alpha = \alpha_{figure\,34} \, \frac{\tan \phi_{rc}}{\tan 30} \tag{61}$$

Figure 34. Factor α for smooth Category 1 or 2 IGM's.

Alternately, f_a can be set equal to f_{max} from equation 37 for Category 2 IGM's. The relevance of this equation has not been established for Category 1 IGM's. This approach also requires that split tensile tests be conducted on cores of the geomaterial.

- If E_m/E_i is < 1, adjust f_a for the presence of soft geomaterial within the IGM matrix using table 8. Define the adjusted value of f_a as "f_{aa}". This adjustment is based on research reported in reference 3.

Table 8. Adjustment of f_a for presence of soft seams.

E_m/E_i	f_{aa}/f_a
1.0	1.0
0.5	0.8
0.3	0.7
0.1	0.55
0.05	0.45

- Estimate σ_n, the normal stress between the concrete and borehole wall at the time of loading. This stress is evaluated at the time the concrete is fluid. If no other information is available, general guidance on the selection of σ_n can be obtained from figure 35, which is based on measurements of Bernal and Reese.[35] In figure 35:

$$M = \frac{\sigma_n}{\gamma_c z_c} \qquad , \tag{62}$$

in which γ_c is the unit weight of the concrete and z_c is the distance from the top of the completed column of concrete to the point in the borehole at which σ_n is desired, (usually the middle of the socket). The values in the legend are values of z_c. Figure 35 may be assumed valid if the rate of placement of concrete in the borehole exceeds 12 m/h and if the ratio of the maximum coarse aggregate size to borehole diameter is less than 0.02. Note that σ_n for slump outside the range of 125 to 225 mm is not evaluated. Unless there is information to support larger values of σ_n, the maximum value of z_c should be taken as 12 m in these calculations. This statement is predicated on the assumption that arching and partial setting will become significant after the concrete has been placed in the borehole for more than 1 hour.

Note that α decreases with increasing q_u in figure 35 for a given value of σ_n. As q_u increases, the normal stress and side shear at failure ($w_t = 25$ mm) increases due to the Poisson's effect, because E_m also increases with increasing q_u, producing higher values of side load transfer at the frictional interface. However, the increase in normal stress does not increase as rapidly as q_u increases; hence, the decreasing α. Furthermore, σ_n has a reduced effect as it increases because plastic conditions are produced in the IGM.

- Determine the "characteristic parameter" n, which is a fitting factor for the load-settlement syntheses produced by the finite element analyses. If the IGM socket is ROUGH:

$$n = \frac{\sigma_n}{q_u}$$

(63)

If the IGM socket is SMOOTH, estimate n from figure 36. Note that n was determined in figure 36 for $\phi_{rc} = 30$ degrees. However, it is not sensitive to the value of ϕ_{rc}. α, however, is sensitive to ϕ_{rc}, as indicated in equation 61.

- If the socket is:
  - Relatively uniform and the geomaterial beneath the base of the socket has a consistency equivalent to that of the geomaterial along the sides of the shaft,
  - $2 \leq L/D \leq 20, 0.5 \, m \leq D \leq 1.53 \, m$, and
  - $10 \leq E_c/E_m \leq 500$,
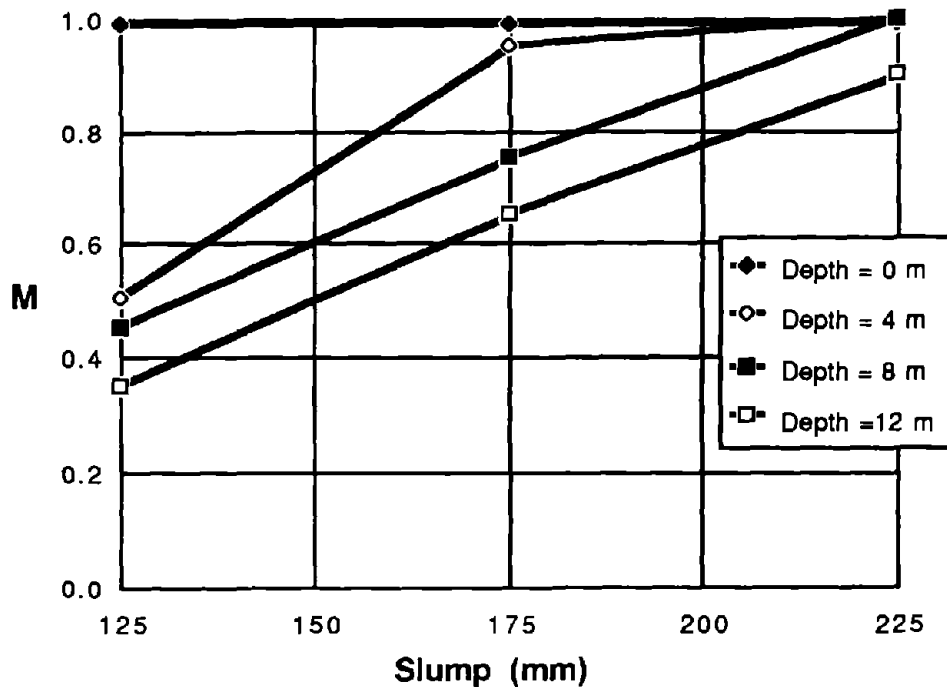
Figure 35. Factor M vs. concrete slump.

then compute the load-settlement relation for the IGM socket as enumerated in the following. Under the same general geometric and modulus conditions, if the socket is highly stratified and/or if the geomaterial beneath the base of the socket has a consistency different from that along the sides of the socket, use the unit load transfer function version of this method described later in this chapter. See figure 1 for geometric terms.

89
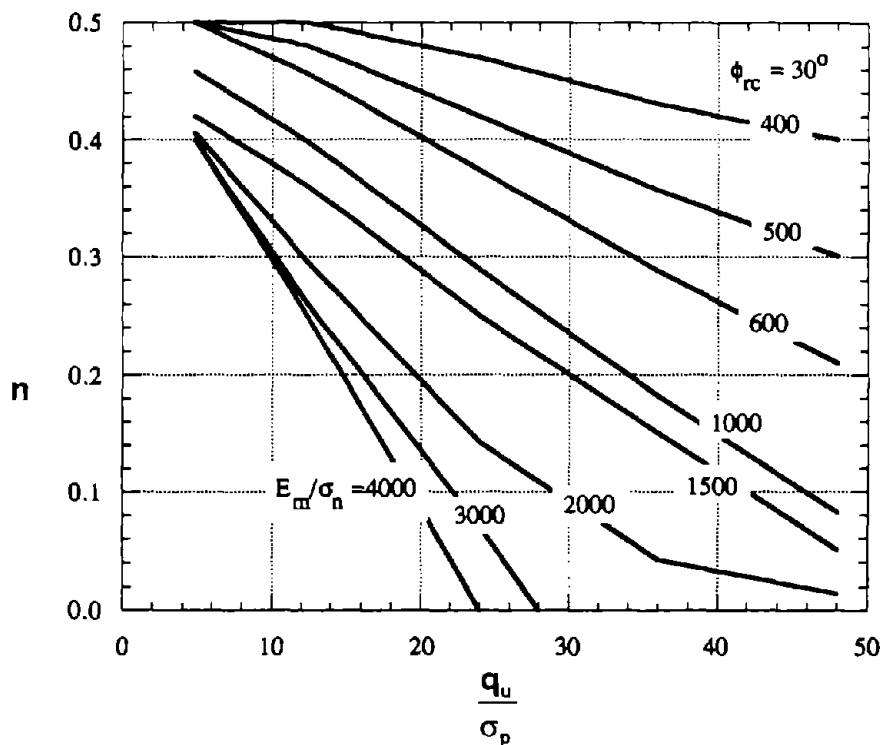
Figure 36. Factor n for smooth sockets for various combinations of parameters.

- Compute Q_t vs. w_t (settlement at top of socket) from equation 64 or equation 65, depending on the value of n. These equations apply to both rough and smooth sockets. Note that application of this method is best performed using a programmable calculator or a spreadsheet program.

$$Q_t = \pi DL\,\Theta_f\,f_{aa} + \frac{\pi D^2}{4}q_b\ , \qquad \Theta_f \leq n \quad .\tag{64}$$

$$Q_t = \pi DL\,K_f\,f_{aa} + \frac{\pi D^2}{4}q_b\ , \qquad \Theta_f > n \quad .\tag{65}$$

Equation 64 applies in the elastic range before any slippage has occurred at the shaft-IGM interface; and elastic base resistance, as represented by the last expression on the right-hand side of the equation, also develops. Equation 65 applies during interface slippage (nonlinear response). In order to evaluate Q_t, a value of w_t is selected, and Θ_f, which is a function of w_t, is evaluated before deciding upon which equation to use. If $\Theta_f > n$, evaluate K_f and use equation 65; otherwise, use equation 64. Equations 66 and 67 are used to evaluate Θ_f and K_f, respectively.

$$\Theta_f = \frac{E_m \Omega}{\pi L \Gamma f_{aa}} w_t \qquad (66)$$

$$K_f = n + \frac{(\Theta_f - n)(1 - n)}{\Theta_f - 2n + 1} \leq 1 \quad , \qquad (67)$$

in which

$$\Omega = 1.14 \left(\frac{L}{D}\right)^{0.5} - 0.05 \left[\left(\frac{L}{D}\right)^{0.5} - 1\right] \log_{10}\left(\frac{E_c}{E_m}\right) - 0.44 \quad \text{, and} \qquad (68)$$

$$\Gamma = 0.37 \left(\frac{L}{D}\right)^{0.5} - 0.15 \left[\left(\frac{L}{D}\right)^{0.5} - 1\right] \log_{10}\left(\frac{E_c}{E_m}\right) + 0.13 \quad . \qquad (69)$$

Finally,

$$q_b = \Lambda \, w_t^{0.67} \quad , \qquad (70)$$

in which

$$\Lambda = 0.0134 E_m \frac{\left(\frac{L}{D}\right)}{\left(\frac{L}{D} + 1\right)} \left\{ \frac{200 \left[\left(\frac{L}{D}\right)^{0.5} - \Omega\right]\left[1 + \frac{L}{D}\right]}{\pi L \Gamma} \right\}^{0.67} \qquad (71)$$

- Check the values computed for q_b. If sample recovery in the IGM surrounding the base is 100 percent, q_b should not exceed $q_{max} = 2.5 \, q_u$. At the discretion of the designer, if core recovery is less that 100 percent, equations 22 through 24 or the method of Carter and Kulhawy (chapter 2) may be used to establish q_{max}. At working load, q_b should not exceed $0.4 \, q_{max}$.

- Select other values of w_t and graph the load-settlement curve resulting from the computations. Select ultimate and service limit resistances based on settlements. For example, the ultimate resistance might be selected as the load Q_t, corresponding to a settlement w_t of 25 mm; while the service limit resistance might be selected as the load Q_t, corresponding to a value of $w_t < 25$ mm.

Commentary on direct load-settlement simulation method

This method is intended for use with relatively ductile IGM's, in which deformations occur in asperities prior to shear. If the IGM is friable or unusually brittle, the method may be unconservative, and appropriate loading tests should be conducted to ascertain the behavior of the drilled shaft for design purposes. The method is also intended for use with drilled shafts in IGM's that are produced in the dry. If it is necessary to produce the shaft using water, or with mineral or synthetic drilling slurries, the shaft should be treated as "smooth" for design purposes unless it can be proved that "rough" and "unsmeared" conditions apply. The method also carries the assumption that the bearing surface at the base of the socket is clean, such that the shaft concrete is in contact with undisturbed IGM. If base cleanliness cannot be verified during construction, base resistance (q_b) should be assumed to be zero.

The design examples did not consider the effect of placing concrete underwater. This effect can be handled by computing σ_n, assuming that the unit weight of the concrete below the water table is its buoyant unit weight from:

$$\sigma_n = M(\text{figure 35})\left[\gamma_c \, z_w + \gamma'_c (z_c - z_w)\right] \quad , \tag{72}$$

in which γ'_c = buoyant unit weight of the concrete and z_w = depth from top of concrete to elevation of water table. An exception to this, described later, occurs if the concrete is placed in the dry below the water table and the water-bearing formation is cased off during concreting. In this case, the concrete is not treated as buoyant.

Example calculations for direct load-settlement simulation method

Example 1. Rough socket

Consider the example shown in figure 37. Compute the load-settlement relation for the socket, and estimate the ultimate resistance at a settlement, w_t, = 25 mm.

1. Since the core recovery is high, assume $E_m = 115 \, q_u$. Note that $E_c/E_m = 100$.

2. $f_{aa} = f_a = 2.4 / 2 = 1.2$ MPa, or 1200 kPa (equation 59).

3. $z_c = 6.1$ m (depth from top of concrete to middle of socket). Considering concrete placement specifications, $\sigma_n = 0.92 \, \gamma_c \, z_c$, from figure 35, or $0.92 \, (20.4) \, (6.1) = 115$ kPa = $1.14 \, \sigma_p$.

4. $n = 115$ kPa / 2400 kPa = 0.048 (equation 63).

5. $L/D = 6.1 / 0.61 = 10$.

6. $\Omega = 1.14 \, (10)^{0.5} - 0.05[(10)^{0.5} - 1]\log 100 - 0.44 = 2.94$ (equation 68).
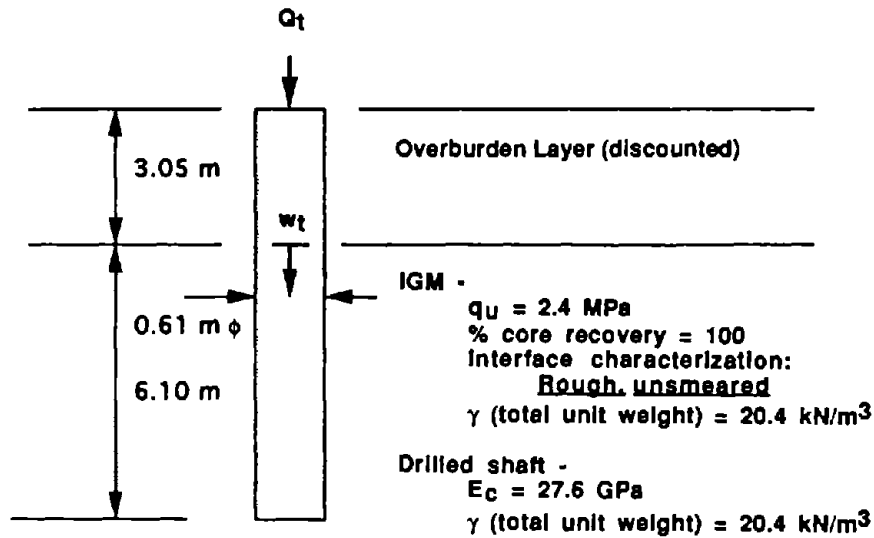
Figure 37. Example 1 for direct method, Model 1.

7. $\Gamma = 0.37 (10)^{0.5} - 0.15[(10)^{0.5} - 1]\log 100 + 0.13 = 0.651$ (equation 69).

8. $\Theta_f = \{[115 (2400) 2.94]/[3.14 (6100 \text{ mm})(0.651) 1200]\} w_t = 0.0542 w_t$ (equation 66).

9. $K_f = 0.048 + (0.0542 w_t - 0.048) (1 - 0.048) / (0.0542 w_t - 0.096 + 1) =$
   $= 0.048 + (0.0542 w_t - 0.048) (0.952) / (0.0542 w_t + 0.904)$ (equation 67).

10. At the end of the elastic stage, $\Theta_f = n$ (implied by equation 64), therefore,
    $w_{te} = n / \Theta = 0.048 / 0.0542 = 0.88$ mm, where w_{te} signifies w_t at the end of the elastic stage. (Note that elastic response occurs only up to a very small settlement in this example.)

11. $q_b = \Lambda w_t^{0.67}$ (equations 70 and 71) $= \{0.0134[(115) (2400) (10/11)]\} \{[200 (10^{0.5} - 2.94) (11)] / [3.14 (6100) 0.651]\}^{0.67} w_t^{0.67} = 383.7 w_t (\text{mm})^{0.67} (\text{kPa})$. ($\Lambda = 383.7$.)

12. $\pi D L = 11.7 \text{ m}^2$; $\pi D^2/4 = 0.2922 \text{ m}^2$.

13. Compute Q_t corresponding to w_{te}, signified by Q_{te}:

$Q_{tc} = 11.7 \, (0.0542) \, (0.88) \, (1200) + (0.2922) \, (383.7) \, (0.88)^{0.67} = 670 + 103 = 773 \text{ kN}$
(equations 64, 70, 71).

Note that at this point, 670 kN is transferred to the IGM in side resistance and 103 kN is transferred in base resistance. (Q_{tc}, w_{tc}) is a point on the load-settlement curve, and a straight line can be drawn from $(Q_t = 0, w_t = 0)$ to this point.

14. Compute the values of Q_t for selected values of w_t on the nonlinear portion of the load-settlement curve. Numerical evaluations are made in table 9.

Table 9. Computations for nonlinear part of load-settlement curve, example 1.

(1)	(2)	(3)	(4)	(5)	(6)	(7)
			$Q_s =$	$q_b =$	$Q_b =$	$Q_t (kN)$
w_t	Θ_f	K_f	$\pi DLK_f f_{aa}$	$\Lambda w_t^{0.67}$	$(\pi D^2/4)q_b$	$=$
(mm)	$= 0.0542 \, w_t$	(Step 9)	(kN)	(kPa)	(kN)	(4) + (6)
5	0.271	0.229	3210	1128	330	3540
10	0.542	0.373	5232	1795	524	5756
15	0.813	0.472	6621	2355	688	7309
25	1.355	0.599	8402	3316	969	9371

Note that q_b at $w_t = 25$ mm $= 3.32$ MPa $= 1.38 \, q_u < q_{max} = 2.5 \, q_u$, OK for definition of ultimate resistance. Based on base resistance, working load should be limited to $q_b = q_u$, or w_t should be limited to about 12 mm at working load. Note also that the compressive stress in the shaft at $w_t = 15$ mm is 25 000 kPa (7309 kN / cross-sectional area), which may be approaching the structural failure load in the drilled shaft. Refer to reference 2 for further information on structural considerations.

15. The numerical values from Steps 13 and 14 are graphed in figure 38. Also shown on that figure is the finite element solution for the same problem and other finite element and design method solutions for the same socket, showing the effects of both E_m/q_u and E_c/E_m on the solution.

The physical significance of the parameters Θ_f and K_f is evident from the numerical solution. Θ_f is a proportionality constant for elastic resistance for side shear, and K_f is a proportionality parameter for actual side shear, including elastic, plastic, and interface slip effects.

Example 2. Smooth socket

Consider the same problem as above, but with a smooth (or rough-smeared) interface. Estimate that $\phi_{rc} = 30$ degrees. The calculations proceed as per example 1, except for the

94

following:

1. $f_a = f_{aa} = \alpha\, q_u$.
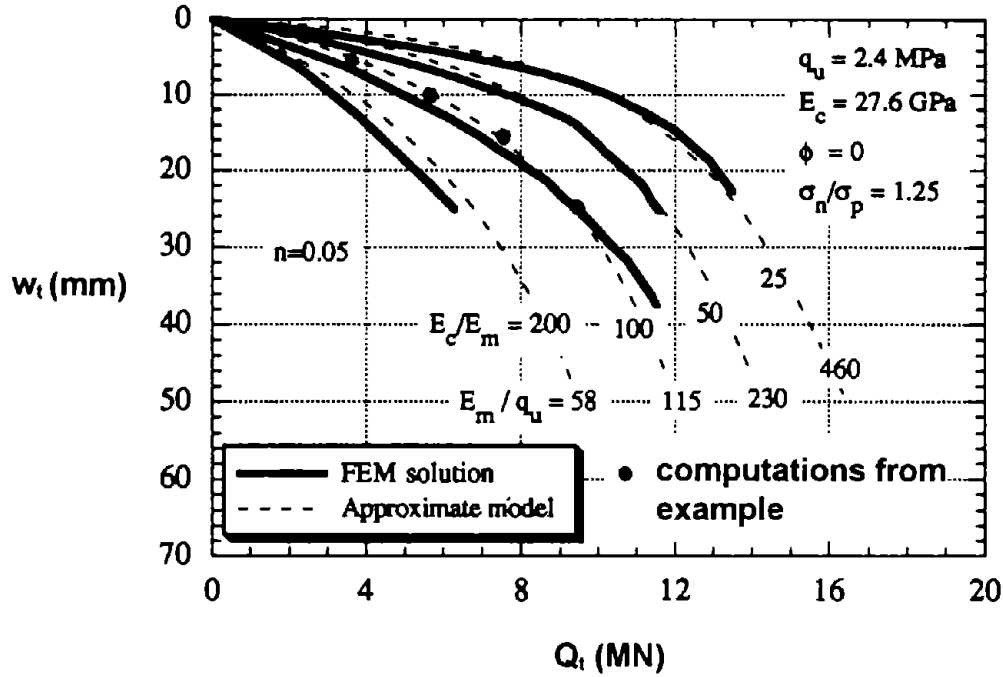
Figure 38. Load-settlement relationship for example 1.

2. Referring to figure 34, for $\sigma_n/\sigma_p = 1.14$ and $q_u = 2.4$ MPa, $\alpha = 0.12$.

3. $f_a = f_{aa} = 0.12\,(2400) = 288$ kPa.

4. $q_u / \sigma_p = 2400 / 101.3 = 24;\ E_m / \sigma_n = 115\,(2.4)\,(1000) / 115 = 2400$.

5. From figure 36, $n = 0.11$.

6. $\Omega = 2.94$ (unchanged); $\Gamma = 0.651$ (unchanged).

7. $\Theta_f = \{[115\,(2400)\,2.94]/[3.14\,(6100\ \text{mm})(0.651)\,288]\}\ w_t = 0.226\ w_t$ (equation 66).

8. $K_f = 0.11 + [(0.226\ w_t - 0.11)(1 - 0.11)]/[0.226\ w_t - 2\,(0.11) + 1] = 0.11 + (0.226\ w_t - 0.11)(0.89)/(0.226\ w_t + 0.78)$.

9. At $\Theta_f = n$, $w_{te} = 0.11/0.226 = 0.487$ mm.

10. $q_b = 383.7\ w_t\,(\text{mm})^{0.67}\,(\text{kPa})$ (equations 70 and 71) (unchanged).

11. $Q_{te} = 11.7 (0.226) (0.487) (288) + (0.2922) (383.7) (0.487)^{0.67} = 371 + 69 = 440$ kN (equation 64).

12. $Q_{te} = 440$ kN, $w_{te} = 0.487$ mm is the point at the end of the linear portion of the load-settlement curve.

13. Compute the values of Q_t for selected values of w_t on the nonlinear portion of the load-settlement curve. Numerical evaluations are made in table 10.

14. The numerical values for example 2 are graphed in figure 39 in comparison with the values from example 1 to illustrate the effect of borehole roughness in this problem.

Table 10. Computations for nonlinear part of load-settlement curve, example 2.

(1) w_t (mm)	(2) Θ_f $= 0.226\ w_t$	(3) K_f (Step 8)	(4) $Q_s =$ $\pi DLK_f f_{aa}$ (kN)	(5) $q_b =$ $\Lambda w_t^{0.67}$ (kPa)	(6) $Q_b =$ $(\pi D^2/4)q_b$ (kN)	(7) Q_t (kN) $=$ (4) + (6)
5	1.13	0.585	1971	1128	330	2301
10	2.26	0.739	2490	1795	524	3014
15	3.39	0.810	2729	2355	688	3417
25	5.65	0.877	2955	3316	969	3924

Note again that $q_b < 2.5\ q_u$.

Simulation by load transfer function analysis

The direct simulation method in the preceding section is easy to use and is appropriate for relatively uniform IGM conditions. In some cases, the designer may wish to use a load transfer function analysis, as described in reference 2. This is a numerical method that requires the use of unit load transfer relations, or nonlinear Winkler stiffness bodies between the concrete and the IGM, sometimes referred to as "t-z" and "q-z" curves. The terms "f-w" and "q_b-w_b" relations will be used here. Computer software not described in this report is required to execute the load transfer function (LTF) analysis.

This approach to design may be appropriate whenever the socket is very short (L/D < 2) or very long (L/D > 20); where there is strong layering in the formation, including a hard layer at the base of the socket; or where part of the socket is artificially roughened and part is smooth or smeared. The f-w and q_b-w_b relations must be constructed before an LTF analysis can proceed. A methodology for constructing these relations is outlined in the following. Note that the method for constructing LTF relations given below actually

produces load and settlement information for the layered IGM socket, which may be sufficient for design purposes without a full LTF analysis.
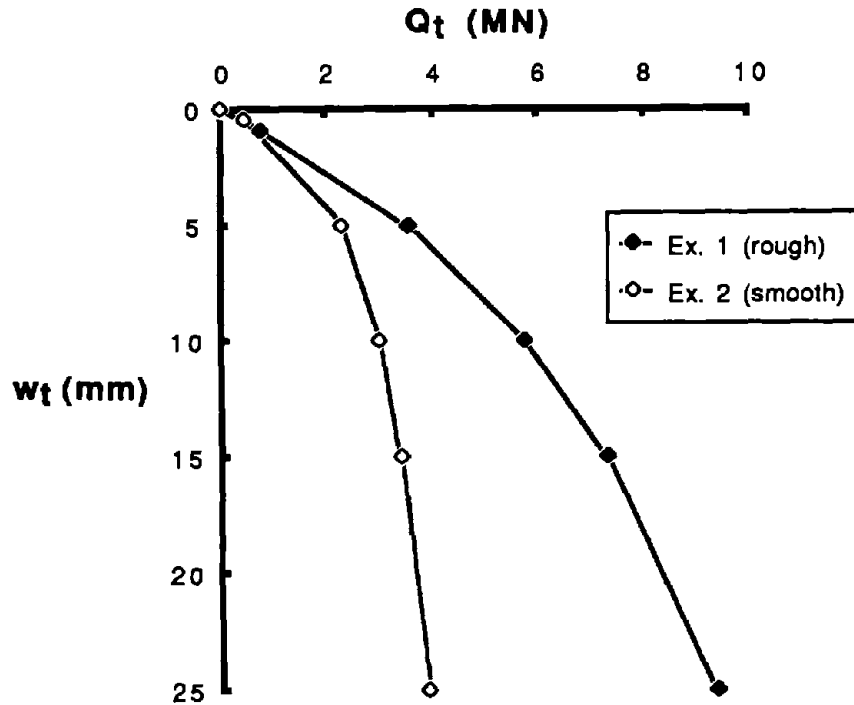
Figure 39. Comparison of solutions from examples 1 and 2.

Construction of f-w and q_b-w_b relations

General procedure

Construction of the unit load transfer relations uses the following approximate procedure:

- Compute weighted averages of E_m and f_{aa} along the sides of the socket, as follows. Refer to figure 40. Begin by computing f_a for each layer k according to equation 59 or 60, as appropriate, reducing f_a to f_{aa} using table 8 or other appropriate means if necessary.

$$E_m \text{ (weighted avg.)} = \frac{\sum_{k=1}^{N} E_{mk} L_k}{\sum_{k=1}^{N} L_k} \quad , \qquad (73)$$

97

$$f_{aa} \text{ (weighted avg.)} = \frac{\sum\limits_{k=1}^{N} f_{aak} L_k}{\sum\limits_{k=1}^{N} L_k} \quad , \tag{74}$$

in which k is the layer number, L is the layer thickness, and N is the total number of layers.

• Compute Ω from equation 68, Γ from equation 69, followed by the average Θ_f for the socket from equation 66.

• Determine n for each separate layer k using equation 63 in rough layers and using figure 36 in layers that are classified as smooth. Then, compute the weighted average value of n along the socket using equation 75.

$$n(\text{weighted avg.}) = \frac{\sum\limits_{k=1}^{N} n_k L_k}{\sum\limits_{k=1}^{N} L_k} \quad . \tag{75}$$

• Determine whether side load transfer is in the linear range by comparing the average Θ_f to n(weighted avg.). Select any value of w_t and then compute the average mobilized value of unit side load transfer f by using either equation 76 or 77, as appropriate:

$$f = \Theta_f \, f_{aa} \text{ (weighted avg.)} \quad , \Theta_f \leq n \quad , \tag{76}$$

$$f = K_f \, f_{aa} \text{ (weighted avg.)} \quad , \Theta_f > n \tag{77}$$

• Compute q_b according to equations 70 and 71, using E_m as the value appropriate for the layer on which the base bears.

• Compute the mean side resistance, base resistance, and total resistance:

$$Q_s = \pi D \sum\limits_{k=1}^{N} L_k \, f \quad , \tag{78}$$

$$Q_b = \frac{\pi D^2}{4} q_b \quad , \tag{79}$$

$$Q_t = Q_s + Q_b \quad . \tag{80}$$

98

- Assume temporarily a linear load distribution along the shaft and calculate the local settlements at the base of the shaft, w_b, and at the middle of each kth layer, w_k from equations 81 and 82.

$$W_b = W_t - \left[\frac{2(Q_t + Q_b)L}{\pi E_c D^2} \right] \quad , \tag{81}$$

$$W_k = W_t - \frac{z_k}{L}(W_t - W_b) \tag{82}$$

In the above equations, L is the total length of the socket and z_k is the distance from the top of the socket to the middle of layer k.

- Determine the value of f mobilized in each layer (f_k) at settlement w_k. First, compute Θ_{fk} and K_{fk} for each layer k from equations 66 and 67, substituting $f_{aa\,k}$ for f_{aa} and w_k for w_t. Then:

$$f_k = \text{minimum of } \Theta_{fk} f_{aak} \text{ and } K_{fk} f_{aak} \tag{83}$$

- Since the relations must be developed using several points, each determined through repeating this procedure with different values of w_t, a presuperscript i will be used to denote the point number. $^i q_b$, $^i w_b$ is a point on the unit load transfer curve for the base, and $^i f_k$, $^i w_k$ are points on the unit load transfer curves for each layer k along the shaft.

- Additional values of w_t are chosen and the computations are repeated to develop the complete unit load transfer curves for each layer and for the base. The process is illustrated in the following example.

Example 3. Unit load transfer function formulation

Consider the socket shown in layered IGM in figure 40. Construct f-w and q_b-w_b relations for this socket for later use in a unit load transfer function analysis. $E_c = 27.6$ GPa.

- E_m (weighted avg.) = $[115(2.4)(3.05) + 115(1.0)(3.05)]/6.1 = 195.5$ MPa.

- $f_{a1} = f_{aa1} = q_{u1}/2 = 2.4/2 = 1.2$ MPa (rough socket).

- $f_{a2} = f_{aa2} = \alpha \, q_{u2}$ (smooth socket).

To determine α, first compute σ_n:

At middle of layer 2, $z_2 = 3.05 + 3.05 + 1.525 = 7.625$ m. From figure 35, M = 0.79. $\sigma_n = 0.79(20.4)(7.625) = 123$ kPa (equation 62). $\sigma_n/\sigma_p = 123 / 101.3 = 1.21$. From figure 34, $\alpha = 0.16$ for $q_u = 1.0$ MPa.

- $f_{aa2} = 0.16(1.0) = 0.16$ MPa.

- f_{aa}(weighted avg.) = $[1.2(3.05) + 0.16(3.05)] / 6.1 = 0.68$ MPa = 680 kPa.

- $\Omega = 1.14(10)^{0.5} - 0.05[10^{0.5} - 1] \log[27600/195.5] - 0.44 = 2.93$.

- $\Gamma = 0.37(10)^{0.5} - 0.15[10^{0.5} - 1]\log[27600/195.5] + 0.13 = 0.603$.

- $\Theta_f = [195.5 \ (2.93)] / [\pi \ (6.1) \ (0.603) \ (680)] \ w_t = 0.0729 w_t$ (equation 66). Note that this is an average value for the socket as a whole.
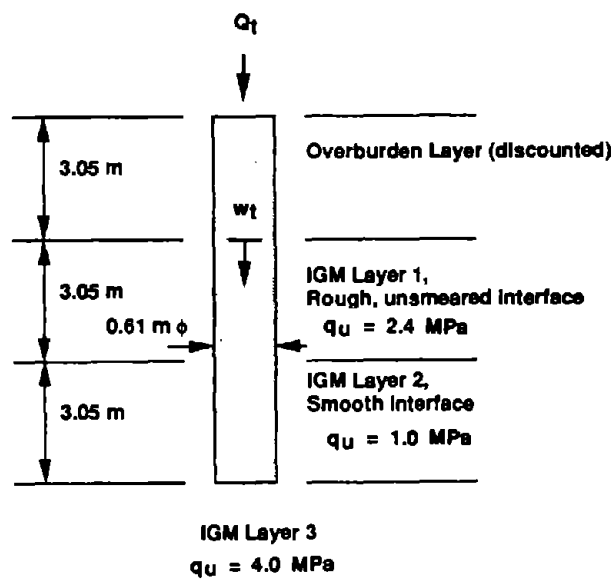
Figure 40. Example 3 for unit load transfer method, Model 1.

- Compute n values for each layer:

  Layer 1: $n_1 = \sigma_{n1} / q_{u1}$
  M (figure 35) at $z_1 = 4.575$ m = 0.94. $\sigma_{n1} = 0.94(20.4)(4.575) = 87.7$ kPa (equation 62). $n_1 = 87.7/2400 = 0.0366$.

  Layer 2: M (figure 35) at $z_2 = 7.625$ m = 0.78. $\sigma_{n2} = 123$ kPa. Use figure 36. $q_{u2}/\sigma_p = 1000/101.3 = 9.9$. $E_{m2}/\sigma_{n2} = 115(1000)/123 = 935$. Read $n_2 = 0.42$.

100

- n (weighted avg.) = [0.0366(3.05) + 0.42(3.05)]/6.1 = 0.228.

- The preceding steps do not vary from point to point on the unit load transfer curves, so the parameters need to be computed only once for any given problem. The following computations need to be made separately for each point on the unit load transfer curves.

- ★ Select any value of w_t. In this case, $w_t = 2.0$ mm will be selected. Then, compute the approximate settlements for the middle elevations of the layers along the sides of the socket and for the base. This is accomplished by determining approximately the elastic compression in the socket and subtracting the compression between the top of the socket and points of interest to obtain w values on the unit load transfer curves, as follows. The following steps can be avoided if it is assumed that the settlement along the socket and at its base is equal to the settlement at the top of the socket, that is, that the socket is rigid under load. While this is often acceptable for drilled shafts in soils, it is usually not acceptable in IGM's, because the elastic compression of the drilled shaft will be considerable unless the shaft is overdesigned structurally with respect to axial loading.

- Θ_f (avg.) = 2.0(0.0729) = 0.1458 < 0.228, so that elastic behavior can be assumed for average computations.

- f (avg.) = 0.1458 (680) = 99.1 kPa.

- Compute $q_b = \Lambda\, w_t^{0.67}$, evaluating Λ as per equation 71:

  $\Lambda = 0.0134\, E_m(\text{base})\, [10/(10 + 1)]\, [200(10^{0.5} - 2.93)\, (11)] / \pi\, (6100)\, 0.603]^{0.67}$
  $= 0.00151\, E_m(\text{base}) = 0.00151\, (115)\, (4000) = 693\ \text{kPa mm}^{0.33}$.
  $q_b = 693\, (2)^{0.67} = 1103\ \text{kPa}$.

- $Q_s = \pi DL\, (99.1) = 11.7\, (99.1) = 1158\ \text{kN}$.
  $Q_b = [\pi D^2/4]\, (1103) = 0.2922\, (1103) = 322\ \text{kN}$.
  $Q_t = 1158 + 322 = 1480\ \text{kN}$.

- Assuming a linear distribution of load along the drilled shaft, compute base settlement, then settlements at the middle elevations of the two layers along the socket.

  $w_b = 2.0 - [2(1480 + 322)\, 6100]/[\pi\, (27,600,000)\, (0.61)^2]$ (equation 81)
  $= 2.0 - 0.000112\, (6100) = 1.32$ mm. (Compare with 2.0 mm at top of socket.)

  w_1 (middle) = 2.0 - [1.525/6.1] (2.0 - 1.32) = 1.83 mm (equation 82).
  w_2 (middle) = 2.0 - [4.575/6.1] (2.0 - 1.32) = 1.49 mm (equation 82).

- (If rigid behavior of the socket is assumed, computations should resume here.) Compute the values of load transfer in the two layers along the side for this point (point 1) on the unit load transfer curves.

$^1\Theta_{f1} = 0.0729\,(1.83) = 0.136 > n_1 = 0.0366$. Side shear response is not linear, so compute K_f. $^1K_{f1} = 0.0366 + [(0.133 - 0.0366)(1 - 0.0366)]/[0.133 - 0.0732 + 1] = 0.124$ (equation 67).

$^1f_1 = 0.124\,(1200) = 149$ kPa (equation 77).

$^1\Theta_{f2} = 0.0729\,(1.49) = 0.109 < n_2 = 0.42$, so

$^1f_2 = 0.107\,(160) = 17.4$ kPa.

- First (non-zero) points on the unit load transfer curves are:

$^1f_1 = 149$ kPa, $^1w_1 = 1.83$ mm;
$^1f_2 = 17.4$ kPa, $^1w_2 = 1.49$ mm;
$^1q_b = 1103$ kPa, $^1w_b = 1.32$ mm.

The process then repeats from the point of the ★(on previous page) to this point. The calculations for several other points are summarized in table 11. Note that it is necessary to compare Θ_f for each layer and for each assumed value of w_t to the value of n for the layer to determine whether to compute $f = \Theta_f\,w_t$ or $f = K_f w_t$. Observe in table 11 that, in addition to the socket load-settlement relation, the distribution of load between the various layers along the shaft and the base at various values of settlement are produced by this process. Since this is normally the objective of a load transfer function analysis, further computations may not be required. However, if the designer wishes to model the load-settlement behavior of the socket considering small changes in shaft diameter, composite concrete modulus, and IGM layer thickness, the unit load transfer curves derived from this process can be reasonably assumed to be appropriate. Thus, the load transfer function analysis can be used to optimize the design. The final f-w and q_b-w_b curves for use in a load transfer function analysis are plotted in figures 41 and 42, respectively. The performance of the load transfer analysis itself is beyond the scope of this report.

MODEL 2 (Category 3 IGM's)

For Category 3 IGM's (dense, granular decomposed rock or granular glacial till), the method of Mayne and Harris (outlined in chapter 2) is recommended, with one exception. Based on recent studies by Majano et al., good practice in slurry construction appears to yield an angle of wall friction of about 0.75 ϕ'.[36] Therefore, equation 44 is modified to give $f_{max} = K_o \tan(0.75\phi')\,\sigma'_{vo}$ for cases where drilling fluid meeting acceptable specifications for good practice is used to drill the borehole.[2] Otherwise, computations for the Mayne-Harris method are prescribed in equations 41 through 54. Concrete pressures are not used in the computations, as with Model 1. It is assumed with this

102

method, however, that fluid concrete is used and placement occurs rapidly enough that K_o conditions are maintained in the ground. The method is demonstrated by the example problem that follows. This method produces a three-branched load-settlement curve that culminates in a plunging resistance for the socket. Where possible, the correlations should be calibrated to load tests in specific geological formations.

Table 11. Summary of computations for unit load transfer curves, example 3.

Parameter Point No.	1	2	3	4
w_t (mm)	2.0	5.0	15.0	25.0
$\Theta_f = 0.0729\ w_t$	0.1458	0.3645	1.094	1.823
K_f	N/A	0.344	0.636	0.748
f(avg.) (kPa)	99.1	234	432	501
q_b (kPa) $= \Lambda\ w_t^{0.67}$	1103	2037	4253	5989
Q_s (kN)	1158	2735	5054	5953
Q_b (kN)	322	595	1243	1750
Q_t (kN)	1480	3330	6297	7703
w_b (mm)	1.32	3.51	12.15	20.77
w_1 (mm)	1.83	4.63	14.29	23.94
w_2 (mm)	1.49	3.88	12.86	21.83
Θ_{f1}	0.133	0.338	1.042	N/A
K_{f1}	0.124	0.266	0.492	0.653
Θ_{f2}	0.109	0.283	0.938	N/A
K_{f2}	N/A	N/A	0.693	0.808
f_1 (kPa)	149	319	590	783
f_2 (kPa)	17.4	45.3	111	129

Warning: $f_c = 26.4$ MPa at $w_t = 25$ mm. Structural failure imminent.
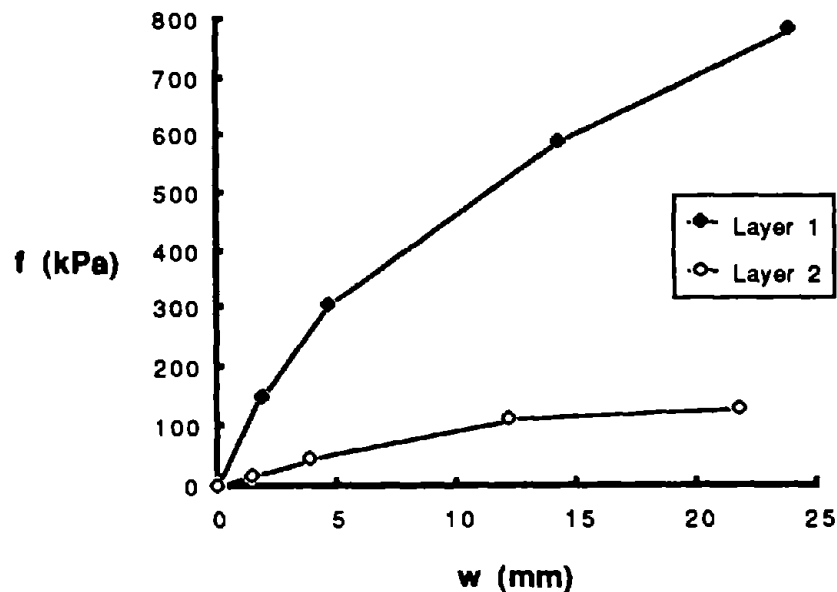
Figure 41. f-w curves for example 3.
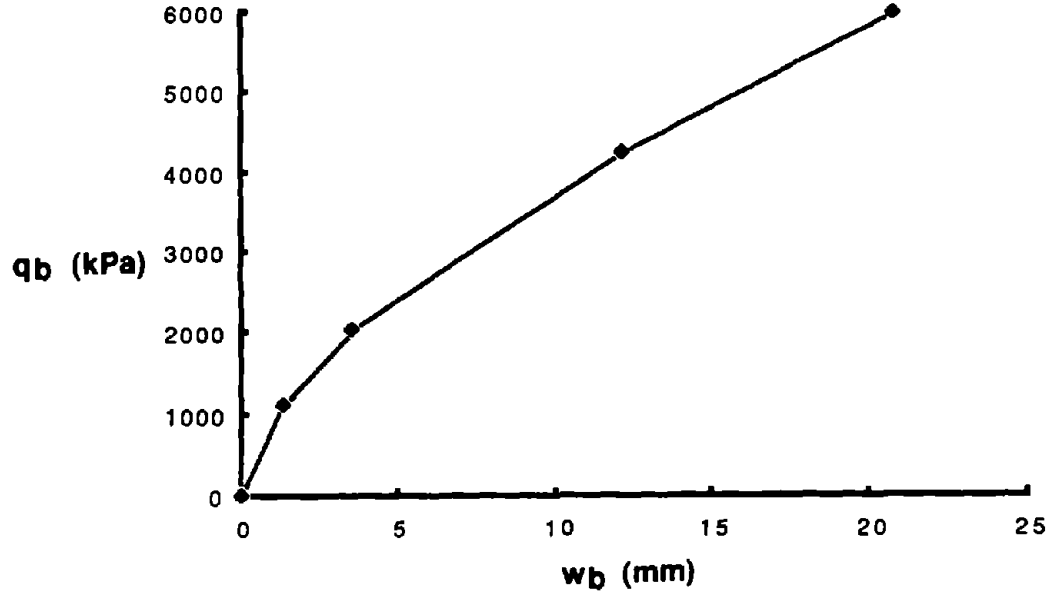
Figure 42. q_b-w_b curve for example 3.

Example 4. Model 2 for Category 3 IGM's

Consider the socket for the drilled shaft in figure 43. Calculations for the geomaterial load transfer factors proceed as shown in table 12. The following calculations are also made:

- q_{max} (base) = 9.33 (0.23) (230) $(8.78)^{0.80}$ = 2806 kPa (equations 46 and 47).

- Assessment of moduli:

E_s (layer 1) = 22 (101) $75^{0.82}$ = 76 600 kPa (equation 49).
E_s (layer 2) = E_{sL} = 22(101) $90^{0.82}$ = 89 000 kPa (equation 49).
E_{sm} (avg.) = [6.1(76 600) + 3.05(89 000)]/9.15 = 80 700 kPa.
E_b = 22(101)$100^{0.82}$ = 97 000 kPa (equation 49). Modify as per p. 34: E_b = E_{sL} / 2.5
= 35 800 kPa, using ξ = 2.5 (empirical correction).

- Preliminary parameters for computing influence factor I, as per pages 33 and 34:

L/D = 9.15 / 0.915 = 10.
λ = 2(1+0.4) [27,600,000/89,000] = 868.
ζ = ln {[0.25 + (2.5(80,700/89,000)(1-0.4) - 0.25)2.5]20} = 4.10.
μL = 2[2/(4.10)(868)]$^{0.5}$ (10) = 0.474.
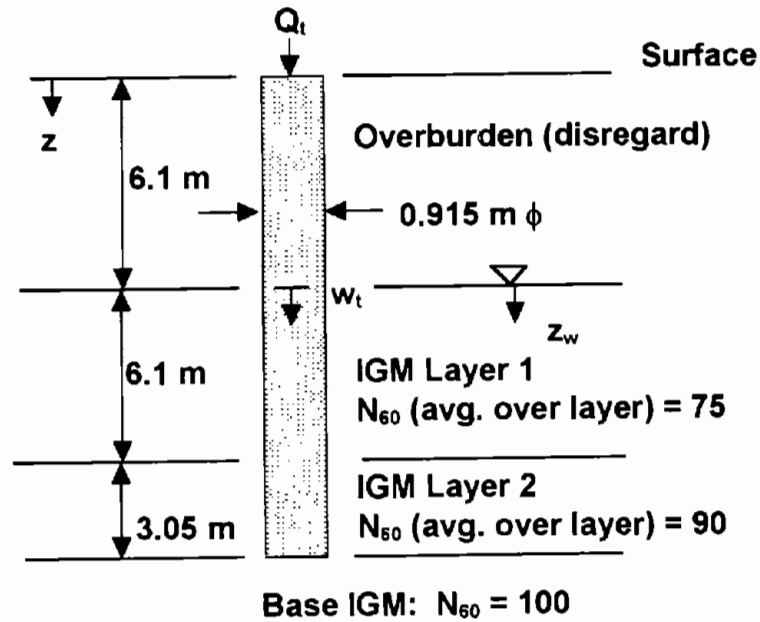
104

Figure 43. Conditions for example 4.

Table 12. Numerical computations for load transfer factors, example 4.

Layer	N_{60} (B/0.3 m)	σ'_p (eq. 41) (kPa)	σ'_{vo} in middle of layer = $\gamma z - \gamma_w z_w$ (kPa)	OCR (eq. 42)	σ'_{vo}/σ_p	ϕ' (deg.) (eq. 43)	K_o (eq. 45)	f_{max} (kPa) (eq. 44)
1	75	1515	162	9.35	1.60	50.0	1.30	162
2	90	1818	213	8.54	2.11	49.8	1.21	197
Base	100	2020	230	8.78	-	-	-	-

Note: f_{max} is computed using $\underline{0.75\phi'}$ due to construction under drilling slurry.

• Compute the influence coefficient, I, according to equation 50:

$$I = 4(1+0.4)\frac{1+\dfrac{8\tanh(0.474)}{\pi(868)(1-0.4)(2.5)(0.474)}10}{\dfrac{4}{(1-0.4)(2.5)}+\dfrac{4\pi\dfrac{80,700}{89,000}\tanh(0.474)}{4.10(0.474)}10} = 0.20$$

- $$Q_{t1} = \frac{4568 \text{ kN}}{1 - \dfrac{0.20}{2.5 \cosh(0.474)\left[(1-0.4)(1+0.4)\right]}} = 4995 \text{ kN} \quad (\text{equation 52}).$$

- $w_{t1} = 4995\ (0.20)\ /\ [89{,}000\ (0.915)] = 0.0123\ \text{m} = 12.3\ \text{mm}\ (\text{equation 48}).$

- $Q_{t\,max} = 4568 + 2806\ [\pi\ (0.915)^2/4] = 6413\ \text{kN}\ (\text{equation 53}).$

- $\Delta w_b = (6413 - 4995)[0.6(1.4)]/[(97{,}000/2.5)(0.915)]\ \text{m} = 33.6\ \text{mm}\ (\text{equation 54}).$

- $w_{t2} = 33.6 + 12.3 = 45.9\ \text{mm}$ at $Q_{tmax} = 6413\ \text{kN}.$

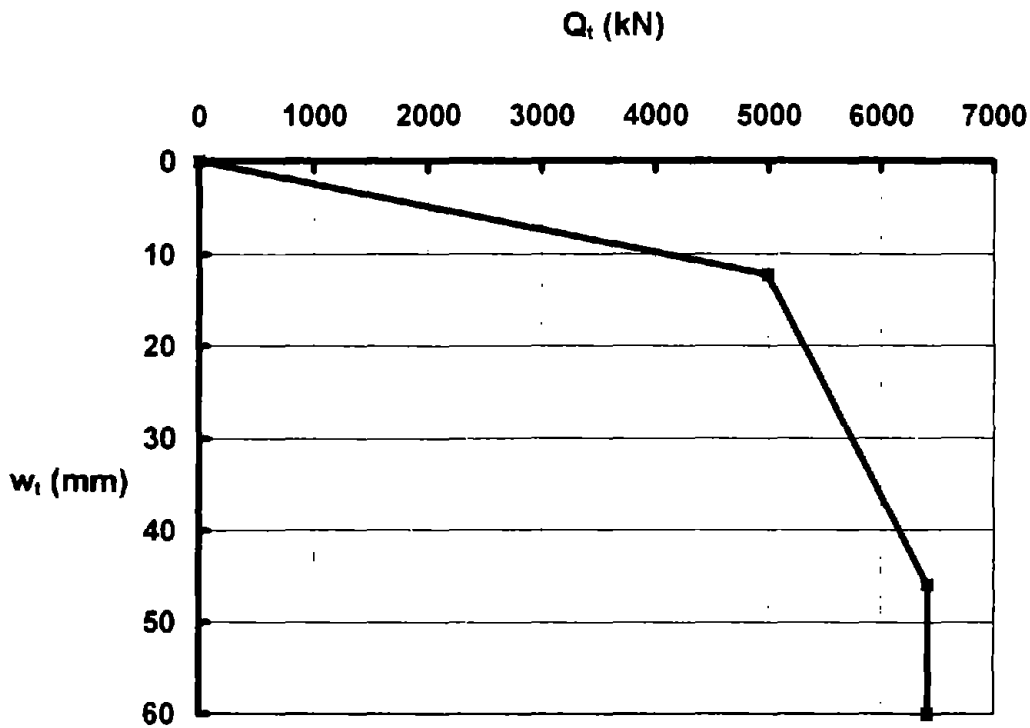The results of the calculations, Q_t versus w_t, are shown in figure 44.

Figure 44. Load-settlement relation for example 4.

CHAPTER 5: FIELD TEST SITES

PURPOSE

Field loading tests were conducted at several sites in order to verify the design models presented in chapter 4. These tests were conducted on full-sized drilled shafts in all three types of intermediate geomaterials. Emphasis was placed on side-shear sockets, so that most of the tests were performed on drilled shafts having a void beneath the base to ensure side shear failure or by shafts loaded by means of bottomhole hydraulic load cells, known commonly as "Osterberg cells." Five of the tests were conducted as an integral part of this project. One test was conducted for another project with which one of the authors was associated. One site was the site of a loading test taken from the literature, in which the author of the paper was interviewed personally. This site was included in order to test the method for predicting behavior of drilled shafts in Category 1 and 2 geomaterials with rough interfaces, because the interfaces for the test shafts at the other Category 1 and 2 geomaterial sites were classified as smooth.

Additional analysis of one complete (side shear plus end bearing) drilled shaft test reported in the literature in Category 1 IGM was performed using the proposed design model, and an additional analysis of a side-shear-only socket test in Category 1 IGM reported in the literature was made. These two analyses are not documented in this chapter, but are documented in Appendix C. Excellent correlation between measured load-settlement relations and predicted relations were obtained for those two tests. Thus, a total of nine full-scale tests, including five associated with this project, were analyzed using the proposed design models: seven ordinary compression tests (including five with voided bases) and two Osterberg cell tests.

GEOMATERIAL AND CONSTRUCTION DATA

Geomaterial data are summarized in table 13, and general construction data are summarized in table 14 for each of the seven test sites documented. Where data are missing, they were not obtained. Properties are given for the geomaterials in the test socket, not for those in the overburden. Note that the site in Dallas, Texas, was the most heavily investigated site. Notation used for geomaterial properties is standard notation for soils, as follows:

w_L = liquid limit,
w_P = plastic limit,
γ = total unit weight,
w = water content,
p_L = limit pressure from Menard-type pressuremeter test,
E_o, E_r = initial and reload Young's moduli from Menard pressuremeter test,
c, ϕ = Mohr-Coulomb shear strength parameters (prime indicating effective stress),
K_o = earth pressure coefficient at rest,
RQD = rock quality designation, and

107

N = uncorrected SPT blow count in B/0.3 m.

The remaining parameters have been explicitly defined previously.

Table 13. Average geomaterial properties in test sockets.

Site: Property	Dallas, Texas	TAMU NGES, Texas	Owensboro, Kentucky	Coweta County, Georgia	Boston, Mass.	Tampa, Florida	Toronto, Ontario
Part of this program?	Yes	Yes	Yes	Yes	Yes	No	No
IGM Type	1 (clay-shale)	1 (hard clay)	1,2 (shale / sandstone)	3 (weath. granite)	3 (glacial till)	2 (lime-stone)	2? (shale)
% - 200	100	100	-	-	-	-	-
w_L (%)	60	-	-	-	-	-	22
w_P (%)	30	-	-	-	-	-	19
γ (kN/m^3)	20.9	19.6	-	-	-	-	25.9
w (%)	19.8	23.0	11 shale 3.5 s'stone	-	-	-	4.6
p_L (MPa)	3.0 (4.3 m) 4.8 (7.3 m)	4.3	-	-	-	-	-
K_o	2.3 - 2.7	-	-	-	-	-	-
E_o (MPa)	134 (4.3) 331 (7.3 m)	154	-	-	-	-	1085 (Goodman jack)
E_r (MPa)	304 (4.3 m) 406 (7.3 m)	312	-	-	-	-	-
% Recovery	100	Not cored	100	-	-	-	-
RQD (%)	30	Not cored	72-85	-	-	-	70
ϕ' (deg.)	24.8	-	-	-	-	-	43
c' (kPa)	0.38	-	-	-	-	-	1.2
ϕ_{rc} (deg.)	30	-	-	-	-	-	-
c_{rc} (kPa)	0	-	-	-	-	-	-
N (avg.) (B/0.3 m)	49	40-90	-	>100	88	-	-
$q_u/2$ (kPa)	385	400	1250 s 6075 ss	-	-	1150	3375

Note: q_u = maximum principal stress difference in UU triaxial compression tests, with confining pressures approximately equal to the total vertical stress except where noted.

108

Table 14. Construction and concreting data.

Site: / Property	Dallas, Texas	TAMU NGES, Texas	Owensboro, Kentucky	Coweta County, Georgia	Boston, Mass.	Tampa, Florida	Toronto, Ontario
Construction date	19 June 1991	23 Nov. 1993	6 Feb. 1993	12-13 Feb. 1993	12 Sept. 1994	29 Mar. 1989	-
Testing date	15 Aug. 1991	29 Nov. 1993	13 Feb. 1993	25 Feb. 1993	10 Oct. 1994	4 April 1989	-
Drilling tool	Soil auger	Soil auger	Rock auger	Soil auger	Rock auger	Rock auger	Rock auger
Time between excavating and concreting (h)	4	3	2	18	4	4	<12
Slurry type	Dry	Dry	Vinyl polymer	PHPA polymer	Light bentonite	Dry	Dry
Concrete slump (mm)	138	150	175	200	187	212	-
Rate of placement (m/h)	15	18	~4	20	7-8	40	-
Method of placement	Directed free fall	Directed free fall	Pump	Tremie	Tremie	Directed free fall	Directed free fall
f'_c (avg.) at time of loading test (MPa)	46.3	31.0	33.1	34.7	27.5	14.5	49.0

DETAILS OF TEST SITES

The Dallas and Owensboro test sites are described in detail in Appendix C, and the Boston test site is described in detail in Appendix D. Sufficient information is given here on the geotechnical characteristics and properties of the test shafts at those test sites and at the remaining test sites to allow use of the design models described in chapter 4. Note that average values of q_u are slightly out of the range specified for IGM's in some layers; however, the results should still provide a reasonable check of the design models.

Dallas Site

The Dallas test site was located on the property of Southwestern Laboratories, Inc., on Lone Star Drive, about 7 km west of downtown Dallas, Texas, and about 0.3 km north of I-30 west. The site consists of about 3 m of fill, underlaid by undisturbed clay-shale, with calcareous pockets. This geomaterial is part of the Arcadia Park member of the Eagle Ford formation, a Cretaceous age marine deposit. The clay-shale is strongly laminated in horizontal planes, with laminations spaced less than 1.0 mm vertically. Three test shafts, denoted E1, E2, and R, were constructed and tested at this site, as shown in figure 45. Test shafts E1 and E2 were constructed of expansive concrete, were not part of the contracted study, and were not considered in this report; however, details of the behavior of these shafts are given in Appendix C.

IGM samples for laboratory testing were recovered with both 75-mm-diameter thin-walled steel tubes and 50-mm-diameter double-walled core barrels at the locations shown in figure 45. Menard pressuremeter tests were also conducted at two depths in the clay-shale. These tests included measurements of creep and relaxation behavior of the clay-shale, as documented in Appendix C. It was concluded from these tests that relaxation would stop within a few days of casting a drilled shaft, so that resistance measured in a load test conducted at the time the load test for this shaft was conducted (60 days after concreting) should remain unaltered with time.

Laboratory testing consisted of UU triaxial compression tests, with isotropic confining pressures equal to 6.2 kPa for every 0.3 m of depth (75-mm samples); CID triaxial compression tests (50-mm cores); CD direct interface shear tests on smooth and rough interfaces with shearing imposed perpendicular to the laminations, as will exist during drilled shaft loading; and index tests, including carbonate content tests. The test results for the UU triaxial tests are shown in figure 46, and those for the CID triaxial tests (ϕ' and c') and direct interface shear tests (ϕ_{rc} and c_{rc}) are summarized in table 13. No tests were conducted in the overburden fill material.

A perched water table was observed atop the clay-shale, but there was no evidence that this water controlled the pore water pressures in the IGM.

A profile of the test shaft is shown in figure 46. Since the primary purpose of this test was to observe the development of shaft resistance, a 0.15-m-thick Styrofoam® plug was
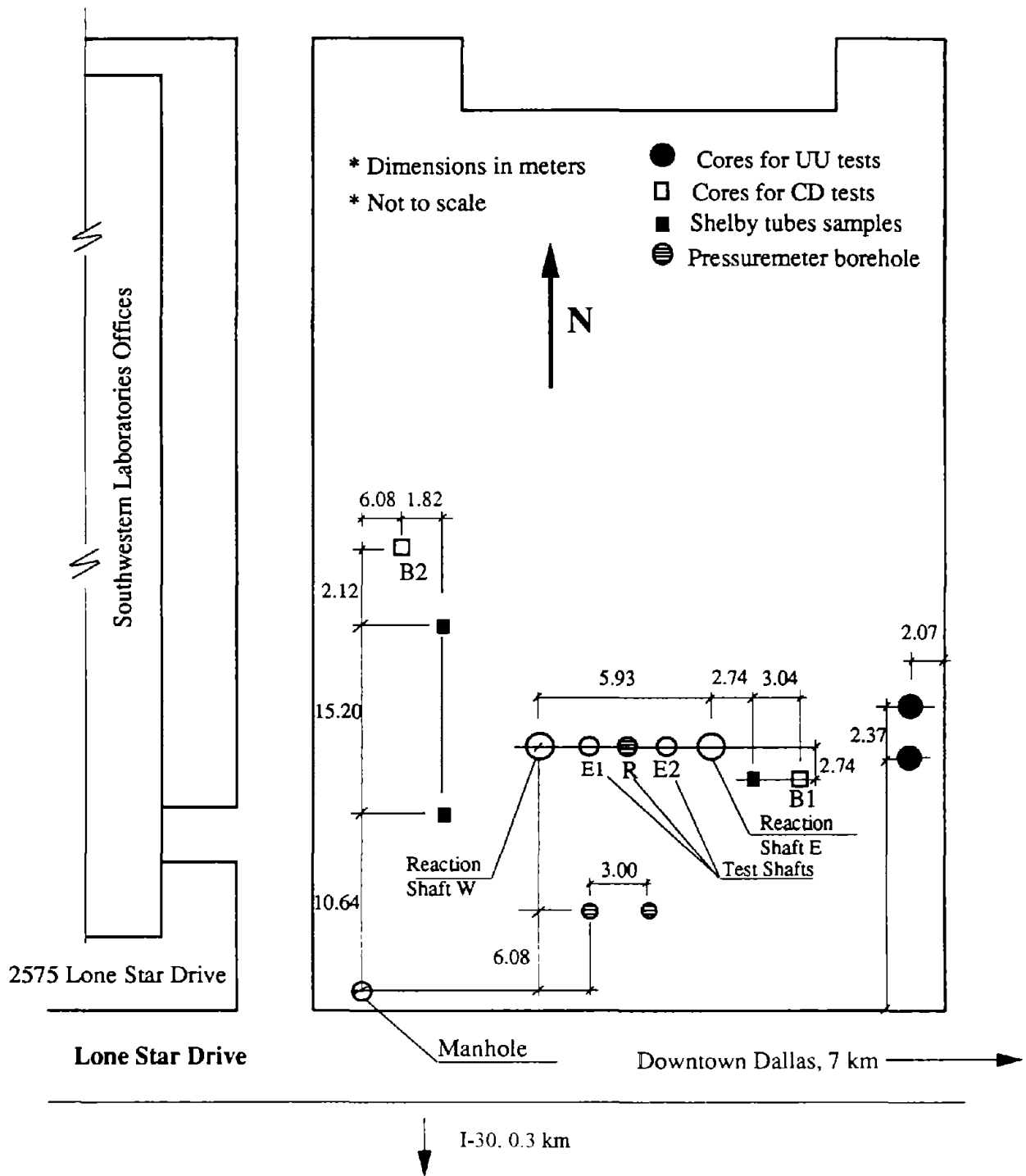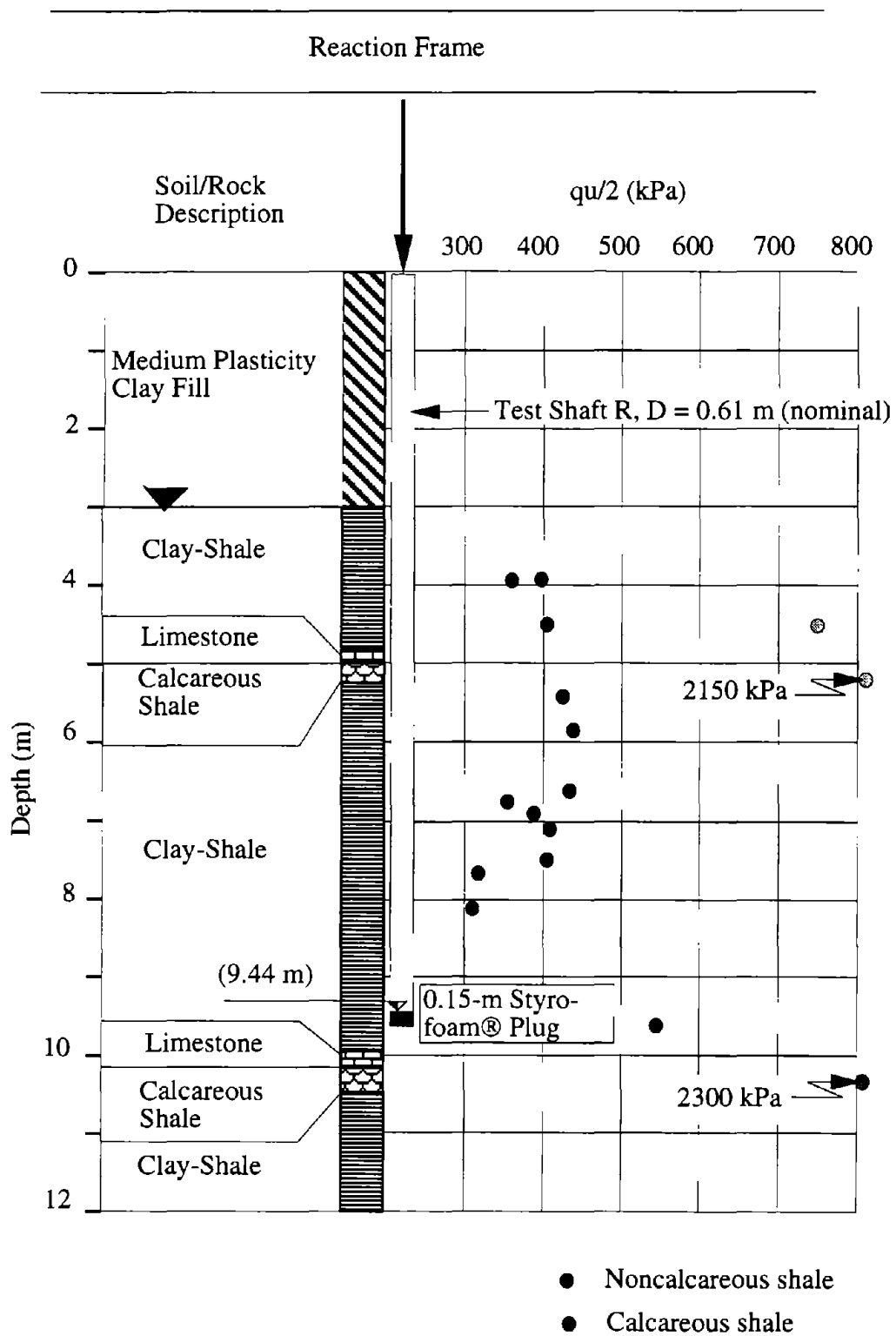
110

Figure 45. Plan view of Dallas test site

111

Figure 46. Profile of test shaft at Dallas site

placed on the bottom of the borehole before casting the shaft in order to minimize base resistance and ensure that complete side shear failure could be achieved with the loading system that was available. In this case, loading was provided through a standard hydraulic jack and electronic load cell reacting against a steel reaction frame anchored by two reaction shafts.

The test shaft borehole was entered for inspection prior to concreting. Its walls contained disturbed material about 5 mm thick, and the walls had a roughness pattern in which the wavelength was about 0.2 m and the amplitude was about 10 mm. The walls were visibly wet, possibly due to the presence of the perched water, which seeped into the borehole as drilling progressed.

After the loading test was completed, the test shaft was exhumed and the roughness profile was measured along a longitudinal line, as described in Appendix C. The measurements are shown in figure 47. The shaft was essentially smooth, except in the area noted, which coincided with a zone of calcareous clay-shale. In particular, the undulation pattern noted on the borehole wall during construction was absent on the exhumed shaft, possibly because some of the smeared material was displaced by the concrete as it was placed (material from the asperities was sheared and moved to the troughs). From this analysis, this test shaft was classified as "smooth."

The test shaft instrumentation system is depicted schematically in figure 48. The primary instrumentation device was a bonded foil resistance gauge sister bar, wired in half-bridge configuration, and tied to the reinforcing cage. The sister bars were #4 deformed bars, Grade 60, with lengths of 0.76 m. The bridge completion was made with dummy sister bars buried beneath the surface, as shown in figure 48. Five levels of sister bars were installed. Three levels had four bars at the ends of two diameters and two had two bars at the ends of one diameter. The top level served as a calibration level, giving instrument output in millivolts versus known applied load, which was then applied to the instruments at the remaining levels to obtain relationships of load to depth during the loading test. Settlement at the shaft head was measured by means of four electrical transducers backed up by optical survey measurements.

The test method was the quick test method, in which loads corresponding to about 10 percent of the expected capacity were applied every 3 to 4 minutes. Once it was interpreted that failure had occurred, loads were then removed in decrements.

TAMU NGES Site

The second test site was the Texas A & M University (TAMU) National Geotechnical Experimentation Site (NGES), approximately 12 km west of Bryan, Texas, on the TAMU Riverside campus. The test area was one of two test areas at the TAMU NGES known as the "sand" site, approximately 0.7 km east of the main entrance road and 1.1 km south of the existing (1993) alignment of State Highway 21. The upper 11 m of the site is a sand

113

10 mm

Top of socket

0.91 m
Amplitude less than 2 mm

1.22 m

4.27 m
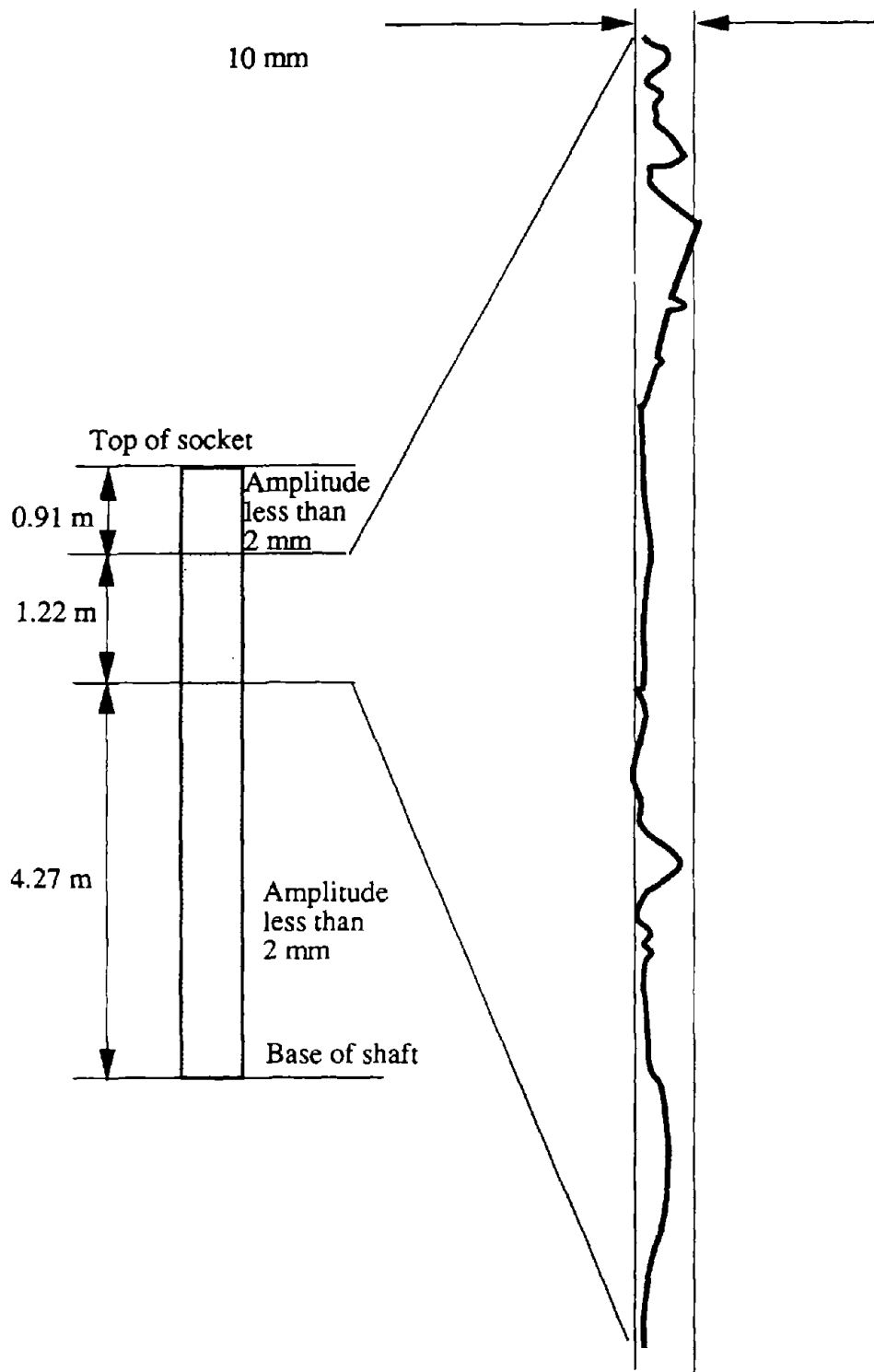Amplitude less than 2 mm

Base of shaft

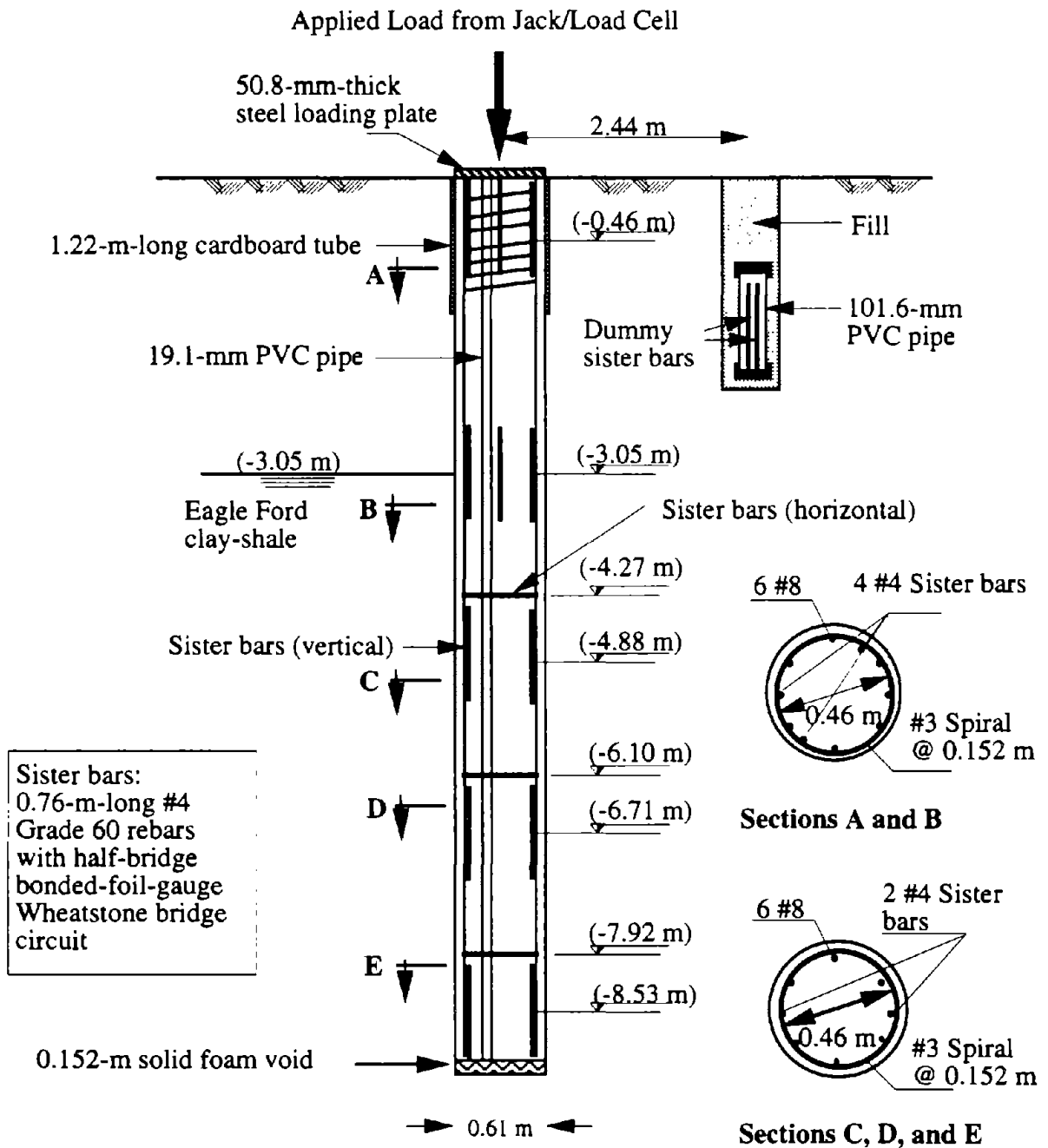Figure 47. Roughness profile for Dallas test shaft.

Figure 48. Schematic of instrumentation for Dallas test shaft.

deposit that was the site of extensive full-scale surface footing tests in 1993. The sand is underlaid by a thick deposit of hard, heavily overconsolidated clay of the Navarro group, a series of Upper Cretaceous marine clay deposits found in central Texas through northern Louisiana and southern Arkansas. The level of the phreatic surface in the surface sand is not clear. It appears to vary seasonally. There is no information on the level of the phreatic surface in the hard clay that underlies the sand at this site. For analysis purposes, it has been assumed that any water in the sand is perched.

The test shaft was installed at the location shown in figure 49.[37] Prior to the installation of the shaft, a 1-m by 1-m surface footing was installed and load tested to failure in compression in the sand. Considerable geotechnical data for the sand are available and are given in reference 37. The footing test had no effect on the hard clay at a depth of 11 m, in which the socket test was conducted. Following the footing test, the footing was removed and the test drilled shaft was installed at the location of the center of the footing in order to take advantage of an existing reaction system. An elevation view of the test shaft is shown in figure 50. Bentonitic drilling slurry with unknown properties was used to drill through the overlying sand, and a temporary casing was set to the depth of the top of the clay. The slurry was then evacuated from the casing, and the borehole was completed in the dry with a nominal diameter of 0.61 m to the depth shown in figure 50, and the borehole was calipered with an Atlas Wireline Co. commercial electronic oil well caliper, with a diameter resolution of 3 mm. The caliper log obtained in the field is given in figure 51. The borehole was classified as "smooth" except for one long asperity produced by a sand seam near the middle of the socket. A foam plastic plug was placed at the bottom of the socket to destroy the end bearing before the concrete was placed. The borehole was not entered for inspection because the socket was too small and too deep to be entered safely. However, surface observation indicated no evidence of water seepage or sloughing of the sides of the borehole.

Following placement of the instrumented reinforcing cage and placement of concrete, the shaft was loaded to failure in compression using the reaction shafts already in place for the footing test, using a procedure identical to that for the Dallas site test. Following the loading test, 75-mm-diameter, thin-walled steel tube samples were taken in the clay and subjected to UU triaxial compression testing in a manner similar to the samples for the Dallas site. Most of these tests were conducted in the University of Houston geotechnical laboratory. Two were conducted in the University of Florida geotechnical laboratory. The results are given in figure 52. Again, q_u in this figure represents the principal stress difference at failure in the triaxial test and not an actual unconfined compression test. The total unit weight of the sand and clay were assumed to be 18.8 kN/m^3 for purposes of computing confining pressures for the UU triaxial tests. The Navarro clay is ductile, as indicated in figure 53, and it exhibits a typical stress-strain relation from a triaxial test.

Owensboro Site

Two loading tests were conducted at the site of the main piers of the U.S. 231 cable-stayed bridge across the Ohio River at Owensboro, Kentucky, located as shown in figure 54.
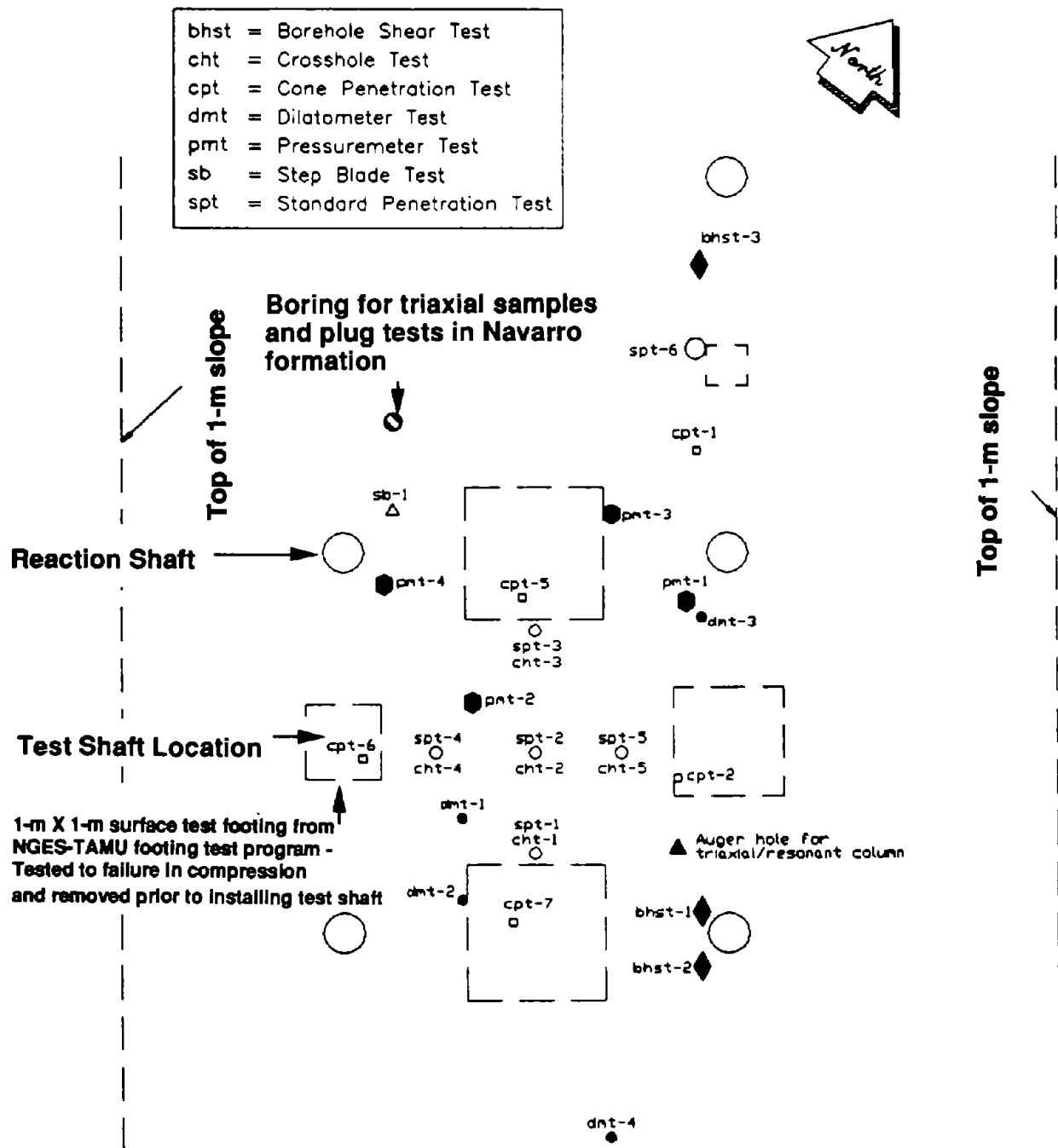
Figure 49. Plan view of TAMU test site.

117

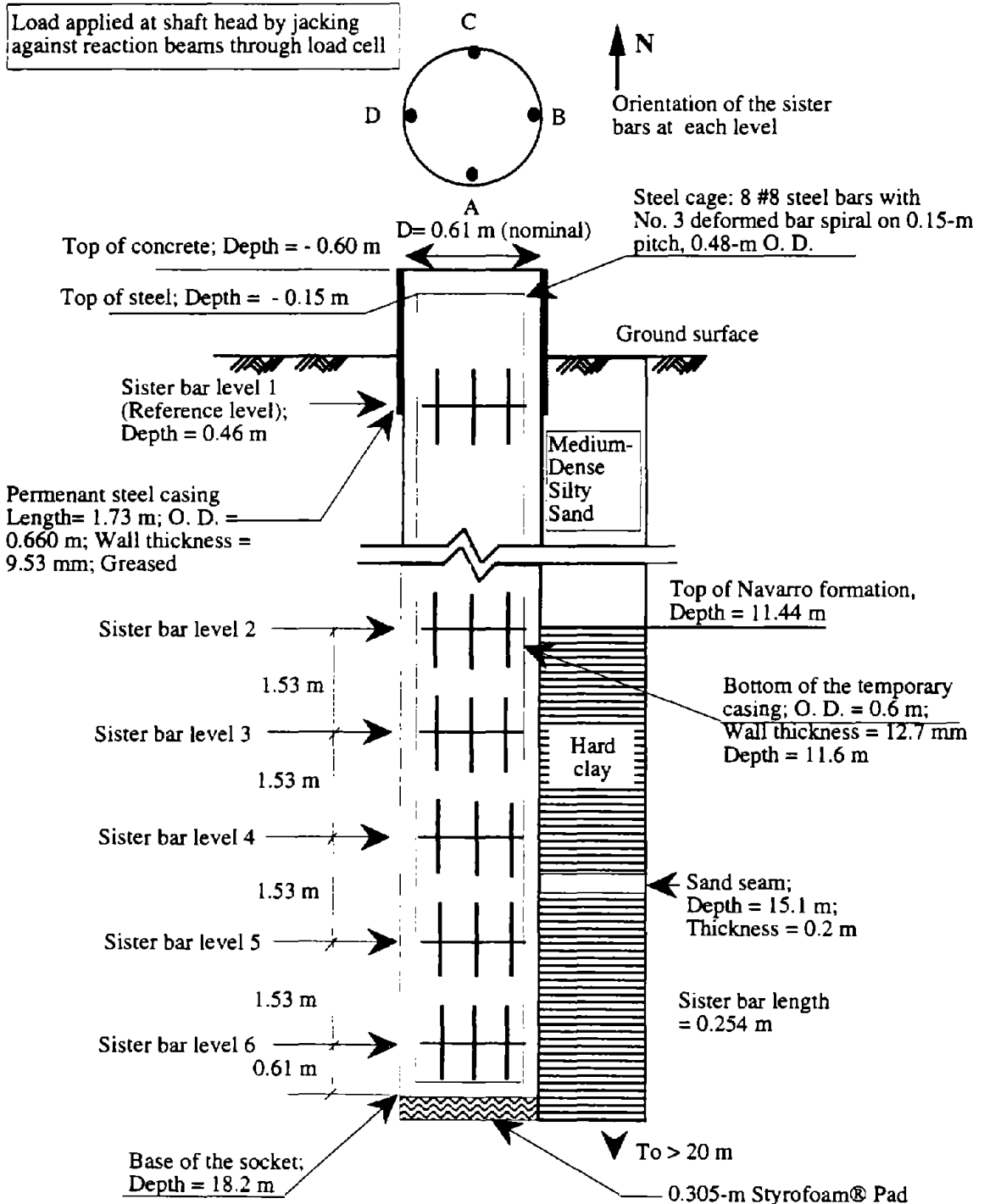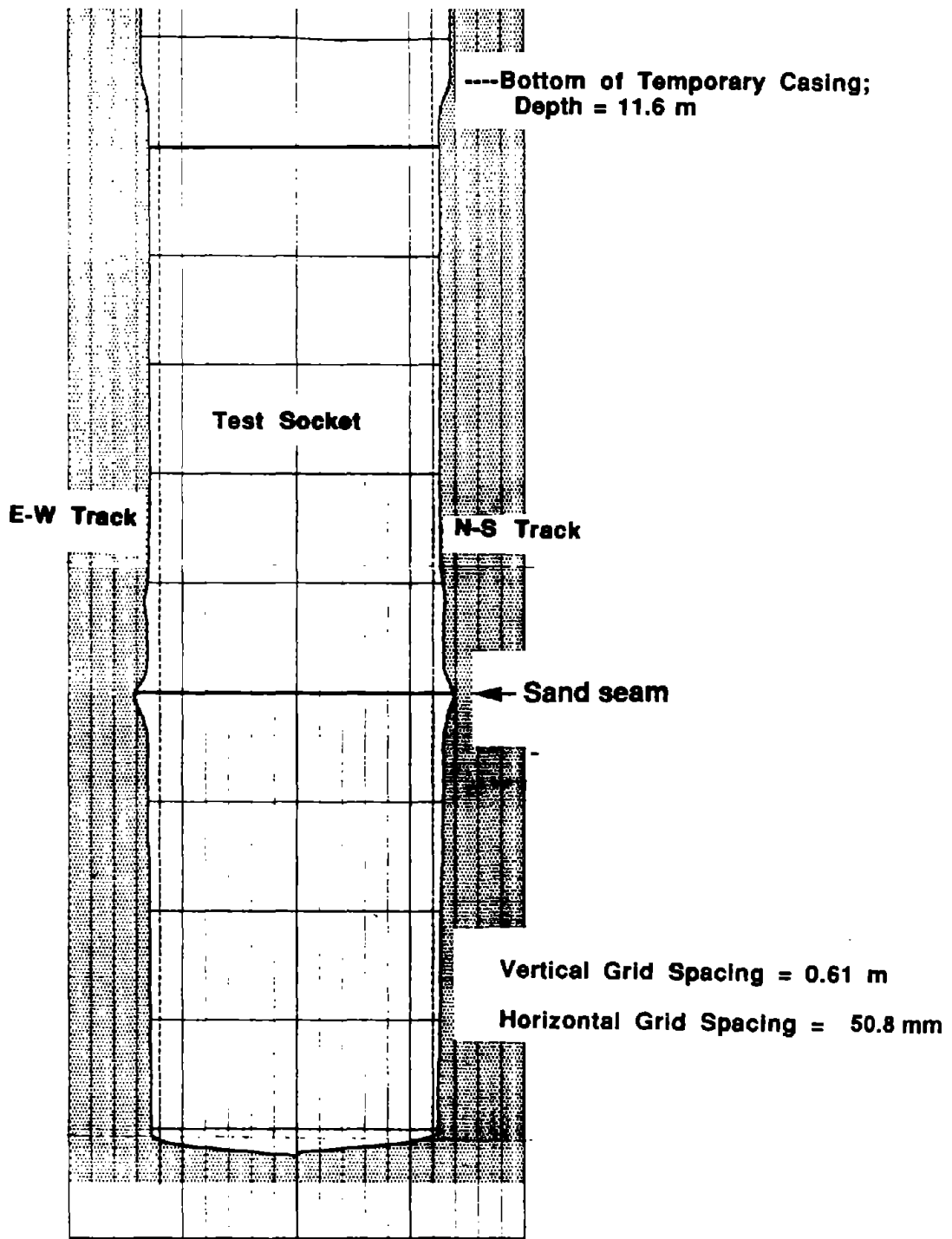Figure 50. Instrumentation and geomaterial profile for TAMU test.

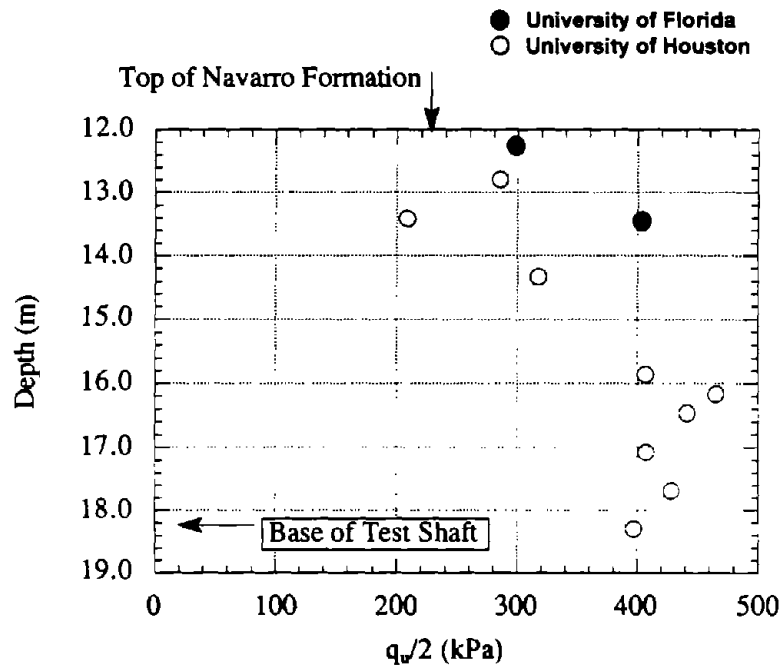Figure 51. Caliper log for TAMU test shaft borehole.

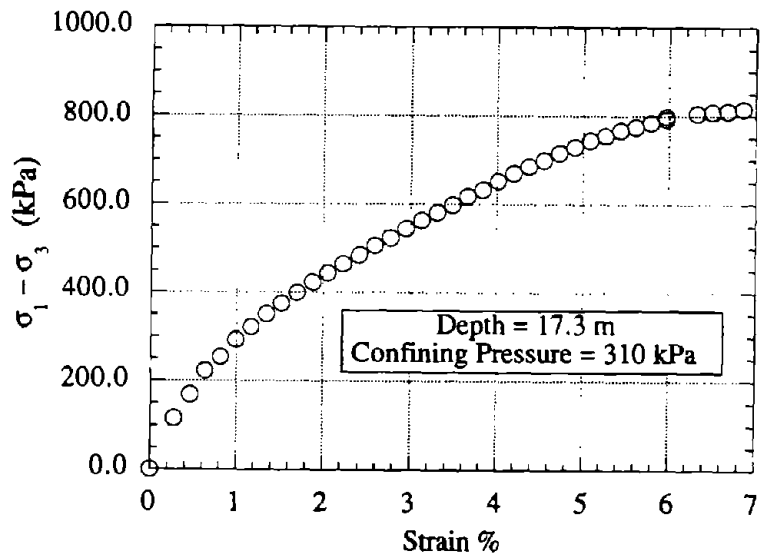Figure 52. Undrained shear strength profile for TAMU site.

Figure 53. Typical UU triaxial compression stress-strain curve for Navarro clay.

The tests were performed for design purposes for the Kentucky Transportation Cabinet; however, personnel from the study team for this project assisted in the planning of the tests and observed the shaft installation. A detailed report on these tests may be found in reference 38.

The geomaterials at this site are a complex series of shales, sandy shales, and sandstones of mid-Pennsylvanian age. The two main piers, situated in the Ohio River, were designated Pier 8 (near south bank) and Pier 9 (near north bank). They consisted of 44 drilled shafts each in a rectangular group pattern, indicated in figure 55. Production shafts were used as test shafts. At Pier 8, the drilled shaft designated 43 was tested, hereafter called shaft 8-43. Only the shaft designated 42 was in place at the time of the construction and testing of shaft 8-43. At Pier 9, the drilled shaft designated 42 (9-42) was tested. Shaft 41 was the only other shaft in place in that pier at the time of the construction and testing of shaft 9-42.

Both piers were constructed within the banks of the river. Cofferdams were first constructed, and the soil was excavated inside the cofferdams to an elevation of 90.5 m, as shown in figure 56. Permanent steel casing was set inside the cofferdams at the test shaft locations from about 2.6 m above the river level to the top of the test socket, which lies beneath sand and gravel alluvium. The sockets were then excavated with a rock auger under lightweight solid vinyl polymer drilling slurry; Osterberg cells were placed at their bases; and the shafts were concreted to the elevation shown in figure 56, which was to be the elevation of the top of the drilled shaft cap in the completed pier. The casing length was approximately 30 m in both test shafts. In shaft 8-43, the socket extended for 13.7 m below the bottom of the casing. In shaft 9-42, the socket extended for only 5.2 m below the bottom of the casing. The instrumentation scheme for the socket for shaft 9-42 is shown in figure 57. Load distribution along the shaft was determined directly from the vibrating wire strain gauges, and shaft displacement was determined from telltales located at the top of the Osterberg cell and at the top of the socket.

Prior to concreting, both shafts were calipered electronically with an Atlas Wireline Co. electronic oil well caliper that was fitted with "feeler" extensions to allow the large-diameter boreholes to be calipered. The precision for this caliper, which was similar to the caliper used at the TAMU test site, was about 3 mm. Caliper logs for shafts 8-43 and 9-42 are shown in figures 58 and 59, respectively. The nominal diameter of 8-43 was 1.805 m, while that of 9-42 was 1.780 m. Shaft 8-43 can be classified as a rough socket, while shaft 9-42 can be classified as a smooth socket for Osterberg cell testing, since the small "shoulder" just below the shale/sandstone interface is tapered downward, opposite to the direction of loading.

Osterberg cells with capacities of 26.7 MN were used to load both shafts. The shafts were loaded in about 30 equal increments in a period of about 4 hours until the maximum capacity of the cells were reached. However, because the socket in 8-43 was both rough and very long, no indication of side shear failure could be identified from the load test records. Furthermore, base failure also did not occur. In shaft 9-42, impending side
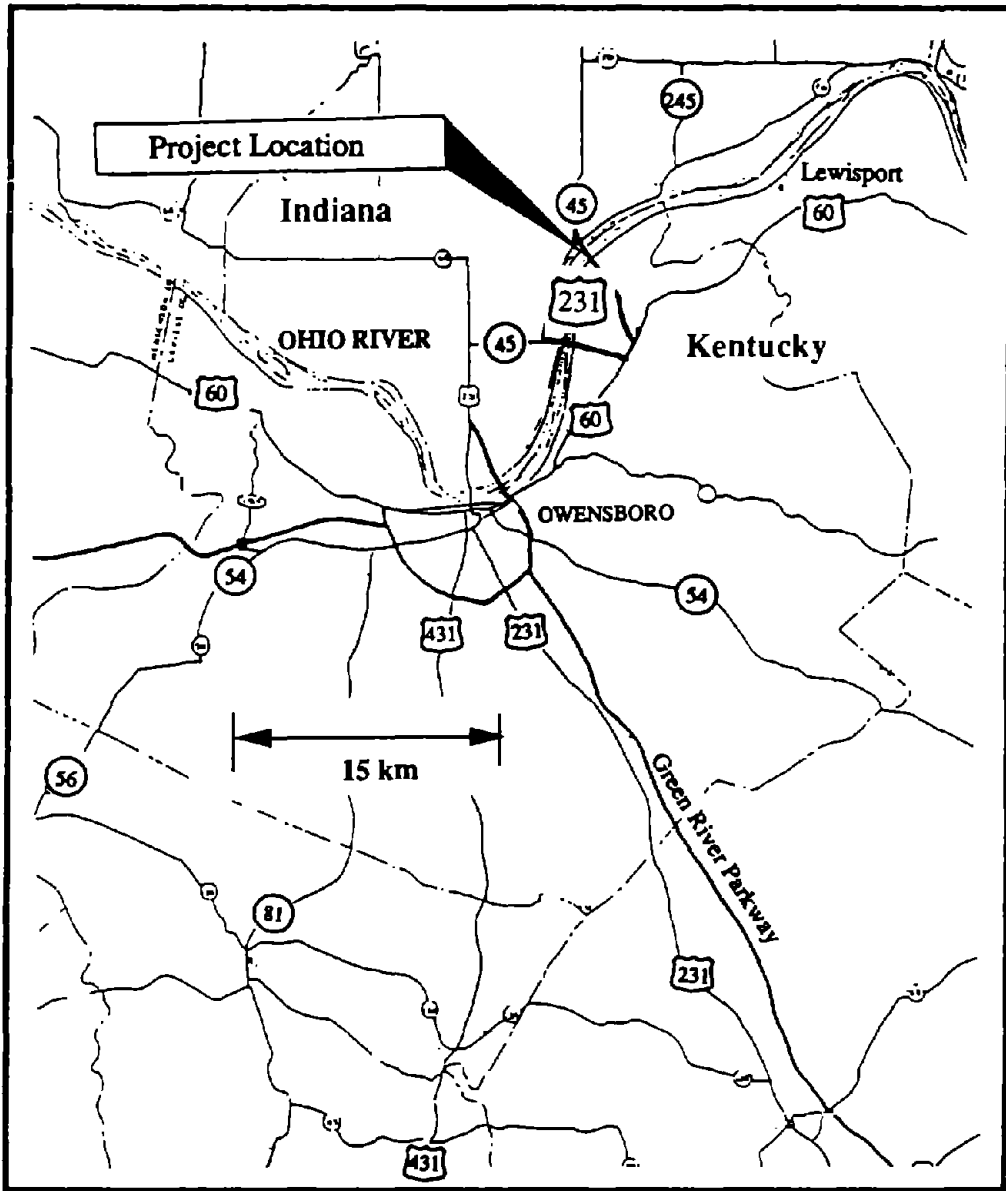
Figure 54. Location map for Owensboro test site.
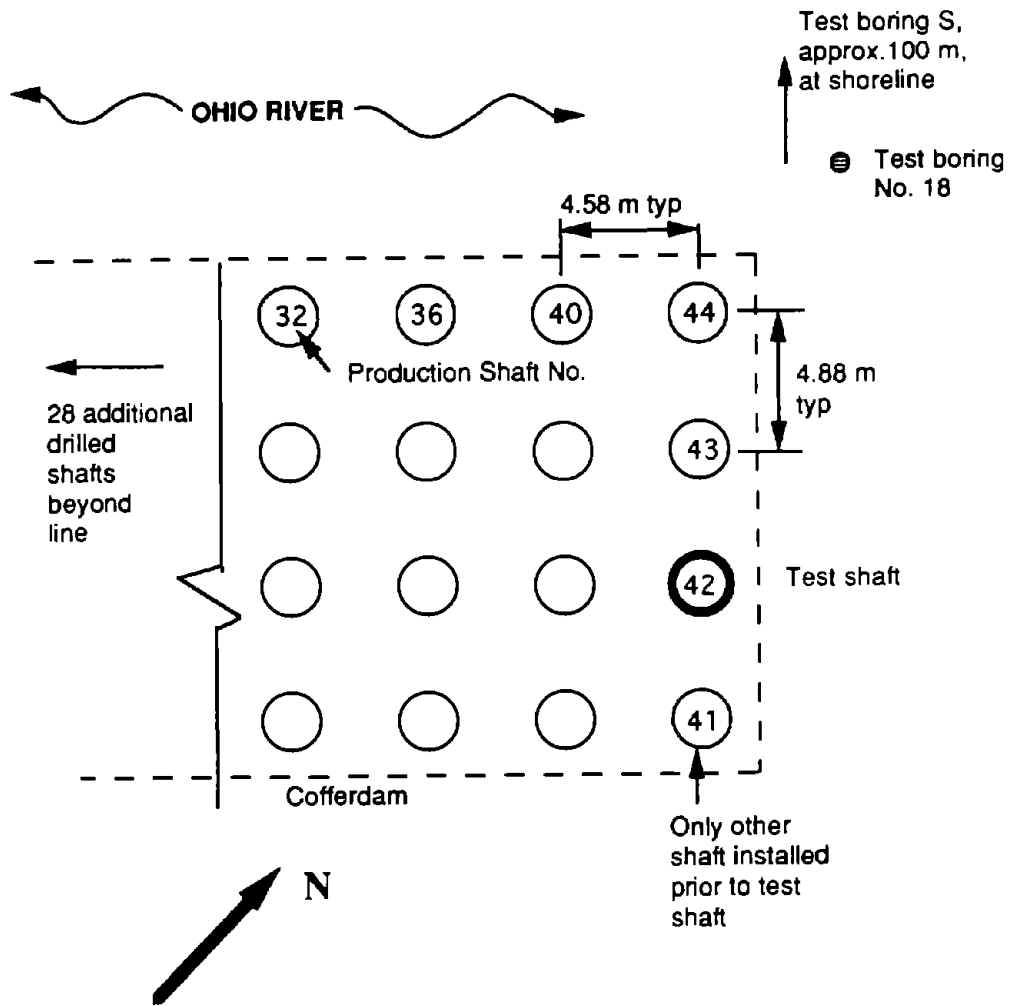
Figure 55. Layout of test and production shafts for Pier 9, Owensboro site.

resistance failure was observed during the loading test, but no base failure could be observed. For this reason, only shaft 9-42 was analyzed using the proposed design model.

At the time the test shafts were constructed and tested, almost no quantitative strength data for the IGM were available. Following the tests, cores were carefully taken in the socket material about 100 m from shaft 9-42 on the north (Indiana) bank of the river and were returned to the University of Houston for compression testing. The results of these tests are shown in figure 60. A layer of shale, which extended slightly more than 2 m below the bottom of the casing in the test shaft, was encountered at the same elevation in the sample boring, giving some confidence that the sample boring was representative of the geomaterials at the test location. Below the shale was a harder, but heterogeneous, geomaterial that was classified as a sandstone, although others have classified it as a sandy shale. The shale was differentiated from the sandstone primarily on the basis of natural moisture contents, also shown in figure 60. The shale and sandstone are Category 1 and 2 IGM's, respectively. The average unconfined compression strength values within the
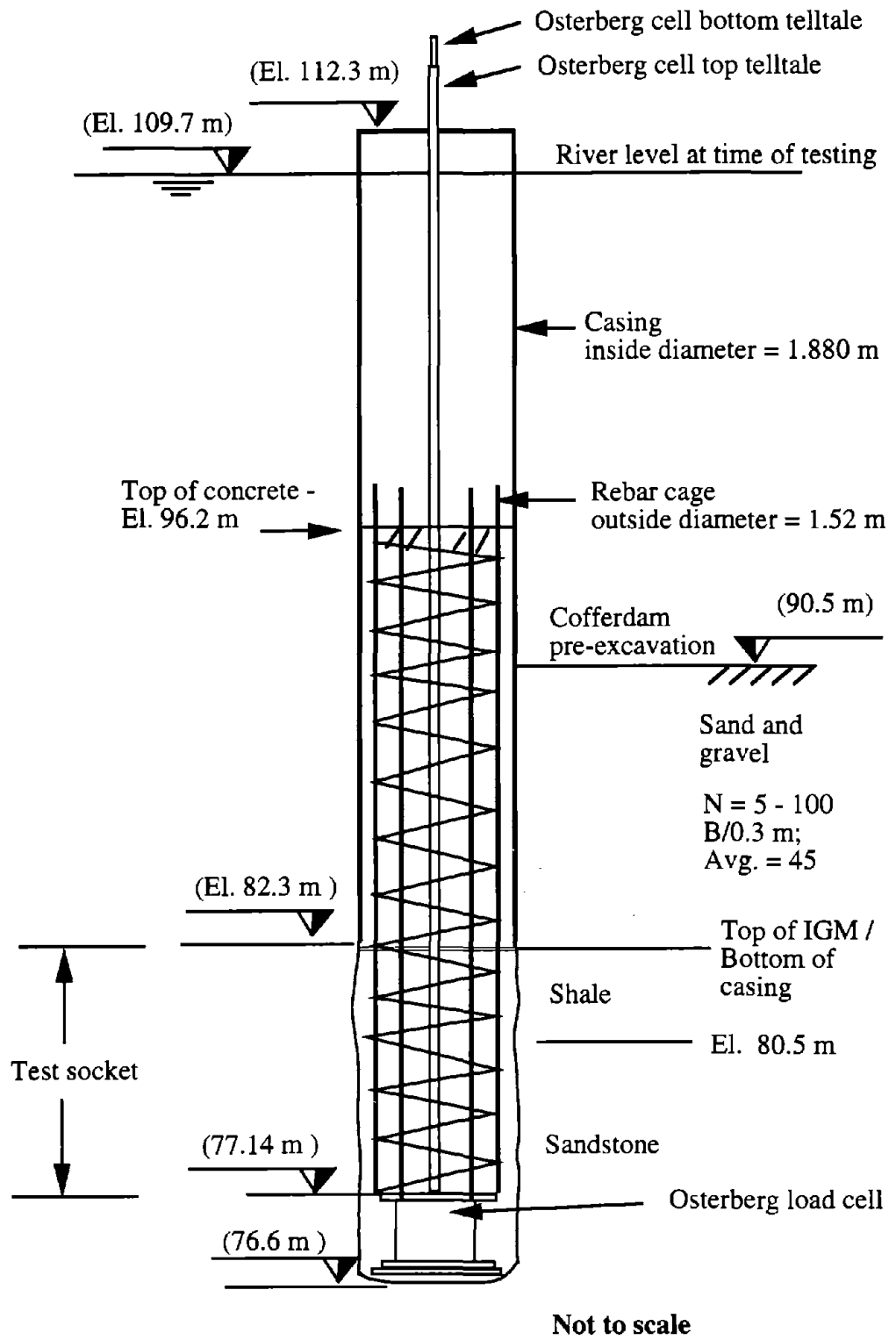
Figure 56. Elevation view of shaft 9-42, Owensboro.

124

Note: There were two levels of sister bars above El. 83.6

El. 83.6 m

82.4 m

Casing

Top of socket

Longitudinal steel:
32 #10 bars,
equal spacing,
2-bar bundles

Spiral steel:
#6 at 0.3 m
pitch,
1.53-m O. D.

Shale,
qu =2.5 MPa

81.3 m

El. 80.5 m

Nominal socket
wall, d = 1.78 m

80.1 m

Sandstone,
qu =12.15 MPa

79.1 m

77.9 m

Top of Osterberg cell,
El. 77.2 m
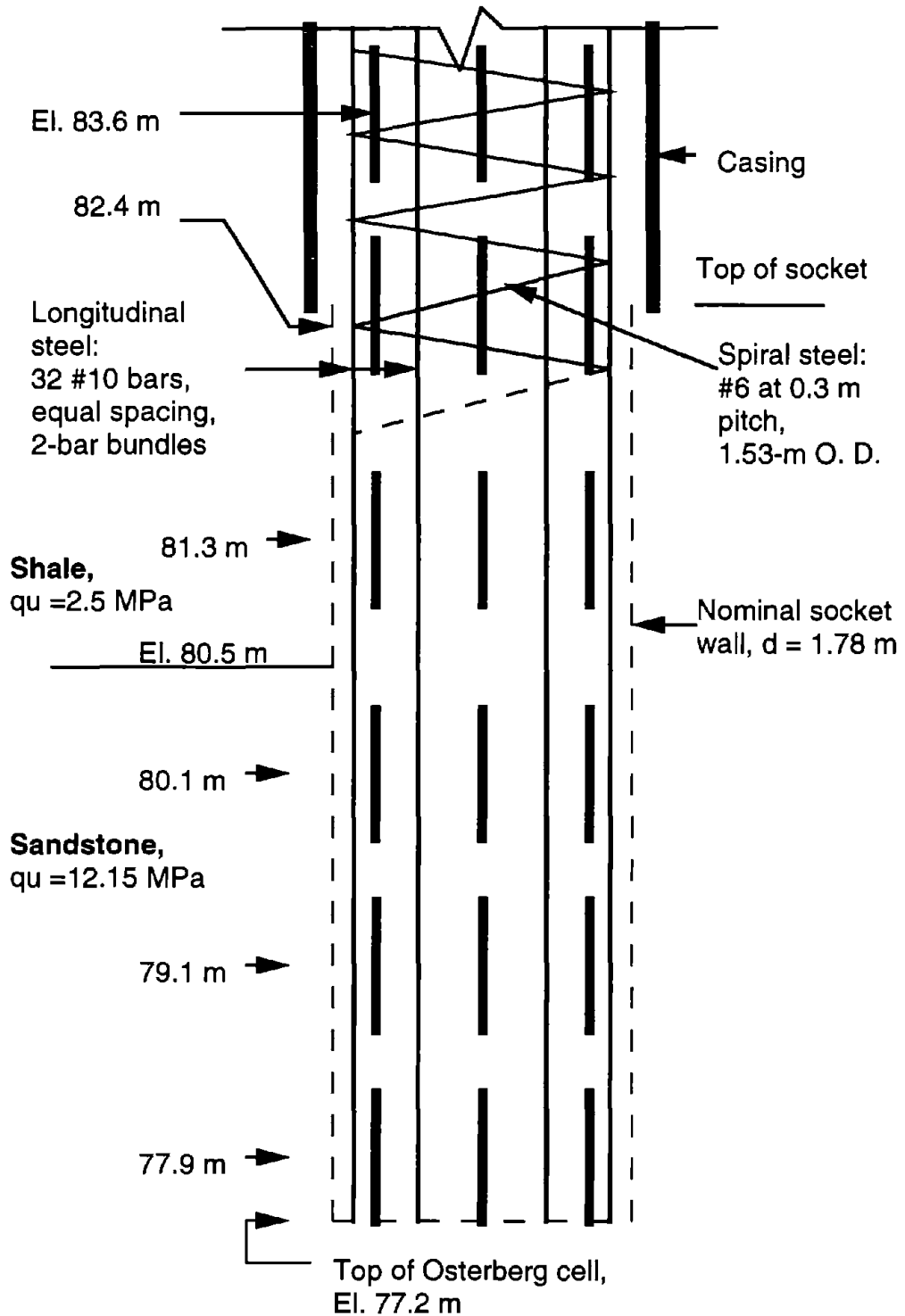
Sister bars: 4 per level. Geokon Model #4911
vibrating wire gauges connected to #4 Grade 60
deformed rebar 1.37 m long.

Figure 57. Schematic of instrumentation for shaft 9-42, Owensboro.

125
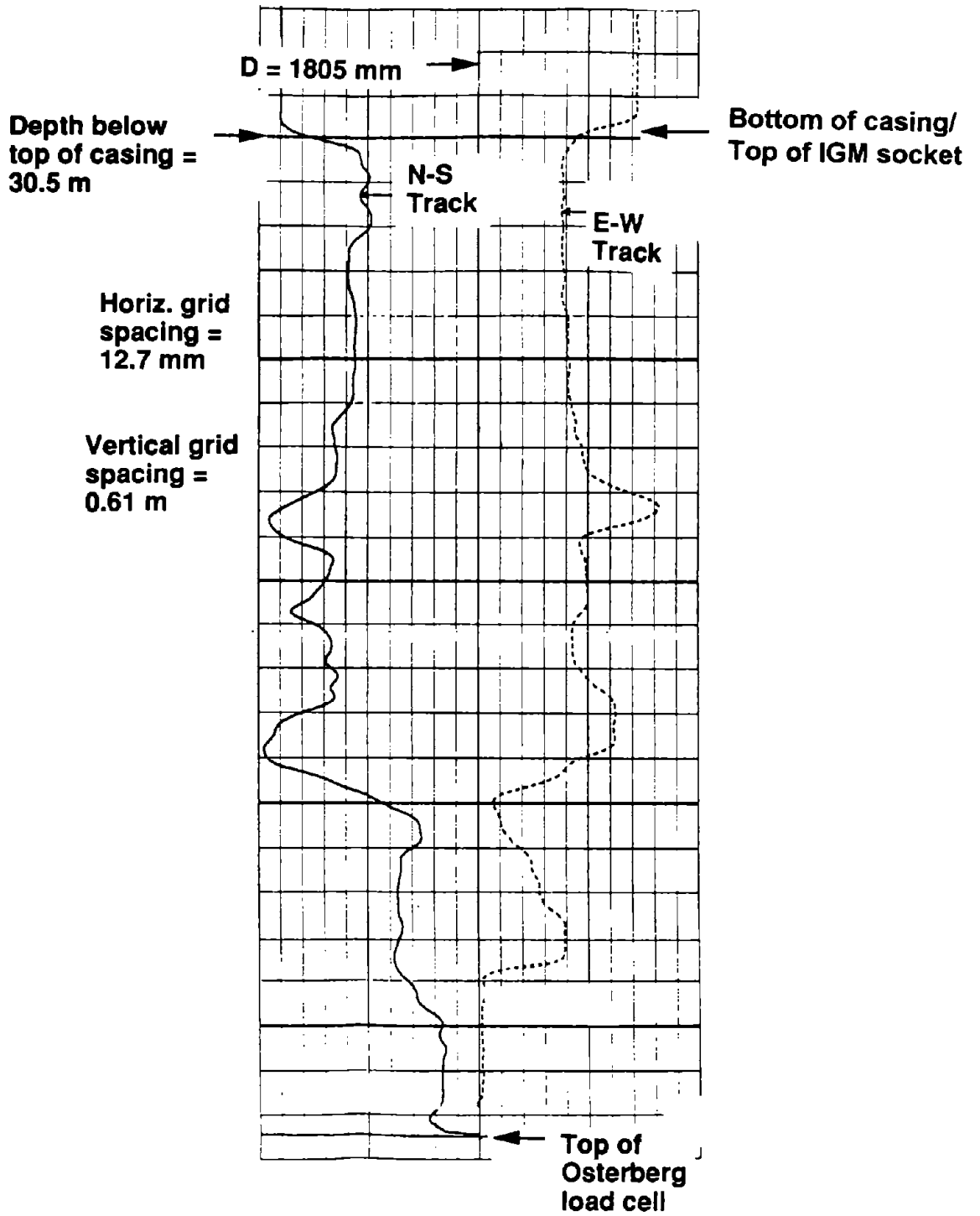
Figure 58. Caliper log of shaft 8-43, Owensboro.

126
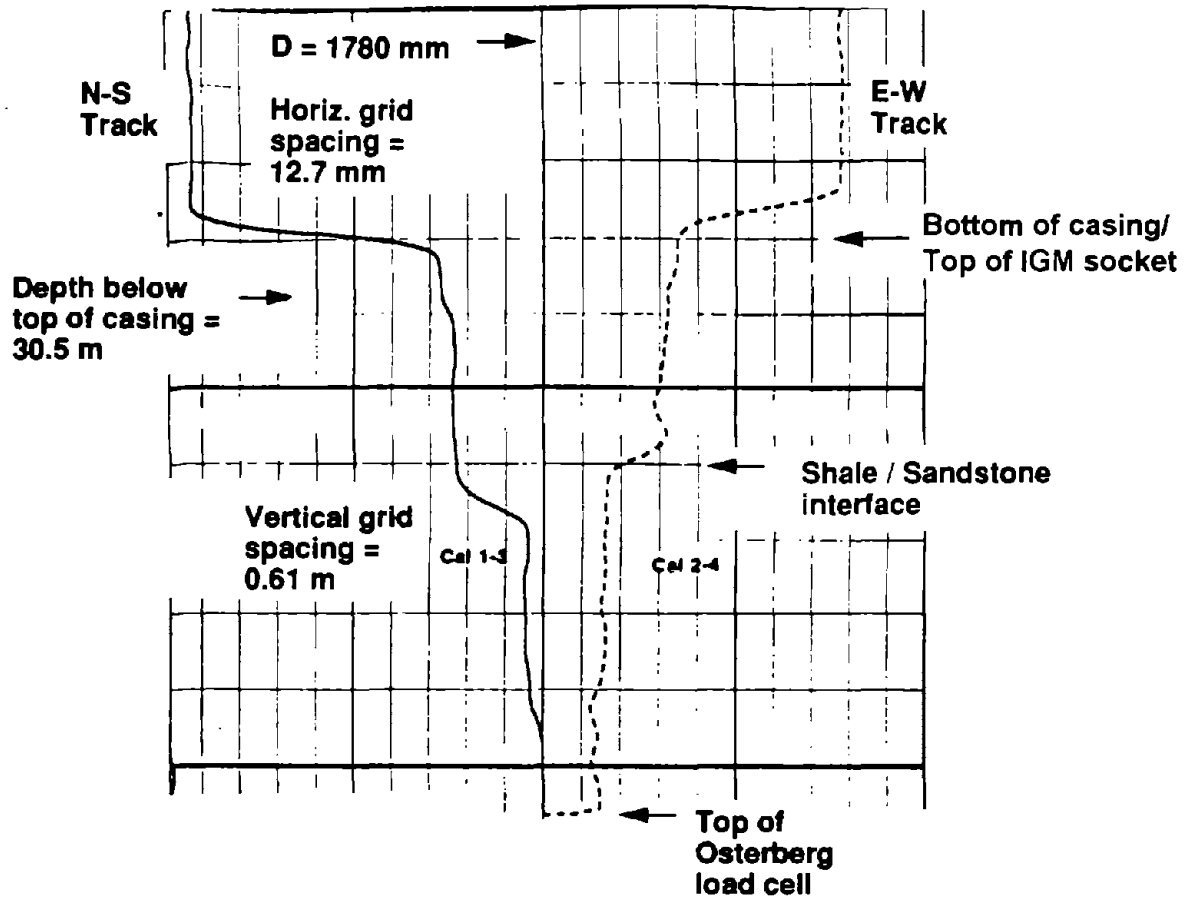
Figure 59. Caliper log of shaft 9-42, Owensboro.

socket for shaft 9-42 for each of the layers are shown in figure 57. These values were used in the design model calculations

Since this test and the test at the Boston site were conducted using Osterberg cells, rather than ordinary compression loading, a comment about the Osterberg cell testing method is in order. An Osterberg cell test does not represent the manner in which the shafts will be loaded in operation or the manner in which loading was assumed in developing the design model. The reversal of the direction of loading by the Osterberg cell produces higher Poisson (lateral) strains in the concrete shaft in the socket than would be produced by normal compression loading. This phenomenon would be expected to produce higher load transfer with a frictional interface. However, mean effective stresses in the geomaterial surrounding the socket are reduced because tension is developed in the geomaterial in the horizontal plane of the cell (plane of the socket base). These actions

127
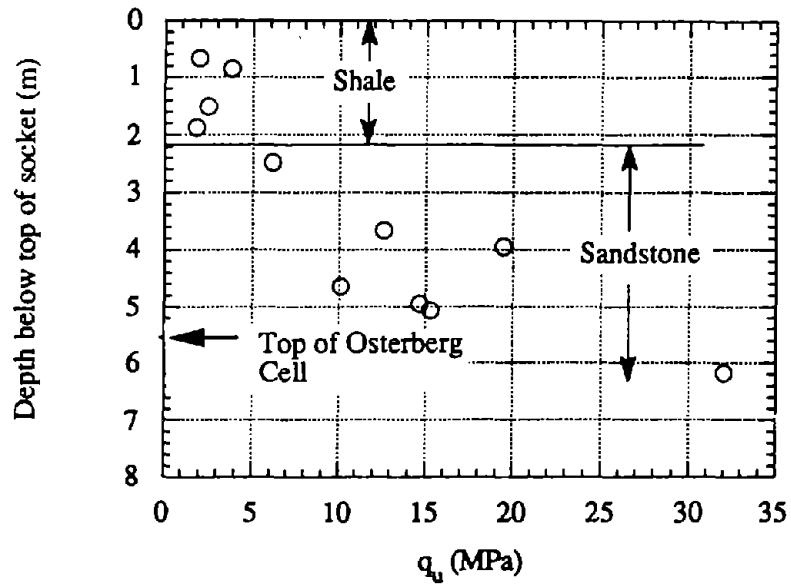
(a) Unconfined compression strength
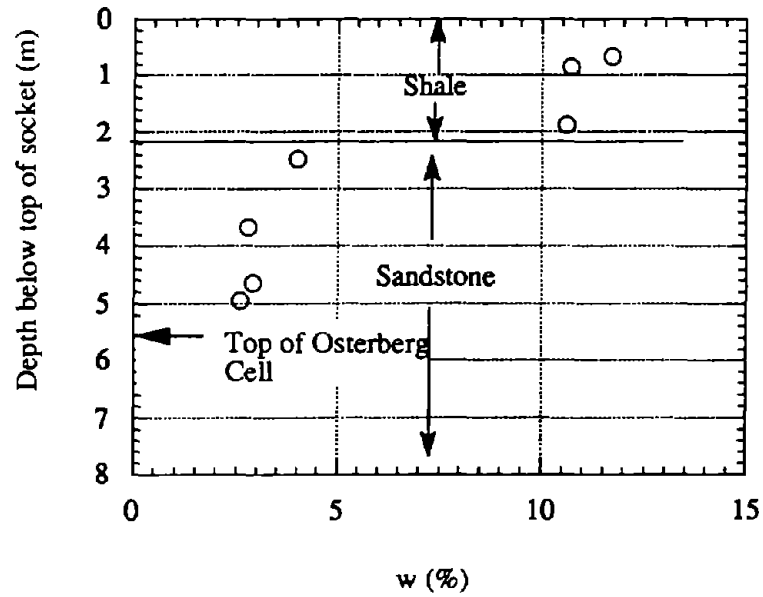
(b) Moisture content

Figure 60. Unconfined compression and moisture data for shaft 9-42, Owensboro.

produce effects that tend to cancel out each other. McVay *et al.* (reference 39) have shown through detailed finite element studies that relatively minor differences in ultimate side resistance exist between ordinary compression loading and Osterberg cell loading in Florida limestone. As a result, the Osterberg cell tests will be assumed to produce results identical to ordinary compression loading tests in this report.

Coweta County Site

An ordinary compression loading test was conducted for design purposes by the Georgia Department of Transportation on the alignment of I-85 southwest of Atlanta. The site is located in figure 61. This site is in the Piedmont province and consists primarily of residual soils. The profile of the test shaft and geomaterial layers is shown in figure 62. The geomaterials of interest at this site are Category 3 IGM's that occur between depths of approximately 14 m and at least 22.9 m, as indicated in an SPT boring made approximately 3 m from the test shaft. This geomaterial is a very dense, fine-grained, residual sand, weathered in place from a parent granitic mica schist rock. The phreatic level in the sand was located at a depth of 3.0 m. No site-specific unit weight information was available. The total unit weights were taken to be 18.8 kN/m^3 for all layers, which is consistent with local practice.
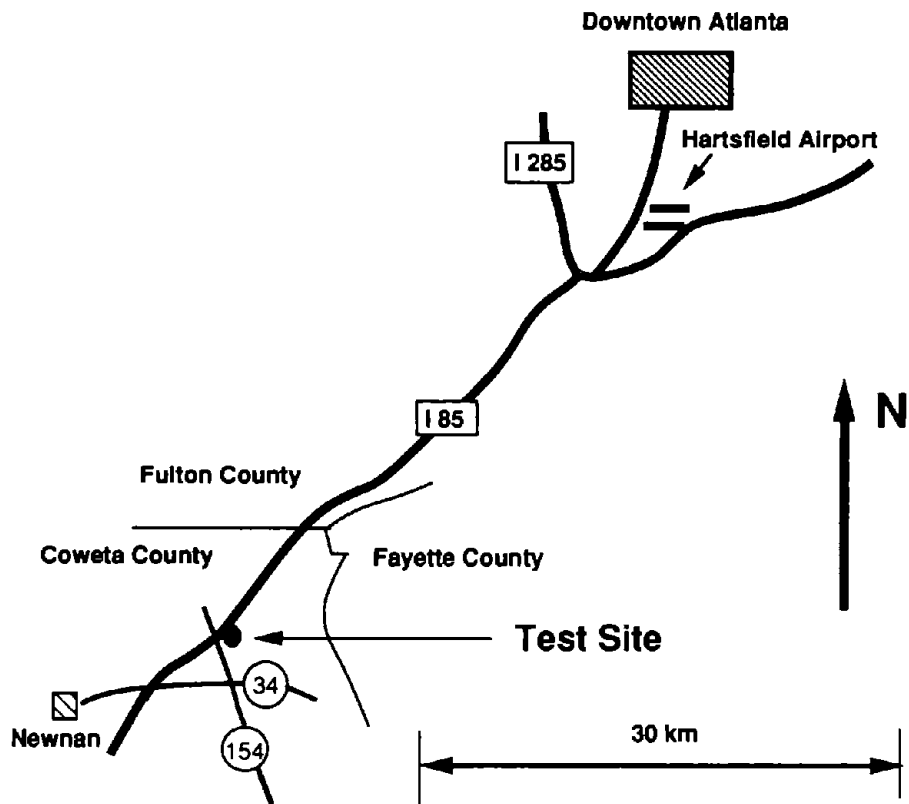
Figure 61. Location map for Coweta County test site.

129
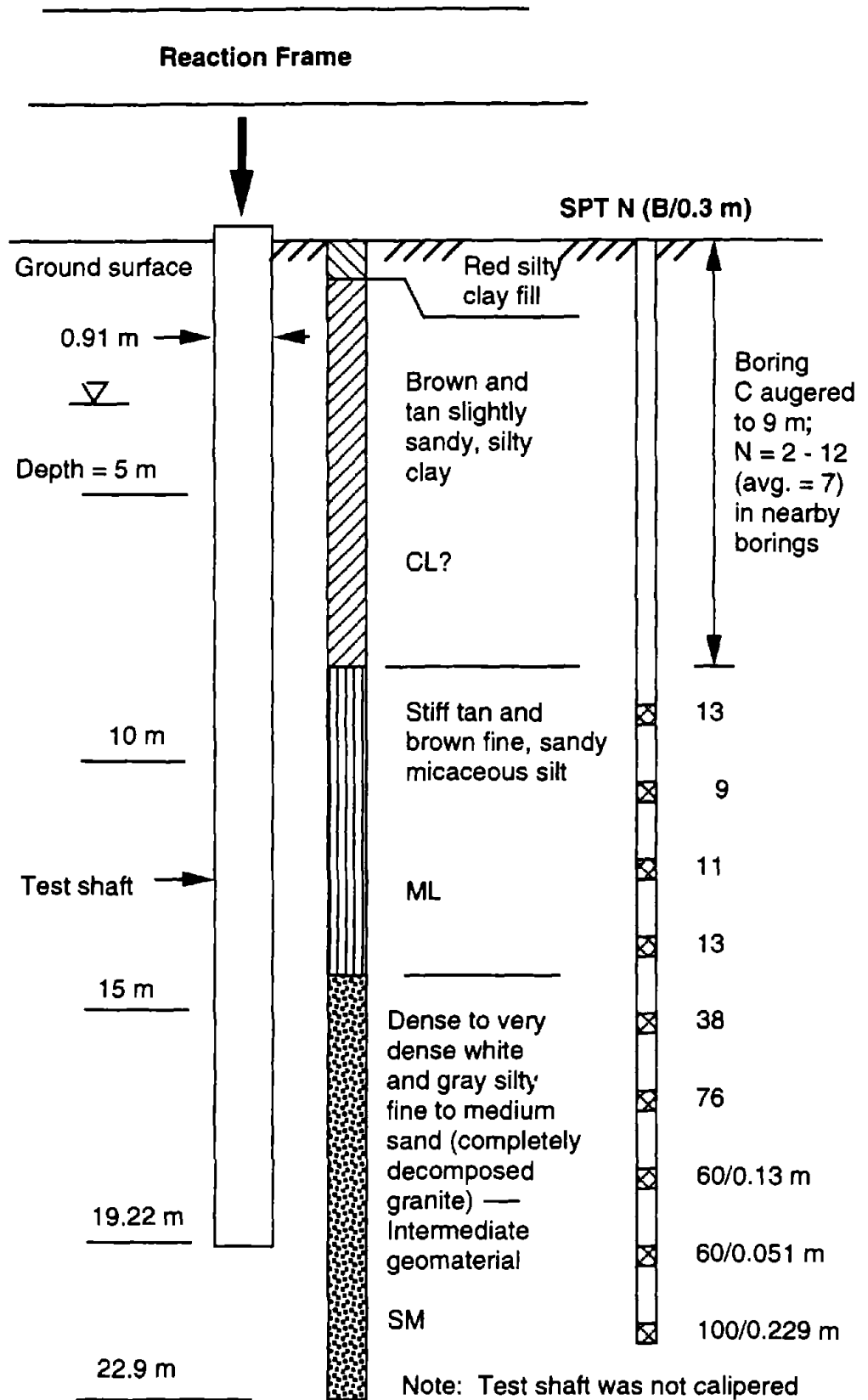
CL, ML, SM — Unified Soil System Classification Symbols

Figure 62. Shaft and geomaterial profile at Coweta County site.

The test shaft was drilled with auger equipment under a polyacrylamide polymer slurry the day prior to setting the reinforcing steel cage and placing concrete. Just prior to setting the reinforcing cage, it was discovered that about 0.5 m of sediment had collected in the bottom of the borehole. The contractor then reentered the borehole and drilled out the sediment and then increased the depth of the borehole beyond the original depth by about 1.0 m. As a result, the instruments, which had already been placed on the cage, were about 1.0 m deeper than planned. The instrumentation scheme is shown in figure 63. For this test, sister bars similar to those used at the Dallas site were employed. However, these instruments consisted of full bridges, so that no external dummy bars were used.

This shaft was a complete shaft, with no void at the base. It was not calipered.
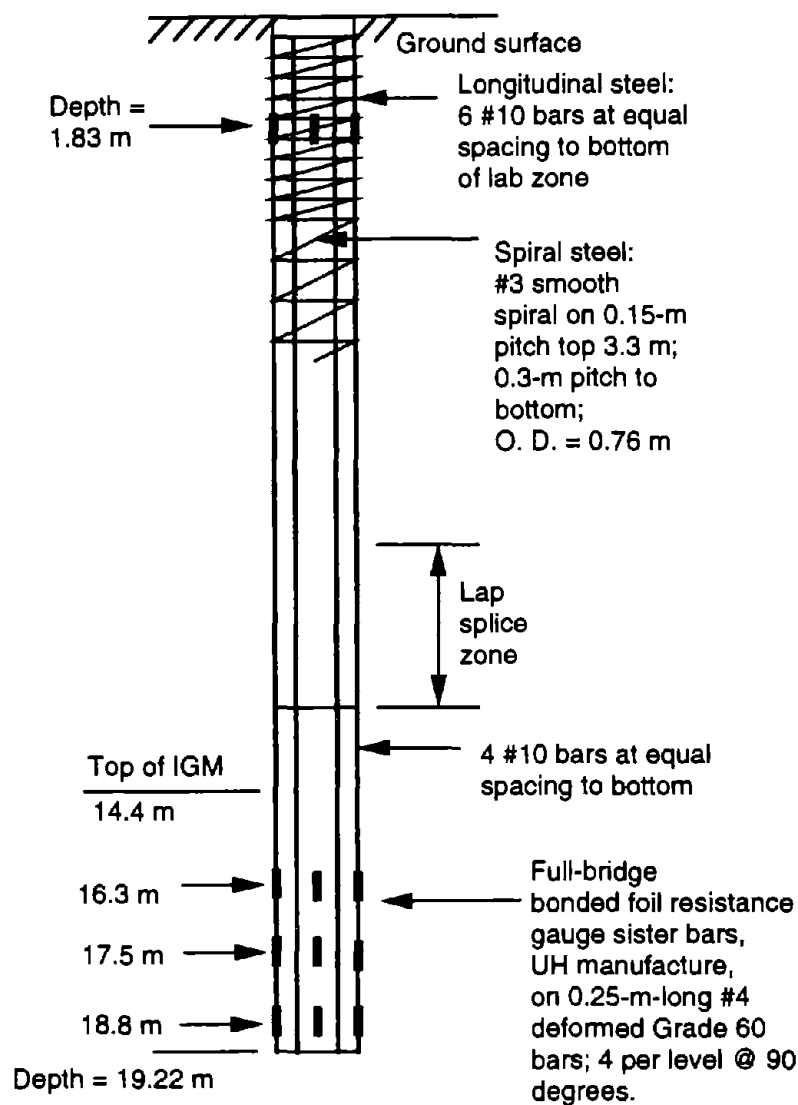
Figure 63. Instrumentation schematic for Coweta County test shaft.

131

The testing procedure was identical to that used at the Dallas site, except that no load cell was used. Applied loads were determined from calibrated jack pressures. Settlements were measured in a manner identical to that used in the Dallas site test.

The design model for Category 3 IGM's was based on correlations in Piedmont residuum similar to that found at this test site.

Boston Site

In order to test the Category 3 IGM design model for granular geomaterials that differ substantially from Piedmont residuum, for which it was calibrated, a loading test was conducted in glacial till at a test site in Boston, Massachusetts. Details are given in Appendix D. The site location is shown in figure 64. This test was conducted by the Commonwealth of Massachusetts for design purposes in connection with the design of the connector between the central artery and the third harbor tunnel.

General profiles of the test shaft and the site are shown in figure 65. The top of the glacial till, a fine-to-coarse-grained glacio-fluvial outwash material, was located at a depth of 36.1 m below the ground surface. The till is 6.0 m thick and is underlaid by an argillite of the Cambridge formation. Overlying the till are a series of soft natural and fill soils, most notably the soft Boston blue clay, which has a thickness of 24.4 m at the test site.

The geomaterials in the socket were characterized by continuous SPT tests, whose results (N blows per 0.3 m) are given in figure 66. The value at a depth of 40.5 m appears to have been influenced by the presence of a large cobble and was omitted from the data for purposes of making the calculations for the design model. The total unit weights of the geomaterials were taken to be 21.2 kN/m^3 in the till and 19.6 kN/m^3 in the geomaterial above the till from local practice. No site-specific unit weight data were available. The piezometric surface in the glacial till was at a depth of 3.0 m below the ground surface, which is the mean water level in the Fort Point Channel immediately adjacent to the test site, which is influenced by tidal fluctuations.

The test shaft, designated CLTP2 by the Commonwealth, was constructed as documented in Appendix D. A permanent steel casing 1.22 m O. D. was set into the till to a depth of 36.5 m through a borehole that was retained by lightweight bentonitic drilling slurry. The socket was then drilled, under the lightweight bentonitic slurry, with auger equipment to a depth of approximately 48.8 m. This placed the bottom of the socket about 6.5 m below the till-argillite contact. The socket within the till and argillite was then calipered by Appalachian Geophysics Company with a three-armed electronic caliper with unknown precision. The nominal socket diameter was 1.07 m. Concrete was placed to near the top of the argillite, and the Osterberg cell and related instrumentation cages were then placed. The 6.5-m length of socket below the Osterberg cell served as a reaction socket for the test on the till socket. The shaft was then concreted all the way to the surface so as to

South Station

Downtown
Boston

N

To Summer Street

Postal Annex

Boring IC 10-11

Test Site

Dorchester Avenue

Boston
Harbor

Test Shaft
(CLTP2)

Fort
Point
Channel

Existing
Bridge

100 m
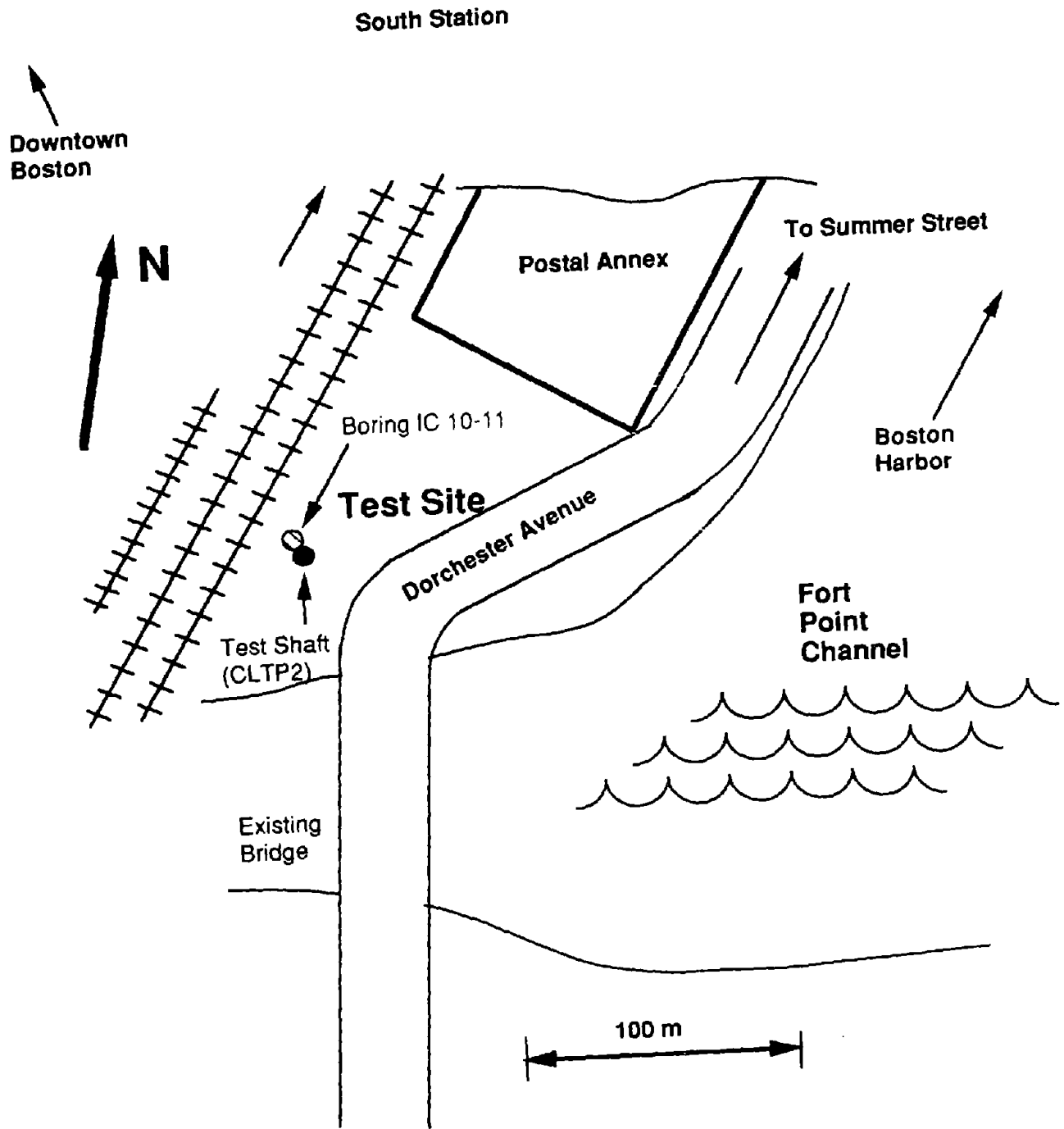
Figure 64. Location map for Boston test site.

Concrete to surface

El. 36.1 m

El. 33.1 m

Miscellaneous fill

El. 28.1 m

Organic soil

El. 24.4 m

"Starter" casing - removed after test

Boston blue clay

Slightly oversized,
slurry-filled borehole

Permanent steel casing

El. 0 m

Glacial till (IGM)

El. - 6.0 m

Test socket

Cambridge argillite (bedrock)

Reaction socket

Osterberg Load Cell

El. - 12.5 m
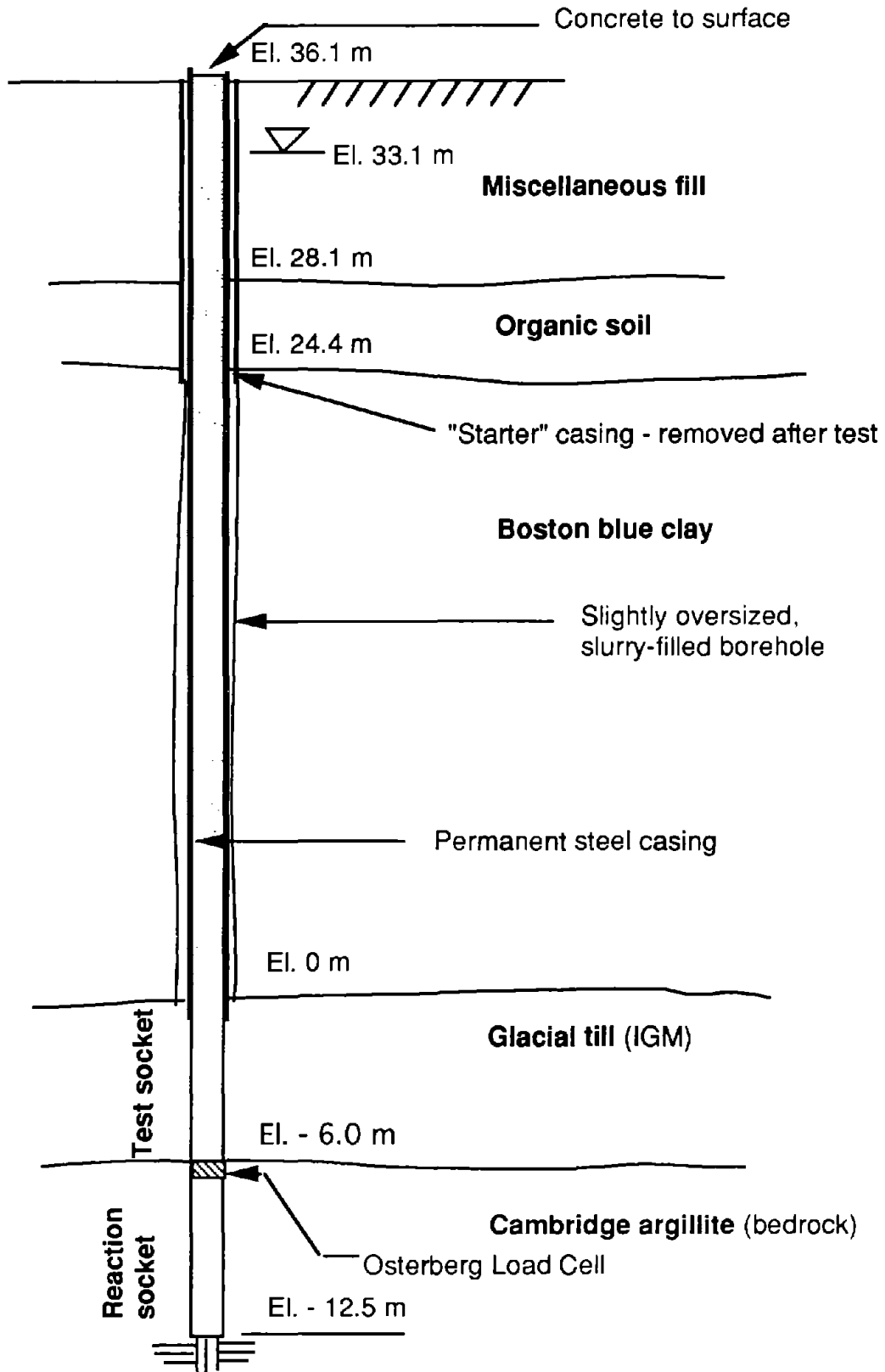
Figure 65. Elevation view of Boston test shaft and geomaterial profile.
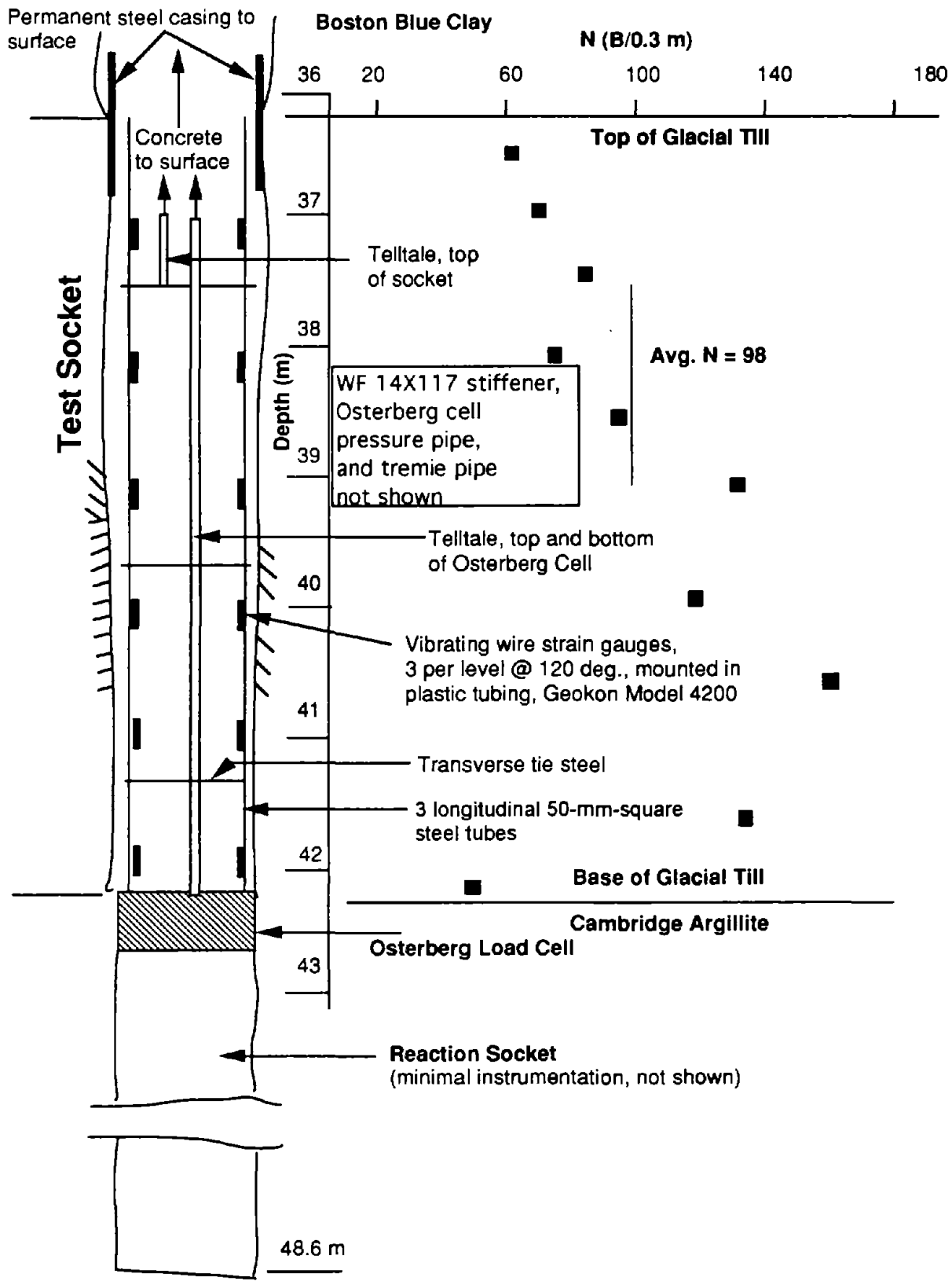
Figure 66. Instrumentation schematic for Boston test shaft.

replicate the fluid concrete stresses that would be present in the till (test) socket during construction of a prototype shaft.

Instrumentation for the socket in the glacial till is shown in figure 66. Loads along the socket were determined from the vibrating wire gauges and displacement of the shaft in the socket was determined from telltales in a manner similar to that done at the Owensboro site. The load test was conducted in a manner similar to the Owensboro test, except that the load was cycled once at a low load value and the load was also held constant until movement had ceased at a load level of 8.9 MN before proceeding to the failure load. In this case, side shear failure was observed in the test socket. Considerable movement of the reaction socket also occurred.

The caliper log (average radius) for both the till and argillite sockets are shown in figure 67. The shaft had a strong inward taper from the top to the bottom of the socket, which suggests that the Osterberg cell test produced a reverse wedge effect that probably made the results of the loading test conservative relative to ordinary compression loading.

Concreting occurred rapidly, and a high-slump concrete was used. However, no measurements of the horizontal concrete pressures in the socket were made. For purposes of executing the design model calculations, it was assumed that the concrete pressures were sufficient to re-establish the effective pressures in the geomaterial in the socket that existed before drilling, in accordance with the suggestions of Mayne and Harris. That is, figure 35 is not used with Model 2 unless concreting rate is slow or concrete slump is low.
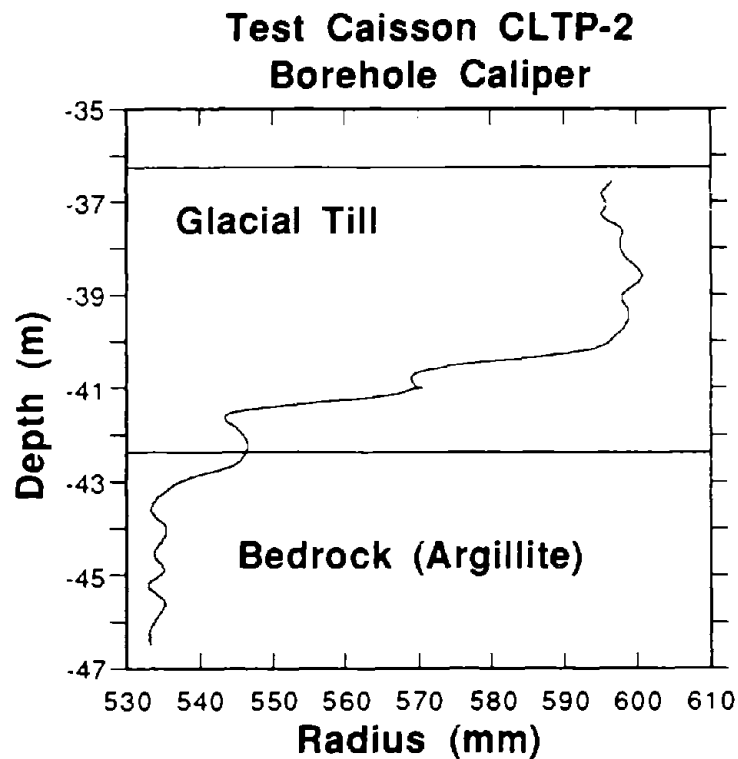
Figure 67. Caliper log for Boston test shaft.

136

Tampa Site

This site was not a formal part of this study, but personnel associated directly with this study from the University of Florida were directly involved in the loading test at this site, so that it was selected as representative of Category 2 IGM's. The test was conducted at the site of a three-story parking garage in the Tampa formation, a Miocene age limestone. More details on this test site can be found in reference 9.

A profile of the site and the test shaft is shown in figure 68. The socket was not calipered, but it was classified visually as "rough" by observers, which is purported to be typical of most sockets drilled into Florida limestone. It will be shown in chapter 6, however, that this shaft behaved as if it had a smooth interface. The loading test was a normal compression loading test that was conducted in a manner similar to the Dallas test.
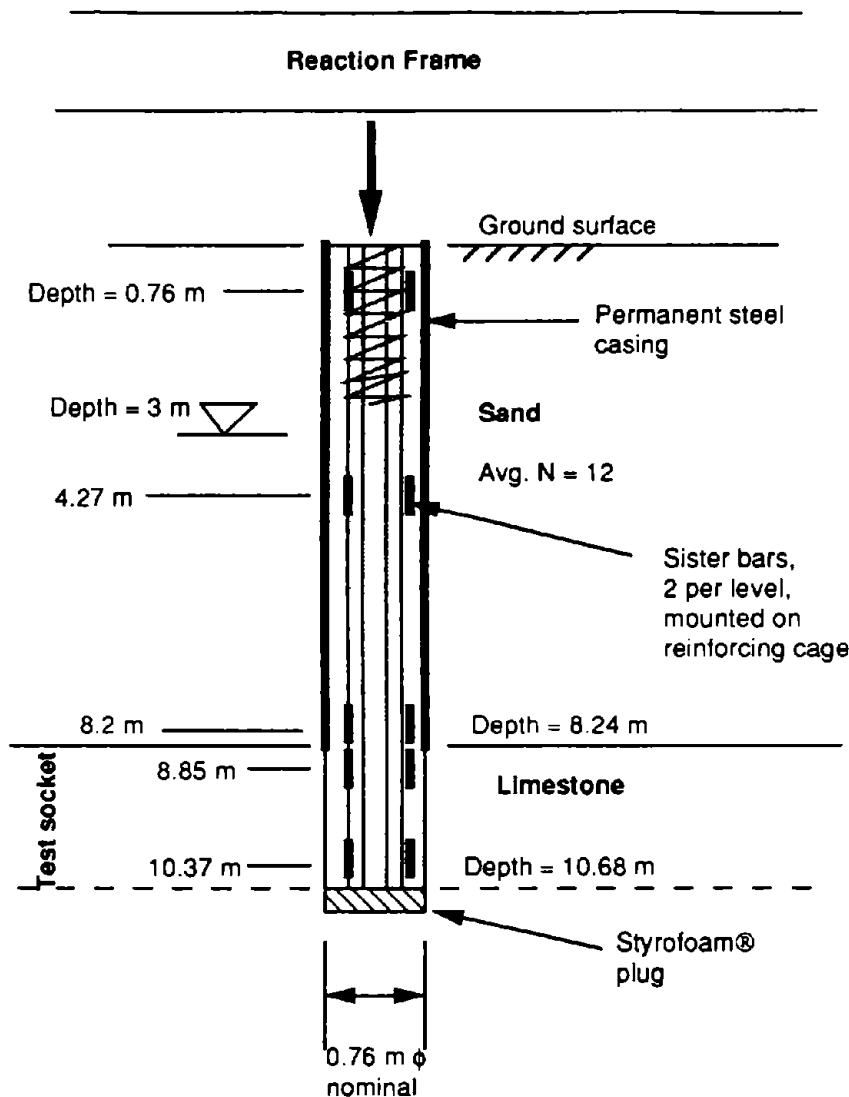
Figure 68. Profile of Tampa test shaft.

137

Toronto Site

The test site was at a shale quarry in Burlington, Ontario, in the greater Toronto area. Detailed description of the shale is given in reference 5. The formation tested was the Queenston shale (technically a mudstone), which is of Ordovician age. It consists primarily of illite, but also contains varying amounts of quartz, calcite, dolomite, and feldspar. Several short drilled shaft sockets were tested at this site as part of a research project. The particular shaft of interest is the one depicted in figure 69. The test shaft was intentionally grooved to produce a rough interface with known roughness features. The socket was calipered by hand before the concrete was placed. A partial tracing of the roughness profile along two axes is given in figure 70. The scale shown applies to both directions. The socket was not smeared. Note that RF = 0.76 is near the low end for "rough" shafts. Until more information can be obtained, it is recommended for design purposes in this report that RF be at least 0.10 for the socket to be considered rough.
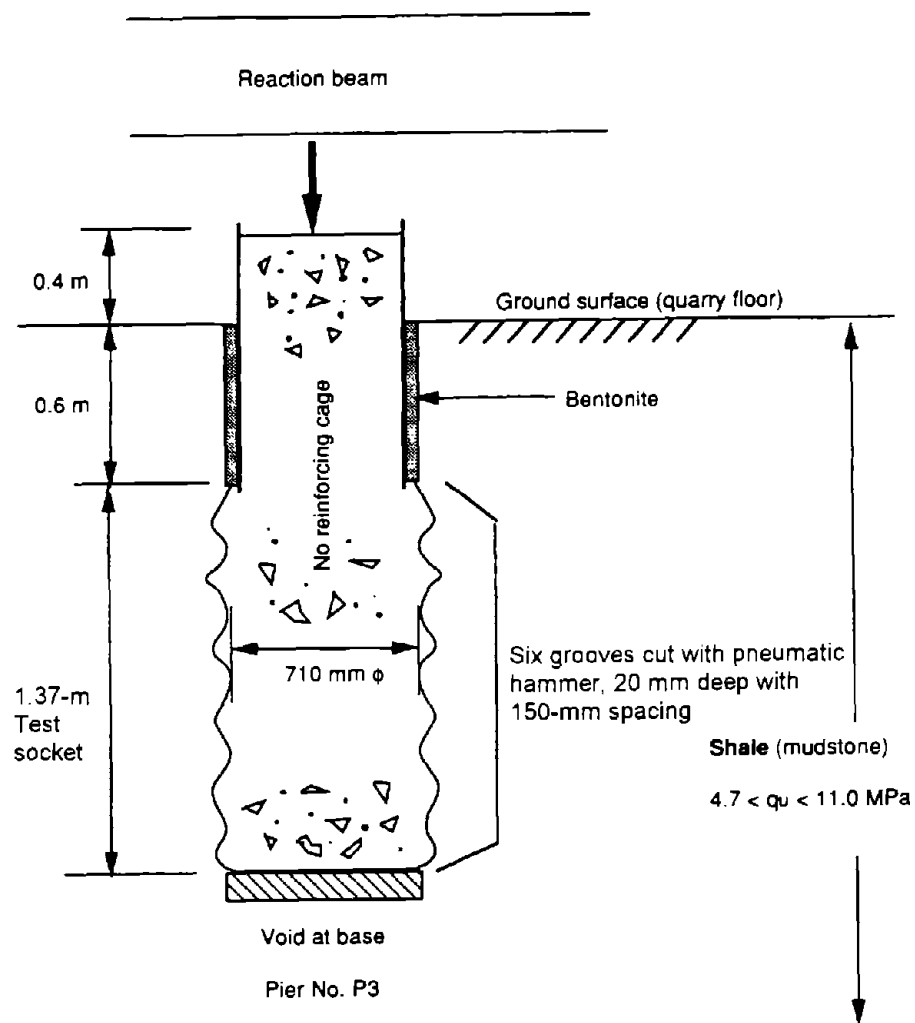
Figure 69. Profile of Toronto test shaft.

138
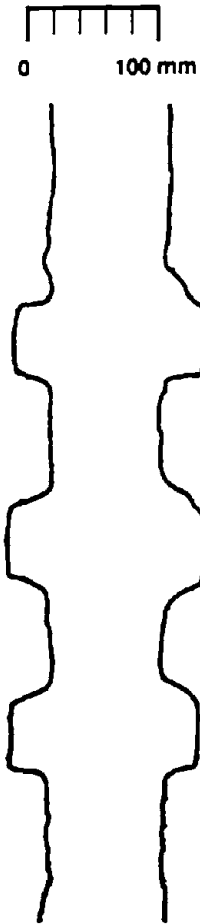
Figure 70. Caliper log of Toronto test shaft.

CHAPTER 6: COMPARISON OF FIELD TEST RESULTS WITH COMPUTED BEHAVIOR

GENERAL

The design models described in chapter 4 are compared in this chapter against loading test results for the test sites and the test shafts described in chapter 5.

The primary inputs for the design models are given in table 15 on a site-by-site basis. The symbols used in table 15 are defined in chapter 4. The design models used to compute load and movement for the test shafts were the "direct" models described in chapter 4. Unit load transfer methods, which are also described in chapter 4 for Category 1 and 2 IGM's, are expected to produce equivalent results. All computations were performed for this report by using simple spreadsheet analysis, systematically applying the appropriate equations from chapter 4. Example spreadsheets are given at the end of this chapter. M (equation 62) was set equal to 1 for Model 1, and K_o was taken as given by equation 45 in Model 2. Judgment was exercised in selecting $M = 1$. In all cases, either the concreting occurred much more rapidly than the rates used to develop figure 35 (Dallas, TAMU, Tampa), the shaft had a very large diameter (Owensboro), or the shaft was very shallow (Toronto), in which case N is approximately 1 in figure 35. Note that figure 35 is still recommended for design. No reduction in side resistance was made for inclusion of soft seams in the IGM at any of the test sites. That is, f_{aa}/f_a (table 8) = 1 in all cases.

The loading test results and comparisons of the computed and measured behavior are given in the following sections. All comparisons were made at the top of the IGM sockets, at which loads were always measured with the shaft instrumentation, rather than at the ground surface, to avoid having to use methods not developed in this study to compute resistance-deformation relations in overburden soils. Where settlements were not measured at the top of the socket, they were calculated from measured loads and estimated concrete moduli using measured surface loads and the column shortening formula. For some tests in which surface loading, as opposed to Osterberg cell loading, was employed, surface load-settlement relations are also given for comparison.

DALLAS TEST

Results for the Dallas test are shown in figure 71 (load vs. settlement) and figure 72 (progression of load vs. depth for selected applied loads). Inputs for the design model are given in table 15. The value of q_u used was the depth-weighted average along with shaft, with the very high values for samples containing thin seams of carbonaceous matter excluded. The mass modulus of the geomaterial was taken as the average value given by a Menard-type pressuremeter upon initial loading, which better represents the geomaterial properties, including any disturbance at the borehole-concrete interface than the reload modulus. The unit weight of the concrete was taken as the total unit weight, not the buoyant unit weight, because the ground water was perched and no evidence of water pressures in the pores of the clay-shale existed.

Use of the Category 1 design model with "smooth" socket formulation was justified based on profiling of the exhumed shaft (figure 47). This analysis yielded a resistance at $w_t = 25$ mm that was higher than that observed. A likely reason for the overprediction is that the angle of interface friction ϕ_{rc} was degraded from the value of 30 degrees that was measured under laboratory conditions. In addition, the design model was developed from

Table 15. Primary input values for design models.

Test	q_u (kPa)	E_m (MPa)	$\dfrac{E_m}{q_u}$	ϕ_{rc} (deg.)	Conc. Buoy.	E_c (GPa)	D (m)	L (m)	Roughness Condition	N Limit (B/0.3 m)
Dallas (Cat. 1)	710	232	327	30	None	46.0	0.61	6.09	Smooth	-
TAMU (Cat. 1)	800	154	193	30	None	31.0	0.61	6.76	Smooth	-
Owens-boro (Cat. 1)	8780	2019	230	30	Fully	34.7	1.80	5.16	Smooth	-
Coweta (Cat. 3)	-	73/151	-	-	Below 3 m	34.4	0.92	3.10	-	100
Boston (Cat. 3)	-	88/176	-	-	Below 3 m	25.4	1.07	6.10	-	None on avg.
Tampa (Cat. 2)	2300	264	115	30	None	15.0	0.76	2.44	Smooth	-
Toronto (Cat. 1)	6750	730	1081	30	None	31.2	0.71	1.37	Rough	-

Notes:
1. For Dallas and TAMU tests, E_m = avg. E_o from Menard-type pressuremeter.
2. For Owensboro test, q_u was depth-weighted average for the two geomaterials; E_m was assumed = 230 q_u (depth-weighted average), since E_m was not measured; and n was computed using values for the shale only.
3. For Coweta and Boston tests, values under "E_m" are modulus computed from N along sides of socket and at base of socket, respectively.
4. For Tampa test, E_m was assumed = 115 q_u, since E_m was not measured.
5. For Toronto test, E_m = avg. E from q_u and Goodman jack tests.

142
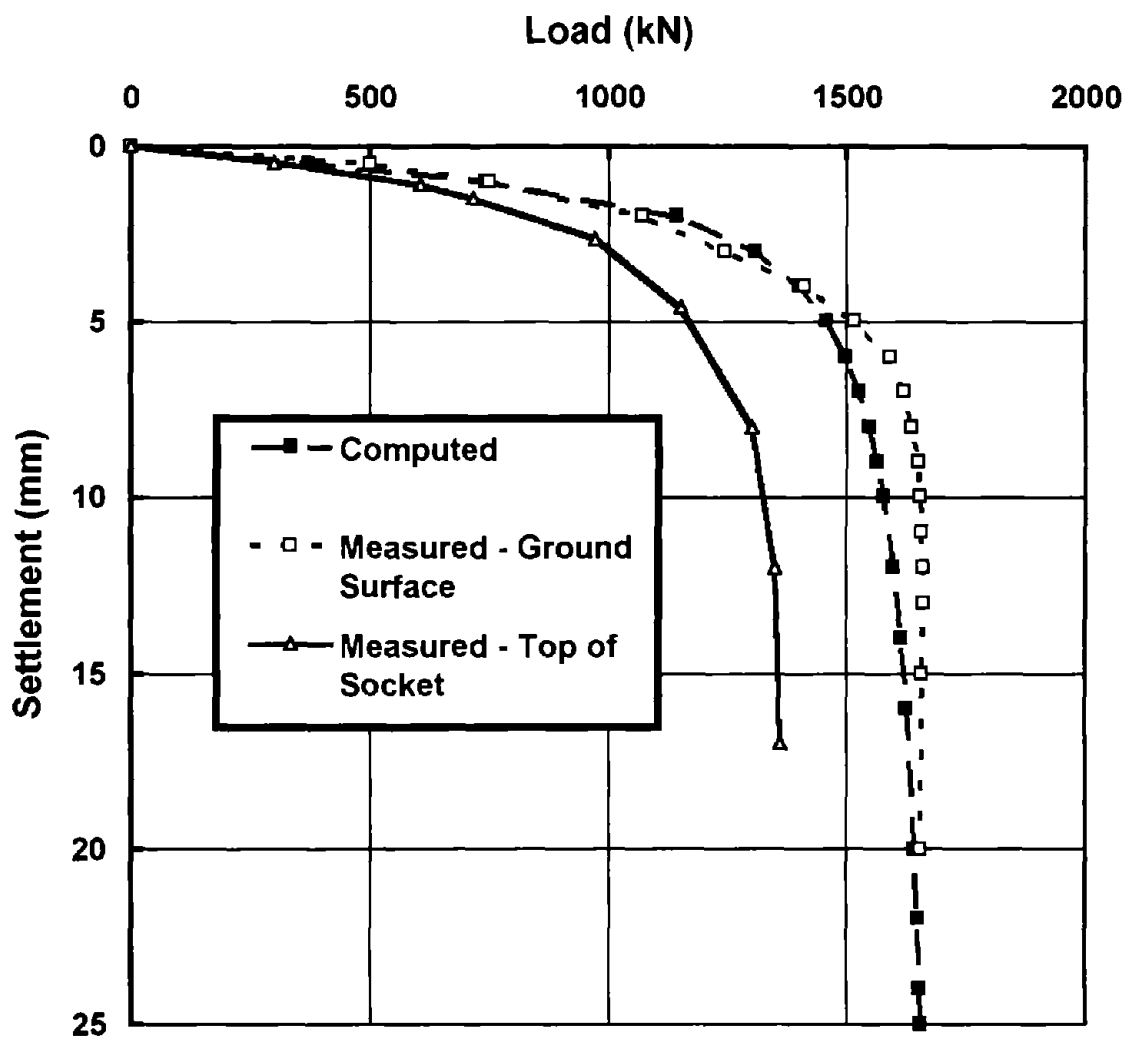
Figure 71. Computed and observed load-settlement results for Dallas test.
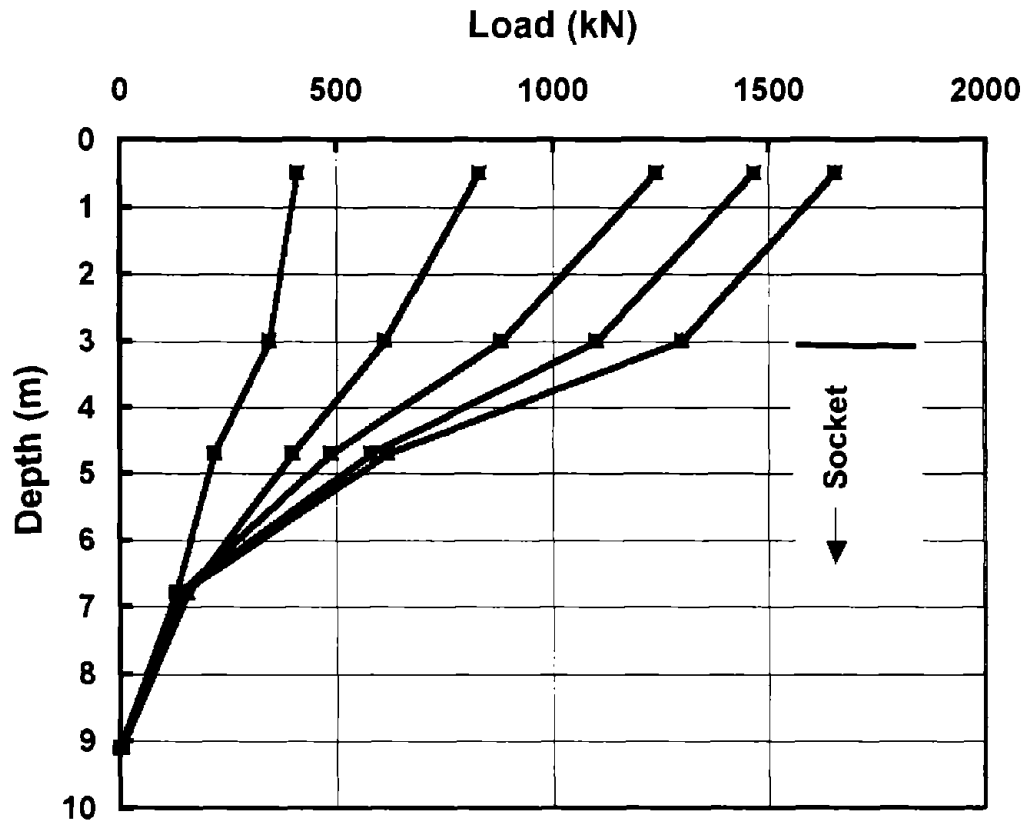
Figure 72. Measured load vs. depth relations for Dallas test.

finite element analyses in which base resistance existed, which will increase side load transfer to a value somewhat above that which will occur in a socket with a voided base, since the Poisson's effect is not produced with a voided base.

The load-depth relations given in figure 72 indicate that the highest load transfer occurred in the top half of the socket. The reduced load transfer in the lower half of the socket correlates with lower values of q_u in that region; but the early side shear failure, indicated by the overlaying of the load-depth relations beginning at very small values of applied load, suggests that the geomaterial at the interface was more severely degraded there, perhaps due to excessive exposure to perched ground water that had entered the borehole, accumulating to a depth of about 0.15 m before concrete was placed. The small inflow of perched ground water was not cased off in this test shaft

144

TAMU TEST

The results from the TAMU test are shown in figures 73 and 74. The undrained shear strengths of the argillaceous geomaterials at the Dallas and TAMU test sites are nearly equal, and both test sockets were of similar dimensions and were smooth; however, the TAMU test socket developed a much higher resistance than the Dallas test socket. This
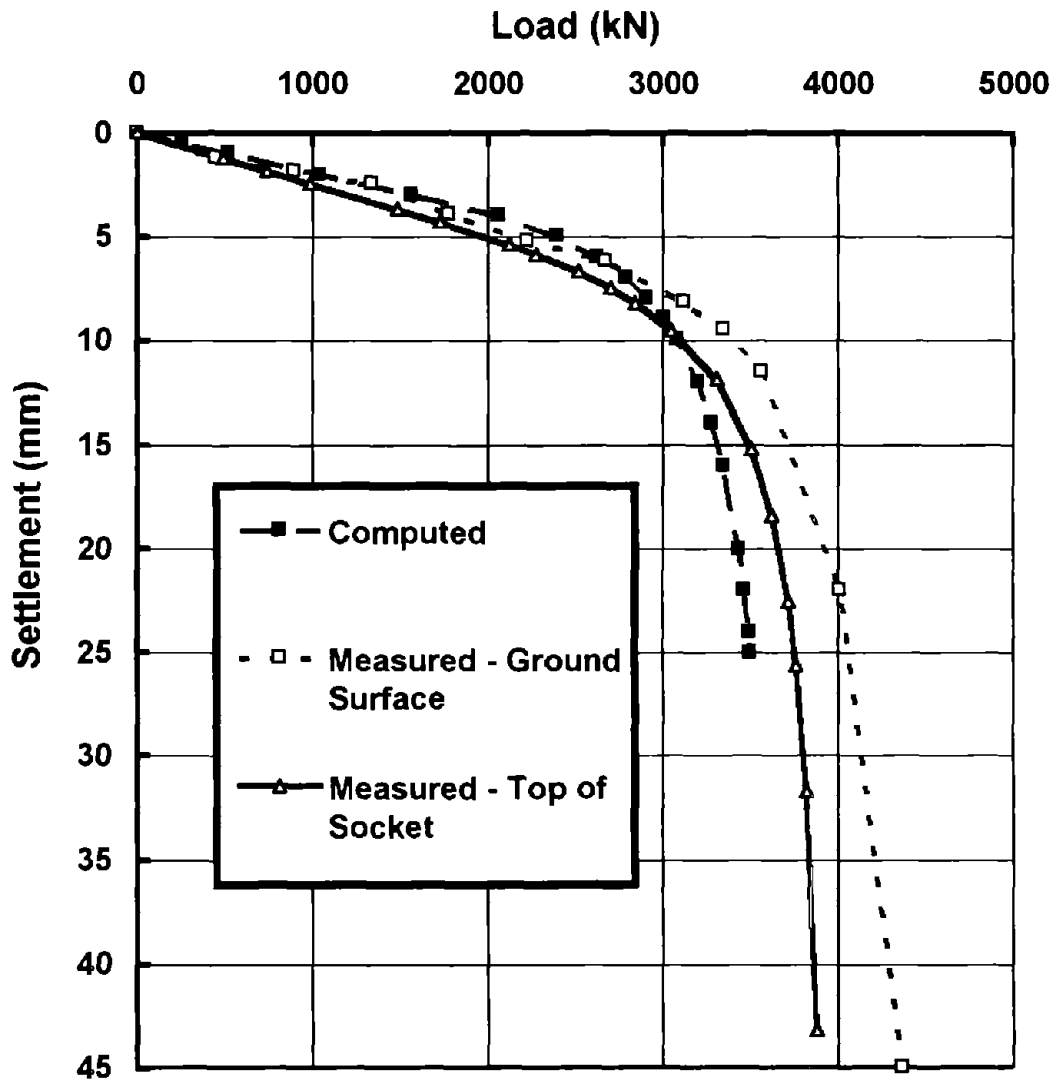
Figure 73. Computed and observed load-settlement results for TAMU test.

145
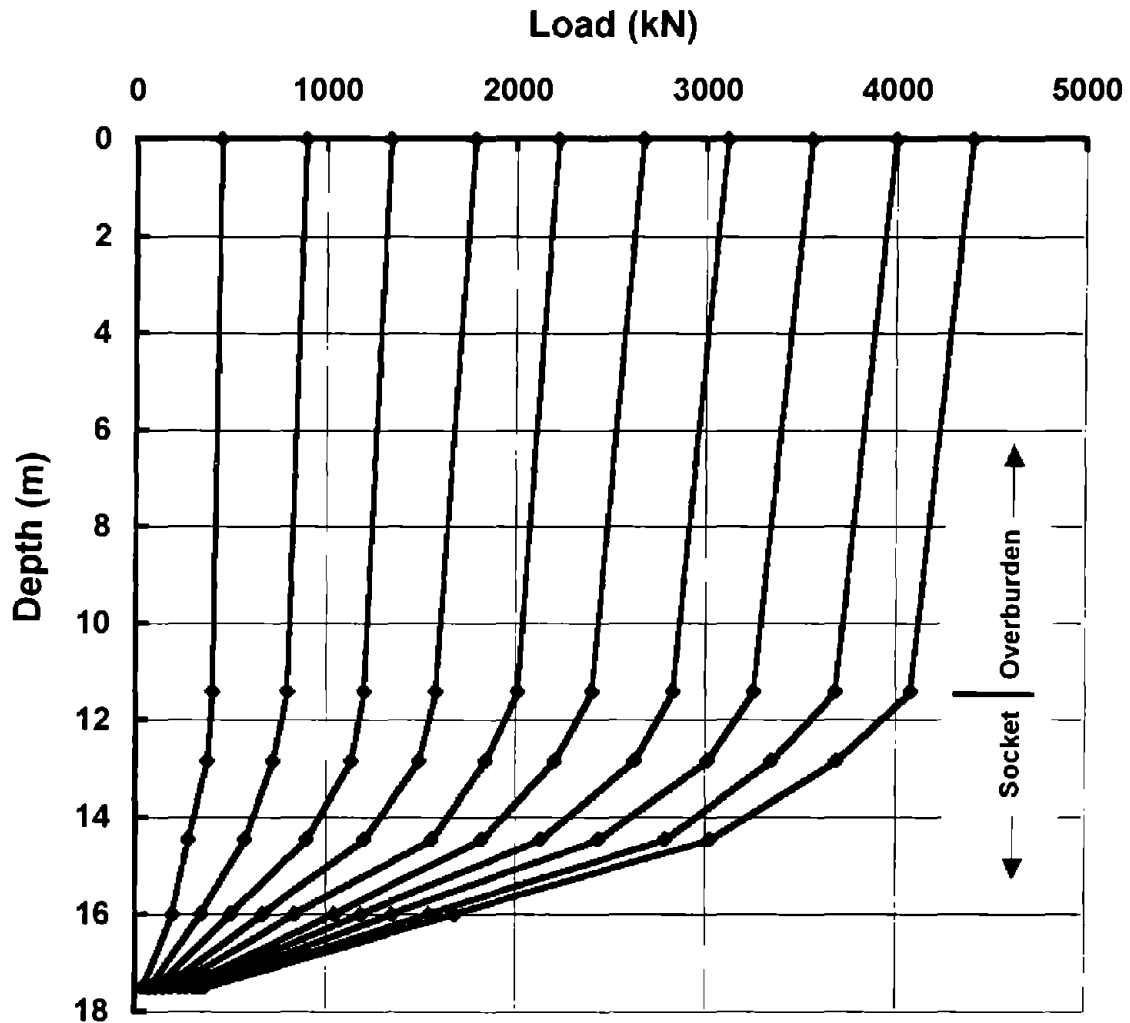
Figure 74. Measured load vs. depth relations for TAMU test.

behavior is predicted by the "smooth" interface model, which relates maximum side resistance to normal stress at the interface after concreting. Examination of figure 51 indicates that the socket is "smooth" according to the definition given in table 1. The mid-depth of the TAMU socket was over twice as deep as that for the Dallas site socket, which produces higher normal concrete stresses and, hence, higher unit side resistances. The waterbearing overburden materials were cased off during the concrete pour, and the socket itself was dry. For this reason, the total unit weight of the concrete was used in the concrete pressure calculations, with which the smooth interface model provided a reasonably close match with the load-settlement relation obtained experimentally at the top of the socket. In this socket, the load transfer pattern (figure 74) also generally followed the pattern of the depthwise variation of q_u.

OWENSBORO TEST

The Owensboro site test at Pier 9 was performed by loading from the base with an Osterberg cell. For purposes of comparison with the design model, it was assumed that the measured load-uplift relation for the socket would be equivalent to the case in which a compression loading test is conducted at the top of the socket, with a void at the bottom of the socket. The term "inverted socket" was used to describe this case, which is the condition for which the design model can be used. The measured and computed load-movement relations are compared in figure 75.
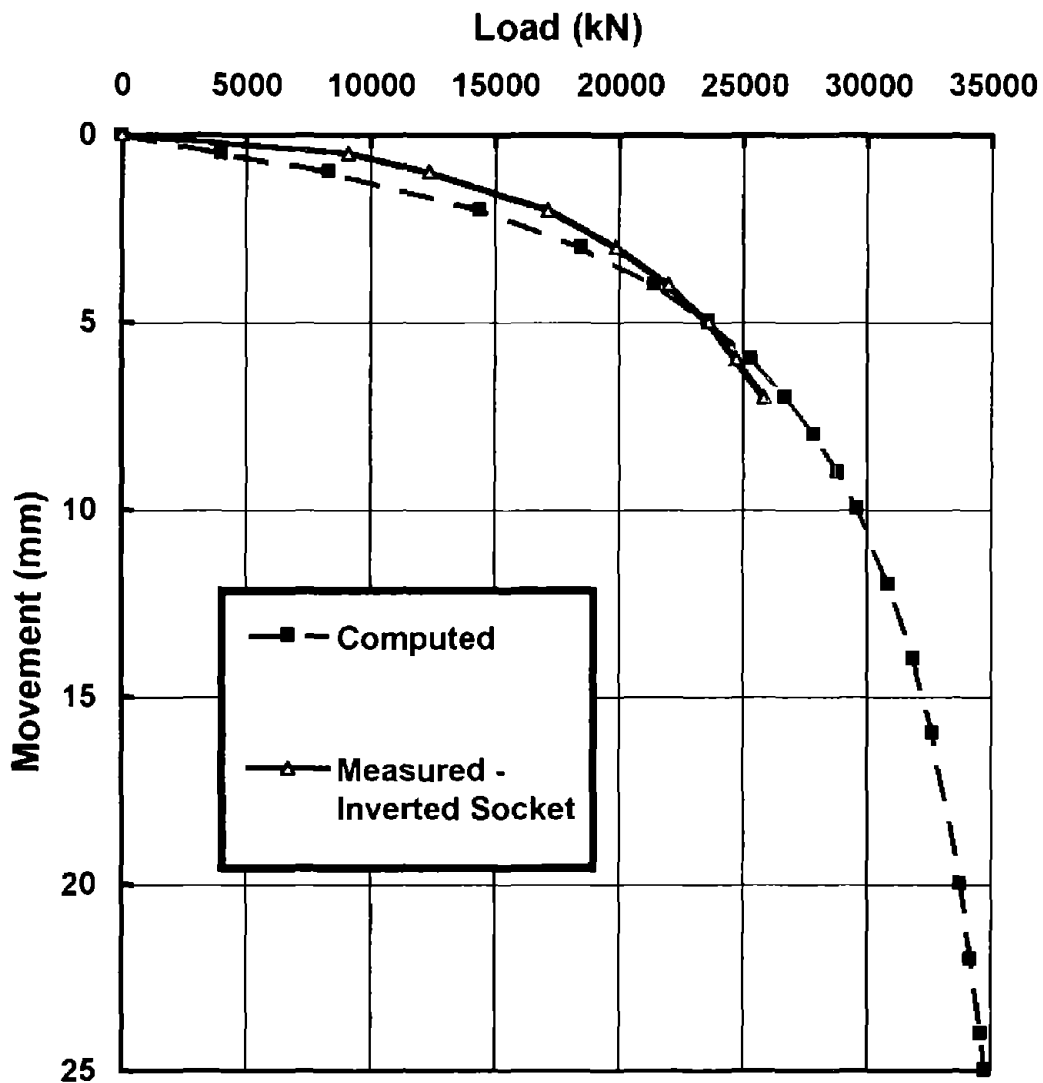
Figure 75. Computed and observed load-settlement results for Owensboro test.

Good agreement between measured and observed load-movement behavior can been seen.
The observed relation was taken from reference 38. In order to make the calculations, it
was necessary to use only the q_u and E_m values for the shale in order to compute the shape
factor n, since the values for the sandstone were out of range for figure 36. That is, it was
assumed that the shale properties completely controlled the shape of the load-movement
relation, which appears to be a good assumption in this case. The shaft was analyzed as a
smooth shaft, as the caliper log (figure 59) indicated asperity heights of less than 2 mm
counter to the direction of taper. This shaft may have behaved more as a rough shaft and
exhibited higher resistance had it been loaded in compression. The role that the polymer
drilling slurry may have played in controlling load transfer is not known; however, the
good correlation between measured and predicted behavior suggests that its effect was not
highly deleterious.

The load vs. depth relations measured for Owensboro test shaft 9-42 are shown in figure
76. Again, the rate of load transfer correlates qualitatively with the measured values of q_u,
the sandstone exhibiting much higher compressive strength than the shale. "Depth" on
figure 76 is distance below the top of the socket.
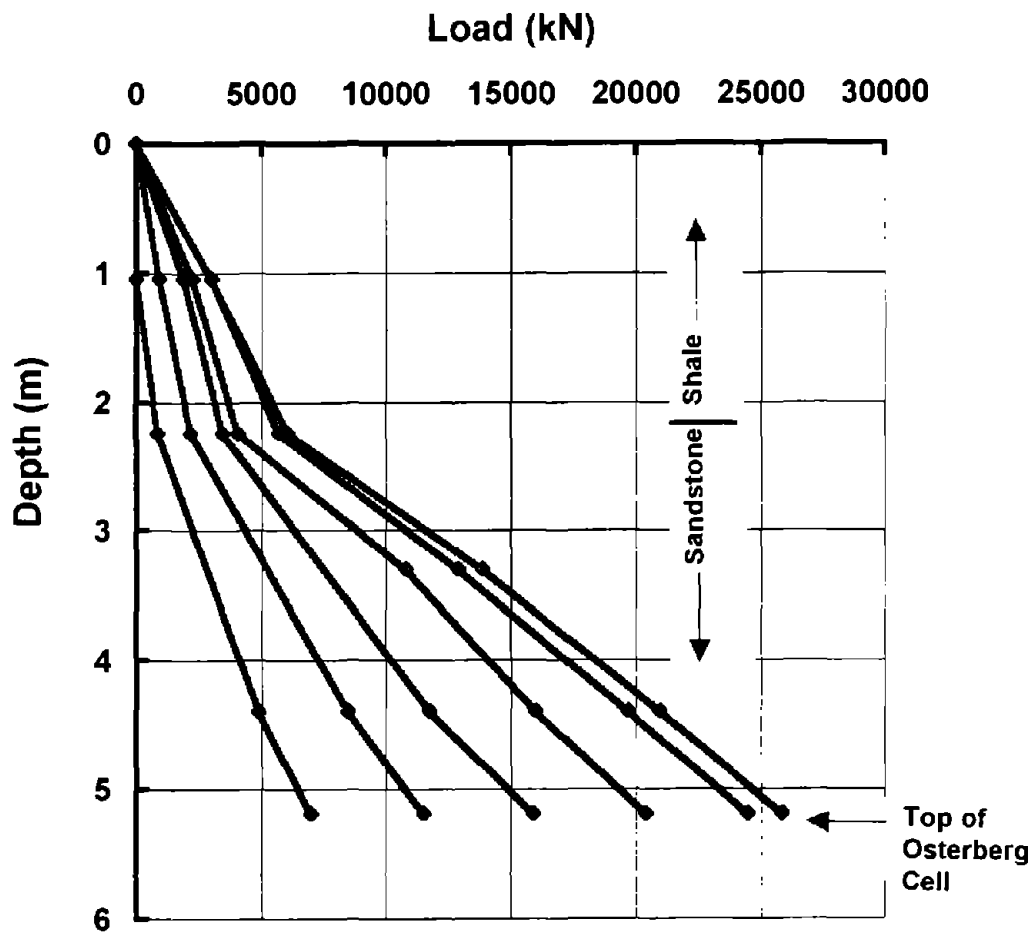
Figure 76. Measured load vs. depth relations for Owensboro test.

COWETA COUNTY TEST

The results for the Coweta County test are shown in figures 77 and 78. In order to make comparisons at the top of the socket, the top of the socket was defined to be at the elevation of the top level of socket sister bars, which was over a meter below the actual top of the socket because of the necessity to excavate the shaft deeper than was planned to clean out sloughed material prior to concreting. The computed and measured load-settlement relations for the top of the socket shown in figure 77 do not compare well if the raw N values are used in the calculations. A value of N exceeding 100 blows / 0.3 m is out of the intended range of the design model. Furthermore, this borehole stood open for about 18 hours before concreting and exhibited some characteristics of "sloughing" before the borehole was concreted, justifying the use of reduced values of N.
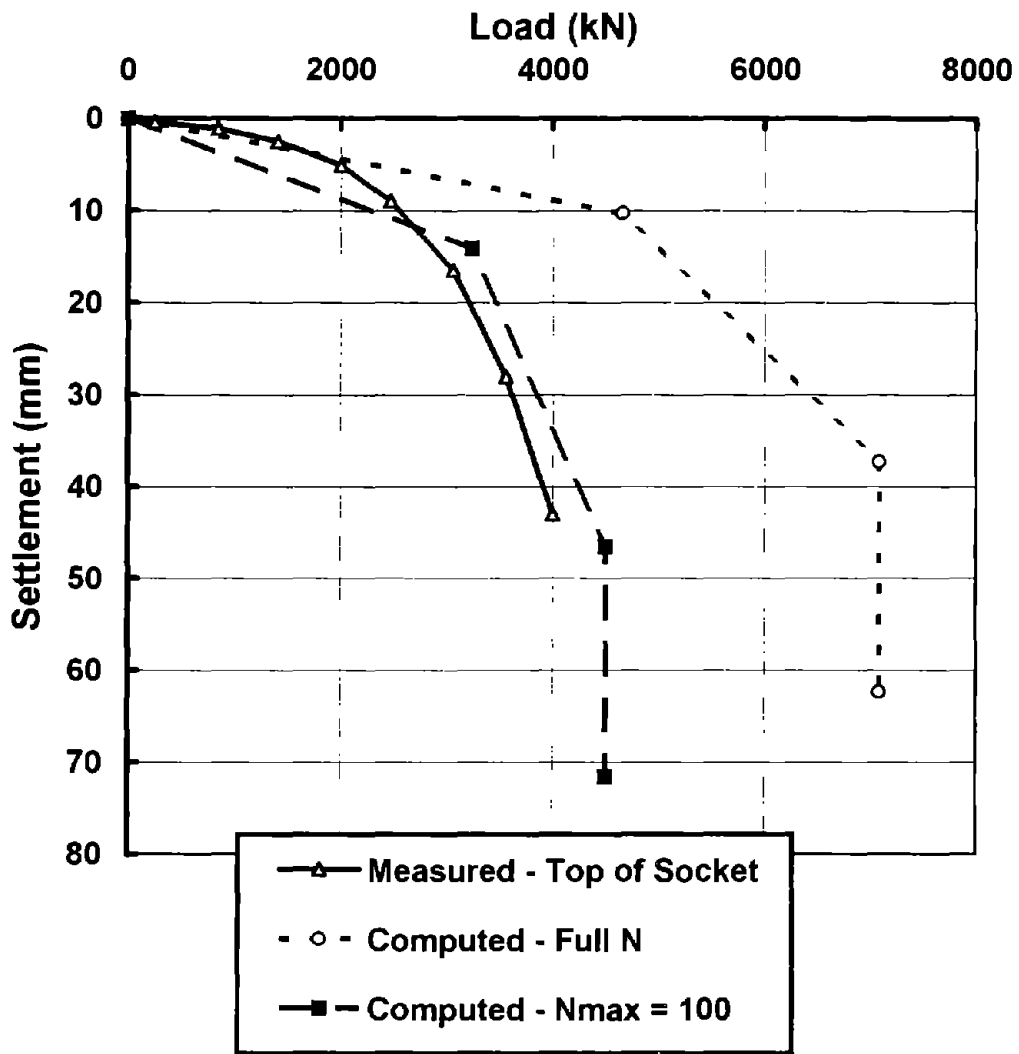
Figure 77. Computed and observed load-settlement results for Coweta County test.

An analysis was conducted in which N was restricted to 100 within any 1.5-m depth interval. Values below 100 were not varied. The results compare favorably with the measured load-settlement relation at the top of the socket. This analysis will be used in the overall comparison of the models with measured behavior. In both of the design model analyses, the concrete was assumed to be buoyant below a depth of 3 m (the depth of the water table) since the socket material was open-pored, with pore water pressures defined by the water table. The concrete was poured under slurry.

Analysis of figure 78 indicates that the load transfer pattern in the socket does not follow the pattern of N values qualitatively. The reason is not clear, but sloughing of the geomaterial near the base may have affected the results.
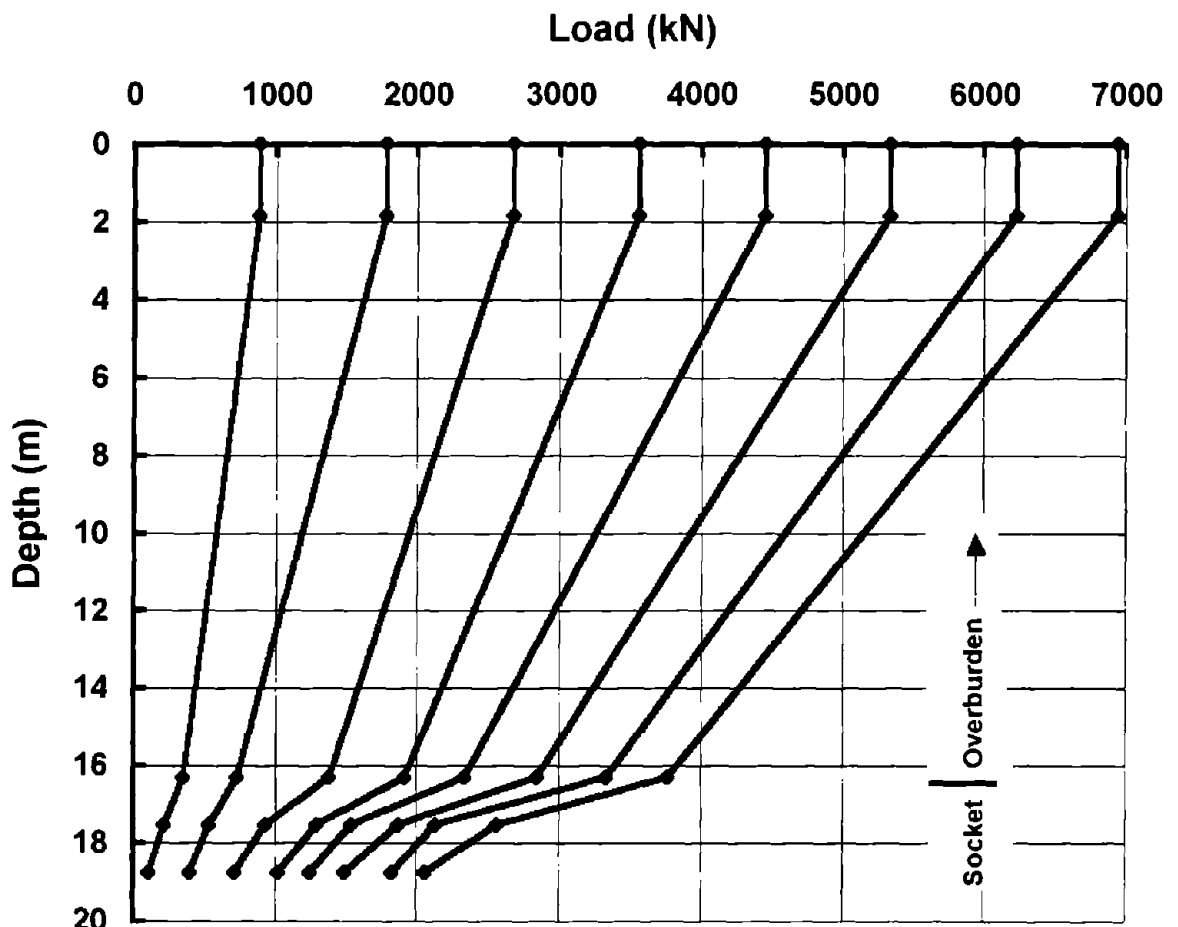
Figure 78. Measured load vs. depth relations for Coweta County test.

BOSTON TEST

This test was incorporated to investigate the applicability of the proposed Category 3 design model to geomaterials other than the residual, sand-like geomaterials for which it was originally calibrated. Like the Owensboro test, the Boston test was conducted using

150

an Osterberg cell to apply the load, and the inverted socket concept was again used to compare computed results with measured results. The pressure registered by the oil pressure gauge at the surface was used to compute the applied load directly. The weight of the shaft overlying the cell was not subtracted because the shaft was buoyant and because the pressure in the cell was higher than that measured at the surface by an amount controlled by the head of the oil. Any error made by this operation will be very small. The load-movement relations for the socket are shown in figure 79, and the load-depth relations measured within the socket are shown in figure 80. As in figure 76, the term "Depth" in figure 80 indicates depth below the top of the socket.
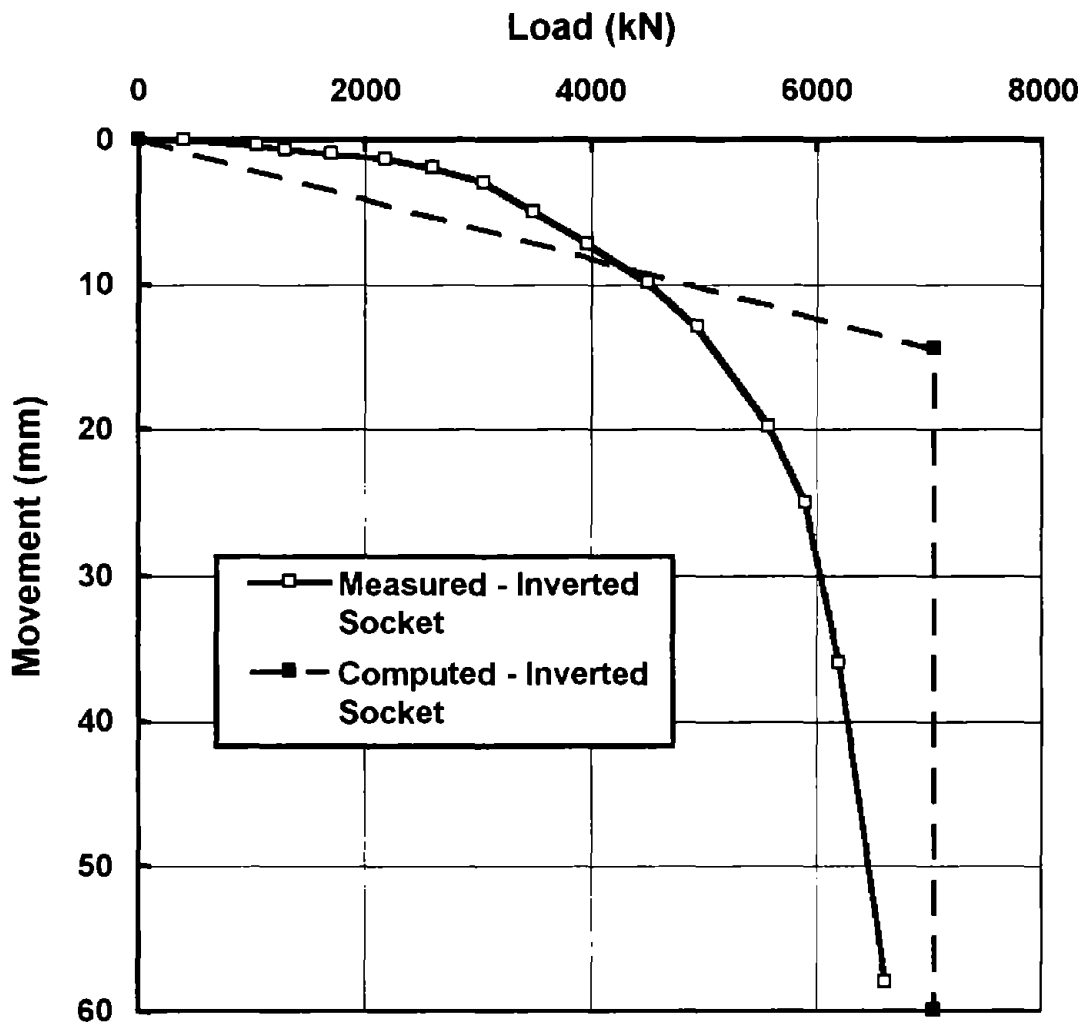
Figure 79. Computed and observed load-settlement results for Boston test.

Load (kN)
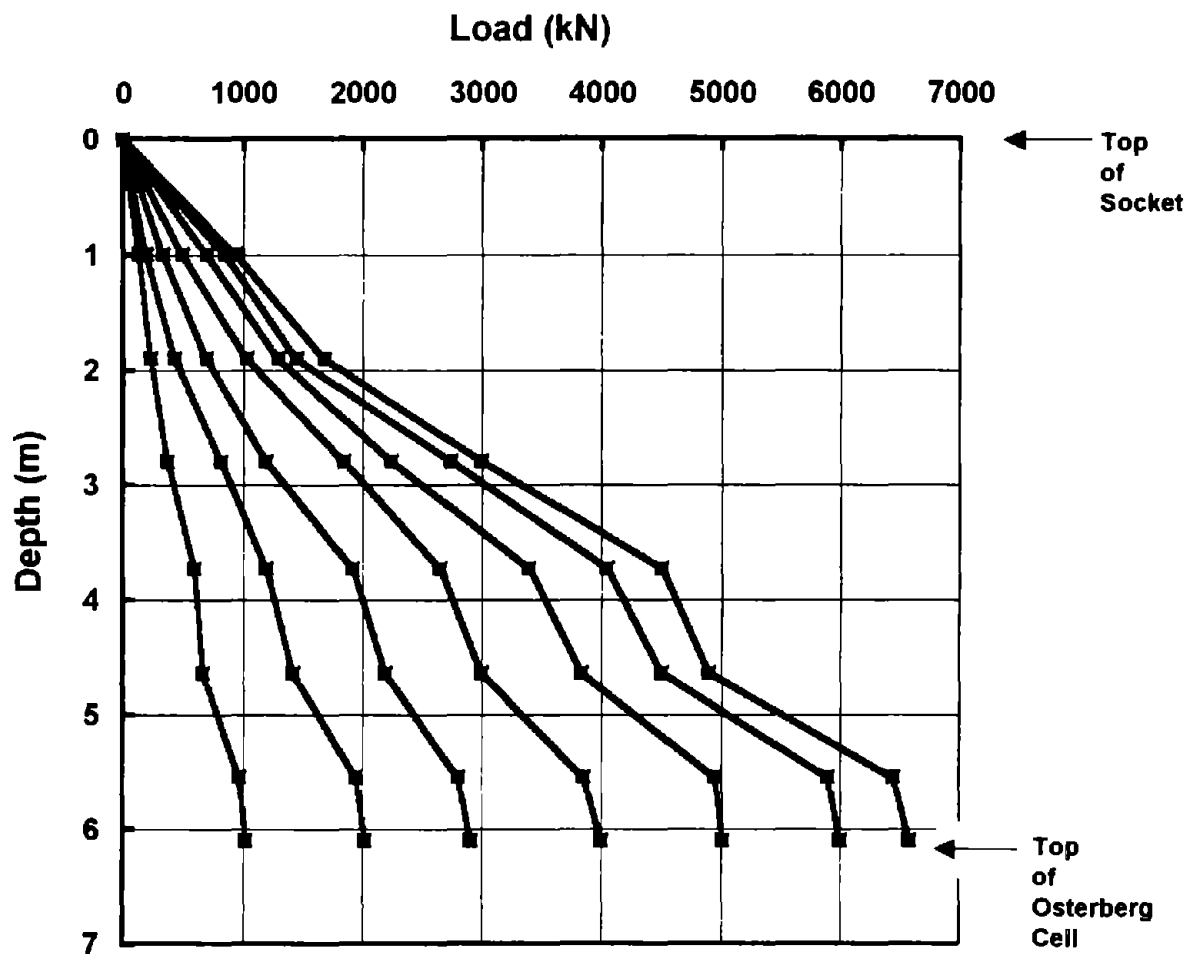
Figure 80. Measured load vs. depth relations for Boston test.

In analyzing this test, no reductions were made in N, despite some values exceeding 100 blows / 0.3 m, because drilling and concreting were carried out in a continuous fashion in one work shift. Note, however, that the average N value over the length of the socket was, in fact, less than 100. One high value was eliminated (depth of 40.6 m, figure 66) because it appeared that this test was performed on cobbles. It is observed in figure 67 that the socket was tapered inward from top to bottom by 60 mm in radius. The socket would likely have had higher resistance if loading had been from the top rather than from the bottom, which may explain the small overprediction of the design model for this site.

Measured load transfer to the geomaterial is seen in figure 80 to be generally uniform with depth. Just above the Osterberg cell, there appears to be a reduction in load transfer, as evidenced by the increase in slope of the load-depth relations. This behavior may be real,

152

or it may be an artifact of the different methods used to compute loads at the level of the Osterberg cell and within the shaft.

TAMPA TEST

The load-settlement and load-depth relations for the Tampa test are shown in figures 81 and 82, respectively. It is striking that the design model for Category 1 and 2 IGM's, when used with the "rough" interface formulation, does not predict the observed behavior well. The rough interface formulation was used because the anecdotal description of the borehole was that it was rough. Since no direct inspection or caliper log of the borehole
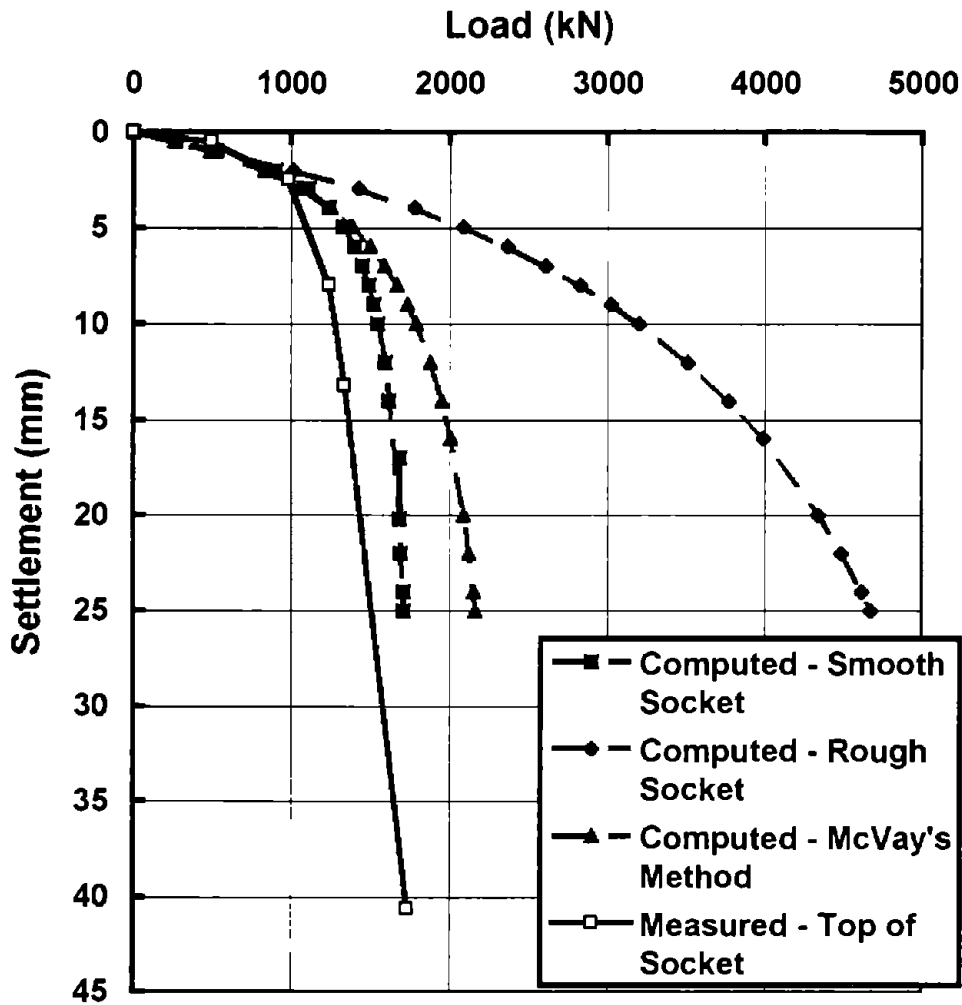
Figure 81. Computed and observed load-settlement results for Tampa test.

153
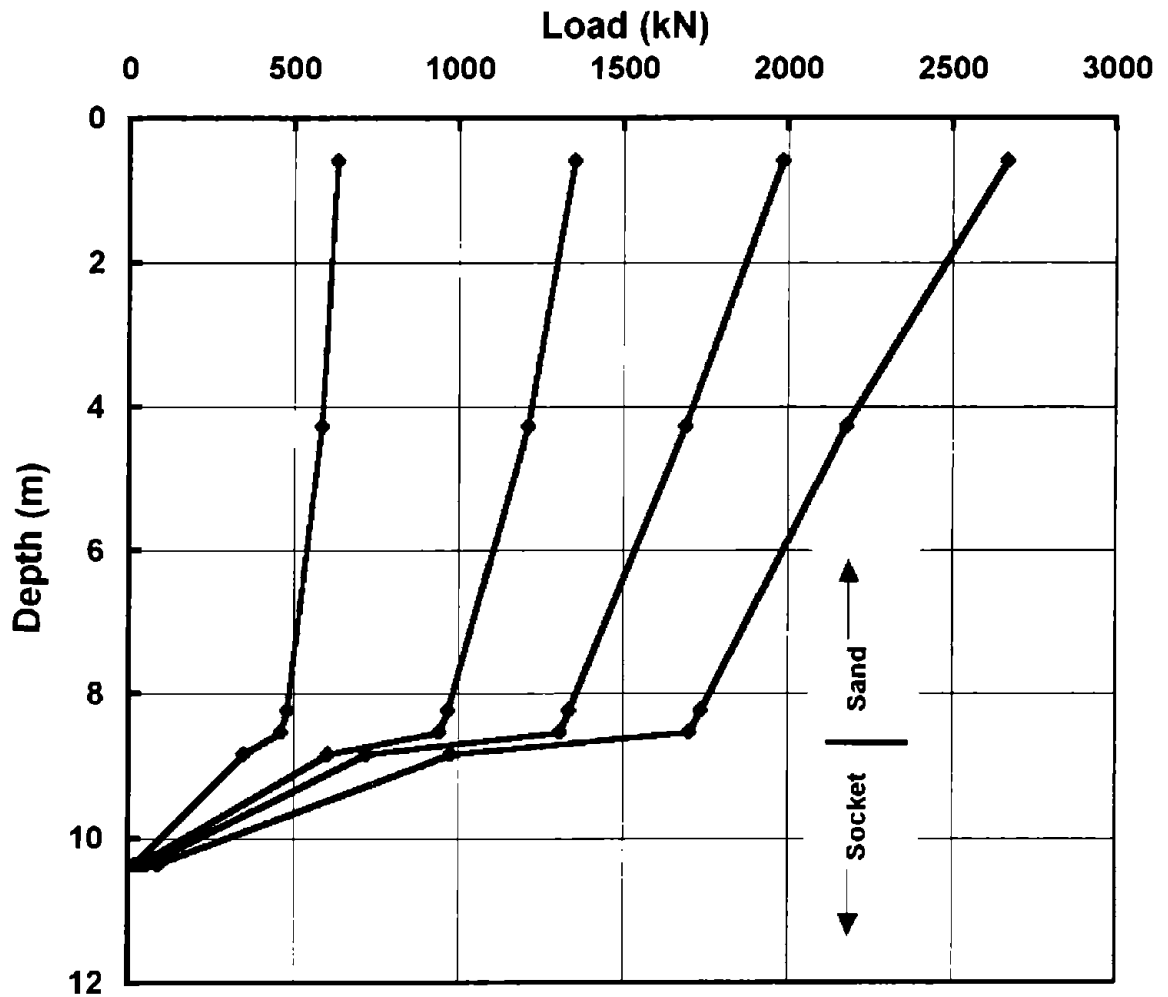
Figure 82. Measured load vs. depth relations for Tampa test.

was made, the existence of a rough interface cannot be confirmed. A "smooth" interface analysis provides a much better simulation of the measured behavior. For reasons that are not clear, it can only be concluded that the smooth interface analysis is more appropriate for soft limestones of the type encountered at this site. Alternatively, the smooth interface analysis was performed using McVay's formulation for f_{max} (equation 37) to be equal to f_{aa}, but otherwise not varying the solution. The results are much improved over the rough interface model.

The load-depth relations suggest that full unit side resistance had developed near the top of the socket at a relatively small settlement (10 to 15 mm), but that side resistance near the bottom of the socket, while lower that that at the top, was continuing to increase at a settlement of 40 mm. This phenomenon could be the result of the Poisson's effect in the shaft or frictional behavior of the base geomaterial.

154

TORONTO TEST

The Toronto test on an artificially roughened socket was selected for analysis, since none of the test sockets in the Category 1 and 2 IGM's investigated for this project by the study team could be confirmed to be rough according to the criteria in table 1. The test was of high quality, and adequate geotechnical property measurements and caliper data existed to permit application of the design model without the need to make excessive assumptions. It is recognized that the test socket had a very small aspect ratio and that the strength of the soft shale that was tested was slightly higher than the upper boundary established in this report for intermediate geomaterials. However, analysis of this test provides good insight into the utility of the "rough" socket model.

Measured and computed test results are compared in figure 83. The match is excellent. It is noted that a high ratio of measured E_m to measured q_u existed at this site, untypical of the ratios experienced at Category 1 IGM test sites. This observation points out the need for making site-specific measurements of the IGM modulus if accurate predictions of settlement are to be made.
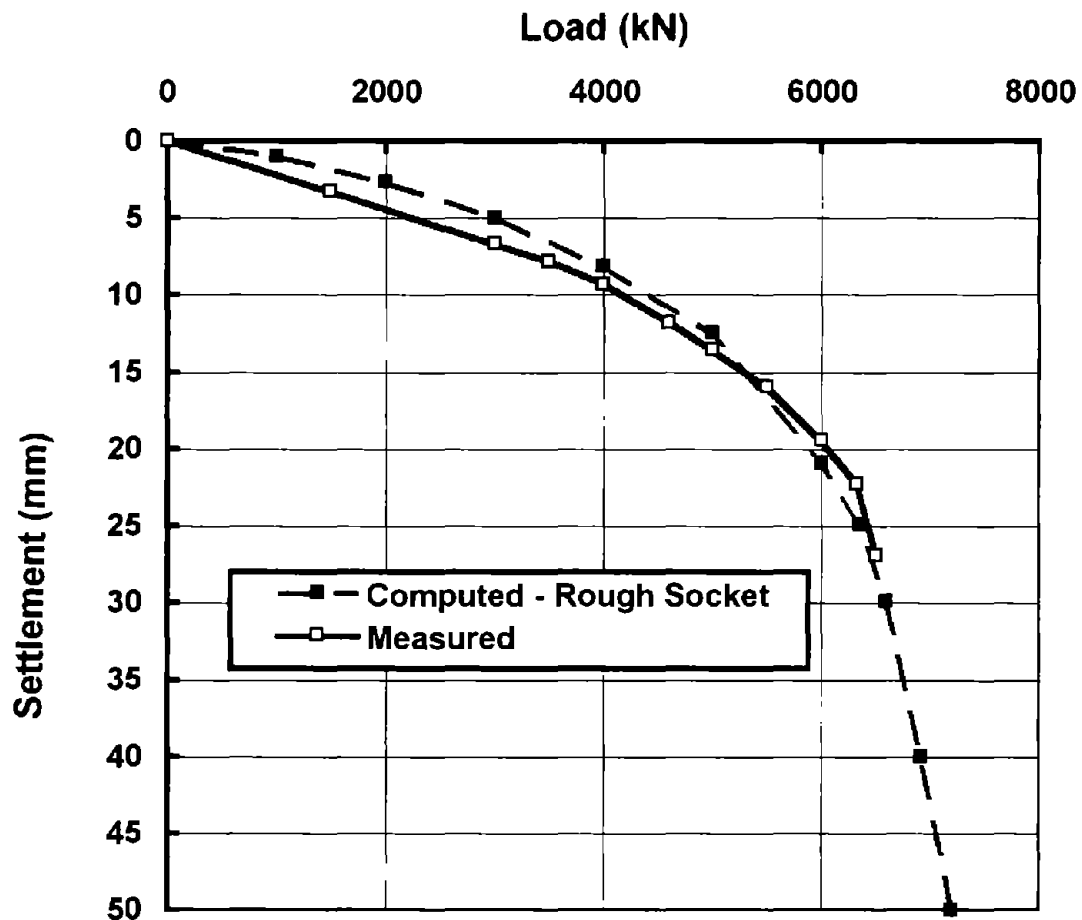
Figure 83. Computed and observed load-settlement results for Toronto test.

DISCUSSION OF RESULTS

A summary analysis of the quality of the matches between the measured and computed response of the test shafts considered here is provided in table 16. Two error metrics were chosen to represent the errors quantitatively. Metric A is the ratio of computed load at the top of the socket to the load measured at the top of the socket when $w_t = 25$ mm or the largest settlement measured in the loading test. Metric B is the ratio of computed settlement to measured settlement at the load equal to one-half of the measured socket load corresponding to $w_t = 25$ mm or to one-half of the maximum measured socket load if a settlement of 25 mm was not reached in the loading test.

Table 16. Error metrics for design models.

Test (IGM Category)	Metric A	Metric B
Dallas (1)	1.20	1.48
TAMU (1)	0.92	0.82
Owensboro (1)	1.04	1.80
Coweta County (3)	1.07	1.80
Boston (3)	1.18	2.18
Tampa (2)	1.13	1.00
Toronto (1)	0.99	0.77
Mean	1.08	1.41
Standard Deviation	0.10	0.55
Coefficient of Variation	0.09	0.39

On the average, the design models with the input conditions described compute ultimate resistances (defined as loads corresponding to settlements at the top of the socket of 25 mm) that are 8 percent too large and settlements at one-half of the ultimate resistances that are 41 percent too large. The coefficient of variation (COV) in predicted ultimate resistance was under 10 percent. Consideration of the two additional tests analyzed in Appendix C has no appreciable effect on these statistical properties.

Observation of the limited measured and computed load-movement relations described in this chapter suggests the following modifications/applications of the design models pending the acquisition and analysis of additional, appropriate field test data:

- **For the Category 1 and 2 IGM design model ("Model 1") for smooth socket analyses, $\phi_{rc} = 27.5$ degrees should be used, not 30 degrees as determined in the laboratory study reported in Appendix C, which translates to $f_a = (\tan 27.5 / \tan 30) \times \alpha \, q_u$ (from equation 61) $= 0.90 \, \alpha \, q_u$.**

156

- For the design model for Category 3 IGM's, N should be limited to 100 B/0.3 m in any 1.5-m depth increment of the shaft.

- A socket should not be treated as "rough" using the design Model 1 for IGM's in Categories 1 and 2 unless clean grooves of at least 25 mm deep and spaced between 0.15 and 0.3 m vertically are specified. Structural capacity of the concrete asperities (grooves) should be verified.

- Measurement of E_m in the field is necessary for optimum application of the design model for geomaterials in Categories 1 and 2. Otherwise, for Category 1 IGM's, E_m/q_u = 250 to 300 appears adequate and generally conservative for design use; for Category 2 IGM's, E_m/q_u = 115 appears justified based on the analysis of the Tampa test.

- It appears that McVay's method for computing f_{max} in massive, soft limestone of the type found at the Tampa test site can be used as a replacement for the variable f_{aa} in the design model for Category 2 IGM's.

- For computing σ_n, the test results suggest that the full head of fluid concrete can be used if concrete with a 175-mm slump (or greater) is placed at the rate of at least 15 m/h or if the shaft has a diameter exceeding about 2 m. However, until this behavior is confirmed to occur consistently in normal construction practice, figure 35 and equation 62 should be used to estimate σ_n for Model 1. The concrete should be taken as buoyant below the water table if the concrete is placed by pump or tremie underwater or under a slurry. That is, the unit weight (γ) of the concrete below the water table should be taken as $\gamma_{concrete} - \gamma_{water}$ when computing the hydrostatic pressure σ_n. If the concrete is placed in the dry, including situations in which a waterbearing overburden is cased off prior to completing a borehole in the dry, no buoyancy in the concrete should be assumed.

It is pointed out that the design models described here, with the interpretations for input outlined above, tend to give resistances that are slightly above the average of the measured resistances and tend to predict settlements under working-level loads that are slightly higher than measured settlements. This behavior should be considered when selecting resistance factors or safety factors for use in static design.

EXAMPLE SPREADSHEETS

An example spreadsheet for performing the calculations for Model 1 is given showing formulas in table 17 and numerical values for the Dallas test in table 18. The spreadsheet is self-explanatory. Symbols used are equivalent to symbols used in this report. This version considers only smooth interfaces. For rough interfaces, α is input as 0.5 in a uniform IGM or 0.5β (figure 6) if the IGM is stratified, and the value for n is calculated as σ_n / q_u. Otherwise, the computations are identical to those for the smooth interface

157

example given in this spreadsheet. When analyzing a smooth interface, n must first be estimated and the program executed. After the program computes q_u/σ_p and E_m/σ_n, n is then re-evaluated by the user from figure 36. If n is sufficiently different from the value that was estimated initially, the new value should be input and the spreadsheet program executed again.

This spreadsheet assumes the geomaterial to be uniform in and below the socket. Both base and shaft resistance can be included, or only shaft resistance can be considered. If base resistance is included, it is understood that the bearing material is massive (not highly jointed).

An example spreadsheet for Category 3 IGM's is presented showing formulas in table 19 and showing values for the Coweta County test in table 20.

Table 17. Formula sheet for Category 1 and 2 IGM's (smooth socket).

	A	B	C	D	E	F	G	H	I	J	K
1	Shaft:					Dallas					
2											
3	Formulas										
4		w_i (mm)	σ_n (kPa)	σ_n/σ_p	q_u (kPa)	λ	q_u/σ_p	α	f_{aa} (kPa)	E_m(kPa)	E_m/σ_n
5	Is base resistance	(input)	(input)		(input)					(input)	
6	to be considered?	0.5	138	=C6/101	710	=(15 - (D6))/27	=E6/101	=((5 - 8.8*F6)*(G6)*F6)/G6	=H6*E6	232000	=J6/C6
7	If it is to be	1	=C6	=C7/101	=E6	=(15 - (D7))/27	=E7/101	=((5 - 8.8*F7)*(G7)*F7)/G7	=H7*E7	=J6	=J7/C7
8	considered, type 1	2	=C7	=C8/101	=E7	=(15 - (D8))/27	=E8/101	=((5 - 8.8*F8)*(G8)*F8)/G8	=H8*E8	=J7	=J8/C8
9	in the box below.	3	=C8	=C9/101	=E8	=(15 - (D9))/27	=E9/101	=((5 - 8.8*F9)*(G9)*F9)/G9	=H9*E9	=J8	=J9/C9
10	If not, type 0.	4	=C9	=C10/101	=E9	=(15 - (D10))/27	=E10/101	=((5 - 8.8*F10)*(G10)*F10)/G10	=H10*E10	=J9	=J10/C10
11		5	=C10	=C11/101	=E10	=(15 - (D11))/27	=E11/101	=((5 - 8.8*F11)*(G11)*F11)/G11	=H11*E11	=J10	=J11/C11
12		6	=C11	=C12/101	=E11	=(15 - (D12))/27	=E12/101	=((5 - 8.8*F12)*(G12)*F12)/G12	=H12*E12	=J11	=J12/C12
13	0	7	=C12	=C13/101	=E12	=(15 - (D13))/27	=E13/101	=((5 - 8.8*F13)*(G13)*F13)/G13	=H13*E13	=J12	=J13/C13
14		8	=C13	=C14/101	=E13	=(15 - (D14))/27	=E14/101	=((5 - 8.8*F14)*(G14)*F14)/G14	=H14*E14	=J13	=J14/C14
15		9	=C14	=C15/101	=E14	=(15 - (D15))/27	=E15/101	=((5 - 8.8*F15)*(G15)*F15)/G15	=H15*E15	=J14	=J15/C15
16		10	=C15	=C16/101	=E15	=(15 - (D16))/27	=E16/101	=((5 - 8.8*F16)*(G16)*F16)/G16	=H16*E16	=J15	=J16/C16
17		12	=C16	=C17/101	=E16	=(15 - (D17))/27	=E17/101	=((5 - 8.8*F17)*(G17)*F17)/G17	=H17*E17	=J16	=J17/C17
18		14	=C17	=C18/101	=E17	=(15 - (D18))/27	=E18/101	=((5 - 8.8*F18)*(G18)*F18)/G18	=H18*E18	=J17	=J18/C18
19		16	=C18	=C19/101	=E18	=(15 - (D19))/27	=E19/101	=((5 - 8.8*F19)*(G19)*F19)/G19	=H19*E19	=J18	=J19/C19
20		20	=C19	=C20/101	=E19	=(15 - (D20))/27	=E20/101	=((5 - 8.8*F20)*(G20)*F20)/G20	=H20*E20	=J19	=J20/C20
21		22	=C20	=C21/101	=E20	=(15 - (D21))/27	=E21/101	=((5 - 8.8*F21)*(G21)*F21)/G21	=H21*E21	=J20	=J21/C21
22		24	=C21	=C22/101	=E21	=(15 - (D22))/27	=E22/101	=((5 - 8.8*F22)*(G22)*F22)/G22	=H22*E22	=J21	=J22/C22
23		25	=C22	=C23/101	=E22	=(15 - (D23))/27	=E23/101	=((5 - 8.8*F23)*(G23)*F23)/G23	=H23*E23	=J22	=J23/C23

Table 17. Formula sheet for Category 1 and 2 IGM's (smooth socket) (continued).

	L	M	N	O	P	Q	R
1							
2							
3							
4	n	L (m)	D(m)	L/D	E_c (GPa)	E_c/E_m	Ω
5	(input)	(input)	(input)		(input)		
6	0.39	6.09	0.61	=M6/N6	46	=P6*1000000/J6	=1.14*(O6)^0.5 - 0.05*((O6)^0.5 - 1)*LOG10(Q6) - 0.44
7	0.39	=M6	0.61	=M7/N7	46	=P7*1000000/J7	=1.14*(O7)^0.5 - 0.05*((O7)^0.5 - 1)*LOG10(Q7) - 0.44
8	0.39	=M7	0.61	=M8/N8	46	=P8*1000000/J8	=1.14*(O8)^0.5 - 0.05*((O8)^0.5 - 1)*LOG10(Q8) - 0.44
9	0.39	=M8	0.61	=M9/N9	46	=P9*1000000/J9	=1.14*(O9)^0.5 - 0.05*((O9)^0.5 - 1)*LOG10(Q9) - 0.44
10	0.39	=M9	0.61	=M10/N10	46	=P10*1000000/J10	=1.14*(O10)^0.5 - 0.05*((O10)^0.5 - 1)*LOG10(Q10) - 0.44
11	0.39	=M10	0.61	=M11/N11	46	=P11*1000000/J11	=1.14*(O11)^0.5 - 0.05*((O11)^0.5 - 1)*LOG10(Q11) - 0.44
12	0.39	=M11	0.61	=M12/N12	46	=P12*1000000/J12	=1.14*(O12)^0.5 - 0.05*((O12)^0.5 - 1)*LOG10(Q12) - 0.44
13	0.39	=M12	0.61	=M13/N13	46	=P13*1000000/J13	=1.14*(O13)^0.5 - 0.05*((O13)^0.5 - 1)*LOG10(Q13) - 0.44
14	0.39	=M13	0.61	=M14/N14	46	=P14*1000000/J14	=1.14*(O14)^0.5 - 0.05*((O14)^0.5 - 1)*LOG10(Q14) - 0.44
15	0.39	=M14	0.61	=M15/N15	46	=P15*1000000/J15	=1.14*(O15)^0.5 - 0.05*((O15)^0.5 - 1)*LOG10(Q15) - 0.44
16	0.39	=M15	0.61	=M16/N16	46	=P16*1000000/J16	=1.14*(O16)^0.5 - 0.05*((O16)^0.5 - 1)*LOG10(Q16) - 0.44
17	0.39	=M16	0.61	=M17/N17	46	=P17*1000000/J17	=1.14*(O17)^0.5 - 0.05*((O17)^0.5 - 1)*LOG10(Q17) - 0.44
18	0.39	=M17	0.61	=M18/N18	46	=P18*1000000/J18	=1.14*(O18)^0.5 - 0.05*((O18)^0.5 - 1)*LOG10(Q18) - 0.44
19	0.39	=M18	0.61	=M19/N19	46	=P19*1000000/J19	=1.14*(O19)^0.5 - 0.05*((O19)^0.5 - 1)*LOG10(Q19) - 0.44
20	0.39	=M19	0.61	=M20/N20	46	=P20*1000000/J20	=1.14*(O20)^0.5 - 0.05*((O20)^0.5 - 1)*LOG10(Q20) - 0.44
21	0.39	=M20	0.61	=M21/N21	46	=P21*1000000/J21	=1.14*(O21)^0.5 - 0.05*((O21)^0.5 - 1)*LOG10(Q21) - 0.44
22	0.39	=M21	0.61	=M22/N22	46	=P22*1000000/J22	=1.14*(O22)^0.5 - 0.05*((O22)^0.5 - 1)*LOG10(Q22) - 0.44
23	0.39	=M22	0.61	=M23/N23	46	=P23*1000000/J23	=1.14*(O23)^0.5 - 0.05*((O23)^0.5 - 1)*LOG10(Q23) - 0.44

Table 17. Formula sheet for Category 1 and 2 IGM's (smooth socket) (continued).

	S	T	U
1			
2			
3			
4	Γ	Θ_f	K_f
5			
6	=0.37*(O6)^0.5 - 0.15*(O6^0.5 - 1)*LOG10(Q6)+0.13	=J6*R6*B6/(3.14159*M6*1000*S6*I6)	=L6 + ((T6-L6)*(1-L6))/(T6-2*L6+1)
7	=0.37*(O7)^0.5 - 0.15*(O7^0.5 - 1)*LOG10(Q7)+0.13	=J7*R7*B7/(3.14159*M7*1000*S7*I7)	=L7 + ((T7-L7)*(1-L7))/(T7-2*L7+1)
8	=0.37*(O8)^0.5 - 0.15*(O8^0.5 - 1)*LOG10(Q8)+0.13	=J6*R8*B8/(3.14159*M8*1000*S8*I8)	=L8 + ((T8-L8)*(1-L8))/(T8-2*L8+1)
9	=0.37*(O9)^0.5 - 0.15*(O9^0.5 - 1)*LOG10(Q9)+0.13	=J9*R9*B9/(3.14159*M9*1000*S9*I9)	=L9 + ((T9-L9)*(1-L9))/(T9-2*L9+1)
10	=0.37*(O10)^0.5 - 0.15*(O10^0.5 - 1)*LOG10(Q10)+0.13	=J10*R10*B10/(3.14159*M10*1000*S10*I10)	=L10 + ((T10-L10)*(1-L10))/(T10-2*L10+1)
11	=0.37*(O11)^0.5 - 0.15*(O11^0.5 - 1)*LOG10(Q11)+0.13	=J11*R11*B11/(3.14159*M11*1000*S11*I11)	=L11 + ((T11-L11)*(1-L11))/(T11-2*L11+1)
12	=0.37*(O12)^0.5 - 0.15*(O12^0.5 - 1)*LOG10(Q12)+0.13	=J12*R12*B12/(3.14159*M12*1000*S12*I12)	=L12 + ((T12-L12)*(1-L12))/(T12-2*L12+1)
13	=0.37*(O13)^0.5 - 0.15*(O13^0.5 - 1)*LOG10(Q13)+0.13	=J13*R13*B13/(3.14159*M13*1000*S13*I13)	=L13 + ((T13-L13)*(1-L13))/(T13-2*L13+1)
14	=0.37*(O14)^0.5 - 0.15*(O14^0.5 - 1)*LOG10(Q14)+0.13	=J14*R14*B14/(3.14159*M14*1000*S14*I14)	=L14 + ((T14-L14)*(1-L14))/(T14-2*L14+1)
15	=0.37*(O15)^0.5 - 0.15*(O15^0.5 - 1)*LOG10(Q15)+0.13	=J15*R15*B15/(3.14159*M15*1000*S15*I15)	=L15 + ((T15-L15)*(1-L15))/(T15-2*L15+1)
16	=0.37*(O16)^0.5 - 0.15*(O16^0.5 - 1)*LOG10(Q16)+0.13	=J16*R16*B16/(3.14159*M16*1000*S16*I16)	=L16 + ((T16-L16)*(1-L16))/(T16-2*L16+1)
17	=0.37*(O17)^0.5 - 0.15*(O17^0.5 - 1)*LOG10(Q17)+0.13	=J17*R17*B17/(3.14159*M17*1000*S17*I17)	=L17 + ((T17-L17)*(1-L17))/(T17-2*L17+1)
18	=0.37*(O18)^0.5 - 0.15*(O18^0.5 - 1)*LOG10(Q18)+0.13	=J18*R18*B18/(3.14159*M18*1000*S18*I18)	=L18 + ((T18-L18)*(1-L18))/(T18-2*L18+1)
19	=0.37*(O19)^0.5 - 0.15*(O19^0.5 - 1)*LOG10(Q19)+0.13	=J19*R19*B19/(3.14159*M19*1000*S19*I19)	=L19 + ((T19-L19)*(1-L19))/(T19-2*L19+1)
20	=0.37*(O20)^0.5 - 0.15*(O20^0.5 - 1)*LOG10(Q20)+0.13	=J20*R20*B20/(3.14159*M20*1000*S20*I20)	=L20 + ((T20-L20)*(1-L20))/(T20-2*L20+1)
21	=0.37*(O21)^0.5 - 0.15*(O21^0.5 - 1)*LOG10(Q21)+0.13	=J21*R21*B21/(3.14159*M21*1000*S21*I21)	=L21 + ((T21-L21)*(1-L21))/(T21-2*L21+1)
22	=0.37*(O22)^0.5 - 0.15*(O22^0.5 - 1)*LOG10(Q22)+0.13	=J22*R22*B22/(3.14159*M22*1000*S22*I22)	=L22 + ((T22-L22)*(1-L22))/(T22-2*L22+1)
23	=0.37*(O23)^0.5 - 0.15*(O23^0.5 - 1)*LOG10(Q23)+0.13	=J23*R23*B23/(3.14159*M23*1000*S23*I23)	=L23 + ((T23-L23)*(1-L23))/(T23-2*L23+1)

Table 17. Formula sheet for Category 1 and 2 IGM's (smooth socket) (continued)

	V	W	X	Y	Z
1					
2					
3					
4	AA	AB numer	AB denom	A	Q$_b$ (kN)
5					
6	=A13*0.0134*J6*((O6)/(O6+1))	= 200*(((O6)^0.5) -R6)*(1+O6)	=3.14159*S6*M6	=V6*((W6/X6)^0.67)	=(3.14159*N6*N6/4)*Y6*((B6/1000)^0.67)
7	=A13*0.0134*J7*((O7)/(O7+1))	= 200*(((O7)^0.5) -R7)*(1+O7)	=3.14159*S7*M7	=V7*((W7/X7)^0.67)	=(3.14159*N7*N7/4)*Y7*((B7/1000)^0.67)
8	=A13*0.0134*J8*((O8)/(O8+1))	= 200*(((O8)^0.5) -R8)*(1+O8)	=3.14159*S8*M8	=V8*((W8/X8)^0.67)	=(3.14159*N8*N8/4)*Y8*((B8/1000)^0.67)
9	=A13*0.0134*J9*((O9)/(O9+1))	= 200*(((O9)^0.5) -R9)*(1+O9)	=3.14159*S9*M9	=V9*((W9/X9)^0.67)	=(3.14159*N9*N9/4)*Y9*((B9/1000)^0.67)
10	=A13*0.0134*J10*((O10)/(O10+1))	= 200*(((O10)^0.5) -R10)*(1+O10)	=3.14159*S10*M10	=V10*((W10/X10)^0.67)	=(3.14159*N10*N10/4)*Y10*((B10/1000)^0.67)
11	=A13*0.0134*J11*((O11)/(O11+1))	= 200*(((O11)^0.5) -R11)*(1+O11)	=3.14159*S11*M11	=V11*((W11/X11)^0.67)	=(3.14159*N11*N11/4)*Y11*((B11/1000)^0.67)
12	=A13*0.0134*J12*((O12)/(O12+1))	= 200*(((O12)^0.5) -R12)*(1+O12)	=3.14159*S12*M12	=V12*((W12/X12)^0.67)	=(3.14159*N12*N12/4)*Y12*((B12/1000)^0.67)
13	=A13*0.0134*J13*((O13)/(O13+1))	= 200*(((O13)^0.5) -R13)*(1+O13)	=3.14159*S13*M13	=V13*((W13/X13)^0.67)	=(3.14159*N13*N13/4)*Y13*((B13/1000)^0.67)
14	=A13*0.0134*J14*((O14)/(O14+1))	= 200*(((O14)^0.5) -R14)*(1+O14)	=3.14159*S14*M14	=V14*((W14/X14)^0.67)	=(3.14159*N14*N14/4)*Y14*((B14/1000)^0.67)
15	=A13*0.0134*J15*((O15)/(O15+1))	= 200*(((O15)^0.5) -R15)*(1+O15)	=3.14159*S15*M15	=V15*((W15/X15)^0.67)	=(3.14159*N15*N15/4)*Y15*((B15/1000)^0.67)
16	=A13*0.0134*J16*((O16)/(O16+1))	= 200*(((O16)^0.5) -R16)*(1+O16)	=3.14159*S16*M16	=V16*((W16/X16)^0.67)	=(3.14159*N16*N16/4)*Y16*((B16/1000)^0.67)
17	=A13*0.0134*J17*((O17)/(O17+1))	= 200*(((O17)^0.5) -R17)*(1+O17)	=3.14159*S17*M17	=V17*((W17/X17)^0.67)	=(3.14159*N17*N17/4)*Y17*((B17/1000)^0.67)
18	=A13*0.0134*J18*((O18)/(O18+1))	= 200*(((O18)^0.5) -R18)*(1+O18)	=3.14159*S18*M18	=V18*((W18/X18)^0.67)	=(3.14159*N18*N18/4)*Y18*((B18/1000)^0.67)
19	=A13*0.0134*J19*((O19)/(O19+1))	= 200*(((O19)^0.5) -R19)*(1+O19)	=3.14159*S19*M19	=V19*((W19/X19)^0.67)	=(3.14159*N19*N19/4)*Y19*((B19/1000)^0.67)
20	=A13*0.0134*J20*((O20)/(O20+1))	= 200*(((O20)^0.5) -R20)*(1+O20)	=3.14159*S20*M20	=V20*((W20/X20)^0.67)	=(3.14159*N20*N20/4)*Y20*((B20/1000)^0.67)
21	=A13*0.0134*J21*((O21)/(O21+1))	= 200*(((O21)^0.5) -R21)*(1+O21)	=3.14159*S21*M21	=V21*((W21/X21)^0.67)	=(3.14159*N21*N21/4)*Y21*((B21/1000)^0.67)
22	=A13*0.0134*J22*((O22)/(O22+1))	= 200*(((O22)^0.5) -R22)*(1+O22)	=3.14159*S22*M22	=V22*((W22/X22)^0.67)	=(3.14159*N22*N22/4)*Y22*((B22/1000)^0.67)
23	=A13*0.0134*J23*((O23)/(O23+1))	= 200*(((O23)^0.5) -R23)*(1+O23)	=3.14159*S23*M23	=V23*((W23/X23)^0.67)	=(3.14159*N23*N23/4)*Y23*((B23/1000)^0.67)

Table 17. Formula sheet for Category 1 and 2 IGM's (smooth socket) (continued).

	AA	AB	AC	AD	AE	AF
1						
2						
3				Values to be graphed		
4	$Q_{s\Omega} + Q_b$ (kN)	$Q_{sK} + Q_b$ (kN)		Q_t (kN)	w_t (mm)	
5				0	0	From Col. AA
6	=3.14159*N6*M6*T6*I6 +Z6	=3.14159*N6*M6*I6*U6 + Z6		371.6008924569	=B6	since $\Theta_t < n$
7	=3.14159*N7*M7*T7*I7 +Z7	=3.14159*N7*M7*I7*U7 + Z7		743.201784913799	=B7	From Col. AB
8	=3.14159*N8*M8*T8*I8 +Z8	=3.14159*N8*M8*I8*U8 + Z8		1142.31065040754	=B8	since $\Theta_t > n$
9	=3.14159*N9*M9*T9*I9 +Z9	=3.14159*N9*M9*I9*U9 + Z9		1308.31872444742	=B9	
10	=3.14159*N10*M10*T10*I10 +Z10	=3.14159*N10*M10*I10*U10 + Z10		1399.10661763134	=B10	
11	=3.14159*N11*M11*T11*I11 +Z11	=3.14159*N11*M11*I11*U11 + Z11		1456.35584415124	=B11	
12	=3.14159*N12*M12*T12*I12 +Z12	=3.14159*N12*M12*I12*U12 + Z12		1495.75352515236	=B12	
13	=3.14159*N13*M13*T13*I13 +Z13	=3.14159*N13*M13*I13*U13 + Z13		1524.523181924	=B13	
14	=3.14159*N14*M14*T14*I14 +Z14	=3.14159*N14*M14*I14*U14 + Z14		1546.4542560356	=B14	
15	=3.14159*N15*M15*T15*I15 +Z15	=3.14159*N15*M15*I15*U15 + Z15		1563.72604576606	=B15	
16	=3.14159*N16*M16*T16*I16 +Z16	=3.14159*N16*M16*I16*U16 + Z16		1577.68077844333	=B16	
17	=3.14159*N17*M17*T17*I17 +Z17	=3.14159*N17*M17*I17*U17 + Z17		1598.84552735908	=B17	
18	=3.14159*N18*M18*T18*I18 +Z18	=3.14159*N18*M18*I18*U18 + Z18		1614.13685854931	=B18	
19	=3.14159*N19*M19*T19*I19 +Z19	=3.14159*N19*M19*I19*U19 + Z19		1625.70176055484	=B19	
20	=3.14159*N20*M20*T20*I20 +Z20	=3.14159*N20*M20*I20*U20 + Z20		1642.03332110791	=B20	
21	=3.14159*N21*M21*T21*I21 +Z21	=3.14159*N21*M21*I21*U21 + Z21		1648.01319756631	=B21	
22	=3.14159*N22*M22*T22*I22 +Z22	=3.14159*N22*M22*I22*U22 + Z22		1653.01332550049	=B22	
23	=3.14159*N23*M23*T23*I23 +Z23	=3.14159*N23*M23*I23*U23 + Z23		1655.21826810206	=B23	

Table 18. Values sheet for Category 1 and 2 IGM's (Dallas test).

	A	B	C	D	E	F	G	H	I	J	K	L	M	N	O	P	Q	R	S
1	Shaft:					Dallas													
2																			
3	Values																		
4		w_t (mm)	σ_n (kPa)	σ_n /σ_p	q_u (kPa)	λ	q_u/σ_p	α	f_aa (kPa)	E_m(kPa)	E_m/σ_n	n	L (m)	D(m)	L/D	E_c (GPa)	E_c/E_m	Ω	Γ
5	Is base resistance	(input)	(input)		(input)					(input)		(input)	(input)	(input)		(input)			
6	to be considered?	0.5	138	1.37	710	0.50	7.03	0.21	150.45	232000	1681.16	0.39	6.09	0.61	9.98	46.0	198.28	2.91	0.55
7	If it is to be	1	138	1.37	710	0.50	7.03	0.21	150.45	232000	1681.16	0.39	6.09	0.61	9.98	46.0	198.28	2.91	0.55
8	considered, type 1	2	138	1.37	710	0.50	7.03	0.21	150.45	232000	1681.16	0.39	6.09	0.61	9.98	46.0	198.28	2.91	0.55
9	in the box below.	3	138	1.37	710	0.50	7.03	0.21	150.45	232000	1681.16	0.39	6.09	0.61	9.98	46.0	198.28	2.91	0.55
10	If not, type 0.	4	138	1.37	710	0.50	7.03	0.21	150.45	232000	1681.16	0.39	6.09	0.61	9.98	46.0	198.28	2.91	0.55
11		5	138	1.37	710	0.50	7.03	0.21	150.45	232000	1681.16	0.39	6.09	0.61	9.98	46.0	198.28	2.91	0.55
12		6	138	1.37	710	0.50	7.03	0.21	150.45	232000	1681.16	0.39	6.09	0.61	9.98	46.0	198.28	2.91	0.55
13	0	7	138	1.37	710	0.50	7.03	0.21	150.45	232000	1681.16	0.39	6.09	0.61	9.98	46.0	198.28	2.91	0.55
14		8	138	1.37	710	0.50	7.03	0.21	150.45	232000	1681.16	0.39	6.09	0.61	9.98	46.0	198.28	2.91	0.55
15		9	138	1.37	710	0.50	7.03	0.21	150.45	232000	1681.16	0.39	6.09	0.61	9.98	46.0	198.28	2.91	0.55
16		10	138	1.37	710	0.50	7.03	0.21	150.45	232000	1681.16	0.39	6.09	0.61	9.98	46.0	198.28	2.91	0.55
17		12	138	1.37	710	0.50	7.03	0.21	150.45	232000	1681.16	0.39	6.09	0.61	9.98	46.0	198.28	2.91	0.55
18		14	138	1.37	710	0.50	7.03	0.21	150.45	232000	1681.16	0.39	6.09	0.61	9.98	46.0	198.28	2.91	0.55
19		16	138	1.37	710	0.50	7.03	0.21	150.45	232000	1681.16	0.39	6.09	0.61	9.98	46.0	198.28	2.91	0.55
20		20	138	1.37	710	0.50	7.03	0.21	150.45	232000	1681.16	0.39	6.09	0.61	9.98	46.0	198.28	2.91	0.55
21		22	138	1.37	710	0.50	7.03	0.21	150.45	232000	1681.16	0.39	6.09	0.61	9.98	46.0	198.28	2.91	0.55
22		24	138	1.37	710	0.50	7.03	0.21	150.45	232000	1681.16	0.39	6.09	0.61	9.98	46.0	198.28	2.91	0.55
23		25	138	1.37	710	0.50	7.03	0.21	150.45	232000	1681.16	0.39	6.09	0.61	9.98	46.0	198.28	2.91	0.55

Table 18. Values sheet for Category 1 and 2 IGM's (Dallas test) (continued).

	T	U	V	W	X	Y	Z	AA	AB	AC	AD	AE	AF	AG
1														
2														
3											Values to be graphed			
4	Θ_f	K_f	ΛA	ΛB numer	ΛB denom	Λ	Q_b (kN)	$Q_{s\,a} + Q_b$ (kN)	$Q_{sK} + Q_b$ (kN)		Q_i (kN)	w_t (mm)		
5											0	0	From Col. AA	
6	0.21	0.14	0.00	539.76	10.62	0.00	0.00	371.60	242.18		371.60	0.50	since $\Theta_f < n$	
7	0.42	0.42	0.00	539.76	10.62	0.00	0.00	743.20	740.18		740.18	1.00	From Col. AB	
8	0.85	0.65	0.00	539.76	10.62	0.00	0.00	1486.40	1143.27		1143.27	2.00	since $\Theta_f > n$	
9	1.27	0.75	0.00	539.76	10.62	0.00	0.00	2229.61	1317.32		1317.32	3.00		
10	1.69	0.81	0.00	539.76	10.62	0.00	0.00	2972.81	1414.35		1414.35	4.00		
11	2.12	0.84	0.00	539.76	10.62	0.00	0.00	3716.01	1476.22		1476.22	5.00		
12	2.54	0.87	0.00	539.76	10.62	0.00	0.00	4459.21	1519.12		1519.12	6.00		
13	2.96	0.88	0.00	539.76	10.62	0.00	0.00	5202.41	1550.60		1550.60	7.00		
14	3.39	0.90	0.00	539.76	10.62	0.00	0.00	5945.61	1574.70		1574.70	8.00		
15	3.81	0.91	0.00	539.76	10.62	0.00	0.00	6688.82	1593.73		1593.73	9.00		
16	4.23	0.92	0.00	539.76	10.62	0.00	0.00	7432.02	1609.14		1609.14	10.00		
17	5.08	0.93	0.00	539.76	10.62	0.00	0.00	8918.42	1632.58		1632.58	12.00		
18	5.93	0.94	0.00	539.76	10.62	0.00	0.00	10404.82	1649.57		1649.57	14.00		
19	6.77	0.95	0.00	539.76	10.62	0.00	0.00	11891.23	1662.44		1662.44	16.00		
20	8.47	0.96	0.00	539.76	10.62	0.00	0.00	14864.04	1680.65		1680.65	20.00		
21	9.31	0.96	0.00	539.76	10.62	0.00	0.00	16350.44	1687.33		1687.33	22.00		
22	10.16	0.96	0.00	539.76	10.62	0.00	0.00	17836.84	1692.92		1692.92	24.00		
23	10.58	0.97	0.00	539.76	10.62	0.00	0.00	18580.04	1695.39		1695.39	25.00		

Table 19. Formulas sheet for Category 3 IGM's.

	A	B	C	D	E	F	G
1	Shaft:		Coweta County				
2							
3	Formulas		Note: v is 0.3				
4							
5	End Bearing	Depth interval number	Depth input number	Depth (m)	N (B/0.3 m)	σ'_p (kPa)	σ'_{vo} (kPa)
6	to be Considered?			(input)	(input)		(Input)
7	Enter 1 in the box		1 (top of socket)	16.16	60	=0.2*E7*101.4	176.4
8	below if end bearing	1 (depth 1 to depth 2)	2	16.47	68	=0.2*E8*101.4	179.3
9	is to be considered	2 (depth 2 to depth 3)	3	16.78	76	=0.2*E9*101.4	182.01
10	or 0 if it is to be	3 (depth 3 to depth 4)	4	17.08	90	=0.2*E10*101.4	184.77
11	neglected.	4 (depth 4 to depth 5)	5	17.38	100	=0.2*E11*101.4	187.52
12	(input)	5 (depth 5 to depth 6)	6	17.69	100	=0.2*E12*101.4	190.28
13		6 (depth 6 to depth 7)	7	17.99	100	=0.2*E13*101.4	193.04
14		7 (depth 7 to depth 8)	8	18.3	100	=0.2*E14*101.4	195.8
15		8 (depth 8 to depth 9)	9	18.61	100	=0.2*E15*101.4	198.55
16		9 (depth 9 to depth 10)	10	18.92	100	=0.2*E16*101.4	201.31
17	1	10 (depth 10 to depth 11)	11 (bottom of socket)	19.22	100	=0.2*E17*101.4	204.07
18			12 (below socket)	19.53	100	=0.2*E18*101.4	206.8
19							
20		Depth interval number	D (m)	f_{max} (kPa)	ΔQ_s (kN)		Influence
21			(input)				factor I :
22							E_c (kPa) (input) =
23		1 (depth 1 to depth 2)	0.915	=K8	=3.14159*C23*D23*(D8-D7)		E_{sm} (kPa) =
24		2 (depth 2 to depth 3)	=C23	=K9	=3.14159*C24*D24*(D9-D8)		E_{SL} (kPa) =
25		3 (depth 3 to depth 4)	=C24	=K10	=3.14159*C25*D25*(D10-D9)		
26		4 (depth 4 to depth 5)	=C25	=K11	=3.14159*C26*D26*(D11-D10)		λ =
27		5 (depth 5 to depth 6)	=C26	=K12	=3.14159*C27*D27*(D12-D11)		ξ =
28		6 (depth 6 to depth 7)	=C27	=K13	=3.14159*C28*D28*(D13-D12)		ζ =
29		7 (depth 7 to depth 8)	=C28	=K14	=3.14159*C29*D29*(D14-D13)		μL =
30		8 (depth 8 to depth 9)	=C29	=K15	=3.14159*C30*D30*(D15-D14)		A =
31		9 (depth 9 to depth 10)	=C30	=K16	=3.14159*C31*D31*(D16-D15)		B =
32		10 (depth 10 to depth 11)	=C31	=K17	=3.14159*C32*D32*(D17-D16)		C =
33							D =
34			Shaft Resistance:	$Q_{s\ max}$ (kN) =	=SUM(E23:E32)		E =
35				$Q_{b\ max}$ (kN) =	=(((C23^2)*3.14159)/4)*M18		
36				$Q_{t\ max}$ (kN) =	=SUM(E34:E35)		I =

166

Table 19. Formulas sheet for Category 3 IGM's (continued).

	H	I	J
1			
2			
3			
4			
5	OCR	φ' (degrees)	Ko
6			
7	=F7/G7	=ATAN((E7/(12.2+20.3*(G7/101.4)))^0.34)*57.3	=(1-SIN(I7/57.3))*H7^(SIN(I7/57.3))
8	=F8/G8	=ATAN((E8/(12.2+20.3*(G8/101.4)))^0.34)*57.3	=(1-SIN(I8/57.3))*H8^(SIN(I8/57.3))
9	=F9/G9	=ATAN((E9/(12.2+20.3*(G9/101.4)))^0.34)*57.3	=(1-SIN(I9/57.3))*H9^(SIN(I9/57.3))
10	=F10/G10	=ATAN((E10/(12.2+20.3*(G10/101.4)))^0.34)*57.3	=(1-SIN(I10/57.3))*H10^(SIN(I10/57.3))
11	=F11/G11	=ATAN((E11/(12.2+20.3*(G11/101.4)))^0.34)*57.3	=(1-SIN(I11/57.3))*H11^(SIN(I11/57.3))
12	=F12/G12	=ATAN((E12/(12.2+20.3*(G12/101.4)))^0.34)*57.3	=(1-SIN(I12/57.3))*H12^(SIN(I12/57.3))
13	=F13/G13	=ATAN((E13/(12.2+20.3*(G13/101.4)))^0.34)*57.3	=(1-SIN(I13/57.3))*H13^(SIN(I13/57.3))
14	=F14/G14	=ATAN((E14/(12.2+20.3*(G14/101.4)))^0.34)*57.3	=(1-SIN(I14/57.3))*H14^(SIN(I14/57.3))
15	=F15/G15	=ATAN((E15/(12.2+20.3*(G15/101.4)))^0.34)*57.3	=(1-SIN(I15/57.3))*H15^(SIN(I15/57.3))
16	=F16/G16	=ATAN((E16/(12.2+20.3*(G16/101.4)))^0.34)*57.3	=(1-SIN(I16/57.3))*H16^(SIN(I16/57.3))
17	=F17/G17	=ATAN((E17/(12.2+20.3*(G17/101.4)))^0.34)*57.3	=(1-SIN(I17/57.3))*H17^(SIN(I17/57.3))
18	=F18/G18	=ATAN((E18/(12.2+20.3*(G18/101.4)))^0.34)*57.3	=(1-SIN(I18/57.3))*H18^(SIN(I18/57.3))
19			
20		Load-Settlement Relation:	
21			
22	34700000	Qt (kN)	wt (mm)
23	=(N7+N17)/2	0	0
24	=N17	=E34/(1-((H36*A17)/((H27*COSH(H29))*0.7*1.3)))	=(I24*H36/((H24)*C23))*1000
25		=E36	=J24+1000*(I25-I24)*(1.3*0.7)/((H24/H27)*C23)
26	=2*(1+0.3)*(H22/H24)	=I25	=25 + J25
27	2.5		
28	=LN((0.25+(2.5*(H23/H24)*(1-0.3) - 0.25)*H27)*(2*(D17-D7)/C23))		
29	=(2*((2/(H26*H28))^0.5)*((D17-D7)/C23))		
30	5.2		
31	1		
32	=8*(TANH(H29))*(D17-D7)/(3.1416*H26*(1-0.3)*H27*H29*C23)		
33	=4/((1-0.3)*H27)		
34	=(4*3.14159*(H23/(H24))*(TANH(H29))*(D17-D7))/(H28*H29*C23)		
35			
36	=H30*(H31+H32)/(H33+H34)		

167

Table 19. Formulas sheet for Category 3 IGM's (continued).

	K	L	M	N
1				
2				
3				
4				
5	f_{max} (kPa)	s_u/σ'_{vo}	$q_{b\ ult}$ (kPa)	E_s (kPa)
6				
7		=0.23*H7^0.8		=22*101.4*(E7)^0.82
8	=((G7+G8)/2)*((J7+J8)/2)*TAN(((I7+I8)/2)/57.3)	=0.23*H8^0.8		=22*101.4*(E8)^0.82
9	=((G8+G9)/2)*((J8+J9)/2)*TAN(((I8+I9)/2)/57.3)	=0.23*H9^0.8		=22*101.4*(E9)^0.82
10	=((G9+G10)/2)*((J9+J10)/2)*TAN(((I9+I10)/2)/57.3)	=0.23*H10^0.8		=22*101.4*(E10)^0.82
11	=((G10+G11)/2)*((J10+J11)/2)*TAN(((I10+I11)/2)/57.3)	=0.23*H11^0.8		=22*101.4*(E11)^0.82
12	=((G11+G12)/2)*((J11+J12)/2)*TAN(((I11+I12)/2)/57.3)	=0.23*H12^0.8		=22*101.4*(E12)^0.82
13	=((G12+G13)/2)*((J12+J13)/2)*TAN(((I12+I13)/2)/57.3)	=0.23*H13^0.8		=22*101.4*(E13)^0.82
14	=((G13+G14)/2)*((J13+J14)/2)*TAN(((I13+I14)/2)/57.3)	=0.23*H14^0.8		=22*101.4*(E14)^0.82
15	=((G14+G15)/2)*((J14+J15)/2)*TAN(((I14+I15)/2)/57.3)	=0.23*H15^0.8		=22*101.4*(E15)^0.82
16	=((G15+G16)/2)*((J15+J16)/2)*TAN(((I15+I16)/2)/57.3)	=0.23*H16^0.8		=22*101.4*(E16)^0.82
17	=((G16+G17)/2)*((J16+J17)/2)*TAN(((I16+I17)/2)/57.3)	=0.23*H17^0.8		=22*101.4*(E17)^0.82
18	=((G17+G18)/2)*((J17+J18)/2)*TAN(((I17+I18)/2)/57.3)	=0.23*H18^0.8	=L18*G18*9.33*A17	=22*101.4*(E18)^0.82
19				
20				
21				
22				
23				
24				
25				
26				
27				
28				
29				
30				
31				
32				
33				
34				
35				
36				

Table 20. Values sheet for Category 3 IGM's (Coweta County test)

	A	B	C	D	E	F	G	H
1	Shaft:		Coweta County					
2								
3	Values		Note: v is 0.3.					
4								
5	End Bearing	Depth interval number	Depth input number	Depth (m)	N (B/0.3 m)	σ'_p (kPa)	σ'_{vo} (kPa)	OCR
6	to be Considered?			(input)	(input)		(input)	
7	Enter 1 in the box		1 (top of socket)	16.16	60	1216.80	176.4	6.90
8	below if end bearing	1 (depth 1 to depth 2)	2	16.47	68	1379.04	179.3	7.69
9	is to be considered	2 (depth 2 to depth 3)	3	16.78	76	1541.28	182.01	8.47
10	or 0 if it is to be	3 (depth 3 to depth 4)	4	17.08	90	1825.20	184.77	9.88
11	neglected.	4 (depth 4 to depth 5)	5	17.38	100	2028.00	187.52	10.81
12	(input)	5 (depth 5 to depth 6)	6	17.69	100	2028.00	190.28	10.66
13		6 (depth 6 to depth 7)	7	17.99	100	2028.00	193.04	10.51
14		7 (depth 7 to depth 8)	8	18.3	100	2028.00	195.8	10.36
15		8 (depth 8 to depth 9)	9	18.61	100	2028.00	198.55	10.21
16		9 (depth 9 to depth 10)	10	18.92	100	2028.00	201.31	10.07
17	1	10 (depth 10 to depth 11)	11 (bottom of socket)	19.22	100	2028.00	204.07	9.94
18			12 (below socket)	19.53	100	2028.00	206.8	9.81
19								
20		Depth interval number	D (m)	f_{max} (kPa)	ΔQ_s (kN)		Influence	
21			(input)				factor I :	
22							E_c (kPa) (input) =	34700000
23		1 (depth 1 to depth 2)	0.915	221.49	197.37		E_{rm} (kPa) =	80715.86
24		2 (depth 2 to depth 3)	0.915	246.12	219.32		E_{SL} (kPa) =	97377.95
25		3 (depth 3 to depth 4)	0.915	279.21	240.78			
26		4 (depth 4 to depth 5)	0.915	315.82	272.35		λ =	926.49
27		5 (depth 5 to depth 6)	0.915	331.55	295.45		ξ =	2.50
28		6 (depth 6 to depth 7)	0.915	332.20	286.48		ζ =	3.08
29		7 (depth 7 to depth 8)	0.915	332.84	296.60		μL =	0.18
30		8 (depth 8 to depth 9)	0.915	333.48	297.17		A =	5.20
31		9 (depth 9 to depth 10)	0.915	334.11	297.73		B =	1.00
32		10 (depth 10 to depth 11)	0.915	334.74	288.67		C =	0.01
33							D =	2.29
34			Shaft Resistance:	$Q_{s\,max}$ (kN) =	2691.93		E =	11.19
35				$Q_{b\,max}$ (kN) =	1812.62			
36				$Q_{t\,max}$ (kN) =	4504.55		I =	0.39

169

Table 20. Values sheet for Category 3 IGM's (Coweta County test) (continued).

	I	J	K	L	M	N
1						
2						
3						
4						
5	ϕ' (degrees)	K_o	f_{max} (kPa)	s_u/σ'_{vo}	$q_{b\,ult}$ (kPa)	E_s (kPa)
6						
7	47.27	1.10		1.08		64053.76
8	48.37	1.16	221.49	1.18		70977.05
9	49.33	1.22	246.12	1.27		77754.90
10	50.85	1.33	279.21	1.44		89318.10
11	51.74	1.39	315.82	1.55		97377.95
12	51.64	1.38	331.55	1.53		97377.95
13	51.53	1.37	332.20	1.51		97377.95
14	51.43	1.36	332.84	1.49		97377.95
15	51.33	1.35	333.48	1.48		97377.95
16	51.23	1.33	334.11	1.46		97377.95
17	51.13	1.32	334.74	1.44		97377.95
18	51.03	1.31	335.36	1.43	2756.60	97377.95
19						
20	Load-Settlement Relation:					
21						
22	Q_t (kN)	w_t (mm)				
23	0.00	0.00				
24	3234.71	14.08				
25	4504.55	46.50				
26	4504.55	71.50				
27						
28						
29						
30						
31						
32						
33						
34						
35						
36						

CHAPTER 7: PLUG TESTS

GENERAL

Plug tests, or pullout tests on short, small-diameter columns of concrete, potentially offer a direct and economical means of measuring the maximum unit side resistance for drilled shafts in the stratum in which the plug test is conducted. The low cost of such tests, compared with the cost of conducting a loading test on a full-scale drilled shaft, is small, which should allow plug tests to be used at many points on a construction site to assess the variability of side resistance across the site.

Plug tests were conducted or attempted at four of the test sites described in chapters 5 and 6, at which drilled shaft loading tests were conducted and actual unit side resistances were measured, and at other sites in Florida. Detailed documentation of these tests is given in a series of reports and papers by research personnel at the University of Florida, references 40 through 44, and a short summary of the test results is given in this chapter.

PRINCIPLES OF PLUG TESTING

A schematic of a typical plug test is shown in figure 84. Concrete pressure and borehole roughness similitude must be achieved as closely as possible in the plug test. The cored hole is presumed to represent the borehole for a drilled shaft, and the use of nonshrink grout is an attempt to create normal pressures against the hole wall that would be similar to those that would develop if a full head of concrete were available. The diameter is much smaller than that of a drilled shaft, but the presumption is made that scale effects are minor. This is probably an accurate assumption for IGM-concrete interfaces that do not dilate and where shearing failure occurs through the roots of the IGM asperities. The plug is tested in pullout, normally within a day of placing the grout. The rate for applying the load is similar to that for the standard pile quick loading test. Ten percent of the estimated resistance is applied every 2 to 5 minutes until failure occurs. The maximum side resistance f_{max} is the maximum load measured on the jack, minus the weight of the loading rod and plug, divided by the perimeter area of the plug.

The plug is installed by lowering the rebar cage and loading the rod into the cored borehole along with the fluid grout contained in a tubular sheath that is sealed against a base plug. The sheath is then lifted, allowing the grout to flow out and occupy the borehole, displacing any groundwater or drilling fluid upward. The height of the plug is then measured, and the grout is allowed to set prior to testing.

RESULTS OF PLUG TESTS

Results of the plug tests documented in references 40 through 44 are summarized in table 21. The first three tests were in argillaceous geomaterials, while the last four were in limestone. The underlined tests were conducted in parallel with the research for this project. Plug tests were also performed at the Owensboro site; however, almost zero side

resistance was measured there. These plugs were placed under a polymer drilling slurry at a large depth to simulate the actual construction of the drilled shafts. It is speculated that the grout did not completely displace the slurry. These tests are therefore omitted from table 21. A plug test was also attempted at the Coweta County site; however, a stable borehole could not be achieved, and the attempt to install the plug was abandoned.

The average ratio of the side resistance measured by the plug test to that measured at the same elevation in a nearby test shaft is shown in table 21 to be 2.54. If the extremely high ratio at the Gainesville, FL, site is omitted, the average ratio is reduced to 1.80. An excellent prediction was achieved at the TAMU site. It is not obvious why the plug tests consistently overpredicted the measured unit side load transfer in the drilled shafts. The results are evidently sensitive to borehole roughness and concrete pressure. Further studies are warranted before proceeding to use plug tests in practical applications.
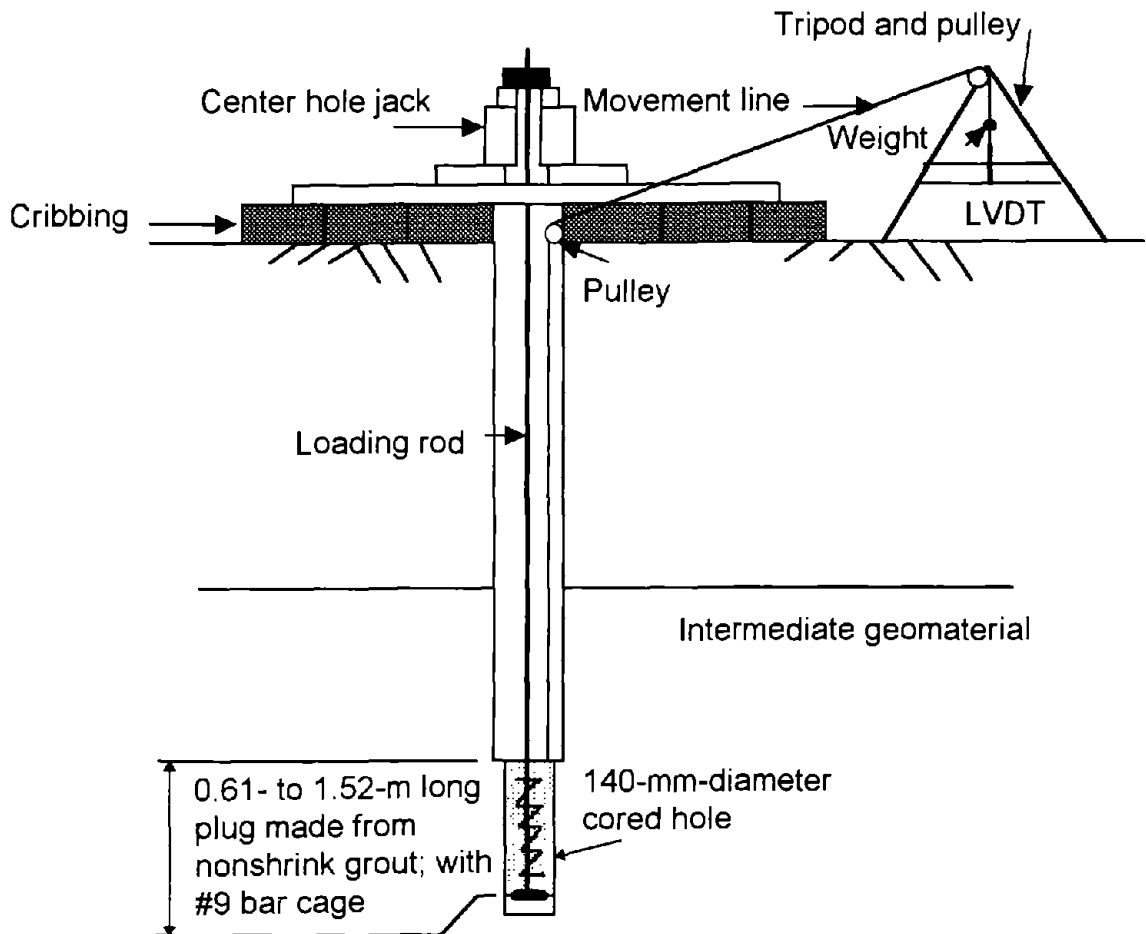
Figure 84. Schematic of plug test.

Table 21. Plug test results.

Plug test site	f_{max} from plug test (kPa)	f_{max} from drilled shaft test (kPa)	Ratio
Dallas (Test 1)	430+	144	2.99
Dallas (Test 2)	249	144	1.73
TAMU	182	172	1.06
Gainesville, Florida	623	89	7.00
Florida Keys (Test 4)	1312	872	1.50
Florida Keys (Test 7)	2280	1466	1.56
I-595, Florida	412	211	1.95
Average			2.54

CHAPTER 8: SUMMARY, CONCLUSIONS, AND RECOMMENDATIONS

SUMMARY

The research study documented in this report focused on predicting the resistance-settlement behavior of individual axially loaded drilled shafts in geomaterials at the boundary of soil and soft rock, herein termed "intermediate geomaterials," or "IGM's."

Three categories of IGM's were established for design purposes:

- Category 1: Argillaceous IGM's, or IGM's derived predominantly from clay minerals and that are prone to smearing according to the definition for water sensitivity in chapter 4
- Category 2: Carbonaceous IGM's, or IGM's derived predominantly from calcite and dolomite (limestones), and soft sandstones with calcareous cementation, or argillaceous IGM's that are not prone to smearing.
- Category 3: Granular IGM's, such as residual, completely decomposed rock and glacial till.

An intensive literature survey was undertaken, and personal visits were made to leading researchers and practitioners in the subject area of drilled shaft behavior. The results of this activity are documented in chapter 2.

A data base of previous loading tests found in the literature was developed and is documented in chapter 3. Analyses of over 100 loading tests of drilled shafts from the data base in Category 1 and 2 IGM's with several existing design criteria that relate drilled shaft side resistance to compressive strength of the geomaterial indicated low correlation with all of the criteria. It was concluded that factors other than geomaterial strength are important in controlling unit side resistance.

Guided by the conclusion from the data base study and by concepts advocated by other researchers, detailed finite element analyses of drilled shaft sockets of smooth, rough, and smeared (degraded) concrete-geomaterial interfaces were performed to investigate the importance of key geometrical and material parameters and to develop a straightforward design-level model for predicting load-settlement behavior of drilled shafts in Category 1 and 2 IGM's. The design model developed for Category 1 and 2 IGM's explicitly considers the effects of interface roughness, including shearing deformation and failure in the IGM asperities and dilation at the interface. This model also considers the IGM at the base of the drilled shaft socket to be as sound as the geomaterial along the sides of the socket; however, a provision is made to eliminate base resistance from the calculations if the user judges end bearing to be unreliable based on geotechnical and/or geological information. If base resistance is included, the computed net unit base resistance, $q_{b\ max}$, should not exceed 2.5 q_u in the geomaterial below the base, and punching failure in a softer stratum underlying the bearing stratum should be checked according to good practice.

The design model for Category 1 and 2 IGM's is described in detail in chapter 4, and three example solutions are presented in chapter 4. This design model is simple and can be applied in practice using spreadsheets, examples of which are shown in chapter 6. The design model only considers the IGM socket portion of the drilled shaft. If side resistance or drilled shaft compression above the socket is to be considered in design, such resistance and compression should be added to the resistance and settlement obtained with the model. Resistance developed in an overburden soil at any given displacement, for example the displacement at the top of the socket, can be estimated by simple load transfer functions described in reference 2.

Primary inputs into the Category 1 and 2 design model (Model 1) are:

- Mass modulus of elasticity of the IGM, including the effects of any inclusions of soft soils.
- Dimensions of the drilled shaft socket.
- Elastic modulus of the reinforced concrete socket.
- Roughness condition of the interface per table 1.
- Smear condition of the interface (indirect input).
- Interface friction angle (30 degrees used in developing the model).
- Compressive strength of the IGM.
- Initial fluid concrete pressure against the sides of the socket at its mid-depth.

A separate design model for Category 3 IGM's was adapted from reference 10. This model combines correlations for critical geotechnical parameters using SPT tests with an approximate elasticity solution for predicting resistance-settlement behavior that is developed in reference 11

Important inputs for the Category 3 design model (Model 2) are:

- N_{60}, the SPT blow count for 60-percent hammer efficiency.
- Vertical effective stress in the socket (requiring estimation of the unit weight of geomaterial in the profile and position of phreatic surface in the IGM socket).
- Elastic modulus of the reinforced concrete socket.

Hand-solution and spreadsheet examples for this model are given in chapters 4 and 6, respectively.

To verify both of the design models, several special full-scale drilled shaft loading tests were conducted, observed, or extracted from the literature in hard clay, clay-shale, shale, residual granular material, glacial till, and soft limestone. Each of the loading tests (nine in all, seven of which are documented in the main body of this report, and two of which are documented in Appendix C) was analyzed with the appropriate load-settlement model using available site-specific data.

Comparison of field test results and model predictions indicates that:

- As formulated, the models predict resistance that is eight percent too high on average (at socket settlement = 25 mm) with a coefficient of variation of under ten percent and conservatively predict settlements at working loads.
- The mass modulus of the IGM for massive Category 1 IGM's (without soft soil inclusions or voids), E_m, can be taken to be 250 q_u if no other data are available. For Category 2 IGM's, E_m can be taken to be 115 q_u. In either case, if soft soil inclusions exist, E_m should be reduced according to equation 7 or table 7.
- The interface friction angle ϕ_{rc} should be reduced to 27.5 degrees in the Category 1 and 2 model until further studies are made (i.e., take f_{max} = 0.9 times the value given by the design model).
- With present knowledge of the roughness and smear produced on IGM borehole walls by various drilling techniques, boreholes should not be considered to be rough for design purposes unless clean grooves at least 25 mm deep and spaced 0.15 to 0.3 m on centers are intentionally constructed into the IGM within the socket.
- McVay's equation (equation 37) can be used as an alternate method to compute maximum unit side shearing resistance in Category 2 IGM's. This method is fundamentally more appropriate than the method developed during this research project for cases in which adhesive bonding develops between the concrete and the IGM and failure occurs through the IGM. The method developed for this project is fundamentally more correct for cases in which the interface is frictional rather than adhesive. That appears to be the case for most argillaceous IGM's in Category 1.
- N_{60} should be restricted to not greater than 100 B/0.3 m in the Category 3 design model.

The design models consider only short-term settlement of the type that will be experienced during a loading test, and they consider only isolated shafts. Long-term settlement potentially can be estimated in shales using the results of a study by Horvath summarized quantitatively in equations 55 and 56. Group behavior is beyond the scope of this study.

CONCLUSIONS

The design models proposed in this report include the proper variables and have a sound analytical basis. Their appropriate use requires high-quality, state-of-the-practice sampling and testing and attention to construction details. Specifically, cohesive geomaterial cores are needed for strength testing and, preferably, *in situ* tests should be conducted to evaluate the modulus of the IGM for the Category 1 and 2 model. For the Category 3 model, it is critical that N values be associated with a known level of hammer efficiency, in terms of energy transferred to the drill string as a function of the theoretical drop energy of the hammer.

Settlement may be important in drilled shafts in IGM's if loads are high relative to the ultimate resistance. The design models allow for the computation of short-term settlement.

Relatively few field tests exist in which sufficient data have been acquired to test these design models. More field test data are needed to evaluate the models further, so that they can be applied with confidence to design.

Plug tests show promise as a means of directly measuring side resistance in IGM's, but at the present time, correlations are not well predicted.

RECOMMENDATIONS

Application of the Design Models

For design purposes, the two proposed models should be used only where full-scale load tests have been made in the same general geological province as the site at which the shaft to be designed is located. This will ensure that the models have been calibrated to local geological conditions.

Use of the models without local calibration may be possible in the future, but more loading tests in a wide variety of IGM's should be conducted and analyzed in light of the design model performance before such action could be considered prudent.

Further Research

Additional high-quality loading tests on drilled shafts in all IGM's are needed in order to verify the design models with a high degree of confidence or to provide a basis for correcting the models. However, further field loading tests will be useful to this end only if:

- Test boreholes are calipered.
- Smear condition of the interface is evaluated.
- E_m is measured.
- Concrete modulus is measured.
- Either N_{60} or q_u, as appropriate, is measured with sufficient numbers of tests to provide statistical significance. (The split tensile strength of the IGM should also be measured in Category 2 IGM's to facilitate evaluation of equation 37.)
- Concrete slump and rate of placement are measured.
- Other construction details, such as properties of drilling slurries, use of casing, effectiveness of casing seal, use of water by the contractor to aid in excavating cuttings in an otherwise dry hole, and length of time between drilling and concreting.

In order to take full advantage of the Category 1 and 2 design model's ability to consider interface roughness, systematic studies should be conducted to obtain reliable correlations between drilling tools and techniques, groundwater states and borehole roughness and smear for the various types of geomaterials should be considered at this time.

178

The Category 1 and 2 design model should be updated eventually to consider interface conditions between rough and smooth, if warranted by roughness correlation studies of the type described in the preceding paragraph.

Plug tests should be investigated on a continuing basis with a view toward developing a coring tool that models, with proper roughness similitude, the interface between the drilled shaft concrete and the borehole wall.

REFERENCES

1. F. H. Kulhawy and K-K Phoon, "Drilled Shaft Side Resistance in Clay Soil to Rock," *Geotechnical Special Publication No. 38, Design and Performance of Deep Foundations: Piles and Piers in Soil to Soft Rock*, Edited by P. P. Nelson, T. D. Smith, and E. C. Clukey, ASCE, pp. 172 - 183, 1993.

2. L. C. Reese and M. W. O'Neill, "Drilled Shafts: Construction Procedures and Design Methods," *Publication No. FHWA-HI-88-042*, Federal Highway Administration, Washington, D. C., 1988.

3. A. F. Williams, I. W. Johnston, and I. B. Donald, "The Design of Socketed Piles in Weak Rock," *Proceedings of the International Conference on Structural Foundations on Rock*, Balkema, Sydney, pp. 327 - 347, 1980.

4. J. Kodikara, I. W. Johnston, and C. M. Haberfield, "Analytical Predictions for Side Resistance of Piles in Rock," *Proceedings of the Sixth Australia-New Zealand Conference on Geomechanics*, Auckland, pp. 157 - 162, 1992.

5. R. G. Horvath, T. C. Kenney, and P. Kozicki, "Methods of Improving the Performance of Drilled Piers in Weak Rock," *Canadian Geotechnical Journal*, Vol. 20, pp. 758 - 772, 1983.

6. P. K. Rowe and H. H. Armitage, "A Design Method for Drilled Piers in Weak Rock," *Canadian Geotechnical Journal*, Vol. 24, pp. 114 - 125, 1987.

7. *Canadian Foundation Manual, Second Edition*, Canadian Geotechnical Society, Vancouver, 1985.

8. J. P. Carter and F. H. Kulhawy, "Analysis and Design of Drilled Shaft Foundations Socketed into Rock," *Electric Power Research Institute Research Report No. EL 5918*, Cornell University, Ithaca, NY, 1988.

9. M. C. McVay, F. C. Townsend, and R. C. Williams, "Design of Socketed Drilled Shafts in Limestone," *Journal of Geotechnical Engineering*, Vol. 118, No. 10, ASCE, pp. 1626 - 1637, 1992.

10. P. W. Mayne and D. E. Harris, "Axial Load-Displacement Behavior of Drilled Shaft Foundations in Piedmont Residuum," *FHWA Reference No. 41-30-2175*, Georgia Tech Research Corporation, Geotechnical Engineering Division, Georgia Institute of Technology, School of Civil Engineering, Atlanta, GA, February, 1993.

11. M. F. Randolph and C. P. Wroth, "Analysis of Deformation of Vertically Loaded Piles," *Journal of the Geotechnical Engineering Division*, Vol. 104, No. GT12, ASCE, pp. 1465-1488, 1978.

12. R. G. Horvath and T. C. Kenney, "Shaft Resistance of Rock-Socketed Piers," *Proceedings of the Symposium on Deep Foundations*, ASCE, pp. 182 - 214, 1979.

13. P. Rosenberg and N. Journeaux, "Friction and End Bearing Tests on Bedrock for High Capacity Socket Design," *Canadian Geotechnical Journal*, Vol. 13, No. 3, pp. 324 - 333, 1976.

14. R. T. Reynolds and T. J. Kaderabek, "Miami Limestone Foundation Design and Construction," Preprint No. 80-546, South Florida Convention, ASCE, 1980

15. C. Gupton and T. Logan, "Design Guidelines for Drilled Shafts in Weak Rock in South Florida," Preprint, Annual Meeting of South Florida Branch of ASCE, Miami, FL, 1984.

16. C. T. Toh, T. A. Ooi, H. K. Chiu, S. K. Chee, and W. H. Ting, "Design Parameters for Bored Piles in Weathered Sedimentary Formations," *Proceedings of the International Conference on Soil Mechanics and Foundation Engineering*, ISSMFE, Rio de Janeiro, 1989.

17. D. K. Crapps, "Design, Construction and Inspection of Drilled Shafts in Limerock and Limestone," Paper Presented at the Annual Meeting of the Florida Section of ASCE, 1986.

18. R. G. Horvath and K-J Chae, "Long-term Settlement of Rock-Socketed Piers," *Canadian Geotechnical Journal*, Vol. 26, pp. 348 - 358.

19. M. W O'Neill and K. M. Hassan, "Drilled Shafts: Effects of Construction on Performance and Design Criteria," *Proceedings of the Conference on Deep Foundations*, U. S. Department of Transportation, Orlando, FL, 1994.

20. M. T. Davisson, "High Capacity Piles," *Proceedings of the Lecture Series on Innovations in Foundation Construction*, Illinois Section, ASCE, 1972.

21. N. R. Morganstern and K. D. Eigenbrod, "Classification of Argillaceous Soils and Rock," *Journal of the Geotechnical Engineering Division*, ASCE, Vol. 100, No. GT10, 1974, pp. 1137 - 1156.

22. Anonymous, *ABAQUS - Finite Element Program*, Version 5.2, Hibbitt, Karlsson and Sorenson, Inc., Pawtucket, RI, 1993.

23. ASTM D1587-94, "Standard Practice for Thin-Walled Tube Geotechnical Sampling of Soils," *Annual Book of ASTM Standards*, Vol. 04.08, Soil and Rock, American Society for Testing and Materials, Philadelphia, PA, 1995, pp. 134 - 136.

24 Anonymous, *Manual on Foundation Investigations*, American Association of State Highway and Transportation Officials, Washington, D. C., 1978.

25. ASTM D2113-83, "Standard Practice for Diamond Core Drilling for Site Investigation," *Annual Book of ASTM Standards*, Vol. 04.08, Soil and Rock, American Society for Testing and Materials, Philadelphia, PA, 1995, pp. 158 - 161.

26. ASTM D3550-84, "Standard Practice for Ring-Lined Barrel Sampling of Soils," *Annual Book of ASTM Standards*, Vol. 04.08, Soil and Rock, American Society for Testing and Materials, Philadelphia, PA, 1995, pp. 345 - 347.

27. ASTM D1586-84, "Standard Test Method for Penetration Test and Split-Barrel Sampling of Soils," *Annual Book of ASTM Standards*, Vol. 04.08, Soil and Rock, American Society for Testing and Materials, Philadelphia, PA, 1995, pp. 129 - 133.

28. ASTM D2664-86, "Standard Test Method for Triaxial Compressive Strength of Undrained Rock Core Specimens Without Pore Pressure Measurement," *Annual Book of ASTM Standards*, Vol. 04.08, Soil and Rock, American Society for Testing and Materials, Philadelphia, PA, 1995, pp. 232 - 234.

29. ASTM D2166-91, "Standard Test Method for Unconfined Compressive Strength of Cohesive Soil," *Annual Book of ASTM Standards*, Vol. 04.08, Soil and Rock, American Society for Testing and Materials, Philadelphia, PA, 1995, pp. 162 - 166.

30. H. G. Poulos and E. H. Davis, *Pile Foundation Analysis and Design*, John Wiley and Sons, New York, NY, 1980.

31. ASTM D1143-81, "Standard Test Method for Piles Under Static Axial Compressive Load," *Annual Book of ASTM Standards*, Vol. 04.08, Soil and Rock, American Society for Testing and Materials, Philadelphia, PA, 1995, pp. 87 - 97.

32. ASTM D4394-84, "Standard Test Method for Determining the In Situ Modulus of Deformation of Rock Mass Using the Rigid Plate Loading Method," *Annual Book of ASTM Standards*, Vol. 04.08, Soil and Rock, American Society for Testing and Materials, Philadelphia, PA, 1995, pp. 586 - 594.

33. ASTM D4395-84, "Standard Test Method for Determining the In Situ Modulus of Deformation of Rock Mass Using the Flexible Plate Loading Method," *Annual Book of ASTM Standards*, Vol. 04.08, Soil and Rock, American Society for Testing and Materials, Philadelphia, PA, 1995, pp. 595 - 603.

34. ASTM D4729-87, "Standard Test Method for In Situ Stress and Modulus of Deformation Using the Flatjack Method," *Annual Book of ASTM Standards*, Vol. 04.08, Soil and Rock, American Society for Testing and Materials, Philadelphia, PA, 1995, pp. 869 - 874.

35. J. B. Bernal and L. C. Reese, "Study of the Lateral Pressure of Fresh Concrete as Related to the Design of Drilled Shafts," *Research Report 308-1F*, Center for Transportation Research, The University of Texas at Austin, Austin, TX, 1983.

36. R. E. Majano, M. W. O'Neill, and K. M. Hassan, "Perimeter Load Transfer in Model Drilled Shafts Formed Under Slurry," *Journal of Geotechnical Engineering*, ASCE, Vol. 120, No. GT12, 1994, pp. 2136-2154.

37. R. Gibbens and J-L. Briaud, *Data and Prediction Request for the Spread Footing Prediction Event Sponsored by FHWA at the Occasion of the ASCE Specialty Conference: Settlement '94*, Department of Civil Engineering, Texas A & M University, June 1993

38. J. W. Goodwin and J. H. Schmertmann, *Report on Osterberg Cell Load Testing, Drilled Test Shaft Nos. 8-13 and 9-12, Owensboro - Indiana State Line Road (U.S. 231) Bridge, Owensboro, Kentucky*, Loadtest, Inc. / Kentucky Transportation Cabinet, March, 1993.

39. M. McVay, S. Huang, and R. Casper, "Numerical Simulation of Drilled Shafts for Osterberg, Pullout and Axial Compression Loading in Florida Limestone," paper submitted for publication to the *Journal of Geotechnical Engineering*, American Society of Civil Engineers, 1995.

40. C. Dunkelberger, F. C. Townsend, D. Bloomquist, and B. Johnsen, *Pullout Tests on Drilled Shafts, Dallas Site*, contract report to the Federal Highway Administration (contract DTFH61-92-9-01211), McLean, VA, June, 1992.

41. B. Johnsen, F. C. Townsend, D. Bloomquist, and G. Dunkelberger, *Pullout Tests on Drilled Shafts, Coweta County, Georgia Site*, contract report to the Federal Highway Administration (contract DTFH61-92-9-01211), McLean, VA, October, 1992.

42. F. C. Townsend, P. Hirshman-Cox, D. K. Crapps, and J. W. Goodwin, *Pullout and Osterberg Load Cell Tests on Drilled Shafts, Owensboro Bridge*, contract report to the Federal Highway Administration (contract DTFH61-92-9-01211), McLean, VA, May, 1993

43. F. C. Townsend, C. E. Dunkelberger, and D. Bloomquist, "Drilled Shaft Friction Evaluation via Pullout Tests," *Geotechnical Special Publication No. 38, Design and Performance of Deep Foundations: Piles and Piers in Soil to Soft Rock*, Edited by P. P. Nelson, T. D. Smith, and E. C. Clukey, ASCE, pp. 64 - 75, 1993.

44. F. C. Townsend and M. W. O'Neill, *Pullout and Load Tests on a Drilled Shaft, National Geotechnical Site, Texas A & M*, contract report to PSC Associates, Mountain View, CA, June, 1994.